Advanced Drug Delivery Reviews 148 (2019) 68–145

Contents lists available at ScienceDirect

Advanced Drug Delivery Reviews

journal homepage: www.elsevier.com/locate/addr

A window into the brain: Tools to assess pre-clinical efficacy of biomaterials-based therapies on central nervous system disorders

Juhi Samal [1], Ana Lucia Rebelo [1], Abhay Pandit *

CÚRAM, Centre for Research in Medical Devices, National University of Ireland Galway, Galway, Ireland

ARTICLE INFO

Article history:
Received 19 September 2018
Received in revised form 4 January 2019
Accepted 28 January 2019
Available online 31 January 2019

Keywords:
Brain
Pre-clinical disease models
Nanoparticles
Histology
Bio-imaging
Molecular
Behaviour

ABSTRACT

Therapeutic conveyance into the brain is a cardinal requirement for treatment of diverse central nervous system (CNS) disorders and associated pathophysiology. Effectual shielding of the brain by the blood-brain barrier (BBB) sieves out major proportion of therapeutics with the exception of small lipophilic molecules. Various nano-delivery systems (NDS) provide an effective solution around this obstacle owing to their small size and targeting properties. To date, these systems have been used for several pre-clinical disease models including glioma, neurodegenerative diseases and psychotic disorders. An efficacy screen for these systems involves a test battery designed to probe into the multiple facets of therapeutic delivery. Despite their wide application in redressing various disease targets, the efficacy evaluation strategies for all can be broadly grouped into four modalities, namely: histological, bio-imaging, molecular and behavioural. This review presents a comprehensive insight into all of these modalities along with their strengths and weaknesses as well as perspectives on an ideal design for a panel of tests to screen brain nano-delivery systems.

Contents

1. Introduction . . . 70
2. Brain-localized nano-delivery systems. . . . 71
   2.1. Polymeric-based systems . . . 82
      2.1.1. Polymeric nanoparticles. . . . 82
      2.1.2. Dendrimers . . . 83
      2.1.3. Micelles . . . 83
   2.2. Lipid-based systems . . . 83

Abbreviations: 2D-PAGE, Two-dimensional polyacrylamide gel electrophoresis; 6-OHDA, 6-Hydroxydopamine; ABI, Acute Brain Ischemia; AchE, Acetylcholinesterase; AD, Alzheimer's Disease; AILA, Amphetamine-induced locomotor activity; ALS, Amyotrophic Lateral Sclerosis; A-NLC, Anionic Nanostrctured Lipid Carriers; APP, amyloid precursor protein; Au, Gold; $AUC_{(0\text{-}t)}$, Area under the concentration-time curve; BAD, Bcl-2-associated death promoter; BAX, Bcl-2-associated X protein; BBB, Blood Brain Barrier; BCEC, Brain Capillary Endothelial Cells; Bcl-2, B-cell lymphoma 2; BCNU, 3-bis(2- chloroethyl)-1-nitrosourea; BDNF, Brain Derived Neurotrophic Factor; bEnd3, Brain endothelial cells; bFGF, basic fibroblast growth factor; BLA, Basal locomotor activity; BNDS, Brain-targeting nano-delivery systems; BrdU, bromodeoxyuridine; CAM, cell adhesion molecules; CAR, two-way conditioned avoidance response; CD31, cluster of differentiation 31, marker for endothelial cells, platelets and lymphocytes; CD68, cluster of differentiation 68, marker for monocytes; CD133, prominin-1, marker for hematopoietic stem cells, endothelial progenitor cells, glioblastoma, neuronal and glial stem cells.; CED, convention enhanced delivery; CeO2, Cerium oxide; CeNPs, Ceria nanoparticles; CFC, Contextual Fear Conditioning; Chol, Cholesterol; C_{max}, Maximum (or peak) serum concentration that a drug achieves in a specified compartment or test area of the body after the drug has been administrated and before the administration of a second dose; c-MET, tyrosine-protein kinase Met or hepatocyte growth factor receptor, marker for tumour cells; C-NLC, Cationic Nanostrctured Lipid Carriers; CNS, Central Nervous System; c(RGDyK), cyclic Arginine-Glycine-Aspartic acid-D-Tyrosine-Lysine; CS, Conditioned stimulus; CSF, Cerebrospinal Fluid; CT, Computed Tomography; CTAB, Cetyltrimethylammonium bromide; DA, Dopamine; DAB, 3'-Diaminobenzidine; DCX, doublecortin, marker for neuronal precursor cells; DCFDA, 2',7'-dichlorodihydrofluorescein diacetate; DDAB, Dimethyl Dioctadecyl Ammonium Bromide; DGL, Dendrigraft poly-L-lysine; DI, discrimination index; DOPAC, 3,4-Dihydroxyphenylacetic acid; DOPE, 1,2-dioleoyl-sn-glycero-3-phosphoethanolamine; DOPAC, dihydroxyphenylacetic; DOX, Doxorubicin; Dox-np, Doxorubicin nanoparticles; DSPE-PEG2k-Ome, 1,2-distearoyl-sn-glycero-3-phosphoethanolamine-N-[methoxy (polyethylene glycol)-2000] liposomes; DTI%, drug targeting index; DTE%, brain targeting efficiency; DTP%, direct transport percentage; d-VAP, retro isomer of l-VAP; EBST, elevated body swing test; EGFP, enhanced green fluorescent protein; EGFRvIII, epidermal growth factor receptor variant III, marker for glioblastoma; ELISA, Enzyme-linked immunosorbent assay; EPM, Elevated plus maze; EPR, Enhanced Permeability and Retention; FC, Flow Cytometry; FDA, Food and Drug Administration; FGF, Fibroblast Growth Factor; FITC, Fluorescein isothiocynate; FRT, Forelimb retraction time; FST, Forced swim test; FGO, Functionalized graphene oxide; GBM, Glioblastoma; GC, Gas Chromatography; GDNF, Glial cell-line Derived Neurotrophic Factor; GFAP, glial fibrillary acidic protein, marker for astrocytes; GI, Gastrointestinal tract; GLUT1, Glucose transporter 1; GMO, Glyceryl monooleate; GMS, Glyceryl monostearate; GR, Glutathione reductase; GRP78, binding immunoglobulin protein (BiP); GSH, Gluthathione; GSHPx, Glutathione peroxidase; GSSG, Oxidized Glutathione; GST, Glutathione-S-transferase; H_2O_2, hydrogen peroxide; HA-LNP,

https://doi.org/10.1016/j.addr.2019.01.012
0169-409X/

2.2.1. Liposomes . . . 84
2.2.2. Lipoplexes . . . 84
2.2.3. SLNs/NLCs . . . 84
2.2.4. Exosomes . . . 84
2.3. Inorganic systems . . . 85
2.3.1. Gold nanoparticles . . . 86
2.3.2. Magnetic nanoparticles . . . 86
2.3.3. Quantum dots . . . 86
3. Classification of evaluation modalities . . . 86
3.1. Histological assessment . . . 86
3.1.1. Bright-field microscopy . . . 86
3.1.2. Fluorescence microscopy . . . 87
3.1.3. Electron microscopy . . . 99
3.2. Bio-imaging assessment . . . 99
3.3. Molecular assessment . . . 103
3.3.1. Chromatographic techniques and Mass spectrometry . . . 103
3.3.2. Spectrophotometry . . . 103
3.3.3. Scintigraphy . . . 105
3.3.4. Proteomic analysis using ELISA/WB/FC . . . 105
3.3.5. Gene analysis . . . 105
3.4. Behavioural assessment modality for nano-delivery systems . . . 105
3.4.1. Parkinson's disease . . . 105
3.4.2. Alzheimer's disease . . . 124
3.4.3. Psychotic disorders . . . 127
3.4.4. Ischemic/haemorrhagic stroke . . . 128
3.4.5. Pain models . . . 129
3.4.6. TBI . . . 130
3.4.7. Epilepsy . . . 131
3.4.8. Glioma/glioblastoma . . . 131
4. Critique . . . 131
Acknowledgments . . . 132
References . . . 132

hyaluronic acid liposomes; HD, Huntington's Disease; HE, Hematoxylin/Eosin; HPLC, High performance liquid chromatography; HRT, Hindlimb retraction time; HSA, Human Serum Albumin; HSPC, hydrogenated soy phosphatidylcholine; HUVEC, Human Umbilical Vein Endothelial Cells; HVA, Homovanillic acid; ICAM, Intercellular adhesion molecules; ICH, Intracerebral haemorrhage; ICP-MS, Inductively coupled plasma mass spectrometry; IHC, immunohistochemistry; IL-1B, interleukin 1B, marker for inflammation; IL-6, interleukin 6, marker for inflammation; Ki67, marker for cell proliferation; k and $t_{1/2}$, denotes elimination rate constant and elimination half life; LC-MS/MS, Liquid chromatography-tandem mass spectrometry; Lf, Lactoferrin; LFPI, Lateral Fluid Percussion Injury; LNC, Lipid nanocarrier; LPNP, large porous nanoparticles; LRP1, Low density lipoprotein receptor related protein 1; LUV, large unilamellar vesicles; MCAO, middle cerebral artery occlusion; MDA, Malondialgehyde; mNSS, modified neurological severity scores; MPEG, methoxy poly(ethylene glycol); MPTP, 1-methyl-4-phenyl-1,2,3,6-tetrahydropyridine; MRI, Magnetic Ressonance Imaging; MRT, mean residence time; MS, Mass spectrometry; MTT, 3-(4,5-dimethylthiazol-2-yl)-2,5-diphenyltetrazolium bromide; MTX, methotrexate; MUV, multilamellar vesicles; MWM, Morris water maze test; NA, Noradrenaline; NAC, N-acetylcysteine; NDS, Nano-Delivery Systems; NGF, Nerve Growth Factor; NeuN, neuronal nuclei, marker for neurons; NIPAAm, N-Isopropylacrylamide; NLC, Nanostructured lipid carriers; NM, Nimodipine; NK012, SN-38 releasing polymeric micelle; NO, Nitric oxide; NOR, Novel object recognition test; Nox, NADPH oxidase; NP, Nanoparticle; NSC, Neural Stem Cells; NSS, Neurological severity score; ODT, Olfactory discrimination test; OVX-D-Gal, ovariectomized administered with D-Galactose; OX-26, anti-transferrin receptor antibody; p75, marker for non-myelinating Schwann cells; PAH, Polyallylamine hydrochloride; PAMAM, Polyamidoamine; PBCA, Polybutyl cyanoacrylate; PCL, poly(ε-caprolactone); PCNA, proliferating cell nuclear antigen, marker for proliferation; PD, Parkinson's Disease; PDCD4, programmed cell death protein 4; PEEP, Polyethyl ethylene phosphate); PEG, Polyethylene glycol; PEG-DSPE, 1,2- Distearoyl-sn-glycero-3-phosphoethanolamine-N-[methoxy (polyethyleneglycol)-2000; PEG-PLGA, Poly-ethylene glycol – poly (D,L-lactic-co-glycolic acid); PEG-PAsp, Poly-ethylene glycol – poly(L-Aspartic acid); PEI, Poly(ethylenimines); PET, Positron Emission Tomography; PEO, Polyehtylene oxide; PEtOz-SS-PCL, poly (2-ethyl-2-oxazoline)-b-poly (ε-caprolactone); PFCE, perfluoro-15-crown-5-ether/perfluorocarbon; PGA, Polyglycolic acid; PLA, Poly(D,L-lactic acid); PLGA, poly (D,L-lactic-co-glycolic acid; PLGA-T7 peptide, poly(lactic-co-glycolic acid) conjugated to T7 peptide; PPI, Prepulse Inhibition of startle reflex; PPG, Polypropylene glycol; PS:80, Polysorbate-80; PS-COOH, Polystyrene carbosyl-functionalised; PSS, Polysturenesulfonate; PTEN, phosphatase and tensin homolog; PTX, Paclitaxel; PTZ, Pentylenetetrazol; PVP, Polyvinylpyrrolidone; QD, Quantum Dot; QSH, QSHYRHISPAQVC; RAM, Radial arm maze; RED, reticuloendothelial system; RGD, arginylglycylaspartic acid (Arginine-Glycine-Aspartic acid peptide); RGD-PF-DP, RGD peptide decorated pluronic-doxorubicin/paclitaxel; Rho-PE, Rhodamine-phosphatidylethanolamine; RID, Ratio of investigation duration; RI-VAP, retro inverso isomer of l-VAP; RNS, Reactive Nitrite Species; RNP, Redox polymer self-assembled nanoparticles (nitroxide radical-containing nanoparticles [RNPs]; ROS, Reactive Oxygen Species; SAH, Subarachnoid hemorrhage; SBE-β-CD, sulfobutylether-β-cyclodextrin; SDH, Succinate dehydrogenase; SLN, Solid Lipid Nanoparticles; SNEDDS, Self-Nanoemulsifying Drug Delivery Systems; SOD, Superoxide dismutase; SPC, Soybean phospholipids; SPECT, single-photon emission computed tomography; SPIONs, SuperParamagnetic Iron Oxide Nanoparticles; SUV, small unilamellar vesicles; SVCT2, Sodium-dependent vitamin C transporter 2; SAPNS, Self-assembling peptide nanofiber scaffolds; TAC, Total antioxidant capacity; TAT, Trans-activating transcriptor peptide (GRKKRRQRRRPQ); TBA, Thiobarbituric acid; TBARs, thiobarbituric acid reactive substances; TBI, Traumatic Brain Injury; TEM, Transmission Electron Microscopy; TGN, TGNYKALHPHNGC; TH, tyrosine hydroxylase; TiO2, Titanium dioxide; t_{max}, time at which the C_{max} is observed; TNF-α, tumour necrosis factor alpha, marker for inflammation; TPGS, d-alpha-tocopheryl polyethylene glycol 1000 succinate; TST, Tail suspension test; TTC, tetrazolium chloride; ^{99m}Tc, metastable isotope of technetium; U87 MG, U87 Malignant glioma cells; UPLC, Ultra performance liquid chromatography; US, unconditioned stimulus; VCAM-1, Vascular cell adhesion protein 1; VEGF, Vascular Endothelial Growth Factor; WB, Western Blot; WGA, Wheat germ agglutinin; Xo, Xanthine oxidase.

* Corresponding author.
E-mail address: abhay.pandit@nuigalway.ie (A. Pandit).
[1] These authors contributed equally to this work.

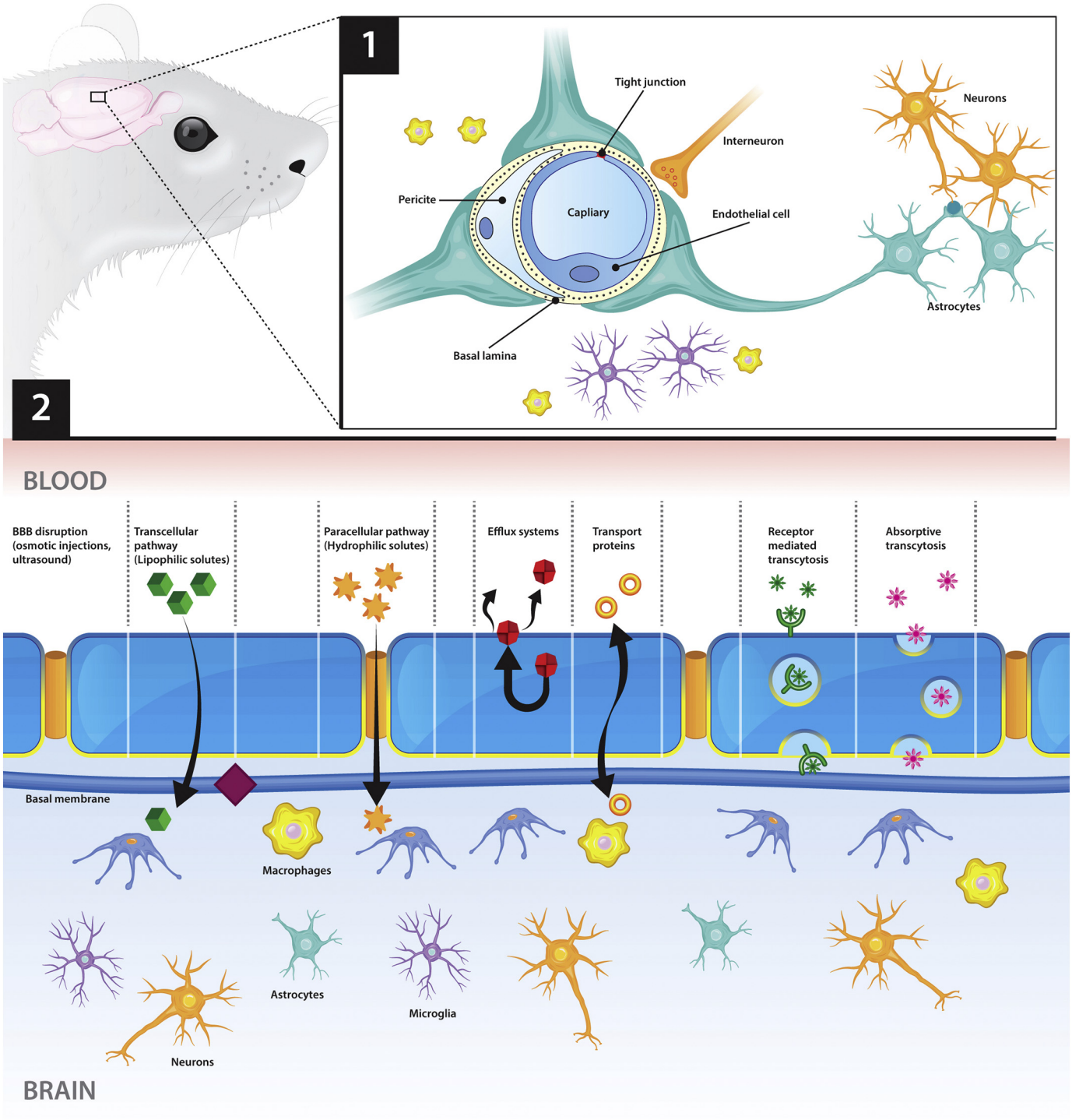

Fig. 1. Brain's protective shield: (1) Representation of blood-brain barrier (BBB) that effectively masks the brain from free access to the molecules in circulation and (2) Mechanisms of evasion of the BBB used by various delivery systems to facilitate the molecules in circulation to gain access to the brain.

1. Introduction

The brain is befittingly protected by layers of fluidic and solid processes along with the cerebrospinal fluid (CSF) that function together to buffer and protect it from challenges in the external environment that might result in brain injuries [1,2]. About 11% of the world poulation is currently suffering from disorders of the central nervous system which is anticipated to increase to 14% by 2020 [3]. A major proportion of this is the elderly population over 70 years of age, where the incidence of central nervous system (CNS) disorders is 50% or more [4]. Two major causes of the CNS disorders are neurodegeneration and neuroinflammation. Neurodegenerative disorders like Alzheimer's disease (AD), Parkinson's disease (PD), Huntington's disease (HD), and Amyotrophic Lateral Sclerosis (ALS) are a substantial proportion of CNS disorders that are characterized by age-related progressive loss of neuronal function followed by cell death [5]. There are many causes and mechanism of neurodegeneration involving a cascade of molecular changes that makes devising an efficient treatment very complicated [6].

Maintenance of brain homeostasis and the exchange of molecules between peripheral circulation and brain is stringently regulated by

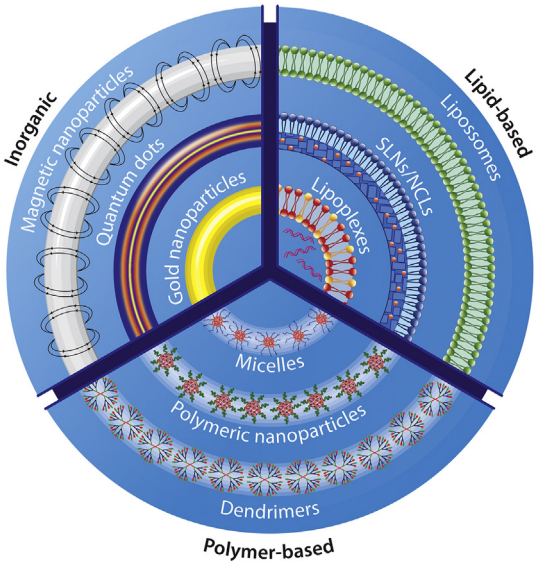

Fig. 2. Systematization of therapeutic nano-systems in the brain: These can either have an intrinsic therapeutic effect or mediate the drug delivery into the site of action. These are divided into inorganic, lipid-base and polymeric-based systems, depending on their composition and structure.

three interfaces or barriers: the blood-brain barrier (BBB), the choroid plexus epithelium and the arachnoid epithelium. Therapeutic delivery to the brain in a systemic injection that is faced with these barriers. BBB is a sieving layer composed of cerebrovascular endothelial cells, astrocytes end-feet, pericytes and basal lamina characterised by the presence of tight junctions between the endothelial cells, transmembrane protein-complexes and minimal fenestra [7]. Molecules in circulation have access through the BBB subject to following criteria (i) low molecular weight lipid-soluble molecules (MW <400 Da) or (ii) endogenous BBB transporter mediated transport. The role of these barriers and various strategies to circumvent them have been represented in Fig. 1.

The unsuitability of large-molecule drug candidates for many CNS disorders hinders their clinical translation as they fail to reach the target site in the brain at therapeutically relevant concentrations. The size-dependent stringency of regulation by these barriers does not allow even the therapeutic molecules to enter the brain, and this renders various therapeutic strategies ineffective. To address this, there is mounting research interest in developing nanotechnology-based strategies to overcome these physical and biological barriers to therapeutic transport for CNS disorders.

Brain-targeting nano-delivery systems (BNDS) provide a solution more suited to the invasive neural surgeries to deliver therapeutics to a target site in the brain. The BNDS could be broadly classified into lipid-based, polymeric and inorganic colloidal systems in the size range of 10–1000 nm [8] fabricated using natural or synthetic polymers. These nano-systems show inherent diversification in their architecture dictated by the fabrication protocols, drug-loading properties, mechanism of brain-targeting, target specificity and stability of the system. BNDS offer an advantage over other delivery systems in terms of the magnitude of therapeutic loading [9]. Encapsulated therapeutics are sheltered against chemical or enzymatic action when these systems are delivered into the body and are in contact with circulation, thereby increasing the odds of their delivery at a pharmacologically relevant concentration. Multiple surface modifications could be used to tailor BNDS for target specificity [10,11]. An effectual BNDS would be a meticulously tailored balance of parameters including stability and reasonable circulation time, immunogenicity and degradation profile. These would enable the transport of a high payload in a spatiotemporally regulated manner while escaping the efflux transporters. Fig. 1 represents the physical and biological barriers for therapeutic delivery into the brain and elucidation of different BNDS with their mechanism of evading the BBB.

Physiological barriers such as reticulo-endothelial system and BBB significantly impede the access to target regions in the brain even in the presence of surface-engineered functional moieties. This makes the need all the more urgent for a multi-modal efficacy evaluation paradigm to comprehensively assess the therapeutic efficacy and potential challenges associated with the BNDS catering to specific CNS disorders. In this review, we stratify all the available efficacy evaluation methods for therapeutic and diagnostic nanoparticles that target the brain while addressing a multitude of CNS disorders. These are grouped into four prime modalities: histological, behavioural, bio-imaging and molecular. Furthermore, we discuss the relevance of each modality and interplay of these modalities in detailed valuation of the success of nano-therapeutic delivery by BNDS in varied disease models in terms of of precise therapeutic targeting and functional recovery. Finally, we summarize the major advantages and critical loopholes of each modality, highlighting the design of an ideal multi-faceted disease-oriented assessment panel for screening the efficacy of the various BNDS in the pre-clinical models.

2. Brain-localized nano-delivery systems

Nano systems have been widely used for the targeting of brain diseases over the last two decades to replace the conventional approaches that still fail to address untreatable conditions [12]. This is due to the capacity of these systems to increase drug bioavailability, while decreasing toxicity [13].

These nano-structures can be classified into distinctive categories according to different criteria. Based on their composition, they can be divided into polymeric, lipid-based nanoparticles and inorganic nanoparticles [12] (Fig. 2). Their targeting and release properties will differ depending on the material used, shape, size and functionalization. With CNS, the existence of BBB increases the difficulty of designing a system which can overcome it and reach the site of action. However, many different systems have already been developed and tested in pre-clinical models of diverse brain disorders such as brain tumors, ischemic stroke and neurodegenerative diseases [14] [Table 1].

For all pre-clinical brain disease models, studies from 1995 till date have been summarized in Fig. 3, further categorized on the basis of disease models and species used for investigation. TBI and hemorrhagic stroke have not been represented in the figure due to fewer studies involving the brain nano-delivery systems catering to these diseases performed till date. In the case of PD, the majority of these studies were performed in Sprague-Dawley rats (*Rattus*), injured by 6-Hydroxydopamine (6-OHDA) (53%). Rotenone and 1-methyl-4-phenyl-1,2,3,6-tetrahydropyridine (MPTP) were also used within other species such as mice (*Mus*) and zebrafish (*Danio rerio*) to induce Parkinsonism; however, the gold standard is still the use of 6-OHDA, because of the plethora of PD features it promotes, which resemble the human disease. Regarding the existing glioma pre-clinical models (Fig. 3b), the only two species used were mouse and rat. There were more studies with rats than with mice. The use of rodents is attractive for the development and testing of new therapies, due to their many genetic, biological and behavioural similarities with those of humans. Most the glioma models (approximately 70%) were achieved post-inoculation with either C6 or U87MG cells, which are rat and human glioma cell lines respectively.

The majority of the studies in AD were conducted on rats (78%) and the chief model used for these studies was the Aβ plaque model as AD is neuropathlogically characterized by the accumulation of Aβ plaques and neurofibrillary tangles. IgG-Saporin, scopolamine and ovariectomized rats administered with D-Galactose (OVX-D-Gal) were the other pharmacological models used for the pre-clinical studies using BNDS as represented in Fig. 3c. Interestingly, transgenic mice overproducing mutant amyloid precursor protein (APP) reproduce the

Table 1
Summary of BNDS used in varied pre-clinical models based on their compositions.

Polymeric-based nano-systems									
Nanosystem tested		Size (nm)	Therapeutic molecule/Drug	Targeting moiety	Disease addressed	In vitro model	In vivo model	Route of administration	Ref.
Core Polymer	Surface Modification								
Polymeric nanoparticles									
PLA	Transferin	120	BiCNU®	Transferin receptor	Glioma	N/A	Adult male Sprague-Dawley rats (200–250 g)	Intracarotid	[15]
PCL	PEG	130–280	Camptothecin™	(EPR effect on cancer)	Glioma	N/A	Female F344 Fisher rats (10–11 week old, 150–175 g)	Intracranial (CED)	[16]
PBCA	Polysorbate80	260 ± 5	Doxorubicin	(LDL receptors)	Glioma	N/A	Adult male Wistar rats (200–250 g)	Intravenous	[17]
PBCA	Polysorbate80, poloxamer188	202 ± 10	Doxorubicin	SR-BI receptor	Glioma	N/A	Male Wistar rats (210–290 g)	Intravenous	[18]
PBCA	Polysorbate80	–	Doxorubicin	(LDL receptors)	Glioma	N/A	White Wistar rats (180–200 g)	Intravenous	[19]
PLGA	Polysorbate80, poloxamer188	239.9–243.4	Doxorubicin	N/A	Glioma	N/A	Adult male Wistar rats (180–220 g)	Intravenous	[20]
PBCA	Polysorbate80	112	Gemcitabine	(LDL receptors)	Glioma	C6 glioma cell line	Adult male Sprague-Dawley rats (220–250 g)	Intravenous	[21]
PCL-PEG	Angiopep-s	90	Paclitaxel	LRP1	Glioma	U87MG cell line	Male BALB/c nude mice (4–5 weeks old, 18–22 g)	Intravenous	[22]
PBCA	Polysorbate80	189.7 ± 7.6	Doxorubicin	(LDL receptors)	Glioma	N/A	Adult male Wistar rats (200–220 g)	Intravenous	[23]
PCL-PEG	Aptamer	156.0 ± 54.8	Paclitaxel	Nucleolin	Glioma	C6 glioma cell line	Adult Sprague-Dawley rats (190–210 g)	Intravenous	[24]
PCL-PEG	PEG	72.5 ± 2.2	Paclitaxel	(EPR effect)	Glioma	C6 glioma cell line	Male BALB/c nude mice(18–22 g); ICR mice (18–22 g)	Intravenous	[25]
PBCA	Polysorbate80	135.8 ± 11.3	Temozolomide	(LDL receptors)	Glioma	N/A	Adult Wistar rats (180–220 g)	Intravenous	[26]
PBCA	Polysorbate80	–	TGF-B antisense oligonucleotide	(LDL receptors)	Glioma	N/A	Fisher rats	Intravenous	[27]
PCL-PEG	Angiopep2	159.9	Doxorubicin	LPR1	Glioma	C6 glioma cell line	Male Wistar rats (200–230 g)	Intravenous	[28]
PEG-PLGA	c(RGDf(N-me) VK)-C (cHP)	97.3 ± 1.7	Curcumin	αvβ3, αvβ5, and α5β1 integrins	Glioma	HUVECs and C6 glioma cell lines	Adult male Sprague-Dawley rats (180–220 g)	Intravenous	[29]
PLGA	–	175 ± 40.75	Carboplatin	N/A	Glioma	GBM cancer cell lines, Primary neuroncultures	Adult male Wistar rats (225–275 g); White pigs (40–45 kg)	Intracranial (CED)	[30]
PLGA-PEG	–	69 ± 4	Paclitaxel	N/A	Glioma	N/A	Adult female Fischer F344 rats	Intracranial	[31]
PEG-PLGA	TGN, QSH, Aβ42	125.5.10 ± 2.26	H102	N/A	Alzheimer's Disease	N/A	Adult ICR mice (18–22 g)	Intravenous	[32]
PEG-PLGA	Solanum tuberosum lectin	118.7	bFGF	N-acetylglucosamine	Alzheimer's Disease	N/A	Adult male Sprague-Dawley rats (200–230 g)	Intranasal	[33]
PLGA	Polysorbate80	138.8 ± 4.3	Estradiol	(LDL receptors)	Alzheimer's Disease	N/A	Adult Sprague-Dawley rats (230–250 g)	Oral	[34]
PEG-PLA	PVP	51.2 ± 2.2	Curcumin	N/A	Alzheimer's Disease	MDCK cell line	Tg2576 transgenic mice	Oral	[35]
PLGA	–	200 ± 20	Curcumin	N/A	Alzheimer's Disease	NSCs from hippocampus	Adult Wistar rats	Intraperitoneal	[36]
PBCA	Polysorbate80	40.5 ± 6.9	Rivastigmine	(LDL receptors)	Alzheimer's Disease	N/A	Adult male Wistar rats (180–220 g)	Intravenous	[37]
PBCA	Polysorbate80	35.58 ± 4.64	Tacrine	(LDL receptors)	Alzheimer's Disease	N/A	Adult Wistar rats (180–220 g)	Intravenous	[38]
Chitosan		41	Tacrine	N/A	Alzheimer's Disease	N/A	Adult Wistar rats (180–220 g)	Intravenous	[39]
PLGA-b-PEG	Ascorbic acid	90.1 ± 5.2–133.1 ± 7.5	Galantamine	SVCT2	Alzheimer's Disease	NIH/3T3 cell line	Adult Sprague-Sawley rats (7–8 weeks old, 180–220 g)	Intravenous	[40]
PLGA	Pluronic 68	139.52 ± 5.35	Tarenflurbil	N/A	Alzheimer's Disease	N/A	Sprague-Dawley rats	Intranasal	[41]
PEG-PLGA	–	–	NGF	N/A	Alzheimer's Disease	N/A	Adult Sprague-Dawley rats (200–250 g)	Intracranial	[42]

Chitosan	–	–	Piperine	N/A	Alzheimer's Disease	N/A	Male Wistar rats (8 weeks old, 180–220 g)	Intranasal	[43]
Chitosan	–	161.3 ± 4.7	Bromocriptine	N/A	Parkinson's Disease	N/A	Adult Swiss albino mice (20–40 g)	Intravenous, intranasal	[44]
Poly (D,L-lactide-co--glycolide)lactide: glycolide	PVP	119.7 ± 2.69	Dopamine	N/A	Parkinson's Disease	SH-SY5Y cell line	Adult Wistar rats (215–235 g)	Intravenous	[45]
Alginate	–	11.3	Curcumin	N/A	Parkinson's Disease	N/A	Transgenic fly lines	Oral	[46]
PLGA	–	250 ± 50	L-DOPA	N/A	Parkinson's Disease	N/A	Adult male Wistar rats (307–363 g)	Intranasal	[47]
PLGA-PFCE	–	210	microRNA-124	N/A	Parkinson's Disease	Subventricular zone primary cell cultures	Adult male C57BL/6 mice (10–12 weeks old)	Intracranial	[48]
PLA	Polysorbate80	200 ± 30	Resveratrol	(LDL receptors)	Parkinson's Disease	N/A	Adult C57BL/6 mice	Intraperitoneal	[49]
PEG-PLGA	Lactoferin	120	Coumarin-6 (dye)	Lf receptor	Parkinson's Disease	bEnd.3 cell line	Adult male Kunming mice (18–20 g), Adult male Sprague-Dawley rats (200–250 g), Adult male Balb/c mice (18–20 g)	Intravenous	[50]
PEG-PLGA	Odorranalectin	114.8 ± 5.6	Urocortin peptide	L-fucose	Parkinson's Disease	N/A	Adult Female ICR mice (25–30 g), Adult female Sprague-Dawley rats (200–220 g)	Intranasal	[51]
Chitosan	–	98–148	Dopamine	N/A	Parkinson's Disease	MDCKII-MDR1 cell line	Male Wistar rats (225–250 g)	Intraperatoneal	[52]
PBCA	Polysorbate80	250 ± 30	Nerve Growth Factor	(LDL receptors)	Parkinson's Disease	N/A	Male C57BL/6 mice (7–8 weeks old, 20–25 g)	Intravenous	[53]
PEG-PLGA	Lactoferin	42.50–141.70	Rotigotine	Lf receptor	Parkinson's Disease	16HBE and SH-SY5Y cell lines	Male Kunming mice (4–5 weeks old, 18–22 g)	Intranasal	[54]
SBE-β-CD	–	214 (±7)–1000	Dopamine	N/A	Parkinson's Disease	Olfactory Ensheating cells	Male Wistar rats (225–250 g)	Intranasal	[55]
PLA	TAT	175	Ritonavir	N/A	HIV	MDCK-wt and MDCK-MDR1 cell lines	Male male FVB/Ntac mice	Intravenous	[56]
			N,N-dimethylacrylamide-PEG	–	124.4 ± 0.823	GABA	N/A	Epilepsy	Cerebellar granular primary cell culture
Adult male Wistar rats (250–350 g)	Intraperitonal	[57]							
PLGA	Poloxamer 407	167–318	Lorazepam	N/A	Epilepsy	Vero cell line	Adult male Sprague-Dawley rats (2–3 months old, 180–200 g)	Intranasal	[58]
PLGA	Poloxamer 407	84.1 ± 2.2–219.1 ± 4.7	Risperidone	N/A	Psychosis	N/A	Adult Swiss albino mice (21–25 g)	Subcutaneous	[59]
PCL	Polysorbate80	261.40 ± 3.52	Haloperidol	(LDL receptors)	Psychosis	N/A	Adult male Wistar rats (150–250 g)	Intraperitoneal	[60]
Chitosan	Polysorbate80	198–257	Doxycycline hydrochloride	(LDL receptors)	Psychosis	N/A	Swiss albino mice (3–4 months old, 25–30 g)	Oral	[61]
PCL	Polysorbate80	230 ± 25–261 ± 03	Haloperidol	(LDL receptors)	Oral dyskinesia	N/A	Adult male Wistar rats (325–395 g)	Intraperitoneal	[62]
PNIPAM	–	615 ± 45–7989 ± 115	Curcumin	N/A	Stroke	N/A	Adult Wistar rats (16 weeks old, 300–400 g)	Intranasal	[63]
Methylcellulose - Docusate sodium salt	–	81 ± 59	Cilostazol®	N/A	Stroke	Red Blood cells	Adult Male Wistar rats (7 weeks old), ICR mice (5 weeks old), rabbits	Intravenous	[64]

(continued on next page)

Table 1 (*continued*)

Polymeric-based nano-systems									
Nanosystem tested		Size (nm)	Therapeutic molecule/Drug	Targeting moiety	Disease addressed	In vitro model	In vivo model	Route of administration	Ref.
Core Polymer	Surface Modification								
							(2.5–3.0 kg)		
PBCA	Polysorbate80	148.9–151.5	Horseradish peroxidase	(LDL receptors)	Traumatic Brain Injury	N/A	Adult male Sprague-Dawley rats (220–325 g)	Intravenous	[65]
PLGA	Poloxamer188	–	BDNF	(LDL receptors)	Traumatic Brain Injury	N/A	Male C57 BL/6 N mice (11–13 weeks old, 25–28 g)	Intravenous	[66]
Chitosan	–	86.89 ± 3.09–328.73 ± 3.04	Rutin	N/A	Cerebral ischemia	N/A	Wistar rats (8–10 weeks old, 300–400 g)	Intranasal	[67]
Chitosan-PEG	PEG+anti transferin antibody	650	Caspase-3 inhibitor	Transferin receptor	Cerebral ischemia	N/A	Swiss albino mice (18–22 g)	Intravenous	[68]
PLGA	Polysorbate80	145.0 ± 1.3	Acetylpuerarin	(LDL receptors)	Cerebral ischemia	N/A	Male wistar rats (200–250 g), Kunming mice (18–22 g)	Intravenous	[69]
PLGA	–	291	Superoxide dismutase	N/A	Cerebral ischemia	N/A	Male Sprague-Dawley rats (250–300 g)	Intravenous	[70]
PLGA	Embedded in fibrin sealant gel	Not specified	Nimopidine	N/A	Intracerebral Haemorrhage	N/A	Wistar rats	Intracisternal	[71]
PCBA	–	125.3 ± 2.5	NT-3 (plasmid containing hormone response element (HRE) with a cytomegalovirus promoter)	N/A	Intracerebral Haemorrhage	RBMEC and iPSCs	Male Sprague-Dawley rats (350–400 g)	Intravenous	[72]
PLGA		220 ± 25	Curcumin	N/A	Intracerebral Haemorrhage	N/A	Male Sprague-Dawley rats (12 weeks, 260–300 g)	Intraperitoneal	[73]
RADA16-I self-assembling peptide nanofiber scaffolds (SAPNS)	–	Not specified	N/A	N/A	Intracerebral Haemorrhage	N/A	Male Sprague-Dawley (11–13 weeks, 420–480 g)	Intrastriatal	[74]
PLGA-PEG	Phage-display pepetide (Pep TGN)	104.17–121.46	–	N/A	–	bEnd.3 cells	Adult male nude mice (16–20 g) and ICR mice (18–22 g)	Intravenous	[75]
PBCA	Polysorbate80	230	Dalargin	(LDL receptors)	–	N/A	Male ICR mice	Intravenous	[76]
PLGA	Alginate hydrogel	400–600	Dexamethasone	N/A	–	N/A	Guinea pigs (300–500 g)	Intracranial	[77]
PBCA	Polysorbate80	27 ± 9	Endomorpin-1	(LDL receptors)	–	N/A	Mice	Intravenous	[78]
PBCA	Polysorbate80	290	Loperamide	(LDL receptors)	–	N/A	Male ICR mice (20–22 g)	Intravenous	[79]
PLGA	Poloxamer188	166.9–168.5	Loperamide	N/A	–	N/A	Female ICR mice (23–28 g), Female Balb/c mice (20–25 g)	Intravenous	[20]
PLGA	PEG	152.3 ± 1.0	Loperamide	N/A	–	RBE4 and C6 cell lines	Male ICR mice (25–30 g)	Intravenous	[80]
PBCA-Chitosan	Polysorbate80	70–345	Methotrexate	(LDL receptors)	–	N/A	Male Sprague-Dawley rats (200–230 g)	Intravenous	[81]
PLA	Maleimide PEG	329 ± 44	Sulpiride	N/A	–	N/A	Male Sprague-Dawley rats	Intravenous	[82]
PBCA	Polysorbate80	230	Tubocurarine	(LDL receptors)	–	N/A	Adult male ACI Wistar rats (180–250 g)	Intracranial	[83]
PLGA	Polysorbate80	259 ± 62	B-Carotene	(LDL receptors)	–	N/A	Male Sprague-Dawley rats (12 weeks old, 410–580 g)	Intravenous	[84]
PBCA	Polysorbate80	166.6 ± 0.33	Quercetin	(LDL receptors)	–	N/A	Male Wistar albino rats (180–220 g)	Oral	[85]
Dendrimers									
DGL-PEG	Angiopep	119 ± 12	DNA (hGDNF)	LRP1	Parkinson's Disease	BCEC, SH-SY5Y cell lines	Adult Male Sprague-Dawley Rats (250–300 g)	Intravenous	[86]
PAMAM-PEG	Lactoferrin	196 ± 10.1	pDNA(hGDNF)	Lf receptor	Parkinson's Disease	BCEC cell line	Adult male Sprague-Dawley rats (250–300 g)	Intravenous	[87]
PAMAM	NAC	–	N-acetyl-L-cysteine (NAC)	Activated mictoglia and astrocytes	Cerebral Palsy	N/A	Newborn New Zealand white rabits	Intravenous	[88]
PAMAM	–	15.10 ± 5.4	Haloperidol	Dopamine D2 receptor	Psychosis	N/A	Adult Sprague-Dawley rats (250–350 g)	Intranasal, Intraperitoneal	[89]

PAMAM	Dexamethasone	208.4 ± 12.1	Heme oxygenase-1 gene	Glucocorticoid receptors	Ischemic stroke	Neuro2A cell line	MCAO Adult male Sprague-Dawley rats (280–300 g)	Intracranial	[90]
DGL-PEG	Leptin30	141 ± 33 nm	DNA	Leptin receptor	–	BCEC, BV-2 microglia cell lines	Male ICR mice (4–5 weeks old, 20–25 g), Nude mice	Intravenous	[91]
PAMAM-PEG	Angiopep	–	DNA (pEGFP-N2)	LRP1	–	BCEC cell line	Male Balb/c mice (4–5 weeks, 20–25 g)	Intravenous	[92]
PAMAM	–	–	–	N/A	–	Primary mouse cortical cell culture	C57/BL6-j mice (3–4 weeks old)	Intracranial, Intraparenchyma	[93]
DAB	Transferin	–	DNA	Transferin receptor	–	bEnd.3 cell line	Female BALB/c mice	Intravenous	[94]
PAMAM-PEG	Lactoferrin	–	DNA	Lf receptor	–	BCEC cell line	Male Balb/c mice (4–5 weeks, 20–25 g)	Intravenous	[95]
PAMAM	(OH neutral groups)	1.0–4.0	–	N/A	–	Primary mouse cortical cell culture	C57 BL/6 J mice (6–15 weeks old)	Intracranial, Intracarotid	[96]
PAMAM-PEG	Serine–Arginine–Leucine (SRL)	150 ± 62	DNA	LRP ligand (clathrin/caveolin endocytosis)	–	BCEC cell line	Male Balb/c mice (4–5 weeks, 20–25 g)	Intravenous	[97]
Micelles									
MPEG-PCL	TAT-modified	73 ± 17	Coumarin (dye)	N/A	Glioma	C6 glioma cell line	Adult male Sprague-Dawley rats (7 weeks old)	Intravenous, Intranasal	[98]
RGD-PF-DP	–	28.5 ± 0.12	Doxorubicin, Paclitaxel	N/A	Glioma	U87MG, BCEC cell lines	Male BALB/c nude mice (18–22 g)	Intravenous	[99]
DSPE-PEG2k-Ome, 3helix bundle	–	19.6 ± 7.4	–	N/A	Glioma	N/A	Male athymic nu/nu rats (250 g)	Intravenous	[100]
vitamin E-TPGS	Transferrin	20.36 ± 3.19	Docetaxel	Transferrin receptor	Glioma	N/A	Charles Foster rats (180–220 g)	Intravenous	[101]
SN-38 loaded micelles	–	–	NK012	N/A	Glioma	U87MG, 9L, F98, GL261 cell lines	Normal Fischer 344 rats (250 g, 12 weeks old)	Intracranial (CED)	[102]
RGD-PLA-PEG	–	118.4 ± 1.6	Docetaxel	alpha v beta3 receptors	Glioma	U87MG, 9L, F98, GL261 cell lines	Nude mice (20 g, 7 weeks old)	Subcutaneous	[103]
Deoxycholic acid-conjugated	–	132	Curcumin/miR21 ASO	N/A	Glioma	C6 glioma cell line	Male Sprague-Dawley rats (7 weeks old)	Intracranial	[104]
PEtOz-SS-PCL	–	88.4–162.4	Doxorubicin, Paclitaxel	N/A	Glioma	C6 glioma cell line	Male ICR mice (18–20 g)	Intravenous	[105]
RI-VAP, d-VAP	–	25	Paclitaxel	GRP78	Glioma	U87MG, HUVEC cell lines	Male BALB/c nude mice (4–6 weeks old)	Intravenous	[106]
Pluronic407	–	26	Panobinostat	N/A	Glioma	F98, U87MG, M059K glioma cell lines	Wistar rats (225–275 g)	Intracranial (CED)	[107]
PLGA-T7 peptide	–	83.31	Carmustine (BiCNU®)	Transferrin receptor	Glioma	BCEC, U87MG cell lines	Male BALB/c nude mice (18–22 g)	Intravenous	[108]
Pluronic P85/F68	–	40.61 ± 1.17	Baicalein	N/A	Parkinson's Disease	MDCK-MRP2 cell line	Zebrafish	Oral	[109]
TPGS	–	26.5 ± 4.8	Paliperidone palmitate	N/A	Psychosis	N/A	Adult Swiss albino mice (21–25 g)	Intramuscular	[110]
Chitosan-PEI-magnetic micelles	–	35–50	DNA	N/A	Traumatic Brain Injury	HT22 cell line	Male Sprague-Dawley rats (250–300 g)	Intranasal	[111]
PE-PEG	Angiopep-2 modified	13.78 ± 1.48	Amphotericin B	LRP1	Fungal infections of CNS	BCEC cell line	Male ICR mice (4–5 weeks, 20–25 g), Male Sprague-Dawley rats (7–8 weeks old, 220–250 g)	Intravenous	[112]
PEG-PPG-PEG	–	83.77–132.7	Clonazepan	P-glycoprotein efflux	Epilepsy	N/A	Male Swiss albino mice (20–25 g)	Intranasal, Intravenous	[113]
methoxyPEG-PLA/TPGS	–	122.9–183.5	Lamotrigine	(inihibition of P-gp)	Epislepsy	N/A	Sprague-Dawley rats (180–220 g)	Intranasal	[114]
Curcumin-Tween80	–	–	Curcumin	N/A	(suitable for Alzheimer's)	PC-12 cell line	Female NMRI mice (8–24 months old)	Oral	[115]
PCL-PEEP	–	20	Coumarin (dye)	N/A	–	BMEC cell line	Male ICR mice (18–22 g)	Intravenous	[116]
Angiopep-2-PEG-PLA	–	38.4 ± 2.1	–	LRP1	–	N/A	Male ICR mice (18–22 g)	Intravenous	[117]
Pluronic F127-TPGS	–	19.19–20.85	–	N/A	–	BCEC cell line	Male Sprague-Dawley rats	Intravenous	[118]

(continued on next page)

Table 1 (*continued*)

Polymeric-based nano-systems									
Nanosystem tested		Size (nm)	Therapeutic molecule/Drug	Targeting moiety	Disease addressed	In vitro model	In vivo model	Route of administration	Ref.
Core Polymer	Surface Modification								
Nano-tubular Pluronic/-phosphatidylcholine/-polysorbate 80 mixed micelles (PPPMM)	Polysorbate 80	571.5 ± 11.87	Nimodipine		Intracerebral Haemorrhage	N/A	(200–250 g) Wistar Rats	Oral	[119]
Lipid-based nano-systems									
p-aminophenyl-alpha-mannopyranoside (MAN) - Transferin		122.80 ± 5.39	Daunorubicin	Transferin receptor, GLUT1	Glioma	BMVEC, C6 glioma cell lines	Male Sprague-Dawley rats (9 weeks old)	Intravenous	[120]
Liposomes nanoparticles									
Pegylated liposomes		100	Doxorubicin	(FUS)	Glioma	N/A	Male Sprague-Dawley rats (200 g)	Intravenous	[121]
Procationic liposomes - Lactoferin		208.97 ± 0.81	Doxorubicin	Lactoferrin receptor	Glioma	BCEC, C6 glioma cell lines	Male Wistar rats (150–180 g)	Intravenous	[122]
Cholesterol-TAT		105.1 ± 2.22	Doxorubicin	N/A	Glioma	BCEC, C6 glioma cell lines	Kunming mice, Wistar rats (8 weeks old, 220–250 g)	Intravenous	[123]
L -a -PC, SA and CH - Transferin		–	5-fluorouracil	Transferin receptor	Glioma	N/A	Albino rats (150–200 g)	Intravenous	[124]
TPGS-Transferin		182.5 ± 1.80	Docetaxel; Quantum dots	Transferin receptor	Glioma	N/A	Charles Foster rats (180–220 g)	Intravenous	[101]
HSPC/DOPE/Chol/CTAB/Didodecyldimethylammonium bromide		187.02	Doxorubicin	N/A	Glioma	C6 glioma cell lines	Adult Sprague-Dawley rats (200–220 g)	Intravenous	[125]
SPC:Cholesterol:Sorbitol		156.70 ± 11.40	Temozolomide	N/A	Glioma	N/A	Adult white New Zealand rabbits (2.0–2.5 kg)	Intravenous	[126]
DSPE- PEG2000-maleimid, DDAB		163 ± 15	VEGF	N/A	Glioma	U87MG, C6 glioma cell lines	Adult female Wistar rats (3 months old, 230–280 g)	Intravenous	[127]
NH2-PEG2000-DSPE-p-aminophenyl-α-D-mannopyranoside		119.7 ± 0.17	Curcumin, Quinacrine	GLUT1	Glioma	bEnd3, C6 glioma cell lines	ICR male mice (18–20 g)	Intravenous	[128]
DPPC:PTX:DSPE-PEG2000:cholesterol		90	Paclitaxel	N/A	Glioma	U87MG cell line	Male BALB/c mice (6–7 weeks old, 18–22 g)	Intravenous	[129]
DSCP:Cholesterol:PEG		106.8 ± 5.5	Donepezil	N/A	Alzheimer's Disease	N/A	Adult male Wistar rats (180–220 g)	Intranasal	[130]
PC:DCP:Cholesterol		67.51 ± 14.2–528.7 ± 15.5	Rivastigmine	N/A	Alzheimer's Disease	N/A	Aldult male Wistar albino rats (240–280 g)	Oral	[131]
OX-26		–	NGF	Transferin receptor	Alzheimer's Disease	N/A	Female Sprgue-Dawley rats (150 g)	Intravenous	[132]
PEG-DSPE-Lecithin:DDAB - Polysorbate80		478 ± 4.94	Rivastigmine hydrogen tartarate	(LDR receptor)	Alzheimer's Disease	N/A	Male albino rabbits (1.5 kg)	Intranasal	[133]
Cardiolipin-conjugated liposomes - WGA		135.2 ± 6.8–142.9 ± 5.4	Curcumin, NGF	N/A	Alzheimer's Disease	HBMEC, Has, SK-N-MC cell lines	Male Wistar rats (8 weeks old, 250–280 g)	Intravenous	[134]
Pegylated immunoliposome (OX-26)		85	DNA (TH plasmid)	Transferin receptor	Parkinson's Disease	U87MG, RG-2 cell line	Male Sprague-Dawley rats (200–250 g)	Intravenous	[135]
DSPE:CHOL:PEG2000 - OX-26		46 ± 4	Dopamine	Transferin receptor	Parkinson's Disease	N/A	Adult male Wistar rats (250–300 g); Adult male Srapgue-Dawley rats	Intravenous	[136]
SPC:CHOL:MPEG-DSPE		98.51 ± 6.82–115.54 ± 9.23	Risperidone	N/A	Schizophrenia	N/A	Male Wistar albino rats	Intranasal	[137]
Heparin-Poloxamer188		128 ± 7.65	bFGF	N/A	Cerebral	N/A	Adult female	Intranasal	[138]

				ischemia reperfusion injury		Sprague-Dawley rats (230–270 g)		
OX-26	–	Methotrexate	Transferin receptor	(Glioma)	N/A	Female Sprague-Dawley rats (100–125 g)	Intravenous	[139]
DSPE-PEG-RMP-7	81.50 ± 0.66	GDNF	N/A	-	BCEC, Acs cell lines	Adult Sprague-Dawley rats (240–260 g)	Intravenous	[140]
SPC:Cholesterol:Rho-PE, NH2- PEG2000-Mal and mPEG2000-NH2	–	–	N/A	–	BCEC, C6 glioma cell lines	Kunming mice	Intravenous	[141]
Procationic liposome - Lactoferin	123.6 ± 22.1	–	Lf receptor	–	BCEC cell line	Kunming mice	Intravenous	[142]
Cholesterol:PEG2000-TAT	147.6 ± 0.6	–	N/A	–	BCEC cell line	Kunming mice, Male Wistar rats (160–200 g)	Intravenous	[143]
POPC, DDAB, DSPE-PEG 2000, DSPE-PEG 2000 - OX-26	73	DNA (luciferase or B-galactosidase plasmid)	Transferin receptor	–	N/A	Male Sprague-Dawley rats (200–250 g)	Intravenous	[144]
POPC, DDAB, DSPE-PEG 2000, DSPE-PEG 2000 - OX-26	>75	DNS (B-galactosidase plasmid)	Transferin receptor	–	N/A	Male Sprague-Dawley rats (250 g)	Intravenous	[145]
SLNs/NLCs								
PNP	109.1 ± 4.3	Temozolomide	N/A	Glioma	U87MG cell line	Adult BALB/c nude mice (5–6 weeks old, 18–22 g)	Intravenous	[141]
SLN	94.6 ± 3.1							
NLC	121.4 ± 5.6							
SLN	111.2 ± 3.1	Edelfosine	N/A	Glioma	C6 glioma cell line	BALB/c mice	Oral	[146]
SLN	117.4 ± 11.7	siRNA	c-MET	Glioma	U87MG cell line	Adult Male BALB/c nude mice (6 weeks old)	Intravenous	[147]
SLN	131.2 ± 7.3–159.7 ± 8.0	Camptothecin™	N/A	Glioma	A172, U251, U373, U87, THP1 cell lines	Adult Male Wistar rats (250–300 g)	Intravenous	[148]
SLN	91.33 ± 41.03–272.33 ± 113.57	Camptothecin™, Rhodamine123 (dye)	N/A	Glioma	Porcine BCEC, RAW 264.7 cell lines	Adult Wistar rats (230–250 g)	Intravenous	[149]
LNC	196 ± 1.40	Curcumin	N/A	Glioma	U251MG, C6 glioma cell line	Adult Male Wistar rats (8 weeks old, 220–260 g)	Intravenous	[150]
SLN	248.30 ± 3.80	Resveratrol	N/A	Glioma	C6 glioma cell line	Adult Female adult Wistar rats (150–200 g)	Intraperitoneal	[151]
NLC	146.8	Curcumin	N/A	Glioma	U373MG cell line	Adult Male Wistar Rats (250–270 g)	Intranasal	[152]
HA-LNP	100.7 ± 3	siRNA	N/A	Glioma	T98G, U251, U87MG cell lines	Athymic BALB/c nude mice	Intracranial	[153]
NLC	178.9 ± 2.7	Temozolomide, DNA	RGD	Glioma	U87MG cell line	Adult BALB/c nude mice (5–6 weeks old, 18–22 g)	Intravenous	[154]
NLC	118.3 ± 2.6	Temozolomide	RGD	Glioma	U87MG cell line	Adult BALB/c nude mice (5–6 weeks old, 18–22 g)	Intravenous	[155]
SLN	179.1 ± 5.2, 181.3 ± 4.1	Vincristine, Temozolomide	N/A	Glioma	U87MG cell line	Adult BALB/c nude mice (5–6 weeks old, 18–22 g)	Intravenous	[156]
NLC	117.4 ± 2.8, 119.8 ± 2.6							
NLC	–	Curcumin	N/A	Glioma	A172 cell line	Adult Female nude mice (5–6 weeks old)	Intraperitoneal	[157]
LPNP	40–135	RNAi	N/A	Glioma	GBM6, GBM12, GBM26, GBM43, MGG8, MES83, bEnd3, C8D1A cell lines	Athymic nude male/female mice (6–8 week old)	Intracranial	[158,159]
SLN	134.6 ± 15.4	Curcumin	N/A	Ischemic Stroke	N/A	Adult Male Wistar rats (250–300 g)	Oral	[160]
SLN	27.20–47.68	Baicalin	Transferin Receptor	Ischemic Stroke	N/A	Adult Male Sprague-Dawley rats (260 ± 10 g)	Intravenous	[161]

(continued on next page)

Table 1 (*continued*)

Lipid-based nano-systems								
NLC SLN LE	373–430 333.1 ± 13.8 435.9 ± 35.2	Apomorphine	N/A	Parkinson's Disease	N/A	Adult Male Sprague-Dawley rats (230–270 g)	Intravenous	[162]
PLN	98.43 ± 3.38–287.26 ± 5.72	Ropinirole	N/A	Parkinson's Disease	N/A	Adult Male Albino Mice (25 ± 2 g)	Intranasal	[163]
A-NLC, C-NLC	82 ± 1.7–314 ± 19	Ropinirole hydrochloride	N/A	Parkinson's Disease	N/A	Adult Male Wistar Albino Rats (200–250 g)	Intranasal	[164]
GNL	143 ± 1.14	bFGF, Apomorphine	N/A	Parkinson's Disease	N/A	Sprague-Dawley rats	Intranasal	[165]
NLC	163–222	Bromocriptine	N/A	Parkinson's Disease	N/A	Adult Male Sprague-Dawley rats	Intraperitoneal	[166]
MEM SLN NLC	148.3 ± 5.1 119.1 ± 6.9 137.1 ± 10.4	Huperzine A	N/A	Alzheimer's Disease	N/A	Adult Male Swiss Albino mice (25–30 g, 4–6 weeks old)	Transdermal	[167]
SLN	152–4620	Quercetin	N/A	Alzheimer's Disease	N/A	Adult Male Wistar Rats (180–200 g)	Intravenous	[168]
SLN	277.6 ± 2.4	Piperine	N/A	Alzheimer's Disease	N/A	Albino Wistar rats	Intraperitoneal	[169]
NLC	92.4 ± 0.9–103.8 ± 0.6	Curcumin	Lactoferrin receptor	Alzheimer's Disease	BCEC cell line	Sprague-Dawley rats (180–220 g) & ICR mice (18–22 g)	Intravenous	[170]
SLN	40–70	Sesamol	N/A	Alzheimer's Disease	N/A	Adult Male Wistar Rats (200–230 g, 3 months old, ICV-STZ)	Intracranial	[171]
SLN	92.0 ± 3.51	Galantamine	N/A	Alzheimer's Disease	N/A	Adult Wistar rats (250–300 g)	Intravenous	[172]
SLN	240.0 ± 4.79	Chrysin	N/A	Alzheimer's Disease	N/A	Adult Male Sprague-Dawley rats (250–300 g)	Oral	[173]
SLN	101–210	MEP, coumarin 6	anti-Nfasc, anti-Cntn2	Multiple Sclerosis	U87MG cell line	Adult C57BL mice (8 weeks old, 30–50 g)	Intravenous	[174]
SLN	180.9–271.18	Simvastatin	N/A	Ischemia	N/A	Adult BALB/c mice (25–30 g)	Oral	[175]
NLC	154 ± 16	Valproic acid	N/A	Bipolar disorder, migraines	N/A	Adult Male Wistar Rats (180–200 g)	Intranasal	
SLN	148 ± 0.85	Risperidone (Risperdal®)	N/A	Schizophrenia, bipolar disorder	N/A	Adult BALB/c mice (25–30 g)	Intranasal	[176]
NLC	163.7 ± 7.52	Asenapine (Saphris®)	N/A	Schizophrenia	N/A	Adult Male Charles Foster rats (200–240 g)	Intranasal	[177]
SLN	134–162	Quetiapine fumarate	N/A	Schizophrenia	N/A	Adult Male albino rats (160–180 g)	Oral	[178]
NLC	137.2 ± 2.88	Duloxetine	N/A	Behavioural disorders	N/A	Adult Swiss Albino Wistar Rats (150–250 g)	Intranasal	[179]
NLC	107–177	Vinpocetine	N/A	(suitable for Ischemic Stroke)	N/A	Adult Male Wistar Rats (200–250 g)	Oral	[180]
NLC	89 ± 21–148 ± 41	Vinpocetine	N/A	(suitable for Ischemic Stroke)	N/A	New Zealand white male rabbits (2.5 ± 0.2 kg)	Oral	[181]
NLC	93.3 ± 1.5–102.5 ± 1.2	Baicalin	N/A	(suitable for Ischemic Stroke)	N/A	Adult Male Wistar Albino Rats (200–250 g)	Intravenous	[182]

Inorganic nano-systems								
TiO_2	–	Dopamine	N/A	Parkinson's Disease	N/A	Adult male Wistar rats (250–280 g)	Intracranial	[183]
CeO_2	200	–	N/A	Parkinson's Disease	N/A	Adult male Wistar rats (200–220 g)	Intraperitoneal	[184]
Au	35.6 ± 8.8	–	N/A	Parkinson's Disease	Mouse TTFs, GM23967 human cells	Male C57BL/6 mice (12 weeks old)	Intracranial	[185]
Fe_3O_4 - Oleic acid-NIPAm-AA-NGF	290.4	shRNA	NGF receptor	Parkinson's Disease	PC-12 cell line	Adult male C57BL/6 mice (7–8 weeks old)	Intraperitoneal	[186]
Au-CLPFFD-THRPPMWSPVWP	13 ± 1.7	–	Transferrin receptor	Alzheimer's Disease	Bovine microvessel brain endothelial cells and newborn rat astrocytes	Male Sprague-Dawley rats (180–200 g)	Intraperitoneal	[187]
QD-aptamer32	20	–	epidermal growth factor receptor variant III (EGFRvIII)	Glioma	U87MG, HUVEC cell lines	Male C57BL/6 athymic nude mice (6–8 weeks old)	Intravenous	[188]
Angiopep2-PEG-DOX-Au	39.96 ± 0.57	Doxorubicin	LRP1	Glioma	C6 glioma cell line	Male Kunming mice (20–24 g)	Intravenous	[189]
PEG/PEI-SPIONs, DMPC	24–31	-	N/A	(Parkinson's Disease)	PC-12 cell line	Adult Female Sprague-Dawley rats (220–250 g)	Intracranial	[190]
SPIONs	10; 25	–	Macrophages	(Brain tumor)	RAW264.7 cell line	BALB/c nude mice (6–11 weeks old, 17 g)	Intraperitoneal	[191]
Au - PSS/PAH and H S A	115 ± 5	–	N/A	(Prion Disease)	PBCEC cell line	Male CD1 mice (6 weeks old, 30 g)	Intravenous	[192]
QD (CdSe core) - PEG	35.4 ± 0.9	–	N/A	(imaging ECS)	N/A	Female Sprague-Dawley rats (160–260 g)	Intracranial	[193]
SPIONs - PEG, PEI, Polysorbate80	11.5 ± 2.2	–	N/A	–	C6 glioma cell line	Adult Female Sprague-Dawley rats (250–300 g)	Intravenous	[194]
Qdot 625 - Monoclonal antibodies Ri7, 8d3	9.15 ± 0.87	–	Transferrin receptor	–	Neuro2A, bEnd5 cell lines	Adult Male Balb/c mice (20–30 g)	Intravenous	[195]
Ceria nanoparticles loaded with Iron-Mesoporous silica nanoparticles with lipid coating	100 nm	–	ROS	Intracerebral Haemorrhage	RAW 264.7 macrophage cell lines	Male Sprague-Dawley rats (8 weeks)	Intracranial	[196]
Ceria, coated with PEG	16.4 ± 3.2 (radius in PBS)	–	N/A	Intracerebral Haemorrhage	U937 cell line and RAW 264.7 macrophage cell lines	Male Sprague-Dawley rats (12 weeks, 260–300 g)	Intravenous	[197]

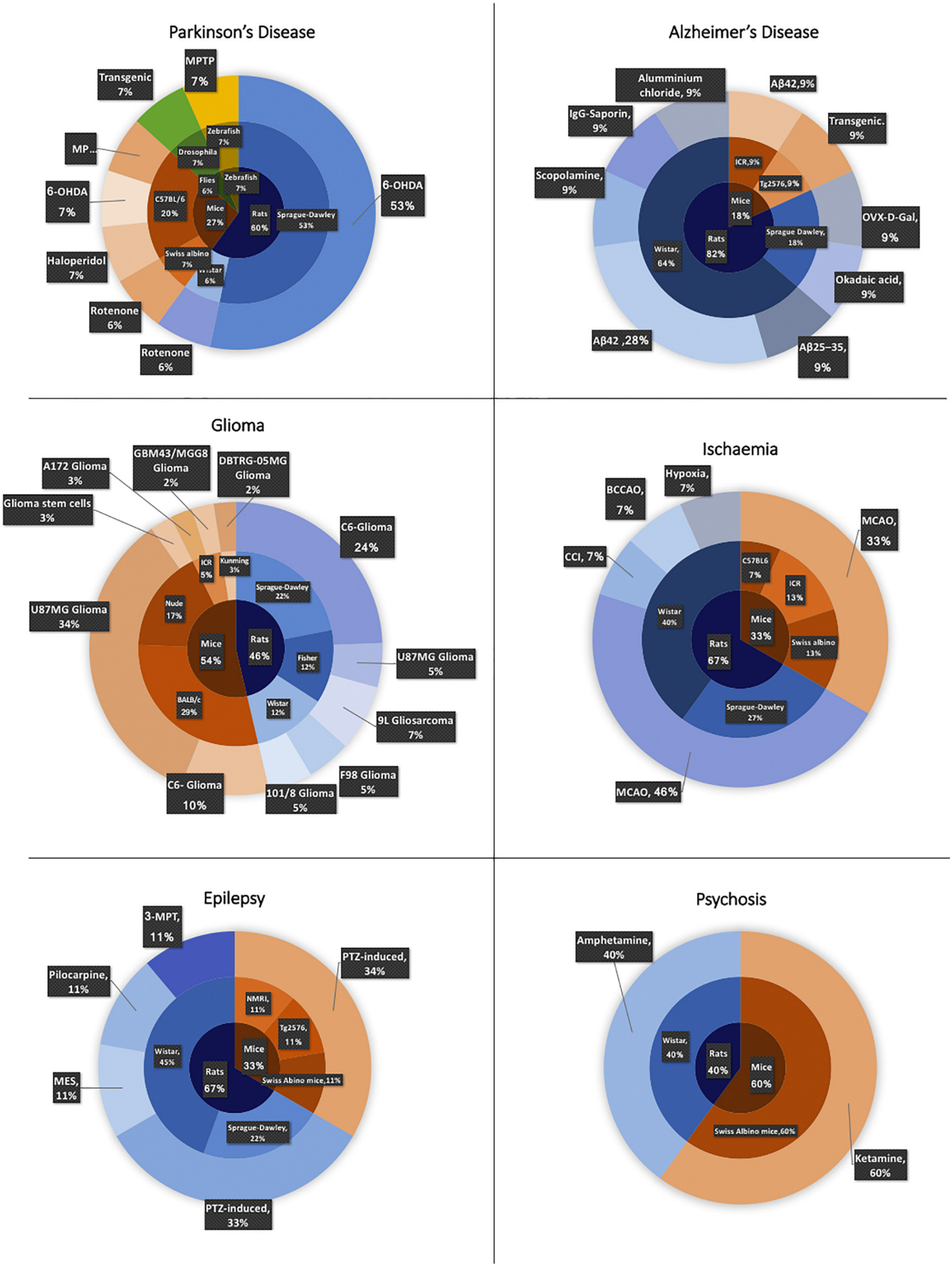

Fig. 3. Pre-clinical models for brain disorders: Categorical representation of pre-clinical models used for (a) PD, (b) Glioma, (c) AD, (d) Epilepsy, (e) Psychosis and (f) Ischemic stroke highlighting the predominant use of rodents because of their genetic and behavioural similarities to humans.

Table 2
Routes of administration used for BNDS and their advantages and disadvantages [207–210].

Route of administration			Advantages	Disadvantages
Local		Intracranial	• Overcomes the BBB • Delivers directly to the site of action	• Invasive • Deep anaesthesia required • Well-trained technical assistance required • Risk of infection • Very low volumes
Systemic	Enteral	Oral	• Easy/convenient • Safe • Ideal for 'slow –release' nanoparticles • Non-invasive • Pain-free • Absorption occurs along the GI tract	• Acidic nature of the GI tract might affect their absorption • First-pass effect by the liver reduces their efficacy • Slow onset of action • Not suitable for formulations unstable in water • Difficult to determine the exact intake • Depends on the animals rate of intake/food preferences • Gavage is needed to ensure precise and accurate dosing of animals • Cannot be used in unconscious animals
	Parenteral	Intrathecal	• Overcomes the BBB • Rapid effects on the brain since the nanoparticles can reach it quicker	• Invasive • Deep anaesthesia required • Well-trained technical assistance required • Intervertebral spaces and meningovertebral ligaments will determine the spread of the formulations being injected • Risk of infection
		Intranasal	• Non-invasive • Easy • Very rapid absorption • Dose required is reduced, which decreases the systemic toxicity • Avoids first-pass effect	• Local irritation, which can increase respiratory secretions • Suitable for administration of small volumes • Rate of injection should be slow • Not suitable for animal with rhinitis
		Intravenous	• Dose and rate of administration are reproducible • Suitable for highly concentrated solutions with low or high pH • Administered dose reaches the systemic circulation immediately (bioavailability of 100%) • First –pass effect and GI avoided	• Semi-invasive • Risk of infection • Less convenient and painful • Requires technical assistance • Unsuitable for oily formulations • Rate of injection should be slow • Possible systemic toxicity
		Intraperitoneal	• Useful to use in smaller animals where IV is challenging • Can be used to administered large volumes • Absorption is slower than in IV • Pharmacokinetics of formulations administered through IP are similar to the orally administered	• Semi-invasive • Risk of infection • Risk of performing subcutaneous injection instead of intraperitoneal • Formulation administered IP might undergo hepatic metabolism • Might be painful if substances injected are irritant
		Subcutaneous	• Minimally painful • Quicker onset than oral administration but slower than the other parental routes • Suitable for slow-release drugs: provides sustained effect • Can be used to deliver aqueous or oily fluids in large volumes	• Only suitable for non-irritant formulations and in small volumes • Requires well-trained personnel to avoid inadvertent intravenous injection

pathology analogous to that of human brain and have been used in the pre-clinical studies (9%) to evaluate the efficacy of BNDS in mitigating the disease pathology. Recently, models of Tau-pathology have also been used in order to test BNDS that focus on targeting the tau aggregation. These models were mainly induced using aluminium chloride [198] or okadaic acid ammonium salt [199] in rodents. In case of epilepsy (Fig. 3d), pentylenetetrazol (PTZ)-induced rodent models (rats:33%, mice:34%) were the predominant choice for pre-clinical analysis as this creates a chemically kindled chronic animal model of epilepsy that can be harnessed to evaluate the therapeutic efficacy of anti-epileptic BNDS.

Non-human primates (NHP) bridge the gap between rodents and humans due to the presence of the pre-frontal cortex regulating such complex brain functions as reasoning and judgement [200]. Also, the close resemblance of human and NHP brains in gene expression, functional and cognitive modalities make NHPs extremely valuable and reliable models for modelling brain disorders. NHPs like rhesus monkeys [201] and tamarins [202] have been used to model both Aβ plaques and Tau pathology in AD. Similarly, MPTP NHP models have been used to model the pathophysiology of PD and screen neuroprotective compounds for diseases associated with motor deficits, such as PD or ALS [203,204]. The rodent models fall short of developing a full spectrum of Parkinson's symptoms using MPTP and hence can not be used to elucidate the neural circuitry implicated in development of the disease in humans. To date, a limited number of studies have catered to the investigation of nano-particles for brain delivery in the NHP models. A study by Saito et al. (2005) investigates the direct visualization of the tissue distribution of drugs infused by convection enhanced delivery (CED) towards successful delivery of therapeutic agents to the brain tumor [205]. This study used gadolinium-loaded liposomes for real time imaging in primate brains. Krauze et al. (2008) also investigated the use of CED of the liposomes into the primate brain [206]. They investigated the parameters associated with CED and whether it has long term pathological consequences in primate brains. These studies draw their motivation from the fact that liposomes are nano-scale particles that allow for a wide range of therapeutic encapsulation and are well distributed in the brain.

Rodents represented the animal model of choice for studies in psychosis as presented in Fig. 3e. For psychosis, all the pre-clinical investigations in rats and mice were performed in the pharmacological models using amphetamine (40%) and ketamine (60%) induction respectively. Ketamine acts through the disruption of glutamate signaling to model psychosis-like effects. Amphetamine can induce a psychotic state in humans and therefore is applied to animals to mimic the biological environment present in a psychotic state.

In regards to ischemic stroke (Fig. 3f), middle cerebral artery occlusion (MCAO) is the most frequently used model for both rats and mice as it offers the benefit of inducing reproducible transient or permanent ischaemia in a relatively non-invasive manner.

All of these models were used to test different BNDS, which were administered through various routes. The main advantages and disadvantages of these routes are summarized in Table 2.

Before presenting the tools to assess the efficacy of these nano-systems for brain delivery, it is crucial to have an overview of the BNDS that were used so far and how their therapeutic effect was evaluated.

2.1. Polymeric-based systems

Majority of the nano-based delivery systems designed for brain targeting use synthetic polymers, which are promising vehicles for local and systemic delivery [211]. The use of polymers provides favorable characteristics such as high loading capacity and stability, control over drug release kinetics and ease of modification and functionalization. Besides, they have been used clinically in a variety of applications [212–214] for the delivery of nucleic acids, drugs, proteins and diagnostic agents [211,215–218]. The polymers used are in general biodegradable, biocompatible, display reduced toxicity, appropriate pharmacokinetics and can be either natural or synthetic [211].

2.1.1. Polymeric nanoparticles

The choice of polymer is decided by the therapeutic aim of the nano-system. Overall, the most frequently employed polymers in the CNS are polysaccharides, proteins, poly(amino acids), poly(ethylenimines), poly (alkyl cyanoacrylates), poly(methylidene malonates) and polyesters (e.g. polyglycolic acid (PGA), polylactic acid (PLA), polycaprolactone (PCL)) [211]. Furthermore, their delivery can be either systemic or local, with the former being highly dependent on their potential for receptor and adsorptive-mediated transcytosis through the BBB in order to be reach the site of action. This can be enhanced by adding cell penetrating peptides or targeting ligands to the surface or by manipulating the charge density [219].

The first polymer to be used for drug delivery in the CNS was poly (butylcyanoacrylate) (PBCA) [220]. It was introduced over 20 years ago and up to date continues to be used for BNDS. It has been employed to carry different drugs such as dalargin [220], doxorubicin [17–19], endomorphin-1 [78], gemcitabine [21], lorepamide [79], tacrine [38] and temozolomide [26], amongst others in pre-clinical studies (Table 1). Even though PBCA presents an interesting choice due to its high biodegradability (reduces its size up to 80% in 24 h post-injection [217]), minimal toxicity and high bio absorbability, it lacks the ability to cross BBB. Therefore, in all the above-mentioned studies the surface of the PBCA nanoparticles was modified with polysorbate 80 (PS 80). PS 80 (also known as Tween80®) acts as an emulsifier that enhances the CNS diffusion of intravenously administered polymeric nanoparticles. It interacts with the endothelial receptors on the BBB surface in a way similar to that of low density lipoproteins and might modulate efflux transporters and tight junctions, facilitating penetration of polymeric nanoparticles in the CNS [221,222]. It has been shown that without PS80 the amount of PBCA that crosses the BBB decreases [223], demonstrating its crucial role in the penetration of BBB by the PBCA nanoparticles.

Other polymers such as PGA, PLA and their copolymer poly(lactic-co-glycolic acid) (PLGA) have been used previously in other biomedical applications, which makes them promising for use in the CNS [224,225]. This is well represented by several studies where these were employed for brain drug delivery in pre-clinical models. For instance, PLA has been extensively utilized with different surface modifications, such as transferrin, polysorbate80 and maleimide PEG. The conjugation with these molecules allowed the delivery of carmustine (BiCNU®) [15], resveratrol [49] and sulpiride [82] respectively into the brain of Sprague-Dawley rats and C57BL/6 mice. PLA nanoparticles have also been functionalized with trans-activating transcriptor peptide (TAT) peptide on their surface, and this increased their uptake into the brain through the BBB via the bypass of efflux transporters [226].

PLGA, as previously described, is a copolymer of PLA and PGA which has been approved for clinical use in humans by the United States Food and Drug Administration (FDA). Since it has been extensively studied for the fabrication of devices for delivery of drugs, proteins and other molecules with low molecular weight and size [227], this makes it a very attractive option to explore in the case of CNS. It has been tested *in vivo* in guinea pigs, rats and mice for the delivery of loperamide [20,22,228], doxorubicin [20] and dexamethasone [229]. It was surface-modified with different molecules (e.g. polysorbate80, poloxamer188) to overcome the BBB. Poly(ethylenimines) (PEIs), on the other hand, because of their cationic properties and proton sponge ability of promoting quick osmotic swelling/lysis of the endosomes [230], are ideal for nucleic acid delivery and have been use in different disease models [231–233].

One noteworthy surface modification used in conjugation with diverse polymers is polyethylene glycol (PEG). This has been used in combination with PCL [16,24,234], chitosan [235], PLGA [236,237] and PLA [238]. PEGylated nanoparticles have improved circulation time, which

increases their bioavailability and accumulation in the brain, making their use an advantageous strategy. In addition to PEG, they also need further functionalisation to facilitate their diffusion through the BBB. It was shown in studies by Hu K. (2011) et al. and Bi C.(2016) et al., that Poly-ethylene glycol - poly (D,L-lactic-co-glycolic acid) (PEG-PLGA) nanoparticles functionalised with lactoferrin are able to improve the brain targeting in a PD model [50,54]. Also, Wen Z et al. (2011) showed that conjugation with odorranalectin is of interest in the delivery of urocortin peptide in another PD model [51].

Even though PEG had been considered inert in the initial studies [239], recent reports have highlighted the physiological presence of anti-PEG antibodies in the host (both pre-existing and therapy-induced), which impacts the use of PEGylated biomaterials [240]. For example, PEG-modified nanocarriers have been reported to induce the generation of anti-PEG antibodies in different animal models [241–244]. This comes associated with the decrease in their therapeutic efficacy and the increase in adverse effects such as the allergic reactions (reviewed in [245]). These hypersensitivity reactions in patients are mainly related to the activation of the complement by the PEG negative charge, which can be tailored by changing the chain length and concentration [246]. However, the understanding of the mechanisms related to the anti-PEG immune response is still at its infancy and, therefore, the systems developed are still in use, mainly due to their distinct advantages. However, this has brought complications to the use of materials functionalised with PEG and led to the design of alternative polymers and to the increased use of natural-based ones.

Natural polymers like chitosan and albumin were also tested in animal models over the past decade for drug delivery [247,248]. Chitosan was successfully used in the delivery of dopamine (DA) [52], rivastigmine [37], piperine [249] and tacrine [38,39] in Wistar rats, as well as being used for the delivery of doxycycline hydrochloride [61] and caspase-3 [235] inhibitor in Swiss albino mice. Albumin, on the other hand, was employed as the carrier of such glioma-targeting drugs as paclitaxel [250] and doxorubicin [251] in U87MG glioma carrying mice models. However, these cases also require functionalisation of the nanoparticles. Without this surface modification (either by the presence of surfactants or ligands to target specific receptors or by the surface display of positive charge), the polymeric nanoparticles have a reduced ability to overcome the BBB once they are systemically injected [252].

Alternatively, if the nanoparticles are delivered locally, the surface modification is less significant. The first intracranial administration of polymeric nano-systems in humans was over 20 years ago, in the case of brain tumors [253], in which 86% of the patients lived more than one year after their diagnosis. Furthermore, 38% of the total number of patients lived more than one year after the intracerebral injection of the nanoparticles loaded with BiCNU®. Even though this route of administration overcomes the hurdle of crossing the BBB, the efficacy of the drug-loaded nanoparticles is limited by the poor diffusion beyond the tumor borders, as was seen in previous studies [254].

Nonetheless, by using convection-enhanced delivery (CED) of these nanoparticles, the influence of an external pressure gradient that is infused uninterruptedly into the brain allows for an enhanced distribution of therapeutics over large volumes, which is of clinical interest when they are delivered intracranially [255–257]. CED has already been used in clinical trials using free drugs for the treatment of glioblastoma [258]. The main advantages of this strategy are its low systemic toxicity and reduced side effects off target. Also, it allows the delivery of higher quantities of therapeutic agents than that of systemic administration. However, its major drawbacks are the limitations in catheter technology and imaging [259], and the need for an intracranial surgery, which is not feasible in the case of some patients.

Even though polymeric nanoparticles have shown promising results in pre-clinical models of PD, AD, brain tumors and cerebral ischemia, there is only one polymer being used in clinical trials on the CNS (poly (isohexyl cyanoacrylate)) due to its reduced degradation rate, which also decreases its toxicity (Trials, 2012) [217,260]. All the others have disadvantages such as inherent toxicity, low encapsulation efficiency of hydrophilic therapeutics, difficulties in scaling up and the use of organic solvents during fabrication, rendering them unsuitable for clinical translation [211].

2.1.2. Dendrimers

Besides nanoparticles, there are other categories of polymeric systems (Fig. 2). Dendrimers are a very-well known class of these systems which have been increasingly used in the CNS over the last ten years [261]. Dendrimers are tree-like polymers which branch out from a core molecule and subdivide into hierarchical branching units composed of alternating layers of two monomers. The main advantages of this system are related to its high density, well defined surface functionalities, monodispersity (which provides reproducible pharmacokinetics, as opposed to the polydispersity of traditional polymers) and its controllable size, [262]. The most commonly used dendrimers are made of polyamidoamine (PAMAM) since it has a low cost of synthesis and is highly compatible with biological tissues due to the combination of the amide bonds in the interior and amines on the surface [262]. Regarding their use in the brain, PAMAM dendrimers have been mainly used to deliver DNA in pre-clinical models. For example, after being functionalised on the surface with angiopep [92], TAT peptide [263] or lactoferrin [95] (all moieties facilitating the targeting of the BBB), PAMAM dendrimers showed an improved transfection efficacy. Also dendrigraft poly-L-lisine (DGL) was used as a delivery system, mainly conjugated with either leptin30 [91] or angiopep [86] and tested in pre-clinical models of PD [86].

2.1.3. Micelles

Another class of polymeric systems is micelles. These are supramolecular assemblies of surfactant molecules dispersed in a colloidal liquid. Over the last decade, many different polymers have been used to fabricate micelles mainly to apply *in situ* and treatment of gliomas [98,101,103,104,106,264–267]. The main cargo tested were anti-tumor drugs, such as paclitaxel [105,106,265], myrcetin [266] and docetaxel [103,268]. The synthetic polymers used to fabricate the micelles are largely the same as those that are present in nanoparticles (e.g. Polypropylen glycol (PPG), PCL, PEG, PLA), but in this case they are usually presented as co-polymers, which allows for an easier formation and dispersion into the colloidal solution. The amphiphilic copolymers are frequently known by their trade name: Pluronic®. For example, Pluronic L121 or Pluronic P123 correspond to PEG-PPG-PEG copolymers, whereas Pluronic F127 or F68 are the equivalent to poloxamer 407 and 188, respectively, both composed of Polyethylene oxide (PEO)-PPG-PEO. Micelle size varies widely from around 13 nm [112] to 162 nm [105], making them suitable for different routes of administration such as intravenous [98,101,105,118,265,267], intranasal [114,269,270], oral [266,271] and intracranial delivery [102,104,264]. In addition to rodents, micelles have also been tested in zebrafish, in a MPTP model of PD where the therapeutic molecule was baicalein [109]. The neuroprotective effect of baicalein was shown by decreasing mitochondrial dysfunction, translating into a good performance of pluronic micelles as drug nanocarriers.

Overall the polymeric systems present numerous advantages as drug carriers into the CNS, including high versatility in synthesis, high loading and encapsulation capacity and long term stability [272]. However, due to their inherent toxicity and the use of organic solvents during their fabrication, further research is needed to improve them and the controlled and targeted delivery into the brain.

2.2. Lipid-based systems

Lipidic nano-systems are composed of molecules of biological origin that are hydrophobic and amphiphilic, which allows them to form different structures (e.g. vesicles, membranes) in an aqueous condition.

These systems can be categorized according to their physicochemical properties and method of fabrication into different groups [273]. However in this section we will only focus on liposomes, lipoplexes, solid lipid nanoparticles (SLNs), nanostructured lipid carriers (NLCs) and exosomes (Fig. 2).

2.2.1. Liposomes

Liposomes are spherical structures made of one or more vesicular bilayers (composed commonly of sphingomyelin, phosphatidylcholine and phospholipids) and encompass the first generation of lipid nanocarriers for drug delivery [274]. They have many advantages such as low toxicity, high loading efficiency, controlled and sustained release and their properties (size, charge and composition) can be easily tailored depending on the cargo. However, they have lower stability than other lipid-based systems, which makes their scale-up and industrial production more arduous [272]. Based on the number of layers (lamellae) and size, they can be classified as small unilamellar vesicles (SUV) with one bilayer and are smaller than 100 nm, large unilamellar vesicles (LUV) with a size above 100 nm and one bilayer, and multilamellar vesicles (MUV), which have multiple lamellae [12]. The use of cholesterol in liposome formulations is of interest since it increases the stability of the liposome and decreases the permeability of the membrane. In liposomes used for brain drug-delivery, cholesterol has been used in combination with TAT peptide to target and overcome the BBB in mice [123,141], to address glioma by carrying doxorubicin [123]. Another example are the pegylated liposomes, where a chain of PEG is added to the surface of the vesicles. These were shown to be effective in the treatment of brain tumor [121] and PD [135]. In some cases, there is the coupling of anti-transferrin receptor antibody (OX-26) with the PEG chains, which targets the transferrin receptor, facilitating their entrance into the brain. These were used to carry different cargo such as methotrexate (MTX) [275], nerve growth factor (NGF) [276,277] or tyrosine hydroxylase (TH) plasmid [135]. The coupling of antibodies to the surface of liposomes (i.e. immunoliposomes) is crucial for a specific targeting since they are highly selective to their antigens [278].

2.2.2. Lipoplexes

Lipoplexes are the designation given to the cationic lipids bound to nucleic acids, which are naturally formed by the simple mixing of both due to their electrostatic interactions. The positive charge of the liposomes in this case facilitates the adsorptive-mediated endocytosis and internalization in endosomes. When the pH decreases inside the endosomes, the 1,2-dioleoyl-sn-glycero-3-phosphoethanolamine (DOPE) fuses and disrupts the endosomal membrane, leading to the release of its contents to the cytoplasm [12,279]. Within the CNS, these have been mainly used in gene silencing [280–283]. Since they are produced from liposomes, they borrow the same advantages as the above-mentioned. Their main disadvantage is that they have high affinity towards the bound nucleic acid, this reduces the transfection efficacy once they are internalized by the cells.

2.2.3. SLNs/NLCs

Solid lipid nanoparticles (SLNs) and nanostructured lipid carriers (NLCs) blend all the features already mentioned for liposomes; however, they do not share the disadvantages, since they present high stability, are able to be produced on a large scale at low cost and can be very small [272] (similar to polymeric nanoparticles, with a diameter as low as 27 nm [161] and up to 277 nm [284]). This facilitates their flow in the blood stream without being uptaken by immune cells, enhancing their stealth profile. Their natural composition allows the release of the cargo through their degradation without raising any toxicity concerns. The combination of the main advantages of polymeric nano-systems and liposomes makes them the best candidates for targeting the CNS. Their main limitation is the low encapsulation efficiency (mainly in the SLNs) and release of drugs during storage, which is likely to be the reason they are not widely exploited within the biomedical industry [12,272].

SLNs were introduced over 25 years ago as an attempt to overcome the limitation of all other nano-systems developed so far [285]. These are fabricated using lipids which share similar features such as low melting point and solid state at body temperature (e.g. stearic acid, stearyl alcohol, glycerol monostearate, Compritol® 888 ATO, cetyl palmitate), and distinct surfactants (such as poloxamer 188, PS 80 and dimethyl dioctadecyl ammonium bromide (DDAB)) [272]. One of their main advantages is the possibility to deliver both hydrophilic and lipophilic drugs and therapeutic molecules. Within the CNS, SLNs have been used in pre-clinical models of glioma to deliver edelfosine [146], camptothecin [148,149], resveratrol [151] and vincristine [156], of ischemic stroke to deliver curcumin [286], simvastatin [175] and baicalin [161] and of AD to deliver quercetin [168], piperine [284], sesamol [171], galantamine [172] and chrysin [173], mainly through intravenous, oral and intraperitoneal routes of administration.

NLCs are essentially the next generation of SLN, modified by the incorporation of a liquid lipid into the solid structure and seen as an attempt to reduce and overcome the limitations of the SLNs, allowing for a higher payload and reduction in the release of cargo during storage [287]. This liquid lipid can be, for instance, oleic acid, olive oil, sesame oil, peanut oil, soybean oil, soy lectin or corn oil [272], and the ratio between the liquid lipid and the solid lipid can go from 1:4 to 4:1. NLCs are divided into three types depending on their structure: imperfect type (imperfectly structured solid matrix with various lipid structures), amorphous type (structure less solid and formation of amorphous matrix with the mixture of certain lipids to prevent the crystal formation) and multiple type [287]. Regarding their use as BNDS, they have also been employed for the release of curcumin [152,288] and temozolomide [154,155] in glioma models, and topinirole hydrochloride and bromocriptine in PD rat models [164,166]. Their bio-distribution was also investigated *in vivo* in rats and rabbits for the delivery of vinpocetine [180,181] and balcalin [182], both drugs suitable for the treatment of ischemic strokes. However, the therapeutic effect of these has not been assessed in diseased models yet. The higher stability and drug loading capacity of these allowed the administration through all the possible routes (oral, intranasal, intravenous, subcutaneous, intraperitoneal) without having to resort to intracranial surgery. This is a major improvement compared to the previous carriers.

2.2.4. Exosomes

Other types of natural lipid-based system are extracellular vesicles (or exosomes) which can be secreted from different types of cells and carry proteins, drugs or even nucleic acids (more specifically RNA) [289]. They comprise the natural ability to cross the BBB, and can encapsulate both hydrophobic and hydrophilic cargo and they remain in the host's circulation for longer periods of time, which increases their interest as drug-delivery vehicles. Addtionally, they have the ability to overcome the cell membranes and deliver their payload into different organelles inside the cell, increasing their attractiveness for this purpose. Exosomes were first studied as delivery vehicles in 2007, when they were shown to mediate the transfer of mRNA and microRNAs between cells [290]. Since then they have been used in different CNS disease models such as brain tumor [291–293], ischemia [294], TBI[295] or PD [296]. Even though exosomes can potentially avoid the endosomal pathway and, therefore, lysosomal degradation, their biological fate is still under investigation. The main disadvantages would be the lack of an optimal purification technique for their isolation, which makes it more difficult to produce in larger scales [297]. Moreover, the heterogeneous components of the exosomes may also show immunogenicity effects based on their cells of origin, so this needs to be further studied.

To sum up the lipid-based nano systems are designated as the next generation of drug delivery systems since they combine the advantages of the polymeric systems without their drawbacks. SLNs and NLCs in particular are of interest, since they are able to cross the BBB without

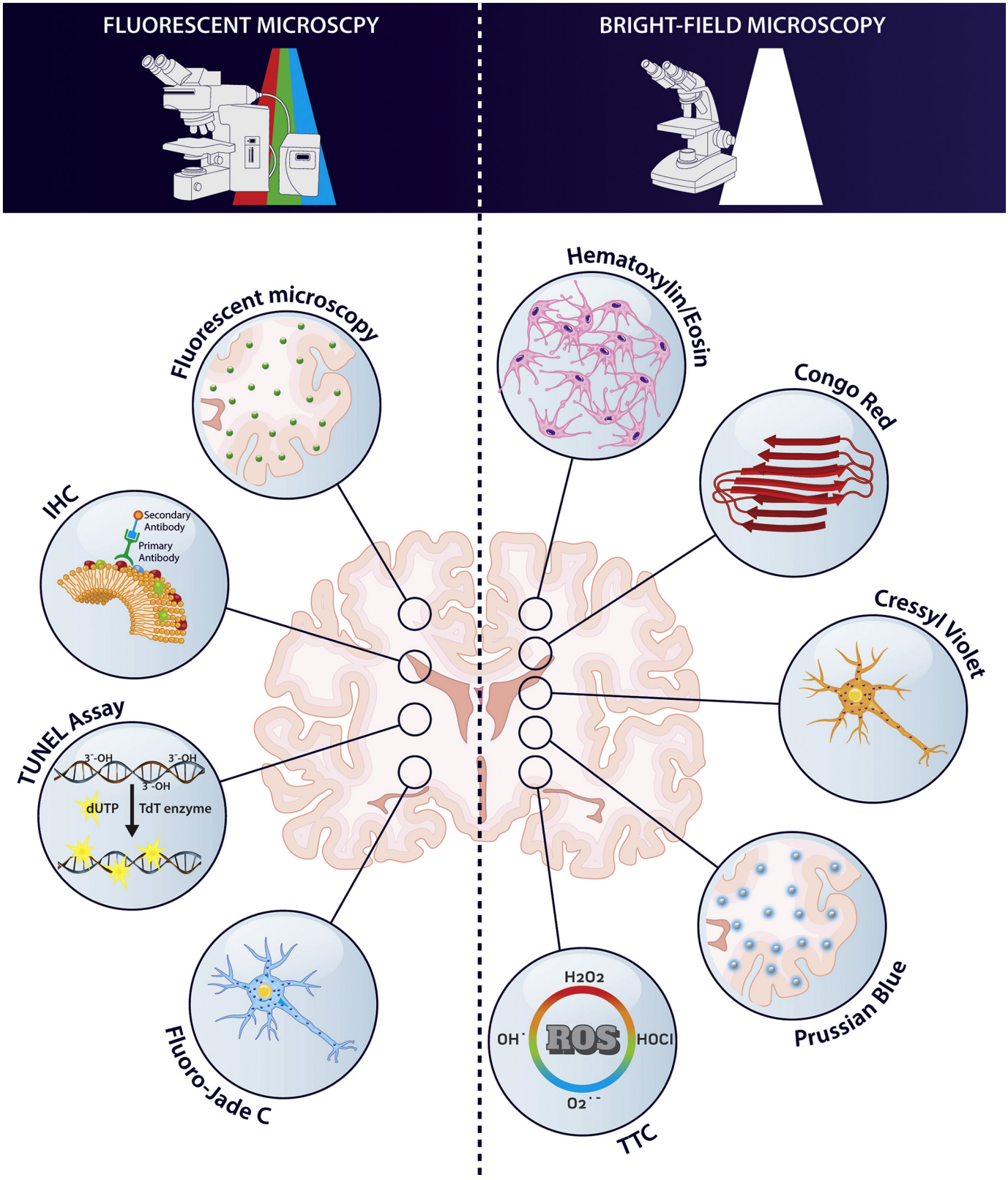

Fig. 4. Categorical distribution of histological techniques for efficacy evaluation: Representation of different assessment staining visualized with fluorescent microscopy or bright-field microscopy.

surface modification, making them excellent candidates for the treatment of brain disorders.

2.3. Inorganic systems

Inorganic nano-systems usually comprise nanoparticles made of gold, silica, titanium oxide, iron oxide and quantum dots (Fig. 2). They

are small in size and usually multifunctional andtherefore, used in theranostics, combining diagnostic (mainly imaging related, and are extensively used in Positron Emision Tomography (PET) scan, Magnetic Resonance Imaging (MRI), X-ray imaging, Computed Tomography (CT) imaging and fluorescence imaging)) and therapeutic tools in a single system [298]. This is highly desirable especially in the case of tumors, where due to the enhanced permeability and retention (EPR) effect, the nano-systems are easily able to reach the tumor site and can co-deliver imaging and therapeutic agents, providing combined integration of diagnostics, treatment and follow-up [299]. The chief drawbacks of these systems are the low biocompatibility and rapid clearance by the reticuloendothelial system if their surface is not modified [272].

2.3.1. Gold nanoparticles

Gold nanoparticles are of significance for intracellular delivery since they can vary in size from 0.8 to 200 nm and can be functionalised on the surface. Besides these traditional features, they also present attractive intrinsic characteristics such as photothermal and light-scattering properties, which allow their trajectories to be tracked in the cells [300,301]. Their optical and thermal properties can be finely tuned depending on their fabrication method. Also, due to their magnetic properties they can be driven through with external electromagnetic fields. For example, Yoo J. et al. (2017) showed that gold nanoparticles can induce a direct lineage reprogramming into dopaminergic neurons in mice [185], which is a promising tool in the treatment of PD. In a pre-clinical AD model gold nanoparticles were used to selectively target toxic Aβ aggregates [302,303], by their surface modification with a custom-made peptide. Regarding gliomas, gold nanoparticles functionalised with PEG have been tested in combination with radiation therapy in a mouse model. It was seen that the use of the nanoparticles significantly increased the DNA and brain blood vessel damages produced by the radiation in tumor [304].

2.3.2. Magnetic nanoparticles

Nevertheless, the main type of inorganic nanoparticles used for tumor treatment are the magnetic ones. These are usually comprise ferromagnetic iron oxide (Fe_3O_4) and can be administered systemically and directed to the site of action through the application of an external magnetic field [305]. In the case of brain tumors, however, this is hindered by the presence of the BBB, which makes intracranial delivery the most appropriate one to reduce the systemic toxicity and increase the therapeutic concentration at the site of action. They can act as imaging agents and upon application of an alternating magnetic field, work as an hyperthermic treatment into the tumor, which is already clinical use(NanoTherm®, Germany). Superparamagnetic iron oxide nanoparticles (SPIONs) are a class of magnetic nanoparticles which have a core of Fe_3O_4 and possess properties such as high field irreversibility and high saturation field, which makes them no longer magnetic-responsive after the external magnetic field is removed [306]. These SPIONS were successfully tested in Sprague-Dawley rats [190] (intracranial administration) and BALB/c mice [191] (intraperitoneal injection), and showed reduced toxicity and high tolerance within the body. Titanium oxide nanoparticles were also tested in the brain of a pre-clinical model of PD, conjugated with DA, which led to a continuous release of the neurotransmitter and reversed the overall motor deficits observed in the lesioned rats [183].

2.3.3. Quantum dots

Quantum dots (QD) are fluorescent semiconductor crystals that present distinct conductive properties, usually made of cadmium sulfide (CdS), cadmium selenide (CdSe), lead selenide (PbSe) and lead sulfide (PbS2). Their physicochemical properties such as versatile surface chemistry, narrow emission profile, high photo stability and brightness, large strokes shift and electron-dense inorganic core make them attractive for use as drug carriers *in vivo* [307]. In the brain, these have been tested in a glioma-bearing mouse model, where they were combined with aptamer32, targeting them to the tumor. Also, there were no tissue lesioning in systemic organs, indicating its reduced toxicity [188]. QD of CdSe have also been used for imaging purposes in Sprague-Dawley rats to study the width of brain extracellular space *in vivo* [308].

In conclusion, inorganic nano- systems offer promising therapies. However, the investigation of these systems for drug delivery in the CNS is still in its very early stages. Therefore, more research is encouraged in this field, given all the promising features it can provide. A summarising representation of the diversity of nano-delivery systems targeting brain is presented in Fig. 2.

3. Classification of evaluation modalities

3.1. Histological assessment

3.1.1. Bright-field microscopy

Histology (from the greek "histos-" (tissue) + "-logos" (study)) is a tool in medicine and biology that allows the microscopic study of the tissue structure from different organs, which is essential to examine the extent and magnitude of a diseased organ and to evaluate the effectiveness of a treatment [309]. Since biological tissues have very low inherent contrast, to better assess and analyse the specimens on the light or electron microscope, histochemical analysis is performed (Fig. 4). The use of histochemistry helps not only to increase the contrast of the samples, but also to highlight specific constituents of the tissue due to an interaction between the dyes and the organelles/chemical environment within the cells [310]

Hematoxylin/Eosin (HE): The gold-standard of histology and most widely used staining. In HE firstly a basic dye (hematoxylin), stains the cell nuclei in dark blue by binding the hemalum (aluminum ions combined with hematein, which is an oxidation product of hematoxylin) to the DNA.This is followed by the counterstaining with an acidic dye (eosin) that stains the cytoplasm (pink). This allows for a first assessment of the morphology of the cells and overall architecture of the tissue, providing a valuable, low cost and easily used tool for the study of the histopathological state of the organs. This is the reason that this technique is almost always used to evaluate the effect of a treatment, mainly one where a biomaterial is employed and mostly to investigate its toxicity and repercussions in regards to tissues integrity and cytoarchitecture.

Regarding the brain and the use of nano-systems targeting the CNS in pre-clinical models, HE was mostly used to 1) confirm the successful development of the disease model; 2) examine the therapeutic effect of the nano-materials in the brain and 3) evaluate the toxicity of the nano-systems in the brain and systemically.

This technique was particularly relevant in the case of glioma-bearing animal models. In the majority of these studies, HE staining allowed a visualization of the formation of tumor approximately two weeks post-glioma cells inoculation (either with C6 cells [21,122,125,189] or U87MG cells [108,147,153,189]), where the nuclear density was significantly higher and cells were less organized than those in the healthy tissue. The onset of this disorder is easy to confirm by this staining since it is characterized by the quick and uncontrolled proliferation of cells.

Besides successfully visualizing the tumor, HE also enables examination of the effect of the nano-systems in the gliomas. The administration of doxorubicin in liposomes with different surface coatings caused a decrease in tumor lesioned cells 48 h post-administration using PEGlylated liposomes [121], higher cell viability and hypocellular tumor tissues [125]. When this drug was encapsulated in polymeric nanoparticles, 18 days post-injection the tumor size decreased significantly [17] and when it was encapsulated in gold nanoparticles, the density of glioma cells in the brain was much lower than in the controls [189]. Even when loaded with other drugs (such as gemcitabine [21], paclitaxel [237,311], myrcetin

[266], cucumin [128,150]) or silencing genes [147], the overall effect after administration of the nano-systems was very similar, all showing a reduction in the cellular density on the tumor site where the nanoparticles were being applied and general disruption of glioma cytoarchitecture [128,266,311].

HE was also used to assess the systemic toxicity of the nano- systems, for the systems administered orally or intravenously. In the case of inorganic nano-systems, gold nanoparticles were functionalized with angiopep-2 while carrying doxorubicin, which made them target the brain. Therefore, no toxicity was seen in the heart [189]. When quantum-dots conjugated with aptamer-32 were used, there were no tissue lesions, necrosis or inflammation in any of the groups analysed in any other organs [188]. When using PCL-based micelles,no lesions were seen in the cardiac tissue [105]. However, while using Doxorubicin-Paclitaxel-based micelles, only the ones functionalized with RGD did not elicit any tissue degeneration and necrosis in the heart, or in the other organs [265]. Chitosan-based micelles were also innocuous to the systemic organs, while exerting their function over the brain and enhancing the anti-tumor activity of myrcetin [266].

Damage at the site of injection can also be assessed by HE when the particles are injected intracranially. For instance, the administration of poly(aspartate) micelles and SN-38 loaded micelles did not exhibit any tissue damage at the site of implantation [102,264].

HE was also used with the same purpose of evaluating the histopathological effect of the nano systems in the brain of other pre-clinical disease models, namely in PD [45,165,186,312], cerebral ischemia [63,69,138,313] and psychotic disorders [314]. In the case of PD, the possible toxic effects were also studied in other organs, using different types of nano- carriers such as iron oxide nanoparticles carrying shRNA administered intraperitoneally [186], gelatin-based nanostructured particles administered intranasally carrying fibroblast growth factor (bFGF) [165] and polymeric nanoparticles for DA delivery [45], showing no effect on the peripheral organs, on the nasal mucosa and in the heart more specifically. In cerebral ischemia models (all induced by MCAO in Wistar rats, Sprague-Dawley rats and Swiss mice), HE staining showed neuronal loss, pycnotic nuclei and numerous vacuolated spaces in the injured groups within the infarcted area in the hippocampus [63,69,138,235,313]. In all the cases referred to there is also a reversal in action by the treatment with the polymeric nano-systems, carrying curcumin [63], rutin [313], caspase-3 inhibitor [235], acetylpuerarin [69] and bFGF [138], all systemically administered, and leading to a decrease in the number of necrotic and abnormal neurons and in the infarcted area. In one model of psychosis (ketamine-induced psychotic Swiss mice), self nanoemulsifying drug delivery systems were employed to deliver olanzapine and no damage was observed in the brain, liver or stomach of the treated groups. In this case, there were no other histological studies to assess the effect of the lipid particles.

In the AD pre-clinical model used to test the effectiveness of polymeric and lipidic nanoparticles, in some cases HE was used in combination with other types of stainings such as Cresyl Violet staining [32,173] or Congo Red [33]. The combination with other histochemical techniques allows for the deeper study of the structures and types of cells present in a certain sample, increasing their significance and providing more information than from morphology and cytoarchitecture.

Cresyl violet: This is used to stain the Nissl substance (mainly composed of RNA), which is found specifically in the neuronal cytoplasm (rough endoplasmic reticulum) in fixed tissues, staining it in purple-blue [315]. This was invented in 1894 by Nissl and is extensively used by neuroanatomists. In Aβ-induced AD models, Nissl was helpful in the evaluation of neurodegeneration triggered by the aggregation of Aβ peptides and the effect of the nano systems in study. This is relevant since Aβ plays a central role in the onset of this neuropathology. It showed that polymeric PLGA functionalized nanoparticles carrying H102 β-sheet breaker peptide had an enhanced action in effectively protecting the neurons, with significantly reduced pathological changes and less cell loss in the hippocampus [32]. The decrease in neurodegeneration was also seen upon administration of liposomes carrying curcumin and NGF [134]. When chrysin was incorporated in SLNs and orally administered it also provided neuroprotection in a dose-dependent manner, reducing the loss of pyramidal cells in the hippocampus [173]. In all the above-mentioned studies the Cresyl violet staining also helped confirm the establishment of the models, highlighting the neuronal loss, shrinkage and nuclear condensation in the lesioned animals.

Congo red: Thisis a dye particularly used in AD studies since it intercalates in amyloid fibers, a hallmark of this pathogenesis, staining them in red [316]. It has been used to assess the neuroprotective effect and safety of PLGA-based nanoparticles loaded with bFGF in the treatment of AD, where the treatment allowed the removal of all detectable Aβ plaques from the diseased animals, showing very little differences from sham [33]. In another study, SLN loaded with piperine led to an advanced decrease in plaques and tangles in the hippocampus of ibotenic acid-lesioned Albino Wistar rats [284]. The high specificity of Congo Red to bind to the amyloid plaques makes it a very useful tool to exploit in the context of AD.

Prussian blue (or Perls Prussian Blue): This is another histopathological staining that has been used in the detection of iron in the tissues since 1867 [317]. It has been used in the brain for the assessment of intracranial hemorrhage, since the breakdown of red blood cells and the onset of the hemorrhage are closely related to the catabolism of heme and processing of iron [318,319]. Regarding its application in the assessment of the efficacy of the BNDS brain disorders, this is an attractive technique used to track and study the bio-distribution of iron oxide or other magnetic nanoparticles. It has already been employed to detect Fe_3O_4 nanoparticles conjugated with alpha-synuclein RNAi plasmid in a model of PD, showing a minimal distribution in all organs except in the spleen [186]. These particles were mainly located in the brain. It was also adopted to assess the presence of magnetic micelles (ferric iron) in the different brain regions. This study showed that more micelles were concentrated in the cortex of the rats that were under a magnetic field and they remained in the cortex and hippocampus even 48 h post-traumatic brain injury followed by the administration of the micelles [269].

Tetrazolium chloride (TTC) is another commonly used stain for the detection of infarcted tissue in stroke. This is a redox indicator that is employed to differentiate between metabolically inactive and active tissues, since TTC is enzymatically reduced to red 1,3,5-triphenylformazan when in contact with hydrogen in living tissues staining these with this color [320]. For this reason it is widely used to identify post-mortem myocardial infarctions [321]. With the same purpose, this became relevant in the recognition and measurement of infarcted brain tissue and was used in pre-clinical models of cerebral ischemia to confirm the establishment of the model and to assess the effect of the nano systems [320]. In all of the MCAO rat models studied, the infarcted area was significantly visible than that in the control and all showed reduction when administered with the polymeric nanoparticles loaded with rutin [313], superoxide dismutase [70] or heme oxygenase-1 gene [90]. In the case of the administration with superoxide-dismutase-loaded PLGA nanocarriers, these endorsed the survival of 75% of the animals 48 h-post injection of the nano carriers, propitiating their continued recovering with time. The main advantage of this method is that it is performed in fresh tissue slices, and is therefore, both simple and fast.

Overall, all the histochemical techniques previously mentioned are convenient for vosualizing the tissue with a bright field microscope, providing a general overview of the tissue as well as their cytostructure and onset/recovery of pathological conditions in the brain.

3.1.2. Fluorescence microscopy

In addition to the histological techniques already described, there is also a panoply of approaches that can be exploited to overcome the lack of information provided by the histochemical staining.

Fluorescence microscopy: By the simple use of fluorescence microscopy it is possible to visualize the nano systems and detect their bio-distribution within the brain tissue. Through the conjugation or loading of the nanoparticles with fluorescent dyes (such as fluorescein isothiocyanate(FITC)), rhodamine-123 or coumarin-6), the nanoparticles can be observed on brain sections in post-mortem analysis. Mainly in glioma models, this has been applied as standard to ensure that the nano-carriers are accumulating within the tumor site. This confirmed that accumulation of PLGA particles coated with cyclic hexapeptide are significantly found more in the brain than the non-coated ones, enhancing the action of the curcumin in that region [29]. Polysterene nanoparticles coated with carboxyl coating remained localized in the site of injection and did not penetrate the brain parenchyma or reach the tumor edge, whereas the particles coated with PEG were able to distribute uniformly in the tumor parenchyma over time, efficaciously delivering paclitaxel [237]. The active metabolite of camptothecin (NK102) was encapsulated in micelles which also enhanced their diffusion in the brain. This additionally reduced their toxicity when compared to the administration of the free NK102 [102]. Other type of micelles were also employed (PCL-based) in glioma pre-clinical models, carrying doxorubicin and paclitaxel, and they were shown to be distributed mostly in the tumor region [105]. In the case of liposomes, when DDAB particles were administered without vector-functionalisation they did not accumulate at the tumor site, whereas when they were coated with anti-VEGF they were mainly concentrated in the center and periphery of the tumor, having an heterogeneous distribution in the brain of C6-glioma bearing Wistar rats [127]. A similar coating influence was seen in the use of SLN coated with polysorbate60 and polysorbate80 to deliver camptothecin. In this case, the particles were not seen in the brain until 120 min post-injection, when the former were observed to be more diffused in the brain than the latter [149].

This technique was also used in the assessment of therapies for pre-clinical models of neurodegenerative disorders such as PD [45,50] and AD [170]. Pahuja R. et al. (2015) went further on to use fluorescence microscopy to visualize polymeric nanoparticles in the peripheral organs besides the brain, observing that at 4 h post-injection, they were detected in the spleen, liver and kidneys of the 6-OHDA lesioned Wistar rats [45]. With the use of PLGA-based nanoparticles covered with lactoferrin, these were detected in the cortex, striatum and substantia nigra 4 h post-injection, which was not seen in the nanoparticles without lactoferrin [50], proving that these particles can reach the site of action in a short period of time. A similar trend was seen with NLC covered with lactoferrin for the delivery of curcumin [170], but in this case the particles reached the brain 1 h post-injection, and so are a more attractive device to use in this case.

All the aforementioned studies contributed to the validation of the fact that surface modification enhanced the distribution of the particles within the region of interest in the brain, becoming crucial to their therapeutic effect. Furthermore, the use of fluorescent probes and a fluorescent microscope to visualize them are valuable tools that allow precise localization of these carriers in the brain. Fluorescence microscopy also allows the application of an array of other techniques, mainly the ones where specific molecules or structures are labeled.

TUNEL assay: The Terminal deoxynucleotidyl transferase dUTP Nick-End Labeling assay (commonly denominated TUNEL assay) has been intended to detect apoptotic cells with high DNA degradation, since the terminal deoxynucleotidyl transferase binds to the blunt ends of the DNA breaks, thereby labeling them [322].

This technique was used to assess of the effect of polymeric micelles on glioma [108,264,266], showing that Am80 encapsulated in PEG-Poly (aspartate) exerted therapeutic effect in six days, increasing significantly the number of TUNEL-positive cells within the tumor site over that in the controls [264]. A rise in these cells was also seen four weeks after the administration of micellar myrcetin [266]. The difference in the time of action can be related with the route of administration (intracerebral for the former and oral for the latter), but also to the fact that the apoptotic cells in the last study were only assessed on the last time point, which does not allow a complete insight as to when the effective action of the loaded-micelles started. The same trend of abundant TUNEL-positive tumortumor cells was seen when liposomes carrying doxorubicin [125] and paclitaxel [323] were used and their effects were enhanced by the use of focused ultrasound. In the case of the doxorubicin-carrying liposomes, the decrease in apoptotic cells was seen as early as 48 h post-injection [323], while with the paclitaxel ones the effect was not seen until 28 days post-injection [125]. In this case, this analysis was the only one performed since this was the sacrificing time point of the study. This highlights the importance of having further methods to assess the effect of the nano-therapeutics on a timeline basis.

TUNEL assay was also employed to evaluate the apoptosis rate in the brain of MCAO lesioned rats and the effect of drug-loaded polymeric nanoparticles [69,70]. In both cases, the assay confirmed the establishment of the model, showing numerous TUNEL-positive cells 6 h [70] and 24 h [69] post-reperfusion. Also, the treated groups displayed significantly fewer apoptotic cells.

Fluoro-Jade C: This is a fluorescent probe which is an alternative to traditional Cresyl violet to label degenerating neurons, and was used to corroborate the presence of a brain injury, exhibiting the majority of Fluoro-jade-positive cells in the cortex, hippocampus and thalamus [111] of lateral fluid percussion injured rats. However, the exact mechanism by which it labels these neurons is still unknown, which is a major drawback for this method.

2',7'-dichlorofluorescein diacetate (DCFDA): DCFDA is a dye which is hydrolysed intracellularly and later oxidized by reactive oxygen species (ROS) into 2',7'-dichlorofluorescein, allowing their detection [324]. This dye was employed to evaluate the effect of superoxide-dismutase loaded PLGA nanoparticles in a MCAO cerebral ischemia model [70]. This study showed that the group administered with the loaded nanoparticles demonstrated a significant decrease in the ROS activity when compared to the control [70], highlighting the importance of this method when an ROS scavenging agent is being tested.

All the aforementioned probes react with chemical moieties/molecules within the cellular environment, providing information about the conditions of that specific tissue, but being unable to allow a deeper analysis of the cellular identity within that region.

Immunohistochemistry (IHC): This is the current gold-standard for the histological recognition of different cell types. It is based on using antibodies that bind specifically to antigens, which in their turn are distinctive identifiers for a certain cell type or a particular signaling pathway. IHC was first implemented in 1941 [325] and it is helpful for several reasons. Firstly, it allows the diagnosis of abnormal cells in a disease condition; secondly, it favors the labeling of specific molecular markers that are characteristic of exclusive cellular events. Thirdly, it facilitates the study of the spatial and temporal distribution of certain proteins within a tissue, thereby providing a more accurate and detailed cellular map of the tissue. Frequently, the antibodies used are tagged with fluorophores which enables easier imaging using the fluorescent microscope and propitiating the labeling of multiple molecules at the same time with different colors (e.g. double and triple stainings). However, secondary antibodies can also be biotinylated instead of conjugating to fluorescent probes. In this case, the biotin will form a complex with a streptavidin-conjugated enzyme (e.g. horseradish peroxidase or alkaline phosphatase), which acts on a substrate that changes its color upon enzymatic reaction. This type of staining (chromogenic staining) can be visualized using the bright-field microscope. Nonetheless, since majority of the studies regarding the usage of BNDS *in vivo* were done using IHC through immunofluorescent detection, this form of detection will be discussed within this section.

Depending on the disease model, different markers where analyzed through IHC. Regarding PD, the major players which are lost during the course of the disease and the ones targeted by most therapies are the dopaminergic neurons [326]. These neurons express idiosyncratically

tyrosine hydroxylase, an enzyme which converts tyrosine to DOPA, the precursor of DA. TH staining has been performed in almost all studies with PD models as an evaluation of the successful establishment of the PD model and as an assessment of the efficacy of the nano systems used [45,50,51,86,87,109,135,165,186,312,327,328]. In every PD model (6-OHDA [109], MPTP [109,186] and retenone [86,328] lesioned), there was a significant decrease in the number of TH+ neurons, confirming the onset of one of the pathological signatures of the disease. Also, all the systems tested showed that the administration of proteins [45,51,109,165,312,327,328] or genes [86,87,135,186] promoted the recovery of dopaminergic neurons in a significant manner when compared to the controls. Regarding polymeric nanoparticles as the carriers, commonly between three to four weeks post-administration of the nano systems, the increase in TH+ neurons was seen in the 6-OHDA lesioned Sprague-Dawley rats [50,51,87]. However, in zebrafish, the therapeutic effect of the drug used (baicalein) was seen two days after administration which can be related to the very small size of the organism and transdermal/oral intake of the micelles, which reduces the time they take to start their action [109]. A short-term effect of two days was also seen in mice, but when ferric iron oxide nanoparticles were used to deliver alpha-synuclein RNAi plamids, a reverse correlation between the TH and alpha-synuclein expression in the substantia nigra was displayed [186]. Lipidic systems were seen to act faster, showing normalized levels of TH in the whole body three days post-injection when TH plasmid was encapsulated in immunolipossomes [135]. In other studies, at from two to four weeks all the systems shared a significant increase in the number of TH+ cells [165,312,327,328]. This suggests that lipid-based systems are a more attractive option to produce an earlier therapeutic effect.

In addition to TH, other markers such as BrdU (proliferating neuroblasts) [48] and DCX (mature neuroblasts) [48] were stained in one study to see the effect of the microRNA-124 on these cells. It had no effect, however, on the number of neuroblasts or proliferating neuroblasts in the subventricular zone, except on the olfactory bulb, where the percentage of these cells increased significantly [48]. This group also chose to assess if there were any inflammatory reactions elicited by the PLGA nanoparticles by staining against CD68 (a marker for immune cells like macrophages and monocytes) in the brain and peripheral organs [48]. It was seen that after administering the particles for one week, there was inflammation in the kidneys, spleen and liver. However, 48 h after stopping the treatment, there were no signs of inflammation. Additonally, there were no CD68+ cells in the brain [48]. Zhao Z-Y et al. (2016) also evaluated the expression of Caspase-3 and c-Jun since they are markers for apoptosis that belong to the same pathway, which means that if they are both expressed, there is an increase in cell death [312]. This was seen in the group administered with blank gelatin nanoparticles. However, the reverse was verified for the group administered with substance P-loaded gelatin particles [312].

Concerning AD, different markers were chosen to assess the effects of the drug delivery systems, both specific to the disease (thioflavin T [35] and Aβ [134] for the detection of amyloid plaques) and broad/indirectly related to the disease (GFAP to detect reactive astrocytes (common in a neurodegenerative environment) [173], P75 to mark Schwann cells (indicative of neuroregeneration) [42], acetylcholinesterase (AchE) (to assess the neurotransmission functionality [42]). As for the density of amyloid plaques, this was significantly reduced when the animals were treated with curcumin (encapsulated either in PEG-PLA particles [35] or in Wheat Germ Agglutinin (WGA) conjugated-liposomes [134]). Reactive astrocytes were shown to be significantly reduced in the groups treated with the encapsulated chrysin, which did not happen when the free drug was administered [173]. Since the neuronal regeneration is greatly dependent on its environment, the existence of myelinating Schwann cells is crucial to regain the neuronal function. Chen Y et al. (2015) studied the expression of P75 in the medial septal nucleus and it was reported that the number of P75+ cells was increased in the group that was administered with NGF-loaded polymeric particles in combination with neural stem cells (NSC) [42]. They also assessed the expression of AchE, an enzyme that is essential to catalyze the breakdown of acetylcholine, which function as neurotransmitters. The expression of this was significantly higher in the treated groups, corroborating the regaining of functional and neuronal regeneration [42].

In the case of cerebral ischemia, the expression of indirect markers was analysed. Kannan S et al. (2012)were interested in the expression of CD11b and myelin basic protein to assess the microglia response and myelination of neurons, upon treatment with N-acetyl-L-cystein loaded PAMAM dendrimers [88]. It was seen that the greater the expression of activated microglia (present in neurodegeneration environments), the less the myelination (MBP+cells), whereas in the treated group the inverse was verified [88]. In another study, the expression the Akt and phosphorylated Akt was assessed, showing that the treated group with bFGF encapsulated in heparin nanoparticles had a significantly increased expression of p-Akt, which is a promoter of neuronal survival [138].

Regarding traumatic brain injury, only the inflammation of the tissue was assessed through the staining of IL-1β, IL-6 and TNFα, all pro-inflammatory markers, in a Lateral Fluid Percussion Injury (LFPI) Sprague-Dawley model [111]. In this case, the magnetic micelles did not elicit any inflammatory response and there were no changes in the expression between the sham and the healthy rats. Even though their expression increased in the traumatic brain injury (TBI) group, this remained at the same levels whether they were treated with micelles or not, confirming that there was not any deleterious effect caused by the nanoparticles [111]. However, in this case the therapeutic efficacy of the system was not assessed through IHC.

In brain tumors, several different markers were studied, mainly divided into apoptotic markers (B-cell lymphoma 2(Bcl-2), Bcl-2-associated death promoter (BAD), Bcl-2-associated X protein (BAX) [266], programmed cell death protein 4 (PDCD4) [104], caspase 3 [108]), cancer markers (vascular endothelial growth factor (VEGF) [17], phosphatase and tensin homolog (PTEN), prominin-1 (CD133), binding immunoglobulin protein (GRP78) [311], tyrosine-protein kinase Met (c-Met) [147], Ki67 [17,311,323], proliferating cell nuclear antigen (PCNA) [323]) and indirect markers (GFAP(reactive astrocytes) [17,188,311], isolectin B4 [17], CD31 [311] (angiogenesis), Nestin [158] (neural stem cells)). In all the above-mentioned studies, at least two or more markers were analyzed at the same time to draw more concise, consistent and accurate conclusions. This allowed a deeper investigation of the efficacy of the nano systems in the tumorand the surrounding environment. All apoptotic markers showed a significantly increased expression in the treated groups: BAD and BAX expression was significantly up-regulated upon the administration of myrcetin-loaded pluronic micelles in glioblastoma bearing mice [266], as well as the expression of PDCD4 in rats administered with curcumin/miRNA in deoxycholic acid-conjugated micelles [104]. Caspase 3 expression was also shown to be localized to the tumortumor core in carmustine treated glioma bearing mice [108]. The significant increase in the expression of apoptotic markers was accompanied by a significant decrease in the expression of cancer markers. VEGF was significantly down-regulated 10 days post-injection of doxorubicin-loaded PBCA particles, while the expression of Ki67 in the same study took another week to decrease significantly [17]. In other reports the same trend was seen in the expression of Ki67, corroborating the reduction in the proliferation of tumor cells after treatment [108,323]. Also, PCNA+ cells and c-Met expression decreased in the groups treated with paclitaxel-loaded liposomes [323] and siRNA-loaded SLN [147], respectively, demonstrating that the tumor growth can be modulated by either a drug or RNA-mediated downregulation of a gene involved in the tumor augmentation. CD133 and GRP78 expression was shown to be co-localized with the micelles signal, which indicates that they were targeting these cancer cells in an effective manner [311]. In this same study, GFAP and Nestin expression were analysed to evaluate the

Table 3
Histological strategies used to evaluate BNDS categorized by disease targets in pre-clinical models.

Nano-delivery systems		Animal model	Route of administration	Therapeutic cargo	Histological assessment	Outcome of histological assessment	Ref
Core polymer	Surface modification						
GLIOMA							
PBCA	Polysorbate 80	101/8 glioblastoma rat model, Adult male Wistar rats (200–250 g)	Intravenous	Doxorubicin	• IHC for GFAP (astrocytes), VEGF (tumor marker), isolectin B4 (vessel density), Ki67 (proliferation); • HE	• Proliferation stable in all groups and decreased significantly on day 18. • Vessel density at day 10 significantly lower on treated animals • Necrosis almost non-existent in the treated group and microvascular proliferation completely absent. • Expression of GFAP not affected • Decreased tumour size following treatment with Dox-np after 18 days. On day 14, the mean tumour size in the control group reached 24.9 ± 7.6 mm^2. Dox-np considerably inhibited the tumour growth.	[17]
PBCA	Polysorbate 80	C6 glioma bearing rat, Adult male Sprague-Dawley rats (220–250 g)	Intravenous	Gemcitabine	• HE	• Formation of the tumour 14 days post-C6 glioma cell inoculation into the rat brain. • Tumour cells in the treated groups were sparse when compared to the control.	[21]
PBCA	Polysorbate 80	F98 glioma bearing Fisher rats	Intravenous	TGF-B antisense oligonucleotide	• HE	• Increased expression of B-galactosidase in brain endothelial cells and liver tissue 24 h post-injection. • High expression seen after 40 h, spreading to spleen, kidneys and stomach. • Tumour cells showed precipitates from the reporter gene.	[329]
PEG-PLGA	c(RGDf(N-me) VK)-C (cHP)	C6 glioma bearing Adult male Sprague-Dawley rats (180–220 g)	Intravenous	Curcumin	• Fluorescence imaging	• Signal of the cHP-NPs in the brain was stronger than the one coming from NP wihtout cHP.	[29]
PEG-PLGA	–	9L gliosarcoma bearing Adult female Fischer F344 rats	Intracranial	Paclitaxel	• HE • Fluorescence imaging	• Region where the NP diffused remained intact and with dense cellularity. • PS-COOH NPs remained localised to the site of injection and did not penetrate the brain parenchyma or reached the tumour edge. • PS-PEG were able to distribute uniformly in the tumour parenchyma over time.	[237]
MPEG-PCL	TAT-modified	C6 glioma bearing Adult male Sprague-Dawley rats (Seven weeks old)	Intravenous, Intranasal	Coumarin (dye)	• Fluorescence imaging	• Fluorescence of coumarin in the brain after intranasal administration was significantly greater than after intravenous administration. • At 4 h post intranasal administration, coumarin fluorescence in brain homogenates was significantly higher in the treated group.	[98]
PEG-PAsp	–	U87MG glioma bearing Male Sprague-Dawley rats (200 g)	Intracranial (CED)	Synthetic retinoid (Am80)	• HE • TUNEL assay	• All animals administered with the highest dose of Am80 micelles showed minor damage at the site of injection and no sign of toxicity. • Six days after the infusion of the micelles, the group treated with micellar Am80 displayed decreased tumour density and increased number of TUNEL--positive cells.	[264]
RGD-PF-DP	–	U87MG glioma bearing Male BALB/c nude mice (18–22 g)	Intravenous	Doxorubicin, Paclitaxel	• HE	• No obvious histopathological abnormalities in the peripheral organs. • Tissue degeneration and necrosis were seen in the heart of the group treated with micelles without RGD	[265]
Chitosan-PEG-PPG-PEG-Poloxamer188	–	DBTRG-05MG blioblastoma bearing athymic Nu/nu mice (18–22 g, 6–8 weeks old)	Intragastric	Myricetin	• HE • TUNEL assay • IHC for apoptotic proteins (Bcl-2, BAD, BAX)	• Treated group showed significantly more apoptosis and necrosis than the controls. • The treated group displayed disrupted tumour cytoarchitecture. • No other significant histological lesions in any of the	[266]

						analysed organs. • TUNEL-positive tumour cells were increased in the treated groups, mainly in the one administered with micelles. • BAD and BAX expression was significantly up--regulated in the treated group.	
DSPE-PEG2k-Ome, 3 helix bundle	–	U87MG glioma bearing Male athymic nu/nu rats (250 g)	Intravenous	–	• HE • IHC against PECAM-1	• Sparse and more numerous large blood vessels within the tumour.	[267]
SN-38 loaded micelles	–	9L glioma/U87MG glioma bearing Normal Fischer 344 rats (250 g, 12 weeks old)	Intracranial (CED)	NK012	• Fluorescence imaging • HE	• The micelles distribution was diffuse and extensive in the brain. • More brain damage was seen in the group treated with free SN-38. • Slight tissue damage in the site of implantation (needle tract)	[102]
Deoxycholic acid-conjugated	–	C6 glioma bearing Male Sprague-Dawley rats (7 weeks old)	Intracranial	Curcumin/microRNA-21 antisense-oligonucleotide (miR21ASO)	• Cresyl Violet • IHC against PDCD4 and PTEN	• Tumour growth repressed by the injection of the micelles with the miR21ASO and curcumin, and this had higher anti-tumour effects compared to the groups treated with free curcumin or free miR21ASO. • Treated groups showed that the delivery of the microRNA increased the expression of both PDCD4 and PTEN, which suggests that the action of miR21ASO over the miR-21 leads to its downregulation	[104]
PEtOz-SS-PCL	–	C6 glioma bearing Male ICR mice (18–20 g)	Intravenous	Doxorubicin, Paclitaxel	• HE • Fluorescence imaging	• Histological examinations showed no lesions in the cardiac tissue in any of the groups. • The micelles distribution was mostly present in the tumour region, where areas of hypercellularity were identified.	[105]
RI-VAP, d-VAP	–	U87MG glioma bearing Male BALB/c nude mice (4–6 weeks old)	Intravenous	Paclitaxel	• IHC against CD31 (blood vessels), CD133 (cancer stem cells) and GRP78. • IHC against NeuN and GFAP	• VAP micelles signal co-localized with CRP78 positive cells. On the other organs the expression of GRP78 was barely detected. • Most of the VAP micelles co-localized with CD31, suggesting that they can bind to the tumour neovasculature and also penetrate in the tumour parenchyma. • VAP peptides showed a high ability to target the cancer stem cells, seen by the co-localization of GRP78 and CD133 expression. • The expression of both markers was similar in treated and untreated animals, both three days and three weeks post-infusion.	[106]
		F98 glioma bearing Fischer-344 rats			• HE	• Control groups showed large necrotic tumours on the stained sections. • Treated group did not show any evidence of the tumour.	
PLGA-T7 peptide	–	U87-Luci glioma bearing Male BALB/c nude mice (18–22 g)	Intravenous	Carmustine (BiCNU®)	• TUNEL assay • HE • IHC against caspase-3 and Ki67	• High apoptosis rate within the tumour region on the group treated with the T7-micelles. • Clearly defined tumour region detected • Accumulated caspase-3 on tumour cells • Lower expression of Ki67 in treated group	[108]
Pegylated liposomes		9L gliosarcoma bearing Male Sprague-Dawley rats (200 g)	Intravenous	Doxorubicin	• HE	• 48 h post-treatment the borders of the tumour treated with doxorubicin and focused ultrasound were characterised by parenchymal vacuolation and lesioned tumor cells. • In the group treated with doxorubicin only the edges remained intact and there were no damaged cells.	[121]
Procationic liposomes - Lactoferin		C6 glioma bearing Male Wistar rats (150–180 g)	Intravenous	Doxorubicin	• HE	• Histopathological stainings showed the differences between the normal and tumour tissue in the brain.	[122]

(continued on next page)

Table 3 (*continued*)

Nano-delivery systems		Animal model	Route of administration	Therapeutic cargo	Histological assessment	Outcome of histological assessment	Ref
Core polymer	Surface modification						
TPGS-Transferin		Charles Foster rats (180–220 g)	Intravenous	Docetaxel; Quantum dots	• Fluorescent imaging	• Fluorescent signal was stronger in the Tf-liposomes, when compared to the control and non-targeted liposomes.	[101]
HSPC/DOPE/Chol/CTAB/Didodecyldimethylammonium bromide		C6 glioma bearing Adult Sprague-Dawley rats (200–220 g)	Intravenous	Doxorubicin	• HE • TUNEL assay	• No pathological morphology present in the peripherical organs one month post-administration of the liposomes. • In the brain, the cell density within the tumour region was much greater than the one in the normal brain tissue. • The rapid tumour growth led to ischemia and damaged cells in the adjacent brain regions. • In the treated group the tumour tissues were hypocellular and with higher cell viability. • Within all the treated groups, the one with focused ultrasound was the one with highest tumour apoptosis and necrosis.	[125]
DSPE- PEG2000-maleimid, DDAB		C6 glioma bearing Adult female Wistar rats (Three months old, 230–280 g)	Intravenous	VEGF	• Fluorescence imaging	• Liposomes without vector did not accumulate in the tumour tissue. • Anti-VEGF-liposomes were accumulated in all tumours (in the centre and periphery of the tumour tissue, with heterogeneous distribution)	[127]
NH2-PEG-DSPE-p-aminophenyl-α-D-mannopyranoside		ICR male mice (18–20 g) bearing glioma stem cells	Intravenous	Curcumin, Quinacrine	• HE	• The tumours within the treated groups were significantly smaller and with more vacuoles. • The shape of the tumours was irregular and without obvious boundaries. • large portions of necrosis and haemorrhage.	[128]
DPPC:PTX:DSPE-PEG:cholesterol		U87MG glioma bearing Male BALB/c mice (6–7 weeks old, 18–22 g)	Intravenous	Paclitaxel	• IHC against Ki-67 and PCNA (proliferating cell nuclear antigen) • TUNEL assay	• Expression of Ki-67 and PCNA was very high in non--treated glioma regions. Between the treated groups there were no significant differences. • The number of Ki-67 and PCNA positive cells decreased in the group treated with paclitaxel loaded liposomes, enhanced by focused ultrasound • Control group showed a small percentage of apoptotic cells, whereas the treated group enhanced by focused ultrasound, showed abundant TUNEL-positive cells within the glioma region.	[323]
SLN		U87MG glioma bearing Adult Male BALB/c nude mice (Six weeks old)	Intravenous	siRNA	• HE • IHC against c-Met	• The nanoparticles decreased the tumour size in a dose-dependent manner. The highest dose showed a 91% tumour volume reduction. • Downregulation in the expression of c-Met after the nanoparticles administration	[147]
SLN		Adult Wistar rats (230–250 g)	Intravenous	Camptothecin™, Rhodamine123 (dye)	• Fluorescence imaging	• The nanoparticles coated with polysorbate 80 were not detected 120 min post-injection. • After this time, both the SLN coated with polysorbate 80 and polysorbate 60 were detected in the brain, being the latter more diffused into the brain.	[149]
LNC		C6 glioma bearing Adult Male Wistar rats (Eight weeks old, 220–260 g)	Intravenous	Curcumin	• HE	• 14 days post-injection, the lowest dose of C-LNC helped to decrease the tumour size when compared to the other treatments. • Curcumin free only exerted significant effects on tumour size at a high dose. • Necrosis and haemorrhages decreased in C-LNC and C50 treatments, while the micro vessel proliferation was similar on the different groups.	[150]
HA-LNP		U87MG glioma bearing Athymic Female BALB/c nude	Intracranial	siRNA	• HE	• Tumour was clearly visible through a high cellular density, with significant differences from the normal tissue.	[153]

		mice (4–6 weeks old, 20 g)					
LPNP		GBM43/MGG8 glioma bearing Athymic nude male/female mice (6–8 week old)	Intracranial	RNAi	• IHC against human Nestin	• The *in vivo* distribution of the LPNP is restricted to the tumour site four days post-injection.	[158,159]
QD-aptamer32		U87 glioma and U87-EGFRvIII glioma bearing Male C57BL/6 athymic nude mice (6–8 weeks old)	Intravenous	–	• IHC against GFAP • HE	• Strong of expression of EGFRvIII in the mice with the U87-EGFRvIII tumours and no expression of this in the mice with U87 tumours. • QD-Apt were only detected in the U87-EGFRvIII tumours. Less astrocytes in this group. • There were no tissue lesions, necrosis or inflammation in any of the groups analysed	[188]
Angiopep2-PEG-DOX-Au		C6 glioma bearing Male Kunming mice (20–24 g)	Intravenous	Doxorubicin	• IHC against LRP1 • TEM • HE	• Tumour cells highly expressed LRP1. • Biodistribution of the nanoparticles was significantly greater than the one of free doxorubicin • Nanoparticles with the angiopep on the surface highly co-localised with LRP1. Distribution in the spleen, liver and kidney of angiopep-NPs was lower than the uncoated NPs 2 h post injection. This result switched 4 h post-injection • Distribution of angiopep-NP in the tumour site was higher than that of NPs without angiopep • In the controls, the glioma was clearly observed. • In the treated groups the density of glioma cells was lower than in the controls • No obvious toxicity was seen in the heart.	[189]
PARKINSON'S DISEASE							
Poly(D,L-lactide-co-glycolide)lactide: glycolide	PVP	6-OHDA lesioned Adult Wistar rats (215–235 g)	Intravenous	Dopamine	• IHC against TH (dopaminergic neurons), GFAP (glial cells) and endoglin (capillaries). • Fluorescence imaging • TEM • HE	• The nanoparticles were not confined within blood capillaries and were detected in the brain parenchyma. The nanoparticles were detected near and inside the neurons and astrocytes, 4 h post-injection. • FITC-labelled nanoparticles were detected also in the spleen, liver and kidneys of the animals, 4 h post--injection. • Polymeric nanoparticles aggregates were detected in the striatal region of the brain. • The administration of the nanoparticles did not cause any lesion or histopathological change in the heart, suggesting that it did not cause any abnormal cardiovascular change.	[45]
Alginate	–	Transgenic fly lines	Oral	Curcumin	• Fluorescence imaging	• The fluorescent intensity decreased in a dose--dependent manner with the administration of ACNC	[46]
PLGA-PFCE	–	6-OHDA lesioned Adult male C57BL/6 mice (10–12 weeks old)	Intracranial	microRNA-124 (miR-124)	• IHC against BrdU, DCX and NeuN	• The nanoparticles delivered into the ventricular lumen were detected one day post-administration. The loaded nanoparticles with miR-124 were not able to change the total number of neuroblasts (DCX+) or proliferating neuroblasts (DCX+/BrdU+) in the subventricular zone of all treated groups, nonetheless in the 6-OHDA group the proliferating neuroblasts were 50% lower than the healthy animals. • Significant increase of DCX+ and DCX+/BrdU+ cells in the Granule cell layer of the olfactory bulb of 6-OHDA treated animals	[48]
PEG-PLGA	Lactoferin	Adult male Kunming mice (18–20 g)	Intravenous	Coumarin-6 (dye)	• Fluorescence imaging	• Lactoferrin-nanoparticles were detected in the cortex, substantia nigra and striatum 1 h post-injection, which was not seen in the nanoparticles without lactoferrin.	[50]
		6-OHDA lesioned Adult male			• IHC against TH	• After 21 days of treatment, the lesioned-control showed significant loss of TH+ neurons.	

(continued on next page)

Table 3 (*continued*)

Nano-delivery systems		Animal model	Route of administration	Therapeutic cargo	Histological assessment	Outcome of histological assessment	Ref
Core polymer	Surface modification						
		Sprague-Dawley rats (200–250 g)				• After treatment in the 6-OHDA lesioned group, there was a significant increase in the number of TH+ neurons.	
		Adult Balb/c mice (18–20 g)			• IHC against CD688	• After administering the nanoparticles for one week, there were dose-related inflammatory reactions in the kidneys, spleen and liver 24 h after that week, which disappeared at 48 h. • No signs of inflammation were seen in other tissues	
PEG-PLGA	Odorranalectin	6-OHDA lesioned Adult female Sprague-Dawley rats (200–220 g)	Intranasal	Urocortin peptide	• IHC against TH	• TH+ neurons decreased in the substantia nigra of the control (6-OHDA lesioned), while there they increased significantly in the nanoparticles-treated groups. • Higher number of TH+ neurons in the groups treated with odorranalectin-nanoparticles.	[51]
DGL-PEG	Angiopep	Rotenone induced Adult Male Sprague-Dawley Rats (250–300 g)	Intravenous	DNA (hGDNF)	• IHC against TH	• The groups administered with the nanoparticles with the angiopep and GDNF showed recovery of dopaminergic neurons, both in striatum and substantia nigra, namely after 5 injections of these nanoparticles, 35 days post rotenone-injection.	[86]
PAMAM-PEG	Lactoferrin	6-OHDA lesioned Adult male Sprague-Dawley rats (250–300 g)	Intravenous	pDNA (hGDNF)	• IHC against TH and CD68	• All the groups administered with the nanoparticles with GDNF showed recovery of dopaminergic neurons in substantia nigra. • In the striatum, substantia nigra and hippocampus almost no cells were CD68+. However, these were detected in the spleen and liver of normal rats	[87]
Pluronic P85/F68	–	MPTP treated Zebrafish	Oral	Baicalein (B-MCs)	• IHC against TH	• Micelles prevented significantly the loss of dopaminergic neurons by exposure to MPTP	[109]
Pegylated immunoliposome (OX-26)		6-OHDA lesioned Male Sprague-Dawley rats (200–250 g)	Intravenous	DNA (TH plasmid)	• IHC against TH	• Total loss of TH+ cells in the striatum where the 6-OHDA was injected. • After administration of the loaded liposomes the levels of TH increased in the striatum, and at three days post-injection they were normalised in the whole body.	[135]
GNL		6-OHDA lesioned Sprague-Dawley rats	Intranasal	bFGF, Apomorphine	• HE • IHC against TH	• No local epithelial damage of nasal mucosa. • Severe loss of dopaminergic neurons in the substantia nigra of the group administered with unloaded particles. • Treated groups showed an increase in the number of TH+ cells	[165]
Poloxamer 188–grafted heparin; gelatin, D,L glyceraldehyde		6-OHDA lesioned Adult male Sprague-Dawley rats (300–320 g)	Intranasal, intravenous	Substance P	• HE • IHC against TH, c-Jun and caspase 3	• The lesioned group showed reduced dopaminergic neurons and proliferation of glial cells. • Treated group showed a significant increase in the number of dopaminergic neurons and reduction in inflammatory cells infiltration. The group where the nanoparticles were administered intranasally had a higher number of neurons with regular arrangement. • Significant loss of TH+ cells in the injured group, which was reverted by the treatment, mainly in the intranasal-administered one. • c-Jun was downregulated in the group treated with saline, while in the lesioned group and in the blank nanoparticles one it was highly expressed. Less staining was seen in the treated group than in the lesioned one. • Caspase-3 signal pattern was similar to the c-Jun.	[312]
Phosphatidylglycerol		6-OHDA lesioned	Intranasal	VP025			[327]

		Adult male Sprague-Dawley rats (225–250 g)			• IHC against TH, MHC Class II and p-p38.	• The administration of VP025 reduces the loss of TH+ neurons at 10 days post administration. However, this trends persists up to 28 days only in the group that received the highest dose of VP025. • Significant increase in microglia expression on the 6-OHDA lesioned rats, which was reduced by the pre-treatment with VP025. The positive expression of activated p38 was seen in surviving dopaminergic neurons on the 6-OHDA lesioned group (28 days). • There is no activated p38 in dopaminergic neurons in the groups pre-treated with VP025.	
GMO-Pluronic F68, vitamine E-TPGS		Adult male Balb/c mice (4–6 weeks old, 12–32 g)	Oral	Curcumin, Piperine	• IHC against TH	• There was accumulation of the nanoparticles within the dopaminergic neurons 2 h post-administration.	[328]
		Rotenone induced male C57BL/6 mice (8–10 weeks old, 25–30 g)			• IHC against TH	• Low density of TH+ neurons in rotenone treated mice, however this is reverted with the treatment, resulting in higher density of dopaminergic neurons in the dual drug loaded nanoparticles group.	
Fe3O4 - Oleic acid-NIPAm-AA-NGF		MPTP treated Adult male C57BL/6 mice (7–8 weeks old)	Intraperitoneal	shRNA	• IHC against TH and alpha-synuclein • Prussian blue • HE	• Reverse correlation was seen between the TH and alpha-synuclein expression in the substantia nigra post-MPTP administration. In the treated groups the number of TH+ neurons increased and there was a down-regulation of alpha-synuclein. • There is a minimal distribution of nanoparticles in all organs except the spleen. • The nanoparticles did not cause any significant lesion or organ damage.	[186]
ALZHEIMER'S DISEASE							
PEG-PLGA	TGN (TGNYKALHPHNGC), QSH (QSHYRHISPAQVC), Aβ42	Aβ 42 induced Adult ICR mice (18–22 g)	Intravenous	H102	• HE • Cresyl Violet	• Damage of nerve cells in the hippocampus region, mainly neuronal loss, shrinkage and nuclear condensation, all in the lesioned rats. • The treatment with TNP/H102 and TQNP/H102 elicited protective effects on neurons, with significant reduced pathological changes and less cell loss	[32]
PEG-PLGA	Solanum tuberosum lectin	Aβ 15–35 & IBO induced Adult male Sprague-Dawley rats (200–230 g)	Intranasal	bFGF	• HE • Congo red	• AD control group showed clear neuronal loss in the hippocampus and dentate gyrus and aggregation of AB plaques. • This was reverted in the group treated with bFGF loaded nanoparticles with STL, showing very few differences from the sham groups. • Cholinergic nerve fibres were intact in the treated groups as well as the architectural organisation of nasal septal mucosas (clear structure and normal cell density). • The peripheral organs showed no obvious lesions or tissue damage, except the kidneys where vacuole-like denaturation and thin tube walls were observed.	[33]
PEG-PLA	PVP	Tg2576 transgenic mice	Oral	Curcumin	• IHC against thioflavin T	• The treated group with curcumin showed a significantly lower amyloid plaque density than the controls.	[35]
PEG-PLGA	–	Adult Sprague-Dawley rats (200–250 g)	Intracranial	NGF	• IHC against P75, synaptophysin and AchE	• There were significantly more P75+ neurons in medial septal nucleus and vertical branches of diagonal bands in the control and treated groups, when compared to the AD rats. • The number of these neurons was higher in the combined treatment group when compared to the NSC transplantation animal.	[330]

(continued on next page)

Table 3 (*continued*)

Nano-delivery systems		Animal model	Route of administration	Therapeutic cargo	Histological assessment	Outcome of histological assessment	Ref
Core polymer	Surface modification						
						• Synaptophysin expression was much weaker in all the groups in comparison to AD rats. • AchE fibres were significantly higher in the treated groups in relation to the AD group	
PC:DCP:Cholesterol		Aluminium chloride-induced Adult male Wistar albino rats (240–280 g)	Oral	Rivastigmine	• HE	• The AD group showed focal area of deep eosinophilic amyloid plaques. • The formation of plaques and the number of necrotic neurons were decreased in the treated group.	[131]
Cardiolipin-conjugated liposomes - WGA		Aβ 1–42 treated Male Wistar rats (8 weeks old, 250–280 g)	Intravenous	Curcumin, NGF	• IHC against Aβ • Cresyl Violet	• Aβ plaque deposition in the hippocampus of the AD rats. • Free curcumin reduced the plaques, but the liposomes were more effective • The AD group displayed more degenerated neurons, which were reduced by the liposomes.	[134]
SLN		Ibotenic acid-lesioned Albino Wistar rats	Intraperitoneal	Piperine	• Congo red	• Amyloid plaques present in nucleus basalis magnocellularis of AD group. • The treated group showed a decrease in plaques and tangles.	[331]
NLC		ICR mice (18–22 g)	Intravenous	Curcumin	• Fluorescence imaging	• Stronger and more distributed fluorescence intensity in the treated group.	[170]
		Aβ 1–42 & D-gal induced Sprague-Dawley rats (180–220 g)			• HE	• In the AD group there was a significant neuronal loss, karyopyknosis and perikaryon shrinkage in the hippocampus. • treatment with curcumin loaded formulations reverted the neuronal loss and the pathological damages were ameliorated. • These effects were more significant in the lactoferrin-coated NLCs.	
SLN		Aβ 25–35 induced Adult Male Sprague-Dawley rats (250–300 g)	Oral	Chrysin	• HE • Crystal Violet • IHC against GFAP	• Treated group displayed as improved neuronal cell configuration in a dose dependent manner if the chrysin is encapsulated. • SLNs per se had no effect on the cell morphology and architecture. • The loss of pyramidal cells in the hippocampus was reduced in the groups treated with SLNs formulations. • Significantly decrease in the expression of GFAP+ cells in the treated groups with SLNs formulations when compared to the AD group and to the free chrysin treated groups.	[173]
STROKE (CEREBRAL ISCHEMIA/ICH)							
PNIPAM	–	Middle cerebral artery occlusion induced Adult Wistar rats (16 weeks old, 300–400 g)	Intranasal	Curcumin	• HE	• MCAO group showed neuronal loss and numerous vacuolated spaces. • Treated group with PNIPAM formulations only displayed partial loss of neurons and intact neurons in between the vacuolated spaces.	[63]
Chitosan	–	Middle cerebral artery occlusion induced Wistar rats (8–10 weeks old, 300–400 g)	Intranasal	Rutin	• HE • TTC assay	• MCAO group exhibited neuronal loss and brain damage with numerous vacuolated spaces. The treated group displayed decreased neuronal abnormalities. • MCAO showed a large lesion area when compared to the control. • The infarct volume decreased significantly in the nanoparticle-treated group.	[332]
Chitosan-PEG	PEG+ anti transferrin antibody	Middle cerebral artery occlusion induced Swiss albino mice	Intravenous	Caspase-3 inhibitor	• HE	• The group pre-treated with the loaded nanoparticles showed significantly reduced infarct volume • The group that was post-treated with the loaded	[235]

		(18–22 g)				nanoparticles showed neuroprotection 2 h post ischemia.	
PLGA	Polysorbate80	Middle cerebral artery occlusion induced Male wistar rats (200–250 g),	Intravenous	Acetylpuerarin	• HE • TUNEL assay	• In the injured group the hippocampus was severely damaged in the infarct area and the neurons disordered and with pycnotic nuclei. • Treated group showed significantly less necrotic neurons. • MCAO group displayed numerous TUNEL+ cells 24 h post-injury. The treatment with the loaded nanoparticles reduced the number of apoptotic cells in a preventive manner.	[69]
PLGA	–	Middle cerebral artery occlusion induced Male Sprague-Dawley rats (250–300 g)	Intravenous	Superoxide dismutase	• TTC assay • TUNEL assay • DCDHF-DA staining	• Treated group showed a reduction in infarct volume and lesions with time. • The animals from the treated group which survived 48 h post-injury continued to recover with time. • Treated group showed significantly less apoptotic cells. • Treated group demonstrated a significant decreased in the ROS activity.	[70]
PAMAM	NAC	E. coli endotoxin injected Newborn New Zealand white rabits	Intravenous	N-acetyl-L-cysteine (NAC)	• IHC against CD11b and MBP	• CP group showed increased activated microglia (CD11b+ cells) and decreased myelination (MBP+ cells). The reverse was seen for the treated groups.	[88]
PAMAM	Dexamethasone	MCAO Male Sprague-Dawley rats (280–300 g)	Intracranial	Heme oxygenase-1 gene	• TTC assay	• The group treated with the loaded and modified dendrimers had the smallest infarct volume.	[90]
Heparin-Poloxamer188		MCAO/reperfusion Adult female Sprague-Dawley rats (230–270 g)	Intranasal	bFGF	• HE • IHC against Akt and p-Akt	• Injured group showed lesions in the hippocampus and intercellular space enlargement, which was significantly reverted upon the administration of the bFGF loaded liposomes. • Expression of p-Akt was significantly increased in bFGF-loaded lipossomes in comparison, while the Akt was lower.	[138]
RADA16-I self-assembling peptide nanofiber scaffolds (SAPNS)	–	Injection of collagenase IV in Male Sprague-Dawley rats (11–13 weeks; 420–480 g)	Intracranial	–	• IHC against MPO (neutrophils), ED-1 (microglia), NeuN, GFAP, Iba-1 • TUNEL assay • EM	• The hematoma-bearing group should high density of MPO+ cells, whereas this was significantly reduced both in the aspiration group and in the saline/SAP administered group. The number of ED-1+cells was the same in the hematoma and aspiration groups, but was decreased in the treated group. Microglia cells were dispersed equally within the scaffold. • High density of apoptotic cells in all groups except the treated one, where these were significantly reduced. • Interaction between the SAPNS and the brain tissue was tight, with cells migrating to the scaffolds.	[333]
Graphene oxide nanosheet	Tat peptide and mPEG	Middle cerebral artery occlusion induced mice	Intravenous	Pirfenidone	• HE	• Untreated group reveals islands of eosinophilic neurons without coagulation necrosis and damage in grey matter, which is reverted upon use of pirfenidone--FGO nanosystems.	[334]
PLGA in fibrin sealant gel		Subarachnoid haemorrhage in Wistar rats	Intracisternal	Nimodipine	• HE • IHC against Iba1 and MAP2	• No subcarachnoidal blood was detected in the animals administered with 40% nanoparticles, whereas in the lowest concentrations and untreated animals there was SAH around the hippocampus. • Accumulation of Iba1+ positive cells (microglia) around the SAH, but these were evenly distributed with no further lesions. There were no significant differences in the expression of MAP2 between injured, treated and sham animals.	[71]
Ceria nanoparticles loaded with Iron-Mesoporous silica	Lipid coating	Injection of collagenase VII in Male	Intracranial	(Ceria)	• IHC against CD68	• The nanoparticles were mainly located in the microglia/macrophages cytoplasm.	[196]

(continued on next page)

Table 3 (*continued*)

Nano-delivery systems		Animal model	Route of administration	Therapeutic cargo	Histological assessment	Outcome of histological assessment	Ref
Core polymer	Surface modification						
nanoparticles		Sprague-Dawley rats (8-weeks)					
PCBA	–	Injection of collagenase IV in Male Sprague-Dawley rats (350–400 g)	Intravenous	NT-3 (plasmid containing hormone response element (HRE) with a cytomegalovirus promoter)	• IHC against NT-3, AIF and caspase-3 • Nissl staining • TUNEL assay	• NT-3 expression was reduced in injured animals up to 2 weeks without treatment and in the ones treated with the free plasmid. The opposite was seen in the group treated with the loaded nanoparticles. The reversed trend was seen in the expression of the apoptotic markers (AIF and caspase-3), with upregulation of these in the untreated group. The TUNEL assay showed a similar distribution pattern to the AIF and caspase-3. • The Nissl staining showed neuronal density in all groups, regardless their treatment. Increased neuronal survival was seen in the group treated with nanoparticles and extensive neuronal loss in the ICH group.	[72]
PLGA	–	MCAO induced Male Sprague-Dawley rats (12 weeks, 260–300 g)	Intraperitoneal	Curcumin	• IHC against ED-1	• Expression of activated microglia (ED-1+) was increased in the injured hemisphere. This was significantly decreased in the curcumin-NPs treated group.	[73]
Ceria	PEG	Injection of collagenase VII in male Sprague-Dawley rats (200–250 g)	Intravenous	(Ceria)	• Fluorescence imaging • IHC against CD68	• CeNPs were mainly distributed in the perihematomal area, where their intensity was higher. They diffused throughout the interstitial space, but did not cross the ventricle or gray matter • The number of CD68+ cells was decreased in the CeNP treated group.	[197]
PSYCHOTIC DISORDERS							
SLN		Ketamine induced Adult Male albino rats (160–180 g)	Oral	Quetiapine fumarate	• IHC against Bcl2	• Ketamine group had no expression of Bcl2 in the hippocampus, which was reverted in the treated groups, where there was a moderate positive expression of Bcl2.	[178]
SNEDDS		Ketamine-induced Swiss albino mice (6–7 weeks old, 30–40 g)	Intraperitoneal	Olanzepine	• HE	• There was no damage or abnormality observed in the organs of the treated groups.	[314]
TRAUMATIC BRAIN INJURY							
PBCA	Polysorbate80	Lateral fluid percussion brain injury Adult male Sprague-Dawley rats (220–325 g)	Intravenous	Horseradish peroxidase	• IHC against EGFP	• The EGFP-loaded nanoparticles were detected 48 h post administration in the brain parenchyma of the control. • On the TBI group, the nanoparticles were seen 45 min post-administration near the injured site.	[65]
Chitosan-PEI-magnetic micells	–	Lateral fluid percurssion injured (LFPI) Male Sprague-Dawley rats (250–300 g)	Intranasal	DNA	• Fluoro-jade • Prussian blue • IHC against IL-1β, IL-6 and TNFα	• TBI group presented neurodegeneration and the majority of FJ+ cells were in the cortex, hippocampus and thalamus. • More micelles were concentrated in the cortex of the rats that were under a magnetic field when compared to the group that was not. • They were present on the cortex and hippocampus even 48 h post-TBI • The micelles did not elicit an inflammatory response in the rats. There was no change in the expression of IL-1B, IL-6 or TNFalfa between the healthy and sham groups.	[269]

toxicity of the micelles. The expression of both markers was similar in all groups, at both three days and three weeks post-injection, highlighting the non-toxic effect of the micelles [311]. A similar unaffected GFAP expression was seen after injection of doxorubicin-loaded PBCA nanoparticles, proving that these did not have a toxic effect over the brain [17].

3.1.3. Electron microscopy

In a minority of the studies, transmission electron microscopy (TEM) was also used to demonstrate the distribution of the nanoparticles in the brain and the ultrastructural changes caused by them [45,189]. This is of interest when metallic particles are used, such as gold nanoparticles. In this study it was shown that the nanoparticles covered with the angiopep-2 in a glioma model had a much higher and wider distribution in the tumor site than uncoated nanoparticles [189]. In another report, TEM allowed the analysis of the effect of nanoparticles on the tissue and showed polymeric nanoparticles aggregated in the striatal region of the brain, corroborating their targeting of the effected tissue in the PD model [45].

Even though there is a much wider range of histological techniques which can be applied to study the efficacy of nano systems, these were the ones used so far in pre-clinical models of brain disorders. Detailed description of their usage can be found in Table 3.

The symbiotic use of these approaches brings a meaningful innovation into the ways to assess the efficacy of the nano systems, allowing a better understanding of how, where and when they act.

It is important nonetheless to the state a proviso by mentioning that these are all qualitative methods, not allowing a precise quantitative analysis of the extent in the expression of each of these markers. Further techniques must be employed as will be discussed in the following sections of this review.

3.2. Bio-imaging assessment

The most recent category of methods to evaluate the efficacy of the nano-systems within the body is bio-imaging. Bio-imaging depends on advanced technologies and equipment that were only developed around 60 years ago [335,336]. These comprise non-invasive methods to visualise biological tissues in real time and are very significant since they can provide an overview of the organ of interest or even the whole body, and are not restricted to a 2D section. This has become a vital part in the field of oncology, particularly for tumor detection, characterisation and the assessment of therapeutic efficacy [337].

Positron-Emission Tomography (PET): This is based on the use of radiotracers which emit positrons that undergo radioactive decay andproduce photons by colliding with electrons, which are detected by the PET scanners. These will then reconstruct the tissue of interest with the corresponding spatial density and the identification of, for example, metabolic and blood flow changes [335]. PET can be used to evaluate the bio-distribution of nano-systems in the brain, such as dendrimers, which were shown to be increased after one day in the brains of animals with cerebral palsy [88]. Currently PET is combined with other modalities, such as computed tomography (CT) or magnetic resonance (MR), to allow the three-dimensional representation of the scanned tissues [335,338]. In another study, PET/MR was used to evaluate how the different sizes of micelles would affect their pharmacokinetics and bio-distribution. This method was useful to see that at 21 h post-injection they ahad ccumulated within the tumor, first in the centre and later on the periphery [267], suggesting a temporal and spatial path of action of this system.

Single-Photon Emission Computed Tomography (SPECT): This method also depends on the use of a radioactive tracer and gamma radiation. However, in this case the radiotracers emit gamma radiation which can be measured directly, contributing to the reduced cost of the SPECT scanners when compared to the PET [339]. In preclinical models of CNS disorders, SPECT has been used in PD, to determine the distribution of the bromocriptine-loaded chitosan nanoparticles in the brain between two different routes of administration [44]. SPECT allowed an easy and quick analysis showing a significantly higher radioactivity in the brain after intranasal administration when than that of the intravenous one.

Magnetic Resonance Imaging (MRI): This has been used in the clinic for over three decades and serves as the primary diagnostic technique [336]. MRI is based on the imaging of paramagnetic chelates and magnetic particles and has no limit of depth for its analysis with a resolution of 10–100um [338]. This is of interest since it does not involve the exposure to harmful radiation, can be used to visualise blood vessels and for soft tissue imaging, making it especially useful in brain imaging. Furthermore, it can show swelling and inflammation, in a three dimensional way [336]. For these reasons, it is already widely used in patients and is also employed in studies to assess the efficacy of treatments in pre-clinical disease models. In the case of brain disorders, MRI is mainly applied (like the majority of bio-imaging modalities) in the follow up of glioma sizes and glioma treatments [102,121,125,188,267,323]. In the majority of the reports where MRI is applied to assess the tumor size after therapeutics, the imaging is preformed between one and five weeks post-administration of treatment [121,125,188,323]. C6 glioma-bearing rats injected with doxorubicin-loaded liposomes showed high tumor inhibition up to 22 days [125], as well as the U87MG glioma bearing mice administered with paclitaxel in liposomes, where the suppression was seen until 38 days post-injection [323]. This was also observed in 9L gliosarcoma bearing rats, where the administration of PEGylated liposomes with doxorubicin combined with focused ultrasound led to a decrease in the r tumor size three weeks post-injection [121]. This emphasises the usefulness of this technique in accompanying the tumortumor progression/regression over a timeline. In this regard, it can also be employed to follow the recovery of infarcted areas in MCAO models after administration of therapeutic molecules, such as that of encapsulated bFGF [138]. Moreover, it can also be used to visualise the nanoparticles administered. For example, Zhang R. et al. (2016) labelled polymeric micelles with gandolinium to make them trackable. This tracking showed that after 1 h, they were evenly distributed in the cancer tissue [102]. However, even though it has many advantages, MRI scanners are expensive, and so this is not the first approach chosen when it comes to *in vivo* imaging of pre-clinical models.

Real-time near-infrared (NIR) fluorescence imaging: This technique has high spatial resolution, thorough molecular tracking of fluorescent probes and portability, as well as offering significant real-time display [337]. The use of the near-infrared spectral region is of interest since it has better penetration into the tissue and reduced auto-fluorescence [337]. The principle of this modality is based on the fluorescent property of certain molecules characterised by the absorbance of light in one wavelength and emission at a higher wavelength [338]. There are two types of NIR fluorescence: tomography fluorescence imaging and fluorescence reflectance imaging (FRI), the latter being the most commonly used in the case of brain studies [337]. This has an imaging depth of less than 1cm, a resolution of 2–3mm and a cost that is less than a third of the MRI equipment [338]. Usually this real time imaging is done on early time points after the administration of the nanoparticles, such as 2, 6, 12 and 24 h post administration [25,29,123,311,340], all in glioma bearing models. All of these nano-carriers were labelled with DiR to allow them to be detected in the different regions of the body. In some studies, the polymeric nanoparticles are detected 1 h post-administration and reach the maximum fluorescence signal at 12 h post-injection, declining thereafter [25,29], only in the drug-loaded carriers. On the other hand, in micelles coated with RGD peptide, the signal was the strongest at 48 h post-injection [265]. NIR fluorescence has also allowed the analysis of particle distribution in peripheral organs, showing that most particles also reach the heart, spleen, lungs, liver and kidneys when they are intravenously administered [29,265,340], but they accumulate less in these tissues when they are coated with brain-targeting moieties. Additionally, the use of liposomes enhanced the accumulation of the drug in the brain even after 24 h [123]. This is,

Table 4
Bio-imaging tools used to study the efficacy of BNDS in different brain disease targets.

Nanosystem tested		In vivo model	Route of administration	Therapeutic cargo	Bio-imaging assessment	Outcome of bio-imaging assessment	Ref
Core polymer	Surface modification						
GLIOMA							
PCL-PEG	Angiopep-s	U87MG glioma tumor bearing-male BALB/c nude mice (4–5weeks old, 18–22 g)	Intravenous	Paclitaxel	• Real-time fluorescence imaging	• Dir-labelled nanoparticles were visualized in excised peripheral tissues and were shown to cross the BBB through LRP receptor binding, and to accumulate in the brain via the EPR effect. • Accumulation of the nanoparticles in the reticuloendothelial system was detected in all groups.	[340]
PCL-PEG	PEG	C6 glioblastoma bearing Male BALB/c nude mice(18–22 g)	Intravenous	Paclitaxel	• Real-time fluorescence imaging	• NP were detected in the brain 1 h after injection and showed maximum fluorescence signal at 12 h post-injection, decreasing thereafter. • The signal of MPEG-NP was always stronger than the one of NP alone.	[25]
PEG-PLGA	c(RGDf(N-me)VK)-C (cHP)	C6 glioma bearing Adult male Sprague-Dawley rats (180–220 g)	Intravenous	Curcumin	• Real-time fluorescence imaging analysis	• Treated group showed a weak signal in the brain 1 h post-injection, but it increased up to 12 h, when it reached the maximum of fluorescence. • In the group without cHP, the signal appeared only 4 h after injection. • NPS were also present in the peripheral organs. • The signal in the brain administered with cHP-NP were significantly stronger than the ones without the cyclic peptide.	[29]
PLGA-PEG	–	Adult female Fischer F344 rats	Intracranial	Paclitaxel	• Bioluminescence *in vivo* imaging	• Bioluminescence signal of the tumor for the group treated with with Paclitaxel-NPs was 45% of the control group 2 weeks post--intratumoral administration	[237]
RGD-PF-DP	–	U87MG glioma bearing Male BALB/c nude mice (18–22 g)	Intravenous	Doxorubicin, Paclitaxel	• *In vivo* Near--infrared optical imaging	• The signal in the group treated with the RGD-micelles was stronger at 48 h post-injection compared to the group without RGD. However, the micelles accumulated in the brains of both groups. • Accumulation of RGD-micelles in the heart, liver and spleen was lower than that of micelles without the peptide.	[265]
DSPE-PEG2k-Ome, 3helix bundle	–	U87MG glioma bearing Male athymic nu/nu rats (250 g)	Intravenous	–	• PET/MR imaging • Autoradiography	• Large blood vessels in the tumour centre and highly localised glioblastoma. • 21 h post-injection of the micelles, they were accumulated within the tumour, first in the centre and later on the periphery of the tumour. • Autoradiography confirmed the enhanced tumour radioactivity shown in the PET/MR images.	[267]
SN-38 loaded micelles	–	9L glioma/U87MG glioma bearing Normal Fischer 344 rats (250 g, 12 weeks old)	Intracranial (CED)	NK012	• MRI	• Clearly defined distributions of the micelles were observed immediately after infusion.	[102]
PEtOz-SS-PCL	–	C6 glioma bearing Male ICR mice (18–20 g)	Intravenous	Doxorubicin, Paclitaxel	• Real-time fluorescence imaging • Bioluminescence	• Fluorescence intensity of free doxycycline was almost inexistent where as the intensity for the micelles loaded with doxycycline was significantly higher, mainly in the tumour region. • Fluorescence in peripheral organs was similar in the all the groups administered with micelles. • The tumour size by day 24 was approximately 12 fold bigger than at day 10 post-implantation.	[105]
RI-VAP, d-VAP, l-VAP	–	U87MG glioma bearing Male BALB/c nude mice (4–6 weeks old)	Intravenous	Paclitaxel	• Real-time imaging *in vivo*	• RI-VAP and d-VAP led to the highest intratumoural fluorescence intensity, reaching its peak at 1 h post-injection. • Semi-quantitative analysis of *ex vivo* organ images displayed strong fluorescence accumulation in tumours.	[106]
PLGA-T7 peptide	–	U87-Luci glioma bearing Male BALB/c nude mice (18–22 g)	Intravenous	Carmustine (BiCNU®)	• Bioluminescence • Real-time imaging *in vivo*	• Signal accumulation at the mice's tumour region on the group treated with the T7-micelles. • These were less present in the liver when compared to the group treated with micelles without T7. • The concentrations of both type of micelles were similar in the peripheral organs.	[108]
Pegylated liposomes		9L gliosarcoma bearing Male Sprague-Dawley rats (200 g)	Intravenous	Doxorubicin	• MRI	• Tumour in the group treated with doxorubicin only grew exponentially even after treatment, which was not seen in the group treated with doxorubicin and focused ultrasound.	[121]

Cholesterol-TAT		Kunming mice, Wistar rats (8 weeks old, 220–250 g)	Intravenous	Doxorubicin	• Near-infrared *in vivo* fluorescence imaging	• Four hours post-injection there was a defined fluorescent signal on the brains from the treated group, which became stronger after 12 h and 24 h. The control groups displayed weak signals.	[143]
HSPC/DOPE/Chol/CTAB/Didodecyldimethylammonium bromide		C6 glioma bearing Adult Sprague-Dawley rats (200–220 g)	Intravenous	Doxorubicin	• Real-time *in vivo* fluorescence • MRI	• In the treated group with only liposomes the tumour growth was still almost not detected 7 days post-transplantation and it occupied half of the semicerebrum by day 25, but it had a weak fluorescent signal. • In the group treated with liposomes and focused ultrasound, the fluorescent signal was very strong. • The groups treated with liposomes and focused ultrasound was the one with higher tumour growth inhibition.	[125]
DPPC:PTX:DSPE-PEG2000:cholesterol		U87MG glioma bearing Male BALB/c mice (6–7 weeks old, 18–22 g)	Intravenous	Paclitaxel	• MRI	• The tumours in the untreated group showed exponential growth pattern up to 38 days post-tumour implantation. • The group treated without liposomes but with focused ultrasound showed similar tumour growth. • The group treated with liposomes only showed a delay in the tumour growth up to 2 weeks, but afterwards the tumour continued to grow. • On the combined treatment group the tumour growth was suppressed during the 4 weeks of treatment.	[323]
LPNP		GBM43/MGG8 glioma bearing Athymic nude male/female mice (6–8 week old)	Intracranial	RNAi	• Bioluminescence	• The fluorescent signals suggest that the administration of the RNAi--LPNP significantly reduced the tumour growth when compared to the LPNP alone.	[158]
QD-aptamer32		U87 glioma and U87-EGFRvIII glioma bearing Male C57BL/6 athymic nude mice (68 weeks old)	Intravenous	–	• MRI • Real-time fluorescence *in vivo* imaging	• Tumour was visible days post-infusion. • In the U87-EGFRvIII group, animals administered with the QD-Apt had strong fluorescence signals in the tumour region whereas the group treated with QD alone had negligible fluorescence signals. • The groups with U87 tumours showed no significant fluorescence in any of the treated groups.	[188]
PARKINSON'S DISEASE							
Chitosan	–	Haloperidol induced Parkinsonism Adult Swiss albino mice (20–40 g)	Intravenous, intranasal	Bromocriptine	• SPECT (Gamma scintigraphy imaging)	• Significant higher radioactivity observed in the brain after intranasal administration when compared to intravenous administration • Signal was weaker in the intranasally administered group in the gastrointestinal tract. • The intravenously administered group had a strong signal in the tract	[44]
PEG-PLGA	Odorranalectin	Adult Female ICR mice (25–30 g),	Intranasal	Urocortin peptide	• Real-time *in vivo* imaging • Fluorescence and light imaging	• Eight hours post-administration the fluorescent intensity in the brain of the treated group increased. • The increased fluorescence intensity in the odorranalectin was also seen in the peripheral organs.	[51]
ALZHEIMER'S DISEASE							
NLC		Sprague-Dawley rats (180–220 g)	Intravenous	Curcumin	• *In vivo* and *ex vivo* imaging	• Fluorescent signal was significantly stronger in the brain in the group administered with the lactoferrin-coated NLCs when compared to the NLC alone.	[170]
Ceria nanoparticles (CeNP) combined with iron oxide nanocrystals (IONC)		Male Sprague-Dawley rats (300–320 g)	Intracranial	(Methylene blue), T807 ligand	• MRI • PET	• Stronger MRI signal in the group treated with the CeNC/IONC/MSN--T807, showing enhanced retention. These results were further confirmed by PET.	[199]
CEREBRAL PALSY							
PAMAM	NAC	E. coli endotoxin injected Newborn New Zealand white rabits	Intravenous	N-acetyl-L-cysteine (NAC)	• PET	• There was an increased brain uptake of the dendrimer in the CP groups when compared to the controls, where there was no CP but the dendrimers were also administered.	[88]
STROKE (CEREBRAL ISCHEMIA/ICH)							
Heparin-Poloxamer188		MCAO/reperfusion Adult female Sprague-Dawley rats (230–270 g)	Intranasal	bFGF	• MRI	• The different treatments lead to the significant reduction in the infarcted area to distinct extents at 24 h post-injection. • The highest recovery was seen in the group of bFGF-loaded lipossome. • Even 21 days after treatment the long term therapeutic effect was seen.	[138]

(continued on next page)

Table 4 (*continued*)

Nanosystem tested		In vivo model	Route of administration	Therapeutic cargo	Bio-imaging assessment	Outcome of bio-imaging assessment	Ref
Core polymer	Surface modification						
Graphene oxide nanosheet	Tat peptide and mPEG	Middle cerebral artery occlusion induced nude mice	Intravenous	Pirfenidone	• Photoacustic imaging	• GO alone cannot penetrate the BBB, whereas the ones carrying pirfenidone can. This combination provides both effective treatment and monitoring of the brain.	[334]
Ceria nanoparticles loaded with Iron-Mesoporous silica nanoparticles	Lipid coating	Injection of collagenase VII in Male Sprague-Dawley rats (8-weeks)	Intracranial	(Ceria)	• MRI	• Three and five days post-injection, there was a decrease in the signal intensity on the group administered with the nanoparticles since they were likely being uptaken by macrophages.	[196]
MULTIPLE SCLEROSIS							
SLN		Cuprizone-induced Adult C57BL mice (8 weeks old, 30–50 g)	Intravenous	Methylprednisolone, Coumarin 6 (dye)	• *In vivo* real time imaging	• Very strong signal coming from the brain in the SLN-injected animals, showing that the accumulation of these was much higher than the free coumarin-6. • There is no significant difference between the two antibodies used to coat the SLNs.	[174]

therefore, a convenient technique to use for the tracking of the nano systems and to confirm their bio-distribution.

In vivo bioluminescence imaging: This tool is based on the detection of the natural light emission from tissues or organs, through the oxidation of luciferin, which produces photons [341]. Since it is versatile, fast to obtain (in minutes) and allows an analysis upto a depth of centimetres, it is mostly used to track tumor progression (gliomas in the case of the CNS), bacterial infections and therapeutic efficacy [338,341]. This was generally applied to follow the tumor growth/regression upon days or weeks [105,108,158,237]. Nance E et al. (2014) showed for instance that paclitaxel-loaded PLGA particles led to the decrease of 45% of tumor volume two weeks post administration [237]. A similar trend was seen upon the intracerebral injection of large porous nanoparticles (LPNP) with RNAi, where the size of the tumor decreased significantly two weeks later [158]. Besides the assessment of the efficacy of these systems, bioluminescence also allowed the confirmation of the establishment of the glioma model in the mice [105,108].

Mass Spectrometry Imaging (MSI): This technique can be considered as a blend of bio-imaging, histology and molecular assessments since by definition it falls short to be labelled as only one of these approaches. MSI is used to identify and visualize the spatial distribution of numerous different molecules such as proteins, lipids, metabolites or biomarkers through their molecular masses (mass spectrometry-based assessment), allowing the correlation of the chemical organisation of the sample with its physical features in a label-free manner [342]. Briefly, the mass spectrum of each spot of a tissue section is collected during the scanning of the tissue with an ionisation beam and the relative abundance of each analyte will generate a proportional signal, which will translate into a distribution map of intensities [342]. This results in molecular images of the samples which will be created from the information coming from the microprobe (laser ion beam) and the "microscope" (2D position-sensitive detector).

There are several different types of MSI based on the ionization method, but the ones most often used to analyse the brain in animal models are Matrix-Assisted Laser Desorption Ionization (MALDI) imaging and Laser-Ablation Inductively Coupled Plasma MS (LA-ICP MS).

MALDI imaging involves the deposition of matrix on the tissue, which aids in the analyte desorption and ionisation [342]. It has the advantage of being able to detect multiple large molecules simultaneously and, therefore, has been used in pharmacodynamics and toxicodynamic studies [343]. In the case of brain disorders, it was used in combination with silver nanoparticles to visualize lipids and to analyse their changes in rat models of TBI [344–346]. The use of silver nanoparticles is of interest since they tend to bind to lipids, which allows them to segregate from the surrounding salts, facilitating their imaging [347]. Gold nanoparticles have also been used with this aim [348]. So far MALDI in the brain has been mostly used to investigate the changes seen in analytes upon disease. However, there is an emerging field exploring its potential for the study of BDNS, both in terms of distribution as well as in terms of efficacy [349].

In the case of LA-ICP MS the laser beam is used to ablate particles from the sample, which will be transported to a new detector for digestion and ionization of the sampled mass, comprising a very quick and accurate technique for elemental analysis [350]. It is broadly used in diverse fields, but in the case of the life sciences, particularly on the brain, it is mainly focused on metal-protein interactions [351–353]. For this reason it is becoming attractive to use in combination with MRI and the detection of its contrast agents [354,355]. Regarding its use for the assessment of the efficacy of treatments in the brain, Koppen et al (2015) have used LA-ICP MS to assess and quantify the presence of platinum to evaluate the toxic effects of cisplatin (chemotherapeutic drug platinum-based) [356]. However, in this case the drug was not administered in combination with any nanoparticle system. On the other hand, LA-ICP MS in association with MRI has been used separately to assess the efficacy of DNA-loaded liposomes in a rodent brain [357]. Even though this was not tested yet to assess the functional action of the

nanoparticles in any disease model, it shows the promising use of this method with that aim.

To sum up, the higher cost of these macroscopic imaging modalities makes them less widely used within the pre-clinical studies. However, since they offer numerous advantages, mainly the possibility of accompanying in real time the distribution of a pharmaceutical nano-system or the progression of a disease without the need to sacrifice the animal, their use always enables a valuable assessment of the site of action and therapeutic effect of the agents, and are thus widely used within the clinic.

Table 4 is an extensive review of the different bio-imaging techniques used in the context of distinct brain disease animal models where nano-delivery systems were employed.

3.3. Molecular assessment

3.3.1. Chromatographic techniques and Mass spectrometry

Bio-distribution/Organ bio-distribution: Temporal analysis of bio-distribution of therapeutic cargo delivered by nanoparticles (NPs) has been performed in various studies. For the analysis of bio-distribution, tissue and blood samples are collected, including the glioma, heart, liver, spleen, lungs, kidneys and brain. The organ samples are weighed and snap frozen at −80°C for analysis whereas the blood samples are further processed into plasma. This is usually followed by the solvent extraction of the required metabolite followed by its detection using either the chromatographic techniques (High Performance Liquid Chromatography (HPLC), Ultra Performance Liquid Chromatography (UPLC), Gas Chromatography (GC)) [146,358,359] or mass spectrometry [24]. This analysis is imperative to determine if there is any significant potential toxic impact of the NPs. NPs showing higher accumulation in the heart could be at the risk of potential toxicity. Several studies affirm the observation that non-targeted NPs show a marked accumulation in liver and kidneys. However, addition of surfactant (PS-80 or Tween-80) [26] or targeting moieties (lactoferrin [50,170] or transferrin [101,268]) on the surface of NPs facilitate higher permeability of these NPs across BBB and boosts their accumulation in brain.

Brain distribution: The aforementioned techniques are also used for evaluation of regiospecific distribution of therapeutics in the brain using nano-delivery systems [98,238]. Use of targeting strategies such as conjugation to TAT peptide [143] or Angiopep-2 [28] enriches the tumor accumulation of therapeutic NPs, thereby minimising the potential toxicity caused by non-specific tissue accumulation of the anti-tumor drugs. In some cases, the presence of the targeting moiety enhanced the plasma clearance of the targeted NPs [28]. The majority of the studies have validated the increase in brain to plasma concentration of therapeutics at different time points of investigation when the NPs are functionalized by targeting moieties [89,360].

Striatal levels of analytes: This is particularly relevant to nano-delivery systems with PD as the disease target. DA can act as a source of a 6-OHDA which potentiates the progression of the disease [361]. This analysis involves the estimation of DA and its metabolites, dihydroxyphenylacetic acid (DOPAC) and homovanillic acid (HVA) in the striatum of NP-treated vs control animals. There is a significant reduction in the levels of DA and its metabolites (DOPAC and HVA) as compared to the age-matched controls [362]. Augmented levels of DA and/its metabolites is symbolic of successful therapeutic regimen for PD as it restores the depleted DA levels and its metabolism in the lesioned animals [363].

Pharmacokinetics: Pharmacokinetics is the time course study of drug metabolism *in vivo*. This encompasses several kinetic parameters such as C_{max}, T_{max}, $AUC_{0-\infty}$,elimination rate constant (K_e) and mean residence time (MRT) which outline the drug bioavailability, distribution and clearance. C_{max} is the maximum (or peak) serum concentration that a drug achieves in a specified area of the body after it has been administrated and before the administration of a second dose and t_{max} denotes the time at which the C_{max} is observed. K_e is the measure of the rate at which the drug or therapeutic is eliminated from a system and $AUC_{0-\infty}$, is the area under the plot for the therapeutic concentration in blood or tissue of interest vs time. AUC represents the parametric valuation of bioavailability and higher values of $AUC_{0-\infty}$ in the brain implies higher drug uptake. MRT is indicative of the average time spent by the drug in body. UPLC, HPLC and Mass Spectrometry (MS) [28,313,363] have been used in different studies for determination of the pharmacokinetic traits of different BNDS. It is one of the customarily used assessment schemes which summarises the performance of brain-delivery nano-systems in various animal models and establishes the efficacy of the system for therapeutic delivery *in vivo*.

For nasal administration, two new parameters evaluating the efficacy of drug targeting using nano-systems through the intranasal(i.n.) pathway are: percent brain targeting efficiency (DTE%) and direct transport percent (DTP%) which are calculated using the formulae as reported by Md et al. [44].

$$\mathrm{DTE}(\%) = \left[(\mathrm{AUC}_{\mathrm{brain}}/\mathrm{AUC}_{\mathrm{blood}})_{0-24,\mathrm{i.n.}}/(\mathrm{AUC}_{\mathrm{brain}}/\mathrm{AUC}_{\mathrm{blood}})_{0-24,\mathrm{i.v.}}\right] \times 100$$

$$\mathrm{DTP}(\%) = \left[(\mathrm{AUC}_{0-24,\mathrm{brain,i.n.}} - F)/\mathrm{AUC}_{0-24,\mathrm{brain,i.n.}}\right] \times 100$$

Where $F = (\mathrm{AUC}_{0-24,\mathrm{brain,i.v.}}/\mathrm{AUC}_{0-24,\mathrm{blood,i.v.}}) \times \mathrm{AUC}_{0-24,\mathrm{blood,i.n.}}$, $\mathrm{AUC}_{0-24,\ \mathrm{brain,\ i.n.}}$ is the area under the curve of brain following i.n. administration, $\mathrm{AUC}_{0-24,\ \mathrm{brain,\ i.v.}}$ is the area under the curve of brain following i.v. administration, $\mathrm{AUC}_{0-24\ \mathrm{blood,\ i.v.}}$ is the area under the curve of blood following i.v. administration, and $\mathrm{AUC}_{0-24\ \mathrm{blood,\ i.n.}}$ is the area under the curve of blood following i.n. administration.

It has been reconfirmed through studies across multiple disease models (glioma, PD, AD, stroke) that surface modifications of NPs using targeting moieties or surfactants improve their pharmacokinetic properties as well as brain targeting. This also minimises the concerns associated with the uptake or redirection of NPs into reticuloendothelial system (RES) of other organs. Soni et al. (2008) [364] demonstrated a five-fold reduced accumulation of liposomes in liver when they were conjugated to transferrin in a glioma animal model. Wilson et al. (2008) also demonstrated reduction in the uptake of PBCA NPs by RES by coating the NPs with PS-80 for drug delivery application in AD [38].

3.3.2. Spectrophotometry

Oxidative and nitrosative stress: The brain is known to be abnormally susceptible to oxidative damage due to the presence of high level of fatty acids which are more prone to peroxidation and to consume a gigantic proportion of total oxygen uptake. Additionally, the scarcity of antioxidant defences which constitute only about 10% of other organs like the liver as well as a higher level of iron and ascorbate, renders the neural cells more liable to oxidative damage [365,366]. Neurodegenerative disorders are characterized by the progressive loss of neurons translating to loss of motor functions and/or cognition which can be attributed to a complex interplay of factors including oxidative stress and free radical generation [367]. ROS and reactive nitrite species (RNS) include hydrogen peroxide (H_2O_2), nitric oxide (NO), superoxide anions and the highly reactive hydroxyl and monoxide radicals ($OH\cdot$, $NO\cdot$). Endogenous antioxidant architecture keeps the ROS generated from mitochondria, NADPH oxidase (Nox), and xanthine oxidase (XO) at relatively low levels [368].

Accumulation of misfolded proteins constitutes the pathogenesis of several neurodegenerative disorders such as AD and PD and is responsible for activation of microglia and astrocytes. PD is signalized by large cytoplasmic inclusions of α-synuclein in the neurons of substantia nigra called Lewy bodies [369]. Impaired mitochondrial activity reflected in the inhibition of complex I and complex II/III of the mitochondrial electron transport by MPTP causes PD in human beings [370]. Heightened levels of proteins and DNA [371], lipid oxidation [372] and decreased levels of reduced glutathione (GSH) [373] are an

integral part of the pathophysiology of PD. Aggregated human α-synuclein causes activation of microglia and DAergic neurodegeneration [374] and stimulates astrocytes to produce inflammatory modulators [375]. Elevated RNS levels leading to nitration of α-synuclein facilitates the neuroinflammatory responses [376]. Involvement of ROS in apoptosis and caspases chain activation leads to the neuronal loss observed in PD [377].

Oxidative stress induced in AD plays a crucial role in the pathogenesis of AD which is established by the presence of markers of oxidative stress in autopsied brains from AD patients [378]. In AD pathology, Aβ peptide produced in the AD brain activates microglia and astrocytes. Aβ accumulation also distorts the mitochondrial respiratory function, increase ROS production, and changes mitochondrial membrane potential in various brain regions [379,380]. Abatement in the activities of oxidative metabolism enzymes including α-ketoglutarate dehydrogenase complex, pyruvate dehydrogenase complex and cytochrome oxidase was observed in patients with AD [381].

Brain ischemia has been identified as the most common ground for strokes as it results in decreased blood flow to brain, thereby preventing the adequate delivery of oxygen and others nutrients leading to metabolic distortions and probable cell death [382]. Oxidative stress plays a significant role in neuronal death paving the way to acute brain ischemia (ABI) in a series of pathophysiological events. Reperfusion, while it partially replenishes oxygen regionally, and thereby restores neuronal viability, also facilitates the activation of oxidant enzymes and mitochondria resulting in the release of free radicals. This, coupled with arrested detoxification systems and expenditure of antioxidants, causes the breach of the normal antioxidative defence of brain [383]. Significant damage is caused by the free radicals via the impairment of lipids, proteins, and nucleic acids [367].

ROS induce genotoxicity and interrupt vital cellular processes through their interactions with nucleic acids and regulatory proteins, inducing chromosome aberrations and modifying the gene expression patterns. Alterations in regulatory proteins such as oncogenic variant epidermal growth factor receptor variant III (EGFRvIII) causes further accumulation of ROS in the cells and promotes further alterations in the genome of GBM cells [384]. ROS can also mediate varied biological effects which can be successfully harnessed for therapeutic development to target cancer cells in the brain given their high basal metabolic rate [385,386]. Oxidative therapy in GBM exploits the increase in ROS levels to trigger apoptosis or necrosis resulting in cell death [384]. In this case, the therapeutic cargo employs the molecules capable of acting as direct inhibitors of tumor and/or in sensitizing tumor cells to initial treatment.

Augmentation of ROS and RNS is extremely difficult to measure quantitatively in either *in vitro* or *in vivo* systems under pathophysiological conditions as they have extremely short half-lives. However, DNA, lipids, proteins and carbohydrates are altered by ROS *in vivo* and can serve as markers of oxidative stress that are modified by interactions with ROS. These alterations are, therefore, detected using several biochemical assays evaluated through spectrophotometry which cover all the facets of ROS defence mechanisms *in vivo*.

(1) Lipid peroxidation (TBARs)/Malondialdehyde (MDA) assay: This assay is used for determining the level of MDA, which is a marker for lipid peroxidation. Thiobarbituric acid (TBA) assay is the most commonly used method for determination of the MDA in animal tissues [387] which involves spectrophotometric detection of reaction products at 532 nm. However, due to the non-specificity of TBA reactivity with MDA and cross-reactivity with other aldehydes produced as a result of lipid peroxidation, TBA reactive substances (TBARs) are more frequently used as a marker of oxidative stress [388].

(2) Reduced GSH estimation: Reduced GSH is a component of the endogenous antioxidant system which facilitates ROS scavenging and H_2O_2 clearance by reducing it to water. The oxidative stress phenomenon in several brain diseases involve reduction in the levels of GSH which promotes neuronal death by impairing peroxide clearance and elevation of ROS levels [389]. Reduced GSH is estimated using the protocol from Jollow et al. (1974) involving spectrophotometric detection at 412 nm [390].

(3) Glutathione peroxidase (GSHPx) assay: The first step of superoxide neutralization involves SOD catalysing the conversion of superoxide anion into H_2O_2, which is still a potentially harmful ROS. Catalase and GSHPx catalyze conversion of H_2O_2 generated to water and oxygen. However, the expression of catalase in neurons is lower than it is in other organs [391], GSHPx takes the lead in detoxifying H_2O_2 after cerebral ischemia and reperfusion. The enzyme activity is determined by the amount of NADPH oxidized at 340 nm [392]

(4) Glutathione reductase (GR) assay: Glutathione reductase catalyzes the reduction of oxidized glutathione (GSSG) to the reduced form (GSH) in the presence of NADPH as a cofactor. GR is a very important part of antioxidant repertoire against free radicals and ROS as well as protein and DNA biosynthesis, which maintains a high ratio of GSH/GSSG [393]. It involves the spectroscopic determination of NADPH disappearance at 340 nm [392]. It seems to have a significant impact in cerebral ischemia as observed through various genetic models [394] however, the neuronal cell loss in neurodegenerative processes are unlikely to result from reduced activity of brain glutathione peroxidase [395].

(5) Superoxide dismutase (SOD) assay: Manganese superoxide dismutase (SOD2) converts superoxide ion to hydrogen peroxide and serves as the primary defence against mitochondrial oxidative stress. SOD plays a vital role in protection against free radical damage in reperfusion injury and aids the reduction of infarct size during ischemia and reperfusion [396]. It is also a cause of degeneration of neurons in the basal ganglia and brainstem and progressive motor disturbances in the neurodegenerative disease pathophysiology [397]. Its activity is determined by spectrophotometric measurements at 560 nm according to the method described by Kono et al. (1978) [398]

(6) Catalase assay: Catalase is responsible for neutralizing H_2O_2. It has been found to be more impactful than glutathione peroxidase in neurons [399] and may be an alternative source for oxygen, thereby aiding neuroprotection under hypoxic conditions [400]. Catalase activity is determined spectrophotometrically using the protocol Claiborn et al. (1985) at 240 nm [401].

(7) NADH dehydrogenase (NDH)/Complex I assay: Mitochondria are known to be the production factories of ROS in the cells [402]. One of the major causes of neuronal death after cerebral ischemia and reperfusion injury is the reduction in mitochondrial enzyme complex. There is a significant impairment in mitochondrial enzyme complex I (NADH dehydrogenase), that is observed in ischemia reperfusion injured animals. Inhibition of mitochondrial complex I has been one of the proposed mechanisms for DAergic neuron loss in MPTP induced Parkinsonism [403]. Levels of NADH dehydrogenase is estimated spectrophotometrically using the protocol described by King et al. (1967) at 550 nm [404]

(8) Succinate dehydrogenase (SDH) activity/Complex II assay: Inhibition of Complex II has been shown to be involved in neurodegeneration and in eliciting motor impairments in rodent models [405]. Complex II is estimated using MTT assay which is spectrophotometrically determined at 420 nm [406].

(9) Nitrite estimation: NO is a very important signalling molecule in CNS under physiological conditions, which when present in excess displays neurotoxicity and an ability to induce neuronal apoptosis. This was demonstrated by the attenuation of NO-induced apoptosis using antioxidants and reduction in the antioxidant treatments facilitated the NO-mediated neuronal apoptosis [407]. In the case of tumors in the brain, subsequential

impact of NO includes amongst others exggarated proliferation, evasion of apoptosis and acquiring chemotherapeutic resistance [384]. NO estimation is done spectrophotometrically using Greiss reagent [408].

This set of biochemical assays has been used in several studies involving the brain-targeted nano-delivery systems addressing the question of their impact on the oxidative stress in various disease models like PD [272], AD [359] and cerebral ischaemia [63].

Acetylcholinesterase (AChE) activity: AChE is a crucial enzyme in the cholinergic nervous system which is responsible for scavenging acetylcholine, a neurotransmitter associated with memory and learning and quelling its physiological action. AChE interacts with Aβ peptides and promotes the formation of amyloid fibrils [409]. In PD patients with dementia, AChE inhibitors like rivastigmine shows long term therapeutic action through improvement of cognition [410]. Therapeutic approaches in AD focus on the inhibition of AChE and post-mortem analysis after the delivery through nano-systems involve estimation of the AChE activity [359] using the protocol elucidated by Ellman et al. [411] involving spectrophotometric detection at 412 nm.

3.3.3. Scintigraphy

Radiolabelled NPs serve diverse functions that include region-specific irradiation for tumor therapy, imaging and determination of *in vivo* pharmacokinetics of the NPs. In regards to their application for brain delivery, they have been widely used to determine the tissue-specific distribution of these radio-labelled NPs and their efficacy in delivering the encapsulated or conjugated cargo into the brain [176,364,412]. Three cardinal approaches to radiolabel the NPs involve direct labelling, chelator-facilitated labelling and radiolabelling the cargo. The most frequently used radionuclide used for BNDS is a short-lived metastable isotope of technetium (^{99m}Tc). The extensive application of ^{99m}Tc in these studies is attributed to its short half-life (approximately 6 h), a suitable ɣ photon emission energy that is suitable for imaging while catering effectively ti patient safety, ready commercial availability and ease of labelling a broad range of targets [413]. However, certain studies have employed ^{125}I and ^{3}H for labelling the therapeutic cargo [33,136]. Serum stability analysis, which investigates the stability of the radiolabelled complexes in serum reveal the *in vivo* stability upon administration into the animals [414,415]

Most studies employing NPs for brain delivery have used direct conjugation protocols, chiefly using the labelled NPs for estimation of brain uptake of the therapeutic cargo and its accumulation in other organs including liver, lungs and heart etc. Also, scintigraphy studies have been performed across a spectrum of brain disorders from glioma to neurodegenerative and psychotic disorders.

These studies involve the administration of these radiolabelled NPs through various routes followed by isolation and weighing of different organs and screening them under a gamma scintillator for evaluation of NP uptake. The radiolabelled NP uptake is mostly expressed/unit weight of the organ and as a fraction of administered dose [414]. The observed radioactivity in brain and plasma over time is converted into a compatible format for the analysis for different pharmacokinetic parameters using appropriate software. Detailed pharmacokinetic analysis that includes investigation of brain targeting using scintigraphy was demonstrated by Shadab et al. (2013) [44] and Kang et al. (2016) [136]. This analysis uses radioactivity for estimation of pharmacokinetic parameters like T_{max}, C_{max}, AUC and systemic clearance of NPs. Shadab et al. (2013) also probed into the brain targeting efficiency of the NP formulation for intranasal transport. Besides the use of radiolabelled NPs for bio-distribution and pharmacokinetic analysis, these NPs can also be employed for the live imaging of drug distribution following different routes of injection. This could be used to determine the preferred administration route.

3.3.4. Proteomic analysis using ELISA/WB/FC

A protein analysis toolset for investigating BNDS mainly comprises ELISA (Enzyme-linked immunosorbent assay), western blot (WB) and flow cytometry (FC). These techniques are applicable chiefly to address three end points: valuation of the therapeutic delivery, inflammatory response and toxicity elicited by the administration of the NPs.

Under the physiological conditions, cytokines show a low constitutive expression in the brain [416]. On being subjected to inimical changes in the microenvironment in CNS through trauma, infection or ischemic attack, the cytokines are activated by glial cells [417]. These pro-inflammatory cytokines have been shown to interact with the adhesion molecules, where they promote the disease pathophysiology, through induction of cell adhesion molecules (CAM) leading to alteration of the blood-brain barrier integrity. The expression of CAM molecules at BBB like intracellular adhesion molecules (ICAM-1) and vascular cell adhesion protein-1 (VCAM-1) expression at the BBB augments leukocyte entry during autoimmune and neuro- inflammatory diseases [418]. Persistent and unconstrained inflammatory modulations disrupt the fine balance between pro and anti-inflammatory cytokines, further aggravating the neuronal injury.

The panel of cytokines tested as a measure of inflammation in the studies dealing with BNDS includes tumor necrosis alpha (TNF-α), IL-1β, IL-6, IL-10, ICAM-1 & VCAM-1 [359]. Of these, TNF-α, IL-1β, IL-6 constitute the pro-inflammatory cytokine panel and IL-10 represents the anti-inflammatory repertoire. TNF- α is most frequently used marker for outlines inflammation in the majority of these studies [43,359,419]. Another category of molecules detected using ELISA is the adhesion molecules ICAM-1 & VCAM-1. In the traumatic brain injury model, ELISA was used to determine the levels of BDNF in brains isolated from injured site and unlesioned sham animals following the administration of PLGA NPs. This revealed that poloxamer 188 coated NPs had a better targeting profile and a higher concentration of BDNF was detected in brain tissues [418].

Western blot, on the other hand, has been used predominantly to detect the cellular and signalling proteins from the total brain extracts. Few examples include TH and α-synuclein pre- and post- therapeutic NP treatment [186], bFGF levels in brain following its delivery using gelatin NPs [165] and estimation of signalling molecules [36]. Fewer studies used flow cytometry to study the cellular markers after NP treatment to show the enhanced proliferation of specific cell types [329].

3.3.5. Gene analysis

Brain-specific gene expression analysis is another strategy employed for assessing the efficacy of therapeutic nano-delivery systems using qPCR for probing into inflammation, gene knockdown and signalling. RNA used for this analysis is either extracted from the whole brain extracts or specific regions in the brain to demonstrate the region-specific modulation of genes in response to therapeutic delivery. Ismail et al. (2013) [131] investigated the impact of nano-formulation of rivastigmine on the expression of BACE-1. IL- 1β and AChE, in the cerebral cortex, all of which are instrumental in progression of AD and reduction in levels of which are indications of success of therapeutic delivery. It has also been used to explore the impact of gene knockdown in a human GBM model that utilizes Polo-Like Kinase 1 (PLK1) siRNAs (siPLK1) which reduced the expression by 80% [153].

A summary of molecular assessment of different nano-delivery systems addressing different disease targets in brain has been presented in Table 5.

3.4. Behavioural assessment modality for nano-delivery systems

3.4.1. Parkinson's disease

Drug-induced rotations: There is an established relationship between the degeneration of the dopaminergic system and the disruption of motor function. Here an unilateral loss of DA system in hemiparkinsonian models can recreate an experimental scenario where

Table 5
Overview of molecular strategies used for evaluating the therapeutic efficacy of BNDS used in pre-clinical settings.

Nano-delivery systems	Animal model	Route of administration	Therapeutic cargo	Parameters assessed	Tools for molecular assessment	Outcome of molecular evaluation	Ref.
GLIOMA							
PS-80 coated PBCA NPs	Wistar rats	Intavenous	Doxorubicin	Organ bio-distribution	HPLC	• Higher retention of PS-80 coated NPs in circulation. • Reduced accumulation in reticuloendothelial system (RES) ofPS-80 coated NPs. • High brain accumulation doxorubicin through PS-80 coated NPs.	[19]
PS-80 coated PBCA NPs	Wistar rats	Intravenous	Doxorubicin	Distribution in brain fractions	HPLC	• High doxorubicin detection in brain homogenates of PS-80 coated PBCA NP treatment at all time points. • Two-fold increase in supernatant concentration of doxorubicin indicative of higher transport across BBB.	[420]
Transferrin-conjugated D-alphatocopheryl polyethylene glycol 1000 succinate (vitamin E TPGS or TPGS) micelles	Charles Foster rats	Intravenous	Doxorubicin	Brain distribution	HPLC	• Higher drug accumulation in brain in targeted micelle treatment compared to the non-targeted micelles.	[98]
Tat modified MPEG/PCL micelles (MPEG-PCLTat)	Sprague-Dawley C6 tumor model	Intravenous, intranasal	Coumarin-6	Organ bio-distribution	Spectrofluorometry	• Less coumarin detected in non-target tissues through i.n. MPEG-PCLTat treatment than free drug administration. • Stronger fluorescence detection for i.n. than i.v. administration of nanomicelles in brain. • Equal fluorescence detection for both inoculated and non-inoculated sides in i.n. administration contrary to i.v. showing no enhanced permeation and retention with i.n. administration.	[98]
Aptamer functionalized PEG-PLGA NPs	Nude mice bearing glioma xenografts, Sprague-Dawley rats	Intravenous	Paclitaxel (PTX)	• Pharmacokinetic analysis • Organ bio-distribution	LC-MS/MS	• Significantly longer PTXNP and Ap-PTX-NP elimination half-life, slower clearance rate (CL), smaller elimination rate constant and higher AUC than free PTX • Tumor PTX concentration: Ap-PTX-NP > PTX-NP > Taxol™	[24]
Focussed ultrasound and microbubble enabled liposomes	U87MG tumor bearing Nude mice	Intravenous	Paclitaxel (PTX)	• Pharmacokinetic analysis • Organ bio-distribution	HPLC	• Greater accumulation (3 fold) of PTX in tumor for FUS+MB+PTX-LIPO treatment compared to PTX-LIPO. • Accumulation in liver(12.81%) and kidney (27.89%) reduced for FUS+MB+PTX-LIPO treatment.	[323]
PS-80 coated PBCA NPs	Wistar rats with syngenic cerebral tumor	Intravenous	Temozolomide (TMZ)	Organ bio-distribution	HPLC	• Decrease in TMZ accumulation in heart and kidneys following encapsulation in NPs. • Higher accumulation of TMZ in brain especially in PS-80 coated PBCA NPs treatment.	[26]
Transferrin coupled liposomes	Albino Wistar rats	Intravenous	5-fluorouracil	Organ bio-distribution	Scintigraphy	• Low accumulation (fivefold) in liver for coupled liposomes. • High brain targeting of coupled liposomes compared to uncoupled (10 fold) and free drug solution (17 fold).	[364]
PS-80 coated PBCA NPs	Fischer rats	Intravenous	TGF β2-antisense oligonucleotides (AON)	TGF-β2 concentration in plasma & lymphocyte subsets	• Flow cytometry • ELISA	• Significant reduction in TGF β2 in active specific immunization and AON combined treatment compared to other groups. • Combined therapy resulted in significant	[329]

						elevation of the rate of activated CD25+ T cells which correlated with survival.	
TAT-modified cholesterol liposomes (TAT-LIP)	Kunming mice, C6 glioma implanted Wistar rats	Intravenous	Doxorubicin (Dox)	Brain bio-distribution	HPLC	• Higher concentration of Dox detected in brain for all time points for Dox-TAT-LIP treatment compared to free Dox and other liposomal fomulations.	[143]
Angiopep-2-conjugated poly(ethylene glycol)-copoly(ε-caprolactone) Polymersomes (Ang-PS-DOX)	C6 glioma implanted Wistar rats	Intravenous	Doxorubicin (Dox)	• Pharmacokinetic study • Brain bio-distribution	HPLC	• DOX encapsulation in PS decreased plasma clearance. • Angiopep-2 modification increased PS blood clearance. • -DOX-PS and Ang-PS-DOX showed significantly lower DOX accumulation in the heart and Ang-PS-DOX showed higher accumulation in tumour compared to other regions in brain and other treatments.	[28]
Hyaluronan-grafted lipid-based NPs	U87MG tumor bearing Nude mice	Intratumor	Pololike kinase 1 (PLK1) siRNA	Pololike kinase 1 (PLK1) in vivo silencing	qPCR	• 80% knockdown in U87MG CD44v6^{+} cells treated with siPLK1 that was delivered via HA-LNPs.	[153]
Nanostructured lipid carrier (NLC)	Nude mice bearing A172 xenografts	Intraperitoneal	Curcumin (Cur)	Organ bio-distribution	HPLC	• AUC values: Cur-NLC increased the blood levels of Cur by 6.4-fold. • NLC-Cur generated higher levels than Cur in the xenografts.	[288]
Nanostructured lipid carrier (NLC)	Wistar rats	Intranasal	Curcumin (CRM)	Organ bio-distribution	HPLC	• Higher concentration of curcumin in brain was observed for CRM-NLC treatment than free drug solution.	[152]
Compritol® based SLNs	Wistar rats	Intraperitoneal	Resveratol	Organ bio-distribution	HPLC	• 6 fold higher uptake of resveratol when administered as SLNs as compared to free solution with reduced uptake by RES.	[151]
Precirol® and Compritol® based SLNs	BaLB/c mice, C6 glioma implanted NMRI mice	Oral	Edelfosine	Pharmacokinetic study	UHPLC–MS/MS	• Higher brain accumulation of drug when administered in SLNs rather than free solution. • High tissue/plasma ratios of 4.5 and 12.4 for Precirol® and Compritol® LN compared to free drug solution.	[146]
PS-60/80 stabilized Cetyl palmitate (CP) based SLNS	Wistar rats	Intravenous	Camptothecin (CPT)	Organ bio-distribution	HPLC	• For heart, kidneys, and spleen, CPT concentrations were similar for the drug incorporated into SLN and in suspension which decreased in liver and lungs. • Higher accumulation in brain of SLNs treatment compared to free suspension.	[148]
PLGA NPs	Wistar rats	Intrastriatal	Carboplatin	Tissue retention	ICP-MS detection	• Carboplatin NPs showed higher in vivo retention in brain.	[421]
PS-80 coated PBCA NPs	Sprague-Dawley rats	Intravenous	Methotrexate (MTX)	Brain and CSF distribution	HPLC	• PS-80 coated NPs double Cmax and AUC in CSF compared to MTX solution. • PS-80 coated NPs triple Cmax and AUC in cerebellum and cerebrum. • NP size<100 nm: more drug transport to brain and CSF.	[81]
RI-VAP/D-VAP conjugated PEG-PLA micelles	U87MG Tumor bearing Nude mice	Intravenous	Paclitaxel (PTX)	Pharmacokinetic analysis	HPLC	• No impact of peptide modifications on circulation time of micelles.	[311]
c(RGDyK)PLA-PEG micelle (PP)	U87MG tumor bearing Nude mice	Intravenous	Docetaxel (DTX)	• Pharmacokinetic study • Brain distribution	HPLC	• Higher AUC for micellar formulations (3–4 fold) compared to free drug indicating longer circulation time. • Brain targeting and accumulation: RDPP>DPP>DTX solution (1 h post administration)	[103]
Poloxamer-407 (P407) nano-micelles	Bioluminescent	Intravenous	Panobinostat(LBH589)	Synaptophysin asaay	ELISA		[422]

(continued on next page)

Table 5 (*continued*)

Nano-delivery systems	Animal model	Route of administration	Therapeutic cargo	Parameters assessed	Tools for molecular assessment	Outcome of molecular evaluation	Ref.
	syngenic F98/Fischer344 rat glioblastoma model					• No difference between animals treated with P407/aCSF compared to aCSF-treated and untreated controls indicative of no potential neuronal toxicity of nano-micelles.	
Transferrin-coated PLA (Tf-PLA) NPs	C6 glioma-bearing Sprague-Dawley rats	Intra-arterial (carotid)	3-bis(2-chloroethyl)-1-nitrosourea (BCNU)	Organ bio-distribution	Single-photon emission computed tomography (SPECT)	• 2.5 fold increase in brain/plasma radioactivity ratios for Tf-PLA compared BSA-PLA indicative of higher brain targeting	[15]
ALZHEIMER'S DISEASE							
Solanum tuberosum lectin (STL) conjugated PEG-PLGA NPs	$A\beta_{25-35}$ induced Sprague-Dawley rats	Intranasal	Basic fibroblast growth factor (bFGF)	• Pharmacokinetic study • Brain bio-distribution • Choline acetyltransferase (ChaT) activity in hippocampus	• Scintigraphy • ChAT activity assay	• STL modification promotes absorption in nasal cavity and brain transport. • Higher concentration in olfactory bulb than cerebellum and cerebrum. • High AUC values for STL-bFGF-NPs indicate enhanced brain delivery. • High DTI% and DTP% for i.n. STL-bFGF-NPs shows its best brain targeting efficiency compared to other formulations and i.v. administration. • -2.04 folds increase in ChaT activity in i.n. STL-bFGF-NPs treatment group compared to AD controls indicative of significant disease amelioration.	[33]
THR peptide conjugated gold nanoparticles (AuNP-THR)	Sprague-Dawley rats	Intraperitoneal	Cys (C) modified β-sheet breaker peptide LPFFD, (CLPFFD)	Brain targeting	Instrumental neutron activation analysis (INAA)	• Increased accumulation of AuNP-THR--CLPFFD and AuNP-CLPFFD compared to AuNP-THR : possible relation to the structure of peptides after conjugation. • Increased brain accumulation by conjugation to THR peptide. • High uptake by RES due to negatively charged surface.	[302]
Liposomes(PEG-DSPE, DDAB)	Albino rabbits	Intranasal	Rivastigmine	Pharmacokinetic study	LC-MS/MS	• Liposomes permeated through the nasal mucosa, long circulation time with MRT of 3.5 ± 0.3 h in comparison to 1.1 ± 0.1 h in case of solution. • Liposomes maintained a sustained increase in brain levels upto 4 h.	[363]
Liposomes	$AlCl_3$ induced Wistar rat model	Subcutaneous	Rivastigmine	Biochemical analysis • Plasma- CRP Hcy • ADMA • Brain-AChE • ATPase Gene expression in cortex • IL-1β • BACE-1 • AChE	• Spectrophotometry • RT-PCR	• Liposomal formulation restored the activity of AChE and ATPase to normal levels whereas drug solution significantly reduced the AChE and enhanced ATPase activity. • Reduction in plasma levels of CRP, Hcy and ADMA was attained by both liposomal and solution formulations compared to $AlCl_3$ controls. • Gene expression of all the tested genes was significantly reduced by solution and restored to normal levels by liposomal formulation.	[131]
Solid lipid nanoparticles (SLNs)	Isoproterenol induced Wistar rats	Intravenous	Galantamine hydrobromide (GH)	Inflammatory changes in brain • TNF-α • IL-1β	ELISA, Spectrophotometry	• Chronic administration of GH-SLNs improves efficacy of BM-MSCs in inhibition of pro-inflammatory cytokines and restoring the anti-inflammatory cytokines deficits.	[172]

				• IL-6 • IL-10 • ICAM-1 • VCAM-1 • Brain BDNF • Tau protein Biochemical analysis Oxidative stress		• Higher attenuation of oxidative stress profile by chronic administration of GH-SLNs with BM-MSCs compared to BM-MSCs alone. • Restoration of BDNF and Tau protein content by GH-SLNs administered with BM--MSCs compared to BM-MSCs alone.	
Solid lipid nanoparticles (SLNs)	$AlCl_3$ induced Wistar rats	Intravenous	Quercetin	• MDA activity • GSH activity • SOD activity • Cat activity • Nitrite activity • AChE activity • BuChE activity Biochemical analysis: oxidative stress	Spectrophotometry	• Quercetin-loaded SLN significantly ameliorated oxidative stress.	[168]
Solid lipid nanoparticles (SLNs)	$A\beta_{25-35}$ induced Sprague-Dawley rats	Oral	Chrysin (CN)	• Lipid peroxidation • Glutathione levels • Nitrite levels • Biochemical analysis: Oxidative stress • TBARS activity • GSH activity • GPx activity • SOD activity • Cat activity • GR activity • AChE activity • Ascorbic acid levels	Spectrophotometry	• Significant restoration of TBARS and GSH levels by low doses of CN-SLNs compared to CN. • Restoration of catalytic activities of anti--oxidant enzymes by low doses of CN-SLNs compared to CN. • Ascorbic acid levels were significantly increased by low doses of CN-SLNs compared to CN.	[173]
Chitosan NPs (CS-NPs)	Colchicine induced Wistar rats-	Intranasal	Piperine (PIP)	Biochemical analysis • Oxidative stress : MDA activity • Total Antioxidant Capacity (TAC) • SOD activity ACHe activity Brain toxicity analysis • Casapase-3 activity • TNF-α levels	• ELISA • Spectrophotometry	• PIP-NPs decreased MDA, increased SOD and TAC; restoring it to the level of negative controls. • PIP-NPs restored AChE activity indicating retrieval and retention of memory processes. • PIP-NPs restored Casapase-3 activity and TNF-α levels comparable to donepezil but failed to fully reverse the colchicine--induced damage.	[43]
PS-80 coated solid lipid nanoparticles (SLNs)	Ibotenic acid induced albino rats	Intraperitoneal	Piperine (PIP)	Biochemical analysis: oxidative stress • SOD activity • AChE activity	• Spectrophotometry • HPLC	• P-80-PIP-SLN treatment showed a significant and prolonged reduction in oxidative stress compared to other groups and at levels comparable to Donepezil. • Slow and sustained release profile in brain for P-80-PIP-SLN treatment compared to free drug which rapidly declined after treatment.	[331]
Solid lipid nanoparticles (SLNs)	Streptozotocin (STZ) induced- Wistar rats	Oral	Sesamol	Biochemical analysis: oxidative-nitrosative stress • SOD activity • AChE activity • MDA activity	• Spectrophotometry • ELISA	• Antioxidant profile (SOD, Cat, GSH, MDA) improved by administration of both sesamol and sesamol-SLNs, significant difference 16 mg/kg dose. • Nitrite levels reduced by both sesamol and sesamol-SLNs significant difference at 16 mg/kg dose.	[171]

(continued on next page)

Table 5 (*continued*)

Nano-delivery systems	Animal model	Route of administration	Therapeutic cargo	Parameters assessed	Tools for molecular assessment	Outcome of molecular evaluation	Ref.
				• GSH activity • Cat activity • Nitrite assay • TNF-α levels		• TNF-α levels reduced by both sesamol and sesamol-SLNs, significant difference at 8 and 16 mg/kg doses.	
Lactoferrin-modified LDL-mimic nanocarrier (Lf-mNLC)	$A\beta_{1-42}$ and d-gal induced Sprague-Dawley rats	Intravenous	Curcumin (Cur)	Biochemical analysis: oxidative stress (MDA)	Spectrophotometry	• MDA levels reduced for Lf_H-mNLC group was 1.50 and 2.68 folds of that in NLC and Cur solution group.	[170]
Liposomes	$A\beta_{1-42}$ induced Wistar rats	Intravenous	Cardiolipin (CL)	• AChE • Lipid peroxidase activity	Spectrofluorometry	• AChE activity reduction: Curcumin < WGA-Curcumin-LIP <WGA-Curcumin-CL/-LIP. • -Malondialdehyde (MDA) levels: Curcumin < WGA-Curcumin-LIP <WGA-Curcumin-CL/LIP.	[134]
(PEG-PLA) di-block polymer micelles	AD model Tg2576 mice	Oral	Curcumin	Pharmacokinetic study	LC-MS/MS	• Six fold higher MRT and AUC for encapsulated curcumin in brain compared to free curcumin. • No difference in tetrahydrocurcumin levels between the two formulations.	[35]
PLGA NPs	Aβ-Induced Wistar rats	Intraperitoneal	Curcumin (Cur)	• Hippocampal curcumin accumulation • Gene expression and protein analysis • TCF/LEF and Cyclin-D1 levels	• HPLC • Western blot • qRT-PCR • Luciferase • reporter assay	• Increased relative mRNA expression of neurogenic genes like β-tubulin, neuroD1, DCX, neurogenin, neuroligin, neuregulin • Down-regulation of transcription factor Stat3 in the hippocampus of Cur-PLGA-–NP-treated rats.	[36]
PS-80 coated PBCA NPs	Wistar rats	Intravenous	Rivastigmine	Organ bio-distribution	HPLC	• NP encapsulation enhances drug accumulation in RES. • PS-80 coating reduces accumulation in liver and spleen. • PS-80 enhances brain drug targeting compared to free drug.	[37]
PS- 80 coated PBCA NPs	Wistar rats	Intravenous	Tacrine	Organ bio-distribution	HPLC	• NP encapsulation enhances drug accumulation in RES. • PS-80 coating reduces accumulation in liver and spleen. • PS-80 enhances brain drug targeting 4.07 times compared to free drug.	[38]
PLGA NPs (TFB-NPs) and solid lipid nanoparticles (TFB-SLNs)	Sprague-Dawley rats	Intranasal	Tarenflurbil (TFB)	Pharmacokinetic study	HPLC	• Biovailability: TFB-NPs (i.n.) > TFB-SLNs (i.n.) > TFB solution (i.n.) > TFB suspension (oral). • TFB-NPs showed better pharmacokinetic profile with 1.2 times higher AUC, 2.5 times higher $t_{1/2}$, and 2.6 times lower k_e than TFB-SLNs. • Highest brain delivery by TFB-NPs compared to TFB-SLNs and other groups.	[41]
PARKINSON'S DISEASE							
Chitosan NPs (CS NPs)	Haloperidol induced Swiss albino mice	Intravenous, intranasal	Bromocriptine (BRC)	• Pharmacokinetic study • Organ bio-distribution	Scintigraphy	• Brain accumulation i.n. > i.v in BRC-CS NPs treatment. • i.n. administration showed higher accumulation in stomach and intestine contrary to liver, lungs and spleen in i.v. administration. • Brain/blood ratio: BRC CS NPs (i.n.)> BRC CS NPs(i.v.)> BRC solution. • High DTI, DTP% and $AUC_{(i.n.)}/AUC_{(i.v.)}$ revealed the mucoadhesive impact of NPs	[44]

						• Gamma scintigraphy revealed higher uptake of BRC through i.n. pathway than i. v.	
Gelatin nanostructured lipid carriers (NLCs)	6-OHDA induced rat model	Intranasal	Basic fibroblast growth factor (bFGF)	• Brain distribution, Striatal levels of Dopamine and Metabolites	• Western blot • HPLC	• DA, DOPAV and HVA levels enhanced by bFGF-GNLs/IN significantly. • Elevated DA levels by bFGF-GNLs/IN treatment ≈ 37% of sham. • bFGF significantly increased in olfactory bulb and striatum, not in prefrontal cortex or hippocampus with bFGF-GNLs/IN treatment.	[165]
PLGA NPs	6-OHDA induced Wistar rat model	Intravenous	Dopamine	• Striatal levels of dopamine and metabolites • Dopamine-D2 receptor assay	• HPLC • Scintigraphy • Scatchard analysis	• Dopamine & metabolites: Double infusion of DA-NPs >Single infusion>PD model • Decrease in striatal ^{3}H-spiperone binding: Double infusion of DA-NPs >Single infusion> PD model.	[45]
Sterically stabilized targeted Liposomes (SSL-T)	Sprague-Dawley rats	Intravenous	GDNF	Brain uptake	ELISA	• High AUC and GDNF uptake by GDNF--SSL-T compared to conventional liposomes and free GDNF.	[140]
Cerium oxide NPs (CeO_2NPs)	6-OHDA induced Wistar rat model	Intraperitoneal	-	Biochemical analysis in brain • Striatal dopamine levels • TBARS & MDA levels • Caspase-3 activity • Nitrite levels Reduced to oxidized glutathione (GSH: GSSG) ratio	• HPLC • Spectrophotometry	• Normalization of striatal dopamine levels, TBARS, MDA and caspase activity levels by 0.5 mg/kg dose of CeO_2NPs, while significantly ameliorated by 1mg/kg and unaffected by 0.1mg/kg. • 1mg/kg dose administration increased oxidative stress cortical, striatal and hippocampal tissues whereas 0.1 and 0.5 mg/kg doses had no adverse impact after three weeks.	[184]
NGF-coated NIPAM derivative based magnetic NPs (NP-NIPAm-AA)	MPTP induced C57BL/6 mice	Intraperitoneal	α-synuclein RNAi plasmid	• Brain levels of α-synuclein • Tyrosine hydroxylase (TH)	Western blot	• Up-regulation of TH and a down--regulation of α-synuclein in brain tissue after treatment with magnetic NPs with plasmid.	[186]
OX26 Mab conjugated PEGylated liposomes (PLs) (PILs)	Medial forebrain bundle transection induced Sprague-Dawley rats	Intravenous	Dopamine (DA)	• Pharmacokinetic study • Brain uptake	Scintigraphy	• Moderate increase in retention in plasma through encapsulation in PD rats. • 14 (PLs) and 16 fold (PILs) increase in AUC. • 8 fold increase in brain uptake though PILs compared to free dopamine in PD rats.	[136]
PS-80 coated PLA NPs	MPTP induced C57BL/6 mice	Intraperitoneal	Resveratol (RVT)	Biochemical analysis: • TBARS levels	Spectrophotometry	• No significant difference was found between animals from control and MPTP plus PLA-PS80 loaded RVT groups.	[49]
Lactoferrin conjugated PAMAM NPs	6-OHDA induced Sprague-Dawley rat model	Intravenous	Human GDNF gene (hGDNF)	• Striatal levels of Dopamine and Metabolites	HPLC	• Multiple dosing increased DA, HVA and DOPAC content more than single dose. • 5 dose regimen increased monoamine neurotransmitter levels by 70% (DA), 90% (DOPAC) and 90% (HVA)	[87]
Lactoferrin conjugated PEG-PLGA NPs (Lf-NPs)	6-OHDA induced Sprague-Dawley rat model	Intravenous	Urocortin (UCN)	• Organ bio-distribution • Striatal levels of Dopamine (DA)and Metabolites (DOPAC and HVA)	HPLC-ECD	• $AUC_{(Lf\text{-}NP)}$=2.49($AUC_{(NP)}$, $C_{max(Lf\text{-}NP)}$=2.36 $C_{max(NP)}$ (Lf facilitates brain uptake) • Lf-NP concentrated in heart and spleen--potential toxicity issues. • DA, DOPAC and HVA levels significantly higher in Lf-NP treatment compared to PBS controls- Lf-NPS increase DA content.	[50]
Odorranalectin PEG–PLGA NPs (OL-NPs)	6-OHDA induced Sprague-Dawley rat model	Intranasal	Urocortin (UCN)	Striatal levels of Dopamine (DA) and Metabolites (DOPAC and HVA)	HPLC-ECD	• DA levels: OL-NP/UCN(=9.1 OL-NP) >NP/-UCN • DOPAC levels: OL-NP/UCN≈ NP/UCN> OL-NP • HVA levels: OL-NP/UCN≈ NP/UCN> OL-NP	[51]

(continued on next page)

Table 5 (*continued*)

Nano-delivery systems	Animal model	Route of administration	Therapeutic cargo	Parameters assessed	Tools for molecular assessment	Outcome of molecular evaluation	Ref.
Chitosan NPs	Wistar rats	Intraperitoneal	Dopamine (DA)	Striatal levels of Dopamine (DA)	HPLC	• Pulsate release of DA was observed for different doses of NPs thus avoiding the potential neurotoxicity associated with prolonged release of DA.	[52]
Lactoferrin conjugated PEG-PLGA NPs (Lf-NPs)	KM mice	Intranasal	Rotigotine	Brain distribution	LC-MS/MS	• Sustained brain delivery • Targeted delivery to brain : $AUC_{Lf\text{-}NPs}$ (Brain/Plasma)=1.89 • High delivery to all regions of brain compared to uncoated NPs.	[54]
Glycol chitosan/sulfobutylether-β-cyclodextrin (GCS, CS) NPs	Wistar rats	Intranasal	Dopamine (DA)	Striatal levels of Dopamine (DA) and Metabolites (DOPAC and NA)	HPLC	• Single administration: no impact on DA, NA and DOPAC levels. • Repeated administration: Significantly higher DA levels in ipsilateral striatum of DA GCS/DA-CD NPs. • No impact on DOPAC and NA levels across both striatum after DA GCS/DA-CD NPs administration.	[55]
EPILEPSY							
N,N-dimethylacrylamide-based PEGylated polymeric NPs (PNPs)	PTZ-induced acute seizure Wistar rat model	Intraperitoneal	Gamma aminobutyric acid (GABA)	GABA concentration in *Stratum corsatum*	• GABA ELISA Kit • EIA analyser	• No significant differences in GABA levels between NP formulations and GABA solution.	[423]
PLGA NPs	Sprague-Dawley rats	Intravenous, Intranasal	Lorazepam	• Bio-distribution • Pharmacoscintigraphy analysis	Scintigraphy	• Brain accumulation: -^{99m}TcLzp-PLGA-NPs (i.n.)> ^{99m}Tc-LS (i.n.)> ^{99m}Tc-LS(i.v.) • Sustained release from PLGA NPs and higher brain uptake due to transport from nose-brain pathway.	[412]
Nano-lipid carriers (NLC)	MES-induced acute seizure Wistar rat model	Intranasal, intraperitoneal	Valproic acid (VPA)	Bio-distribution	Gas chromatography	• Brain-plasma ratio of VPA was higher for i.n. administration of NLCs than i.p. administration at much lower dose at all time points.	[172]
Pluronics® (L121 and P123) based polymeric micelles (PM7)	Swiss Albino mice	Intravenous, Intranasal	Clonazepam (CZ)	• Bio-distribution • Pharmacoskinetics analysis	Radiochemical yield assessment	• Brain accumulation: CZ-PM7 (i.n.)> CZ-PM7(i.v.)≈CZ(i.n) • Blood levels : CZ-PM7(i.v.)> CZ(i.n) > CZ-PM7 (i.n.) • Higher C_{max} and AUC indicate high brain targeting for CZ-PM7 (i.n.). • Relative bioavailability 812.96% and 11.83% for brain and blood for CZ-PM7 (i.n.).	[270]
PSYCHOSIS							
Tween 80 coated chitosan NPs	Ketamine-induced Swiss albino mice model	Oral	Doxycycline hydrochloride (DC)	Biochemical estimation in brain: TNF-α estimation, AChE activity estimation Neurochemical estimation: DA & GABA level	Spectrofluorometry, Spectrophotometry	• TNF-α levels, GSH levels: DCNP= Olanzapine>DC solution>Ketamine treated animals (lower doses in NP effective as higher dose in free drug formulation) • AChE levels: Olanzapine>DC solution= DCNP =Ketamine treated animals • Decrease in DA levels and increase in GABA levels: DCNP=Olanzapine>DC solution>Ketamine treated animals (greater drug bio-availability for NPs due to tween 80 coat).	[61]
Cationic liposomes	Wistar rats	Intranasal	Risperidone (RSP)	Pharmacokinetic study	HPLC	• Drug concentration in brain higher at all time points for all liposomal than i.v. administration of free drug.	[424]

						• LP-16 shows high MRT indicating higher half-life and longer circulation time with better brain uptake.	
Solid-lipid nanoparticles (SLNs)	BalB/C mice	Intranasal, Intravenous	Risperidone (RSP)	Pharmacokinetic study, bio-distribution	Pharmacoscintigraphy	• RSP concentration in brain following i.n. administration of RSLNs higher than both RSLNs (i.v.) and RS (i.v.). • Higher Cmax and t 1/2 for RSLNs (i.v. and i.n.) compared with RS (i.v.) indicates higher brain uptake, sustained release, and reduction in P-gp efflux from the SLNs.	[425]
Nano-lipid carriers (NLCs)	Swiss albino Wistar rats	Intranasal	Duloxetine (DLX)	Brain bio-distribution	HPLC	• Brain concentration higher with i.n. DLX--NLC than free DLX solution.	[179]
Nano-lipid carriers (NLCs)	Charles-Foster rats	Intranasal, intravenous	Asenapine (ASN)	Pharmacokinetic study	LC-MS/MS	• 1.34 and 2.68 times higher bioavailability of drug in plasma and brain, respectively after i.n. administration of ASN-NLCs compared to ASN. • 2.07 folds increase in brain targeting through i.n. administration of ASM-NLCs compared to i.v.	[177]
Solid-lipid nanoparticles (SLNs)	Ketamine-induced Albino rats	Oral	Quercetin fumarate (QF)	Biochemical analysis • Analysis of excitatory (glutamate) and inhibitory (GABA) amino acids • Catecholamines: norepinephrine (NE), serotonin (5-HT) and DA	HPLC	• QF administration ameliorated the disturbance of the neurotransmitters with more pronounced effect in rats treated with QFSLN, in a dose-dependent manner. • Amelioration of disturbances in GABA and glutamate in the cortex and hippocampus of brain tissues by QF and QF-SLNs; with more pronounced effect in rats treated with QFSLN, in a dose-dependent manner.	[178]
PAMAM NPs	Sprague-Dawley rats	Intranasal, intraperitoneal, oral	Haloperidol	Brain and plasma distribution	LC-ESI-TOF-MS	• Highest concentration detected for i.p administration and No detection in oral administration at the same dose as i.n.	[89]
STROKE (CEREBRAL ISCHEMIA/ICH)							
Polymeric NIPAM NPs	MCAO Wistar rat model	Intranasal	Curcumin (Cur), demethoxycurcumin (DMC), and bisdemethoxycurcumin (BDMC)	Biochemical estimation in brain: • GPx • GR • Lipid peroxidation • SOD activity • CAT activity	Spectrophotometry	• Antioxidant system (GPx, GR, SOD, CAT): Protected using Cur, DMC, BDMC nanoformulations: Cur-NPS (100 μg/kg: best) -Lipid peroxidation: attenuation in TBARS level in all nanoformulations: Cur-NPS (100 μg/kg: best)	[63]
Solid-lipid nanoparticles (SLN)	BCCAO induced Wistar rat	Oral	Curcumin (Cur)	Oxidative-nitrosative stress parameters: • MDA • GSH Cytosolic SOD • CAT activity Nitrite estimation • NADH dehydrogenase activity SDH activity	Spectrophotometry	• Free curcumin didn't affect the Oxidative--nitrosative stress parameters which were restored to sham levels using SLNs.	[426]
Cilostazol (CLZ)NPs	MCAO ICR mice model	Intravenous	-	• Pharmacokinetic study • Brain distribution	HPLC	• CLZ concentration on non-infarct side was equal for CLZ NP treatment, lower concentration was found on the infarct side for 0.1mg/kg dose. • Pharmacokinetic parameters similar for CLZ solution and NPs i.v.	[64]
OX26 antibody conjugated PEGylated cationic solid lipid NPs (OX26-PEG-CSLN)	MCAO induced Sprague-Dawley rats	Intravenous	Baicalin	• Pharmacokinetic study • Excitotoxic index (EI)	• LC-MS/MS • HPLC	• Two peak values of baicalin after injection and reperfusion observed in CSF, high levels for OX26-PEG-CSLN group. • AUC and C_{max} for OX26-PEG-CSLN 5.69	[161]

(continued on next page)

Table 5 (*continued*)

Nano-delivery systems	Animal model	Route of administration	Therapeutic cargo	Parameters assessed	Tools for molecular assessment	Outcome of molecular evaluation	Ref.
						and 6.84 fold higher than free drug. • Significant reduction in EI by OX26-PEG--CSLN compared to curcumin solution restoring the imbalance between excitory and inhibitory amino acids.	
Chitosan NPs (CS-NPs)	MCAO induced Wistar rat model	Intravenous, intranasal	Rutin	• Pharmacokinetic study • Brain targeting	UPLC	• High AUC in brain, lungs, plasma for CS-NPs compared to free rutin. • High DTE% and DTP% for i.n. CS-NPs treatment show higher brain bioavailability.	[332]
PS-80 coated PLGA NPs	MCAO induced Wistar rat model	Intravenous	Acetylpuerarin (AP)	• Pharmacokinetic study • Brain targeting	HPLC	• Increased AUC, Cmax and prolonged MRT and $t_{1/2}$ for AP-CS NPs than AP solution in brain. • Increased AUC and prolonged MRT in all tissues and higher C_{max} in brain and spleen following encapsulation.	[69]
PLGA NPs	MCAO induced Sprague-Dawley rat model	Intravenous, intrajugular, and internal carotid arterial route	Superoxide dismutase (SOD)	Brain targeting	HPLC	• NP uptake in brain: Carotid artery≈ 13 folds (Tail vein/jugular vein) administration.	[70]
RADA16-I self-assembling peptide nanofiber scaffolds (SAPNS)	Type VII collagenase induced ICH Sprague-Dawley rat model	Intrastriatal	-	Hematoma volume	Spectrophotometry	• No significant differences between aspiration only, saline and SAP group. • Significant reduction of hematoma volume by aspiration.	[333]
Nano-tubular Pluronic/phosphatidylcholine/polysorbate 80 mixed micelles (PPPMM)	SAH induced albino wistar rat model	Oral	Nimodipine (NM)	Brain and plasma pharmacokinetic	UPLC-MS/MS	• Improved bioavailability (232%) and longer circulation time of PPPMMs compared to NM solution. • Improved bioavailability but no impact on circulation time in brain for PPPMMs compared to NM solution.	[427]
Quercetin nanoemulsion	Type VII collagenase induced ICH Wistar rat model	Intraperitoneal	Quercetin	• GSH levels in brain • TAC • GST activity in brain • TBARS assay for lipid oxidation	• Spectrofluorometry • Spectrophotometry	• Significant increase in striatal GSH levels in quercetin nanoemulsion treatment. • Preservation of GST and TBARS levels and decresed oxidant capacity by quercetin nanoemulsion treatment after ICH compared to other treatments.	[428]
Redox polymer self-assembled nanoparticles (nitroxide radical-containing nanoparticles [RNPs]	1-MHz focused ultrasound sonication coupled with microbubble treatment induced ICH Sprague-Dawley rat model	Intravenous	-	• 8-hydroxy-2′-deoxyguanosine (8-OHdG) levels in DNA	• ELISA	• Significant suppression of 8-ODdG by RNP administration after ICH induction as compared to control animals.	[429]
PLGA nanoparticles	Intracranial endovascular perforation induced Sprague-Dawley SAH model	Intraperitoneal	Curcumin	• Glutamate Concentration in CSF • COX-2, CINC-1, IL-1β, IL-6, iNOS, ICAM-1, MCP-1, MIP-2, and TNF-α expression • IL-1β, IL-6, TNF-α, MDA, 3-NT, and 8-OHDG levels	• Glutamate assay • RT-PCR • ELISA	• Curcumin NP treatment (20mg/kg) significantly attenuated Glutamate increase in CSF after SAH. • Curcumin-NPs reduced SAH-induced neuroinflammation in brain as indicated by the mRNA expression of chemokines and cytokines. • Curcumin-NPs hindered oxidative stress after SAH as indicated by ROS production and anti-oxidant markers.	[73]
TRAUMATIC BRAIN INJURY							
Poloxamer 188 coated PLGA NPs	Weight-drop C57BL/6N mice model	Intravenous	BDNF	Brain BDNF levels	ELISA	• BDNF levels increased in uncoated NP treatment only ipsilaterally.	[419]

						• Poloxamer 188 coated NPs increased BDNF levels both ipsi-and contra-laterally.	
PAIN MODEL Poloxamer 188 or PS 80 coated PLGA-PEG-PLGA NPs	ICR mice model	Intravenous	Loperamide	Brain distribution	HPLC	• Higher brain accumulation of surfactant coated NPs than controls. • Poloxamer188 more effective than PS-80 for brain targeting (AUC for Poloxamer 188 NPs= 1.68 (PS-80 NPs).	[430]
FUNGAL INFECTIONS Angiopep-2 modified PE-PEG polymeric micelles (PE-PEG-Angiopep)	Sprague-Dawley rats, ICR mice	Intravenous	Amphotericin-B (AmB)	• Organ bio-distribution • Pharmacokinetics	HPLC	• Brain uptake: PE-PEG-Angiopep AmB> PE-PEG AmB> AmB. • Biodistribution comparable for micellar formulations- decreased accumulation in spleen compared to AmB. • Higher AUC (83% and 63% for PE-PEG AmB and PE-PEG-Angiopep AmB)and lower total clearance (46%) values for micellar formulations than free drug.	[112]

pharmacologically induced DA release occurs only on one side. In various rodent models, this imbalance is manifested as a vigorous rotational behaviour after treatment with amphetamine or apomorphine. Spiking of unilateral DA transmission triggered by the administration of these drugs induces a rotational behaviour towards the side ipsilateral (amphetamine) or contralateral (apomorphine) to the DA abundance. These two drugs are most commonly used to relate the behavioural impact to the extent of lesioning and consequently to test the efficacy of various neuro-reparative and neuro-restorative therapeutics. It was observed that ipsilateral amphetamine-induced rotation could stem from 50% depletion of striatal DA, whereas more than 90% depletion was necessary to effect the contralateral apomorphine-induced rotations [431]. DA receptor agonists like apomorphine cause the direct stimulation of supersensitive postsynaptic receptors on the lesioned side, which results in contralateral rotations [432]. This effect is, however, observed only in highly lesioned models (>90%) because of the compensatory mechanisms in the surviving neurons, which bar the accretion of supersensitive postsynaptic receptors. In contrast to this, amphetamine releases DA from nigrostriatal terminals through presynaptic action, which are more abundant on the unlesioned side and cause ipsilateral circling, [433]. The elicited rotational behaviour is quantified as turns per minute versus time in a specially designed 'rotometer' where the animal moves on a spherically shaped surface while connected to the registering device by a thin wire [51,434,435]. A major proportion of the studies investigating the functional recovery post-treatment using BNDS as summarised in Table 6 have used apomorphine induced rotations for behavioural assessment [48,50,51,312]. A significant reduction in apomorphine-induced contralateral rotations was observed in 6-OHDA lesioned animals after the treatment with lactoferrin (lf) conjugated PEG-PLGA nanoparticles (lf-NP) [50]. These nanoparticles were loaded with urocortin peptide which has been reported to arrest the development of 6-OHDA induced PD pathophysiology as reported by Abuirmelleh et al. [436]. In this study and several others, the authors have demonstrated superior brain targeting and minimal side-effects associated with BNDS by coupling them to the vectors with specific receptors on the BBB [48,51,87]. Higher brain targeting and sustained release of the therapeutic cargo also translates to better functional recovery in rotational analysis than that of the controls. Drug induced rotations have been widely used in both mice and rat models.

A major drawback of the rotational analysis is the ambiguity resulting from sensitization, conditioning or priming effects and compensation in the rotational behaviour by grafts or therapeutics while the other deficits remain unaddressed [437,438]. Simplicity, reproducibility and ease of automation are the most important advantages of rotation tests which makes them the most frequently used means of behavioural assessment for Parkinson's and its therapy.

Rotarod test: This test was first described by Rozas et al. (1997) [439] with consistent performance of lesioned rats with the progression of disease over time. The instrumental setup comprises an automated n-lane rotarod unit consisting of a rotating spindle and individual lanes for each rat. This is connected to a data and protocol (rotational speeds) management system. Infrared beams are used to detect when a rat has fallen onto the grids beneath the rotarod. Recorded parameters include the time of fall and time spent on the rotating rod with the experimental set-up parameters. Rozas et al. (1997) revealed that learning did not significantly affect test performance, with minimal differences between trained and naive rats. The inability of the lesioned animals to multitask and detrimental impact on equilibrium is well reflected using the rotarod test. Falling in the rotarod analysis also takes into account the loss of ability to apply force with the effected limbs and fatigue of the affected limbs caused by repeated motion [440,441]. In this test, a miscellany of the lesion-induced deficits manifests itself which becomes more evident as rotation speed is increased and this correlates very well to the inaccuracy of movement in PD patients [442]. This test was used to investigate the therapeutic efficacy of curcumin and piperine loaded NPs in a rotenone-induced PD model [328]. Rotarod analysis was used

Table 6
Behavioural assessment tools used to study the functional recovery through the application of BNDS in different brain disease targets.

Nano-delivery systems	Animal model	Route of administration	Therapeutic cargo	Behavioural assessment	Outcome of behavioural evaluation	Ref.
PARKINSON'S DISEASE (PD)						
Odorranalectin (OL) conjugated PEG-PLGA nanoparticles (OL-NP)	Hemiparkinsonian (6-OHDA induced Sprague-Dawley rats)	Intranasal	Urocortin peptide (UCN)	• Apomorphine-induced rotations (30 min)	• Rotational number in OL-NP/UCN group decreased significantly compared to other treatment groups.	[51]
Lactoferrin (lf) conjugated PEG-PLGA nanoparticles (lf-NP)	KM Mice and Hemiparkinsonian (6-OHDA induced Sprague-Dawley rats)	Intravenous	Coumarin-6 (fluorescent probe), Urocortin peptide (UCN)	• Apomorphine-induced rotations (15 min)	• Tight contralateral rotation significantly attenuated in Lf--NP-UCN5 treatment.	[50]
Angiopep-PEG conjugated-Dendrigraft poly-L-lysine (DPA)	Rotenone-induced Sprague-Dawley rats	Intravenous	Therapeutic gene (hGDNF)	Open field tests • Line crossing • Rearing • Head dips • Defecating • Inactive sitting	• Reinforced injections of DPA/hGDNF NPs markedly improve the locomotor activity and decrease the inactive time.	[451]
Rabies virus glycoprotein (RVG) peptide PEG-linked Dendrigraft poly-L-lysines (DGLs)	Rotenone-induced Sprague-Dawley rats	Intravenous	Caspase-3 short hairpin RNA coding plasmid DNA (pshC-3)	Open field tests • Line crossing • Inactive sitting	• High line crossing and low retention time in DPR/pshC-3 NPs injected group.	[450]
Polysorbate 80 (PS80)-coated Poly (lactide) nanoparticles	MPTP induced C57BL/6 mice	Intraperitoneal	Resveratol (RVT)	• Olfactory discrimination task • Social recognition task	• RVT-loaded PLA-PS80 nanoparticles treated animals spent significant higher time in the familiar compartment in olfactory discrimination task • Prevention of deficits in social recognition ability in RVT--loaded PLA-PS80 NP treatment.	[49]
Protamine-coated PLGA nanoparticles	6-OHDA induced C57BL/6 mice	Intraventricular	microRNA-124 (miR-124)	• Apomorphine-induced rotations (45 min)	• Boost of neurogenesis caused in miR-124 treated mice • Rescue of motor impairments of 6-OHDA-lesioned mice.	[48]
TiO_2-Dopamine Nanocomplex	Hemiparkinsonian (6-OHDA induced) Wistar rats	Stereotactic implantation into caudate nucleus	–	• Open field tests • Apomorphine-induced rotations (30 min)	• The number of crossing squares and rearing per 5 min in open field tests increased significantly in nanocomplexes treatment. • Significant reduction in turning behaviour was observed for animals treated with nanocomplexes.	[183]
Polymer–lipid hybrid NPs (PLN)	Chlorpromazine (CPZ) induced albino mice	Intranasal	Ropinirole	• Anti-tremor activity • Riserpine antagonism	• Significant reduction in CPZ induced tremors. • Reduction in riserpine induced rigidity and immobility with PLN treatment at lower doses.	[163]
Solid-lipid nanoparticles (SLN) incorporating glyceryl monostearate (GMS) and polyethylene glycol monostearate (PMS)	Hemiparkinsonian (6-OHDA induced) Wistar albino rats	Oral	Apomorphine	• Apomorphine-induced rotations (45 min)	• Enhanced rotations following administration of SLNs with GMS and PMS representing enhanced bioavailability.	[591]
Gelatin nanoparticles (GNP)	Hemiparkinsonian (6-OHDA induced) Sprague-Dawley rats	Intranasal, Intravenous	Neuropeptide Substance P	• Apomorphine-induced rotations (30 min)	• Motor recovery in terms of rotational behaviour in the order: intranasal SP-GNP > intravenous SP-GNP > intranasal SP solution > intranasal Blank GNP > intranasal PBS ≈ sham group.	[312]
PLGA nanoparticles	Hemiparkinsonian (6-OHDA induced) Wistar rats	Intranasal	L-3,4-Dihydroxyphenylalanine (L-DOPA)	• Placing task • Open field test • Vertical grid holding test • Footfault asymmetry test	• Coordination performance was significantly higher in animals treated with nano-DOPA in placing task. • No differences in animals' endurance, cognition and locomotor activity in response to any treatments. • Comparable scores for nano-DOPA group was similar to control animals in footfault asymmetry tests.	[47]
Magnetic Fe_3O_4 nanoparticles coated with oleic acid	MPTP induced C57BL/6 mice	Intraperitoneal	shRNA (short hairpin RNA) with photoactive NGF (AzPhNGF)	• Gait analysis • Open field test (15 min)	• NP treated mice more active than saline treated group in the open field test. • NPs improve the motor dysfunctions reflective in ambulation time and speed.	[186]
Surfactant-coated glyceryl monooleate (GMO) nanoparticles	Rotenone induced C57BL/6 mice	Oral	Curcumin and piperine	• Rotarod task	• Dual drug loaded NPs improve motor dysfunction by increasing the bioavailability and superior brain targeting.	[328]

Superparamagnetic iron oxide nanoparticles (IONPs)	Bilateral 6-OHDA induced Wistar rats	Intrastriatal	-(stimulated with electromagnetic fields (EMF))	• Open field test • Accelerated rotarod task • Gait analysis	• NP+MF rats showed significant recovery in locomotor activity. • A significant increase in post-surgery score in rotarod task suggesting the attenuation of postural stability deficit. • Significant impact on width of gait and overlap of limbs for NP and EMF post-surgery.	[443]
Thiol-capped and RGD peptide functionalized electromagnetized gold nanoparticles	MPTP induced C57Bl/6 mice	Intrastriatal	-(stimulated with electromagnetic fields (EMF))	• Rearing behaviour analysis • Open field test (10 min)	• EMF-exposed MPTP mice demonstrated striking restoration of movement in open-field tests. • Significant increase in rearing behaviour compared with controls.	[185]
Exosomes	6-OHDA induced C57BL/6 mice	Intranasal	Catalase (exoCAT)	• Apomorphine-induced rotations • (90 min)	• exoCAT treated mice exhibited significantly less rotations than PBS controls.	[296]
Solid lipid nanoparticles	Hemiparkinsonian (6-OHDA induced) Sprague-Dawley rats	–	Bromocriptine (BK)	• Bar test	• Action of encapsulated BK was more rapid in onset and prolonged in attenuating motor asymmetry.	[166]
OX26 murine monoclonal antibody (Mab) conjugated PEGylated immunoliposome (PIL)	Hemiparkinsonian (6-OHDA induced) Sprague-Dawley rats	Intravenous	TH expression plasmid	• Apomorphine-induced • rotations	• Immunoliposomes (PIL) treatment showed reduction in apomorphine-induced rotations.	[135]
Polysorbate 80 –coated cerasomes (CPC)	MPTP induced C57Bl/6 mice	Intravenous	Curcumin	• Rotarod task • Climbing pole task	• CPC with focused ultrasound treatment recovered more effectively than other groups in both the motor tasks.	[444]
Cerium oxide nanoparticles (CeO_2 NPs)	MPTP induced Wistar rats	Intraperitoneal	–	• Open field test (3 mintues) • Rotarod task • Stepping test	• In open field tests, Rats treated with 0.5 mg/kg of CeO_2 NPs optimal for reverting locomotor deficits. • Treated rats showed longer latency to fall on rota rod. • Reduction and delayed performance of right paw was normalized.	[184]
Alginate-curcumin nanocomposite (ACNC)	h-αS expressing PD flies	Culture media	Curcumin	• *Drosophila* climbing assay	• Significant delay in the loss of climbing ability.	[46]
PLGA nanoparticles	Hemiparkinsonian (6-OHDA induced) Wistar rats	Intravenous	Dopamine(DA)	• Amphetamine induced rotations • Spontaneous Locomotor Activity (SLA) through open field test	• A significant decrease in amphetamine-induced in DA- NP treatment, more pronounced in double dosed rats. • Locomotor activity was restored to Sham levels by DA-NP treatments.	[45]
VP025 phospholipid nanoparticles	Hemiparkinsonian (6-OHDA induced) Sprague-Dawley rats	Intramuscular	–	• Amphetamine induced rotations	• Injection of VP025 before lesion induction significantly reduced rotation rates at both doses tested.	[327]
Poly(butylcyanoacrylate) (PBCA) nanoparticles coated with polysorbate 80	MPTP induced C57Bl/6 mice	Intravenous	Nerve growth factor(NGF)	• Open field test (2 min) • Actometer (10 min)	• Improvement in locomotor activity in the "open field" reflected by increased horizontal movements and stride length. • Significant improvement over the MPTP treated animals in actometer measurements.	[53]
Chitosan nanoparticles (CS-NPs)	Haloperidol induced Swiss albino mice	Intranasal	Bromocriptine	• Bar test • Akinesia test	• Encapsulated Bromocriptine in CS-NPs intranasal treatment reversed catalepsy and akinesia.	[44]
Polyamidoamine PEGylated dendrimers targeted with lactoferin	Hemiparkinsonian (6-OHDA induced Sprague-Dawley rats)	Intravenous	Therapeutic gene *h*GDNF	• Elevated body swing test • Apomorphine-induced rotations (30 min)	• Multiple injections of hGDNF loaded Lf-modified NPs demonstrate greater symmetrical swings and lower apomorphine-induced rotation.	[87]
PLGA nanoparticles	Apomorphine-treated Swiss albino mice	Subcutaneous	Risperidone	• Bar test for catalepsy • Antipsychotic activity test	• PLGA-risperidone NPS significantly reduced catalepsy • Prolonged inhibition (from 12 h to 72 h) of apomorphine--induced climbing and sniffing.	[592]
ALZHEIMER'S DISEASE (AD)						
RVG conjugated PEGylated dendrigraft poly-L-lysines (DGLs)	Transgenic C57BL/6 mice expressing a chimeric mouse/human amyloid precursor protein	Intravenous	BACE1-AS shRNA encoding plasmid (pshBACE1-AS)	• Morris water maze • test	• Mice treated with DGLs-PEG-RVG29/pshSc NPs spent least time to reach the platform.	[480]
PLGA nanoparticles	Aβ-Induced Wistar rats	Intraperitoneal	Curcumin	• Two-way conditioned avoidance response	• Cur-PLGA-NPs reversed the Aβ-induced deficits in learning and memory.	[36]
Polyethylene glycol-polylactic acid co-block polymer and polyvinylpyrrolidone nanoparticles	Tg2576 transgenic mice	Oral	Curcumin	• Radial Arm Maze (RAM) • Contextual Fear Conditioning (CFC)	• Nanocurcumin (NC) treated mice exhibited fewer reentry errors. • Cue memory showed significant improvement in NC *vs.* control without any alteration on context memory.	[35]

(continued on next page)

Table 6 (*continued*)

Nano-delivery systems	Animal model	Route of administration	Therapeutic cargo	Behavioural assessment	Outcome of behavioural evaluation	Ref.
Tween 80 (T-80) coated polylactide-co-glycolide (PLGA) nanoparticles	D-galactose (d-gal) treated ovariectomized (OVX) Sprague-Dawley rat model of AD	Oral, Intravenous	Estradiol	• Open field tests • Elevated plus maze	• Impairment in anxiety-related behaviour (central platform behaviour) was attenuated with NP treatment.	[34]
Solid lipid nanoparticles (SLNs)	$AlCl_3$ induced Wistar rats	Intravenous	Quercetin	• Spatial navigation task • Elevated plus maze	• Decrease in escape latency for SLN treatment. • Mean transfer latency was reduced for quercetin-SLN was significantly reduced.	[168]
Microemulsion (ME), solid lipid nanoparticles (SLNs), and nanostructured lipid carriers (NLCs)	Scopolamine induced Albino mice model	Transdermal	Huperzine A (HupA)	• Elevated plus-maze	• Mice treated with ME, SLNs and NLCs based gel showed significant difference in transfer latency. • Comparable transfer latency of normal control and formulation treatment groups.	[167]
Solid lipid nanoparticles (SLNs)	Streptozotocin (STZ) induced- Wistar rats	Oral	Sesamol	• Closed field tests • Elevated plus maze • Morris water maze test • Memory consolidation test	• Decrease in escape latency significantly different for encapsulated and free formulations. • Sesamol-SLNs (16 mg/kg) significant decreased retention transfer latency. No difference in spontaneous locomotor activity observed.	[171]
Solanum tuberosum lectin (STL) conjugated PEG-PLGA nanoparticles	$A\beta_{25-35}$ and ibotenic acid (IBO) induced Sprague-Dawley rats	Intranasal	Basic fibroblast growth factor (bFGF)	• Morris water maze test	• Rats given STL-bFGF-NP showed shorter escape latency and improved learning ability.	[33]
Solid lipid nanoparticles (SLNs)	$A\beta_{25-35}$ induced Sprague-Dawley rats	Oral	Chrysin (CN)	• Morris water maze test • Novel object recognition test • Y-maze test • Radial arm maze training	• Mean escape latency and time spent in target quadrant reduced and enhanced respectively by both CN-SLNs and CN but at a much lower concentration in CN-SLNs in MWM test. • Similar results were obtained for novel object recognition test and the impact on spatial learning and memory and spatial working assessed through RAM and Y-maze test.	[173]
Apolipoprotein E3–reconstituted high density lipoprotein (ApoE3–rHDL) nanoparticles	Senescence-accelerated prone mouse (SAMP8) mice model	Intravenous	–	• Morris water maze test	• ApoE3–rHDL-treated SAMP8 mice exhibited significantly improved spatial learning and memory.	[481]
TGN (TNP/H102) (TGNYKALHPHNGC) and/QSH (QSHYRHISPAQVC) peptides coated PLGA-PEG nanoparticles (TQNP/H102)	Aβ42 induced ICR mice	Intravenous	β-sheet breaker peptide H102	• Morris water maze test	• Mice performance improved in a dose dependant manner to different dosages of TNP/H102 or TQNP/H102. • Best directional performance in the high-dose TNP/H102 and TQNP/H102 groups.	[32]
Polysorbate-80 (PS-80) coated solid lipid nanoparticles	Ibotenic acid induced albino Wistar rats	Intraperitoneal	Piperine	• Forced swim test	• Decreased immobility in P-80-PIP-SLN treatment, better than Donepezil (positive control).	[331]
Chitosan nanoparticles	Colchecine induced Wistar rats	Intranasal	Piperine	• Morris water maze test	• PIP-loaded NPs treatment significantly improve escape latency. • PIP-NP and donepezil treatments significantly increased the retention time.	[43]
Lipid-core nanocapsules (LNCs)	$A\beta_{1-42}$ induced Wistar rats	Intraperitoneal	Indomethacin (IndOH)	• Spontaneous alteration • Novel object recognition test	• IndOH-LNCs at the same dosage as free IndOH was able to attenuate the decrease in spontaneous alteration in the Y-Maze. • Short-term and long term recognition memory restored by IndOH-LNCs not free IndOH.	[593]
Solid- lipid (glyceryl behnate) nanoparticles (SLNs)	Isoproterenol-induced Wistar rats	Oral	Galantamine hydrobromide (GH)	• Elevated plus maze test (EPM) • Morris water maze test (MWM)	• Decline in cognitive function significantly attenuated by co-administration of MSCs along with GH-SLNs. • MSCs alone as well as in combination with GH-SLNs improved memory acquisition and retention as tested by EPM test.	[172]
Tween-modified monoolein cubosomes (T-cubs)	Colchicine- induced Wistar rats	–	Piperine	• Behavioral passive avoidance test	• T-cubs treatment restored cognition to the level of negative controls.	[249]
Liposomes	Aluminium chloride ($AlCl_3$)-induced Wistar rats	Subcutaneous	Rivastigmine	• Morris water maze test	• Restoration of spatial memory with RL treatment concomitantly with $AlCl_3$.	[131]
PSYCHOTIC DISORDERS						
Poly ε-Caprolactone (PCL) nanoparticles	Swiss albino mice	Parenteral (Intravenous)	Risperidone	• Apomorphine- induced climbing	• Prolonged apomorphine-induced sniffing and climbing with risperidone loaded PCL NPs.	[59]

				• Sniffing test • Catalepsy test	• Reduction in extrapyramidal side effects (EPS) liability of risperidone-PCL NPs.	
D-alpha-tocopheryl polyethylene glycol 1000 succinate micelles (TPGS micelles)	Swiss albino mice	Intramuscular	Paliperidone palmitate (PPT)	• Apomorphine- induced climbing and sniffing test • Catalepsy test	• PPT loaded TPGS micelles significantly counteracted the apomorphine induced climbing and sniffing behavior. • Significant reduction in the catalepsy using PPT-loaded TPGS micelles compared to paliperidone palmitate control.	[110]
Tween 80 coated chitosan nanoparticles	Ketamine-induced Swiss albino mice model	Oral	Doxycycline hydrochloride	• Forced swimming test (FST) • Passive avoidance test • Locomotor activity test (actophotometer)	• Reduction in ketamine-induced hyperlocomotor activity by $DCNP_{opt}$ statistically equivalent levels as olanzapine (positive control). • Similar results were observed for stereotyped behaviour induced by ketamine. • Immobility duration in FST was decreased by $DCNP_{opt}$ at statistically equivalent levels to olanzapine. • No significant difference in step down latency in comparison to ketamine in passive avoidance test.	[61]
Polysorbate-coated nanocapsules (NCs)	d,l-amphetamine-(AMPH) induced Wistar rats	Intraperitoneal	Haloperidol	• Oral dyskinesia (OD) • Catalepsy test • Stereotyped head behaviour	• Both groups treated with haloperidol (H-NC and FH) decreased the AMPH-induced stereotyped behaviour. • Prolonged antipsychotic action in H-NC group at the equivalent dose. • FH treatment caused extrapyramidal effects, such as OD and catalepsy. H-NC group showed significantly less motor side effects as compared to FH.	[539]
PAMAM NPs	Sprague-Dawley rats	Intranasal, intraperitoneal, oral	Haloperidol (H)	• Catalepsy test, • Motor suppression	• I.n. administration of H-NPs evokes catalepsy at lower doses than in i.p. or oral administration. • I.n. administration of H-NPs induces motor suppression at lower doses than i.p. and at much higher levels than the same dose given via oral administration.	[89]
Solid Lipid Nanoparticles (SLNs)	Ketamine-induced Swiss albino mice model	Oral	Quetiapine Fumarate (QF)	• Open field test (OFT) • Passive avoidance test (PAT)	• Number of squares in OFT and latency time in PAT significantly increased by treatments with QF and QF-SLNs, with dose-dependent increase in efficiency in QFSLNs.	[178]
Lecithin-based nanoemulsion (Polysorbate-80 with/without)	Wistar rats	Intraperitoneal	Risperidone (RSP)	• Amphetamine-induced locomotor activity (AILA) • Basal locomotor activity (BLA)	• RSP-P80-treated rats travelled significantly longer distance than rats treated with RSP-Sol. • RSP-Sol induced a strong sedative effect which is minimised by nanoemulsions. • For AILA, significant difference was found between SAL/-AMPH and RSP-LS75/AMPH group for both distance travelled and time active indicating more sustained antipsychotic effect of RSP-LS75 nanoemulsion.	[525]
Compritol 888 ATO based solid-lipid nanoparticles	Balb/C mice	Intravenous	Risperidone	• Paw test using Perspex platform	• A significant rise in HRT (hindlimb retraction time--antipsychotic impact) for the RSLNs formulations. • No significant impact on FRT (forelimb retraction time--induction of EPS)	[176]
Nano-lipid carriers (NLCs)	Charles-Foster rats	Intranasal, intravenous	Asenapine (ASN)	• Paw test • Induced locomotor activity test • Catalepsy test	• Catalepsis significantly increased in ASN and decreased in ASN-NLC in higher time points. • Significant count reduction in induced locomotor activity test by ASN-NLC. High HRT observed for ASN-NLC treated animals in paw test.	[177]
Polysorbate 80 coated Fish oil (FO) or Grape seed oil (GSO) containing Poly(ε-caprolactone) nanocapsules	Wistar rats	Intraperitoneal	Haloperidol	Oral dyskinesia (OD)	• At the same doses of the free drug, haloperidol encapsulating nanocapsules (H-NcCCO) reduced OD, with the dose of 0.5 mg kg−1 of haloperidol-loaded nanocapsules suspension (H-NcCCO) being the most effective.	[62]
Polysorbate-80 coated Poly (ε-caprolactone) nanocapsules containing fish oil (FO)	Wistar rats	Intraperitoneal	Haloperidol	• Oral dyskinesia • Catalepsy time • Locomotor activity	• Acute treatment: Stark increase in the frequency of VCM was observed for free haloperidol as opposed to nanocapsules. • Nanocapsules with FO showed no epilepsy and haloperidol containing nanocapsules reduced catalepsy compared to free treatment. • Subchronic treatment: Nanocapsules-treated rats showed lower immobility time than free haloperidol treated rats.	[60]

(continued on next page)

Table 6 (*continued*)

Nano-delivery systems	Animal model	Route of administration	Therapeutic cargo	Behavioural assessment	Outcome of behavioural evaluation	Ref.
Lipid core nanocapsules (LNCs)	D,l Amphetamine-induced Wistar rats	Intraperitoneal	Olanzapine (OLA)	• Stereotyped behaviour • Prepulse Inhibition of Startle Reflex (PPI) • Locomotor and Exploratory Activity	• Rats treated with OLA-LNC showed lower stereotyped behavior. • Significant decrease in crossing and rearing behaviour was observed for OLA-LNC and OLA-FREE groups. • OLA-LNC prevented the deficit induced by apomorphine in the prepulses.	[519]
Lipid based self nanoemulsifying drug delivery system (SNEDDS)	Ketamine-induced Swiss albino mice		Olanzapine (OLZ)	• Open field test • Rota rod test • Tail suspension test	• Decrease in the mobility observed in the animals pretreated with OLZ-SNEDDS. • Increased permanence time on the rod by OLZ-SNEDDS treatment. • Immobility time significantly enhanced by OLZ-SNEDDS in tail suspension test.	[314]
STROKE (CEREBRAL ISCHEMIA/ICH)						
Polyanion-complexed PEG diblock nanoparticles	C57Bl/6 mice focal transient cerebral ischemia model	Intravenous	Brain derived neurotrophic factor (BDNF)	• Neurological deficit score (NDS) • Novel object recognition task (NORT) • Tail suspension test (TST)	• Nano-BDNF treatment showed higher discrimination index (DI) • Improved learning and memory in treatment groups • Reduction in immobility in the tail suspension test compared to controls.	[546]
PLGA nanoparticles	Sprague-Dawley rat focal cerebral (medial cerebral artery occlusion) ischemia-reperfusion injury model (MCAO/reperfusion)	Intracarotid	Superoxide dismutase (SOD)	Neurological severity score • Motor activity • Sensory responses • Behavioural abnormality	• Lower neurological severity scores when compared to free SOD or NP-treated or saline controls in treatment group.	[70]
Cilostazol nanoparticles	ICR mice Focal cerebral ischemia/reperfusion model (MCAO/reperfusion)	Intravenous	–	Neurological deficit score	• Neurological deficits in MCAO/reperfusion mice attenuated by the CLZ nanoparticles.	[64]
Polymeric NIPAM nanoparticles	Wistar rat MCAO/reperfusion model	Intranasal	Curcumin (Cur), Demethoxycurcumin (DMC), Bisdemethoxycurcumin (BDMC)	• Close field activity monitoring • Grip strength	• PNIPAM-curcumin, optimal dose: 100 μg/kg in attenuation of spontaneous activity deficits • PNIPAM-curcumin, DMC and BDMC at same dose showed improvement in grip strength.	[63]
Nanoliposomes	Sprague-Dawley rat MCAO/reperfusion model	Intranasal	Basic fibroblast growth factor (bFGF)	• Neurological deficit score • Locomotor activity	• The neurological deficit score was improved post treatment with bFGF-NL. • bFGF- NL significantly increased the total distances travelled.	[138]
Squalenoyl Adenosine nanoparticles (SqAd NPs)	Swiss albino mice MCAO/reperfusion model	Intravenous	–	Neurological deficit score	• Neurological deficit score improved in a dose-dependent manner by SqAd NPs • Neuroprotective effect of SqAd NPs preserved in the absence of reperfusion.	[552]
Citrate-Capped Gold nanoparticles (Au-NPs)	Sprague-Dawley rat MCAO/reperfusion model	Intraperitoneal	–	Neurological deficit score	• Significant improvements observed in neurological deficit scores after reperfusion with 20 nm Au-NPs treatment.	[594]
Silica-coated superparamagnetic iron oxide nanoparticles (SiO_4@SPIONs)	ICR mice Focal cerebral ischemia/reperfusion model (MCAO/reperfusion)	Intravenous	–	• Modified neurologic severity score (mNSS) • Rotarod task	• Residence time on rotary rod prolonged for magnetic field induced SiO_4@SPIONs-EPCs treated mice compared to controls. • Neurobehavioral deficiency reduced in M-SiO_4@SPIONs--EPCs treated mice compared to controls.	[554]
PLGA nanoparticles	Sprague-Dawley perinatal Hypoxia-Ischemia Exposure Model	Intraperitoneal	Erythropoietin (EPO)	Rotarod task	• For roatarod test starting at 10 rpm, PLGA-EPO-NP (300 U/kg) outperformed the same dose of free rEPO and showed results comparable to therapeutic dose of free rEPO (5000 U/kg) and sham.	[595]
Exosomes	Controlled cortical impact (CCI) Wistar rat model	Intravenous		• Modified neurological severity score (mNSS) test • Footfault test	• Functional recovery assessed by mNSS test and footfault test significantly improved in the exosome-treated groups. • Exosomes from 2D and 3D cultured cells had no significant difference in their impacts on functional recovery.	[295]

				• Morris water maze (MWM) test		
Anti-mouse TfR antibody coated chitosan-PEG nanospheres	Swiss albino mice temporary intraluminal filament occlusion (MCAO) model	Intravenous	N-benzyloxycarbonyl-Asp (OMe)-Glu(OMe)-Val-Asp (OMe)-fluoromethyl ketonePeptide Caspase-3 inhibitor (Z-DEVD-FMK)	• Neurological severity score test	• Significant functional recovery was observed in the high--dose nanospheres treatment compared to low-dose and blank controls. • Low dose groups showed reduction in neurological severity scores compared to controls.	[596]
Chitosan nanoparticles (CS-NPs)	Wistar rat intraluminal filament MCAO model	Intranasal	Rutin (RUT)	• Closed field activity monitoring • Grip strength	• RUT-CS-NPs improved locomotor activity compared to RUT solution at the same dose and MCAO groups. • Grip strength significantly enhanced in RT treated groups compared to MCAO group.	[332]
PS-80 coated Poly (butylcyanoacrylate) Nanoparticles (PBCN)	Wistar rat MCAO/reperfusion model	Intravenous	Peurarin (PEU)	Neurological symptom score test	• Rats treated with PUE-PBCN displayed lower scores than PEU treated and saline treated controls.	[597]
Solid lipid nanoparticles (SLNs)	Wistar rat bilateral common carotid arteries occlusion (BCCAO)/reperfusion model	Oral	Curcumin	• Morris water maze (MWM) test • Elevated plus maze (EPM) test • Actophotometer assessment	• C-SLNs treatment significantly attenuated the increase in initial transfer latency (ITL) and retention transfer latency (RTL) in the EPM. • Significant improvement in memory consolidation in MWM in treatment as opposed to controls.	[286]
PS-80 coated PLGA NPs	MCAO induced Wistar rat model	Intravenous	Acetylpuerarin (AP)	• Neurological deficit score	• Decrease in score following treatment with AP solution and AP-CS NPs.	[69]
RADA16-I self-assembling peptide nanofiber scaffolds (SAPNS)	Type IV collagenase induced ICH Sprague-Dawley rat model	Intrastriatal	-	• Modified limb placing test	• Significant improvement in functional recovery in SAP group at week 10 as compared to week one and two. • No significant difference in serial changes amongst the other three groups.	[333]
Lipid-coated magnetic mesoporous silica Nanoparticles (LMCs)	Collagenase VII induced ICH Sprague-Dawley rat model	Intracerebral	Ceria nanoparticles (CeNPs)	• Corner turn test • Forelimb asymmetry test	• Reduced preferential turning and improved forelimb use asymmetry on day 3 compared to vehicle-treatment	[196]
Quercetin nanoemulsion	Type VII collagenase induced ICH Wistar rat model	Intraperitoneal	Quercetin	• Open field test • Beam walking test • Foot fault test	• Free and QU-loaded nanoemulsions increased the number of crossings and rearings compared to control groups in open field analysis. • Significant decrease in beam walking test score in quercetin nanoemulsion treatment compared to other groups. • No impact of quercentin on foot fault test.	[428]
Redox polymer self-assembled nanoparticles (nitroxide radical-containing nanoparticles [RNPs]	1-MHz focused ultrasound sonication coupled with microbubble treatment induced ICH Sprague-Dawley rat model	Intravenous	-	• Neurological deficit score • Forelimb placing test • Postural reflex test	• All the neurobehavioural analysis confirmed the establishment of ICH in the sonication and microbubble treated animals.	[429]
EPILEPSY						
N,N-dimethylacrylamide-based PEGylated nanoparticles (PNP)	PTZ-induced acute seizure (Wistar rats) model	Intraperitoneal	Gamma-aminobutyric acid (GABA)	Latency to Myoclonus, tonic clonic and tonic seizures	• A significant retardation in latency time observed for both formulations (PEG and non-PEGylated) when compared with controls. • No death and a decrease in the duration of convulsions was observed for both formulation.	[423]
Silica core iron oxide nanoparticles	3-mercaptopropionic acid (3MPA) induced seizure (Wistar rat) model	Intraperitoneal	Phenytoin	Latency to Myoclonus, tonic clonic and tonic seizures	• PHT-NPs treatment showed significant lower prevalence of the clonic and tonic–clonic seizures.	[598]
Solid lipid nanoparticles (SLN)	PTZ-Induced Seizures in Swiss Webster Mice	Intraperitoneal, oral	Clonazepam (CLZ)	• Latency to Myoclonus, tonic clonic and tonic seizures • Behavioral seizure severity (BSS): Racine's scale	• Delay in onset of myoclonus and tonic clonic seizures for IP and oral formulations. • No tonic seizures and mortality in p.o. administration whereas they were still detected for lower doses in IP formulations. • Latency to the onset of paroxystic activity significantly delayed in rats receiving CLZ-SLN.	[587]
Angiopep-2 (ANG) modified electroresponsive hydrogel nanoparticles (ERHNPs)	Maximal Electroshock-induced Seizures (MES), Pentylenetetrazole-induced Seizures, Pilocarpine-induced Seizures (Sprague-Dawley rat) model	Intraperitoneal	Phenytoin sodium (PHT)	Behavioral seizure severity (BSS): Racine's scale	• ANG-PHT-ERHNP most effective: effective at lower therapeutic doses. • In the PTZ model, ANG-PHT-ERHNP showed significant antiepileptic ability compared to other treatments.	[599]

(continued on next page)

Table 6 (*continued*)

Nano-delivery systems	Animal model	Route of administration	Therapeutic cargo	Behavioural assessment	Outcome of behavioural evaluation	Ref.
Chitosan solid lipid nanoparticles	Maximal Electroshock-induced Seizures (MES) Wistar rat model, Isoniazid (INH) induced convulsions	Oral	Carbamazepine (CBZ)	Latency in onset of convulsion phases	• Delayed onset of convulsions in CBZ SLN s treatment.	[600]
Polysorbate 80 coated albumin nanoparticles	maximal electroshock (MES) and pentylenetetrazole (PTZ) induced convulsion Wistar rat model	Intraperitoneal	Gabapentin	Latency in onset of convulsion phases	• Significant reduction in convulsion phases in both MES and PTZ induced convulsion models using Polysorbate 80 coated nanoparticles in comparison with drug solution and nano-particle formulations.	[601]
Chitosan-alginate-STPP nanoparticles	Pentylenetetrazol (PTZ)-induced kindling epilepsy mice model	Intraperitoneal	Curcumin	Morris water maze test	• Short latency for animals under treatment of high dose curcumin-loaded NPs. • Significant preference toward the former platform site representing improved memory consolidation.	[602]
Polymeric micelles (PM)	PTZ-Induced Seizures in Swiss Albino Mice	Intranasal, intravenous	Clonazepam (CZ)	Latency in onset of convulsion phases	• Strong significant delay in the onset of seizures by intranasal delivered PM-CZs as compared to CZ solution.	[270]
TRAUMATIC BRAIN INJURY						
Poloxamer 188 coated PLGA NPs	Weight-drop C57BL/6N mice model	Intravenous	Brain derived neurotrophic factor (BDNF)	• Neurological severity score • Passive avoidance task	• Significant improvement in neurological severity score in Poloxamer 188 coated BDNF loaded PLGA NP treatment. • Reversal of cognitive deficits in TBI model.	[419]
PAIN MODELS						
PS-80 coated PBCA NPs	Mice model	Intravenous	Endomorphin-1	Tail flick test (response to water at 55 $\pm$1°C)	• PS-80 coated NPs have continuous analgesic effect compared to other groups.	[570]
PS-80 coated PBCA NPs	ICR mice model	Intravenous	Loperamide	Tail flick test (response to quartz projection bulb)	• Dose-dependent analgesia observed for NPs. • Prolonged and sustained analgesia in PS-80 coated NPs treatments compared to free solution at the same dose.	[79]
Poloxamer 188 or PS 80 coated PLGA-PEG-PLGA NPs	ICR mice model	Intravenous	Loperamide	• Formalin test • Hot plate test	• Hot plate: Significant anti-nociceptive response for surfactant coated NPs compared to uncoated NPs and drug solution. • Poloxamer188 coating more effective than PS-80 for displaying anti-nociception at same doses. • Formalin test: Significant reduction in licking duration for coated NPs at the same dose as free drugs. • Poloxamer 188 coated NPs more potent for anti-nociception than PS-80 coated NPs.	[430]
PS-80 coated PBCA NPs	ICR mice model	Intravenous	Dalargin	Tail flick test (response to quartz projection bulb)	• PS 80-coated nanoparticles with a dose of 5 mg/kg and above showed significant sustained analgesic effect than controls.	[220]

to assess impaired motor balance and coordination in which mice treated with rotenone spent less time on the rod compared to untreated control. There was a significant extension of time spent on the rod, with dual drug loaded NPs exhibiting more significant amelioration of motor dysfunction than the native drugs combined. Other studies with 6-OHDA PD model [184,443,444] have also shown motor recovery in rotarod analysis through the therapeutic delivery using BNDS.

The most pressing issue addressed by rotarod analysis is the lack of complete dependence on asymmetric motor movements as in the case of drug-induced rotations which makes it an extremely valuable tool in analysing bilateral lesion models. This drug-free analysis of behavioural response in lesioned models could be used for assessment of both maximal as well as partial lesions. This test is also well adapted to be used in both mice and rat models.

Elevated body swing test (EBST): EBST provides an estimate of asymmetrical motor behaviour in hemiparkinsonian animals tested in a drug-free state through the measurement of frequency and direction of the swings of the animal when it is held by the tail. Unilaterally lesioned animals exhibit biased contralateral swings. EBST has an advantage of being a rapid, easy, inexpensive and accurate measure of a DA-mediated motor function; well reflecting the true effects of unilateral lesions on the nigrostriatal pathway. For this test, the animal is placed into a Plexiglas box and allowed to attain a neutral position. It is then elevated to an inch above the resting surface and a swing is recorded using hand counters for a certain period of time whenever the animal moved its head out of the vertical axis to either side with 70% or higher being set as the deciding criterion. Huang et al. (2009) [87] showed that this behavioural test provided significant improvement in locomotor activity in rats treated with NPs loading hGDNF compared to controls. Multiple dosing regimen of therapeutic gene showed improved behaviour of 6-OHDA-lesioned rats compared to a single injection. This test is predominantly used for 6-OHDA-lesioned animals which displayed a decreasing trend of biased swing activity over a period of two months representing habituation due to recurrent handling [445]. Iancu et al. (2005) have shown a poor correlation between cell loss and performance in EBST in the mice models of PD [446].

Stepping test: Unilateral 6-OHDA-lesioned rats display chronic akinesia in a contralateral forelimb. The parameters evaluated in this assessment include initiation time, stepping time, step length and step adjustment as described by Olsson et al. (1995) [447]. Here, the rat is held by the experimenter with one hand fixing the hindlimbs and hind part is raised above the surface. Initiation time was recorded as the time elapsed before the movement initiation by forelimbs, stepping time was recorded as the time required to cover a designated distance by the rats and step length was calculated by dividing the distance covered by the number of steps required. The adjustment of steps was evaluated with the rat being moved slowly sideways in the forehand and backhand directions and counting the number of adjusting steps for both paws in the backhand and forehand direction of movement [184]. These two parameters namely initiation time and adjusting steps are most significantly affected by unilateral lesioning. This test was used by Hegazy et al. (2017) to study forelimb brady/akinesia in the 6-OHDA rat model and the impact of cerium oxide NPs on its amelioration [184] and has been used previously in mice models of PD as well. An inherent demerit of this method is the variability introduced by direct interaction between the experimenter and the animal as well as strain and test condition variations.

Open field tests: This test measures behaviour elicited by placing the animal in a novel confined open space and it remains the mostly widely used behavioural assessment for MPTP induced lesion models [448]. The setup for this test consists of a square or rectangular open space divided into a certain number of equidimensional squares and bound with a wall. Behavioural activity is registered using sets of infrared beams which, when broken are, registered by a software system. After placing the animal in the centre, the following ambulatory and autonomic response parameters are recorded: locomotor activity, speed, thigmotaxis, distance travelled in the centre, time spent in periphery, inactive sitting time, defecation, rearing time and number [449]. Open field tests have been used widely in both rodent models to investigate the reversion of bradykinesia in Parkinson's [47,183,443,450,451]. In a study by Hegazy et al. (2017), treatment using cerium oxide NPs showed a significant amelioration of motor deficits in some locomotor behaviours induced by 6-OHDA treatment assessed by certain components of open field test. However, other dimensions of the test like decrease in latency to move and to rear were unaffected by suboptimal doses of NPs [184]. However, another study by Gambaryan et al. (2014), there were no significant differences detected between the experimental groups suggesting neither the 6-OHDA induction nor the drug treatment affected the animals' cognition and locomotor activity [47].

It provides an exhaustive drug-free assessment of both locomotor and behavioural activity and is an easy to perform, non-invasive protocol not requiring any prior training. Open field activity data suffers from significant variation in behavioural and locomotive activity due to factors like experimenter handling, environmental conditions, cognition, genetics, sex and age [452,453].

Bar test: This is the most routinely used protocol for measuring catalepsy. It involves placing the forepaws of the test animal on a bar, where the height of the bar is adjusted in accordance with the animal's size, so that the hind limbs rest on the floor. The time elapsed before the animal returns to its normal posture is recorded as a measure of catalepsy [454]. The drawback of this assessment is the inconsistency that could be introduced with the selection of bars (shape, diameter and height), weight and strain of the animals, repeated testing and environmental stimuli. However, the inclusion of multiple bars of different diameters should overcome any apparatus limitations as the impact of bar diameter is observable at the extremes of bar height [455]. Its easier to manipulate the bar height than to vary the size of the squares on a grid, the gauge of wire, the distance between four pegs or corks, or the size of platforms or blocks needed for more complicated catalepsy-assessing strategies. This test has been used uniformly for both rat and mice models. Bar test was used as a measure of akinesia in hemiparkisonian rats by Esposito et al. (2008) where they showed a sustained and more rapid onset of attenuation of akinesia for encapsulated bromocriptine compared to the free drug in 6-OHDA treated animals [166]. Another study by Md et al. (2013) using bar test showed that catalepsy in animals receiving bromocriptine either in solution or within chitosan NPs showed a reversal in catalepsy when compared to haloperidol treated mice [44].

Footfault asymmetry test: The foot fault test or grid-walking test is an evaluation of the animal's ability to place its paws while probing an elevated grid, thus addressing the deficits in voluntary motor control and limb movement involved in co-ordination and accurate paw placement [456]. If the paw fell within the cells of the grid or slipped due to an inability to support the weight for both forelimbs and hind limbs, a foot fault was considered. This test for motor dysfunctions has not been used very routinely for evaluating the efficacy of BNDS. However, Gambaryan et al. (2014) used footfault asymmetry test to demonstrate that all PD-positive groups, except for the nano-DOPA treated group differed significantly from the control animals. [47]. Till date, this analysis has been used more frequently with rat models of PD as compared to mice models.

However, Silvestrin et al. (2009) [457] ascertained that context-induced ipsilateral rotational activity (CIIRA) in the foot fault test could be used as a very sensitive and specific screening tool for unilateral 6-OHDA-lesioned animals. Additionally, the test requires only one short session, does not need the administration of a drug to show motor asymmetry and is much more sensitive than open field tests, which require a longer session. Another significant revelation from this study was the comparability of this screening to apomorphine challenge, which is customarily used for behaviour analysis in Parkinson's. On

the debit-side of foot fault test is a sharp fall of CIIRA in the second trial cannot be used twice when both sessions are very close.

Manual gait analysis: PD is characterized by the presence of gait abnormalities reflected in shortened stride length [458] and loss of control in stride frequency [459] leading to postural instability. Prior studies [446,460,461] have established a relatively simple protocol for manual gait analysis using a limb painting procedure. Animals are trained to traverse a horizontal corridor with walls to confine their movement tracks leading directly into their goal box. Stride length was measured as the distance between successive paw prints when the animal was walking continuously at a constant pace. Width of gait and overlap between hind limb and fore limb are other parameters that are recorded from the prints. Gait analysis has been used in both mice and rat models of PD to determine the bradykinesia and postural instability. Umararo et al. (2016) used gait analysis to evaluate the reversion of bradykinesia in 6-OHDA treated rats after subjecting them to superoxide iron oxide NPs in the presence of magnetic field [443]. The authors hypothesized this recovery could be attributed either to reduction in oxidative stress and mitochondrial dysfunction or enhanced release of dopamine from the spared tissue. However, variation in schedules of neurotoxin administration translating in differences in the mechanisms of neuronal death, habituation [462] and strain differences [463] alter gait dynamics and must as a matter of urgency, be assessed while evaluating behavioural responses.

Climbing pole: Originally described by Ogawa et al. (1985) [464], the pole test is used to evaluate the agility and degree of bradykinesia in animals. The animal is placed head-upward on the top of a rough-surfaced vertical pole and two parameters are recorded as a measure for bradykinesia: the time taken for the animals to turn by 180° and the time taken to reach the floor. There is a time lag between the control and lesioned animals to turn and get down the pole; with the control animals being much faster. This procedure is an useful tool for screening the lesioned animals as well for detecting the impact of therapies in them. This is because it can be very well correlated with striatal DA content [465] and can be performed easily and quickly. The limitations of the pole test include the variability introduced with gender and strain of animals as the BALB/c strain showed a stunted tendency to climb down the pole [465]. Furthermore, the impact of environmental conditions like brightness on the performance of animals in pole test must be accounted for.

Placing task: This test is designed to estimate the animals' motor responses and coordination performance after unilateral lesion by evaluating a directed forelimb movement in response to sensory stimuli. The sensory stimulus is provided by brushing the vibrissae of one cheek (either the same side or the contralateral side) across the side of table [466]. Animals are immobilized by holding the torso with free hanging forelimbs, and are moved up and down in space before testing. The animals respond to the sensory stimulus by reaching the forelimbs out to the table-top. Unilaterally lesioned animals do not place the paw on the side of lesion whereas there is a reliable paw placement on the unlesioned side and percentage of flawed placements are recorded as a measure of co-ordination. Adaptation of this protocol for MPTP mice includes immobilization of mice and sensory stimulation to induce the forelimb movement. The parameter recorded here is the paw reach in millimetres. This test is sensitive for detection of DA loss (70%) for weeks after MPTP treatment [384].

Another adaptation to this test is the cross-midline forelimb placing test, where the same side forelimb is immobilized followed by vibrissae stimulation and the successful placement of the opposite forelimb on the table top is recorded. This is instrumental in the analysis of motor and sensory integration across cerebral hemispheres and the extent of damage in different types of lesions [467]. The placing task was used by Gamabaryan et al. (2014) to estimate the animals' coordination performance after unilateral substantia nigra lesion [443]. During the treatment, animals performed the placing task twice a day: 30 min and 24 h after drug administration. In animals treated with nano-DOPA, improved coordination performance was observed compared to all the PD positive animal groups.

There is an inevitable irreversible alteration of sensory signals on being transmitted through DA depleted striatum which is translated into altered limb trajectory. Forelimb placing accurately detects these motor deficits independently of the impact of habituation, making the tests sufficiently sensitive for detection of a dopaminergic lesion and evaluation of circuit recovery and plasticity through various neuroreparative strategies.

Olfactory discrimination test (ODT): This test originally described by Prediger et al. (2005) [468] measures olfactory deficits in odour detection, apperception and discrimination, which are commonplace in the diagnosis of Parkinson's disease. The apparatus consists of a box equally compartmentalized into two and connected by an open door allowing free access to the animal. One compartment contains clean sawdust (non-familiar odour) and the other contains sawdust obtained from cages of animals isolated for 48 h before testing (familiar odour). The ODT consists of placing the animal in the middle of box and recording the time of investigation of each compartment. Equal tendency to spend time in both compartments is indicative of olfactory impairment and absence of discrimination. The discrimination index (DI) is the ratio of difference in investigation time between the two compartments by the total amount of exploration for both compartments. Hyposmia is prognostic to nigrostriatal denervation in the early stages of PD [382], whereas the motor deficits could be manifested much later in disease progression. Therefore, this test could be used in the pre-symptomatic evaluation of PD. Practical advantages of this test include inexpensive apparatus, ease of implementation and rapid acquisition although the sensitivity to potential stress induced by handling is a major downside. This test was used by Lindner et al. (2015) in the MPTP mice model for the behavioural assessment as MPTP-induced PD models do not show motor dysfunctions [469]. The results showed MPTP-infused animals treated with reservatol-loaded PLA-PS80 NPs spent significantly greater time in the familiar compartment than the control animals.

Social recognition task: Social interactions among animals investigate the memory processes which impact the behavioural patterns and could be instrumental in examining the impact of lesions on learning and memory. The social recognition test is based on the domain that adult rodent engages more in the investigation of an unfamiliar juvenile and spends more time in nosing, sniffing, grooming or pawing the new juvenile. Re-introduction of the same juvenile significantly reduces the engagement of the adult with the juvenile [470]. The engagement parameters are recorded as a measure of social recognition that stems from social generated from olfactory innuendo [471]. The ratio of investigation duration (RID) of second and first exposure is indicative of social recognition [472]. It is a very simple and ethologically relevant test, that is not conditioned by additional positive or negative reinforcements, for MPTP models which simulate early phase of PD, where sensory and memory deficits appears with no major motor alterations [473]. However, some of the disadvantages of this assay are: the complications involved in automation, requirement of an acclimatisation period before test and sensitivity to environmental stimuli causing stress in animals [474]. Lindner et al. (2015) found a significant reduction in RID induced by reservatol-loaded NP treatment. There was no significant difference found between animals from control and MPTP plus PLA-PS80 loaded RVT groups which was indicative of prevention of the deficit in social recognition ability induced by MPTP treatment [49].

3.4.2. Alzheimer's disease

Morris water maze (MWM) test: Originally described by Richard G. Morris in 1981 for rats [475], MWM is a behavioural assessment of the long-term spatial memory in rodents. It represents the yardstick of behavioural testing of spatial memory impairment and for assessing the impact of several therapeutic strategies on cognition in the animal models of AD [476,477]. The setup for this test requires the presence of an opaque temperature (25°C) regulated pool with a hidden

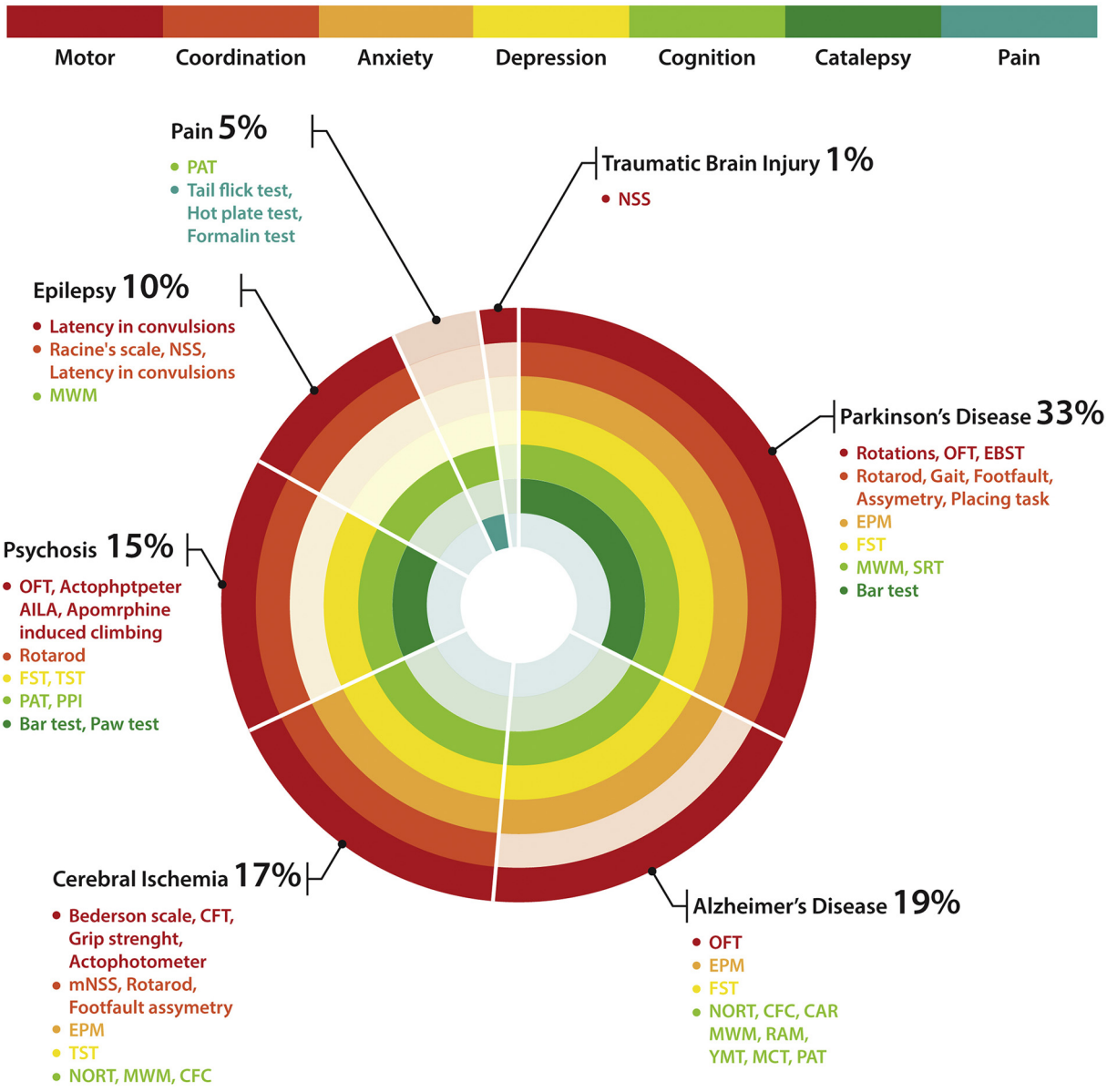

Fig. 5. Stratification of behavioural analysis paradigm: Representation of assessment strategies for multiple facets of functional recovery in pre-clinical models of different brain diseases using BNDS

submerged platform. A very apparent stationary cue for the animals is provided either at the periphery of the maze or on the walls of the testing room which is fitted with camera connected to a video tracking system and software for motion detection. Multiple training trials per day are conducted for 2–10 days before the experimental MWM test is performed for experimental groups. Animals are released in the water facing the wall of the water maze and the time to reach the platform is recorded, with a maximal time limit of 60 s. The tracking is stopped if the animals are delayed more than 60 seconds which is recorded as it is. The time taken to reach the hidden submerged platform (escape latency) is recorded. The animals, however, might be able to reach the platform due to prior learning of sequence of movements, recognizing proximal cues or a spatial navigation strategy. Therefore, Dalm et al. (2000) [478] suggested using a video tracking system to calculate the non-prompt oriented parameters like length of the swimming path, path directionality or cumulative distance to platform to identify the concentric search strategy. Sachdeva et al. (2015) reported a significant improvement in the latency to reach the submerged platform in the animals treated with sesamol-loaded SLN compared to control streptozotocin treated animals. This was indicative of intact learning and memory function in SLN-sesamol treated group which was found to be dose-dependent.

Another arm of this investigation uses a visible test to assess the motivational, visual and motor abilities where the animals undergo trials for two days and the time taken to reach a randomly positioned visible platform in a different place each time is measured [479]. The swimming speed and distance travelled to reach the platform is used to analyse the motor performance of the animals. A detectable deficit in the hidden acquisition test with normal performance in the visible test is indicative of spatial memory impairment independent of motivational, visual and motor skills. MWM is the most widely used behavioural assessment in rat models of AD [33,171,173,480,481]. All these studies have suggested an overall improvement in the memory and learning in the therapeutic carrying nano-system treated AD models. Ismail et al. (2013) studied the effect of free and liposome-encapsulated rivastigmine on spatial memory deficits in $AlCl_3$-treated rats. Restoration of spatial memory was achieved upon treating rats with liposome-encapsulated rivastigmine concomitantly with $AlCl_3$.The most

important limitation of this method comes from the fact that mice perform more poorly than rats [482,483] due to thigmotaxis and passivity which could partially be circumvented by nudging by the experimenter and careful selection of the strain. Lighting is another crucial aspect as MWM does not account for the olfactory capabilities of the rodents [484]. This test could also be significantly impacted by age of the animals and viral, bacterial and nematode infections [485,486]. MWM still is the gold-standard behavioural test because of its simple and fast execution and the ability to resolve the spatial learning and long-term spatial memory, testing of non-spatial abilities such as visual and motor performance alongside the low costs involved.

Radial Arm Maze (RAM): Dry RAM involves the use of a maze consisting of variable number of equally spaced arms radiating from a central platform. The rodents enter one of these arms in the maze to obtain food or water while guiding themselves using spatial cues around the room, with the motivation of acquiring the maximum reward in shortest time and with minimal efforts. This kind of task requires both working memory (WM) when retaining information within the trials and reference memory when retaining memory to avoid the non-baited arms across the maze for a longer time. Impact of spatial learning and memory was evaluated in the Tg2576 mice model for AD by Cheng et al. (2013) using the radial arm maze [35]. Nano-curcumin treated mice exhibited fewer re-entry errors than either the control or free curcumin treatment group. This suggested that curcumin is involved in prevention of Aβ induced damage to the hippocampus. Major limitations are the use of food or water deprivation, the presence of olfactory confounds that are not accounted for and less sensitivity in detection of search strategies when compared to MWM. [487,488]. RAM is more useful for investigating changes of error patterns than for searching patterns. The advantages of this method includes the simultaneous detection of working and reference memory and low costs involved.

Contextual Fear Conditioning (CFC): Fear conditioning provides an estimate of hippocampal-dependent associative learning wherein the dependant parameter is the freezing response that happens by coupling of an unconditioned stimulus (US) such as a foot shock with a conditioned stimulus (CS) such as a particular cage or tone. It has been previously demonstrated that several transgenic mouse models of AD display impairments in fear and anxiety and it is hypothesized that the hippocampal function used in fear conditioning is different from that of learning in a spatial task [489]. During this test, the animal is placed in a cage/box and is presented with a tone (usually 80 dB) (conditioned stimulus) that is paired with a mild shock (unconditioned stimulus) at the end of the trial. This results in the tone eliciting a freezing response in the animals. Increasing the time lag between CS and US provides a good estimate of prefrontal cortical activity. Cue-dependent fear conditioning is measured by placing the animal in a new box that is different in color, shape, etc., and presenting it with the tone as it explores the new environment. Freezing response associated with the tone is measured. Study by Cheng et al. (2013) uses CFC to evaluate the improvement in associative memory after treatment with nano-curcumin in transgenic AD mice model [35]. The study indicated that treatment with nano-curcumin had no effect on the contextual memory of the mice but enhanced the cue memory of the treatment group compared to that of the controls.

Shortcomings in this investigation include the non-associative freezing to US caused by the exposure of rodents to foot shock in a new environment [490]. There is an augmentation observed in the freezing response to the tone stimulus in the novel environment for the animals that have received contextual conditioning [491]. The strains and age of animals used for the investigation can have a major impact on the outcomes as in some strains of mice, retinal degeneration is a background genetic defect that may affect contextual freezing. However, it is a useful long-lasting and quickly acquired strategy for investigating both emotional and contextual memory which can be used both in animal models and humans [492].

Two-way conditioned avoidance response (CAR): *The* CAR protocol is related to the classicconditioning concept first presented by Pavlov in 1927 [493] and further elucidated by B.F. Skinner [494]. Antipsychotic efficacy for a compound is defined by the ability of a compound to inhibit the conditioned avoidance response (CAR) to an adverse stimulus. Avoidance is represented by the tendency of the animals to move, within a certain time frame, from one compartment to another upon presentation of auditory or visual stimulus (CS) after training. A delay in avoidance is coupled to an unconditioned stimulus (UCS; usually a weak electric shock) until the animal responds by moving into the other compartment. This behaviour is regarded as escape from the negative reinforcer. Once the animals have been trained, both typical and atypical antipsychotics are effective in decreasing the CAR to the conditioned stimulus without altering the escape response elicited by the unconditioned stimulus. Tiwari et al. (2013) investigated whether curcumin loaded PLGA NPs can reverse Aβ-mediated inhibitory effects on hippocampal neurogenesis and learning and memory defects in a rat model. Using CAR, they demonstrated that both free and encapsulated curcumin can mediate a significant reversal of the learning and memory deficits in AD rat model. However, curcumin loaded NPs are effective at much lower doses *in vivo* than curcumin solution [36]. Specific downsides to the CAR test is that it is primarily efficacious in predicting the general antipsychotic activity of a drug, rather than its comparative therapeutic efficiency or prediction of therapeutic activity against specific symptoms. This necessitates the use of additional animal models/screening tests to assess EPS liability profile [493]. Doses of antipsychotics effective in inhibiting CAR while preventing the induction of catalepsy provides a convenient measure for therapeutic index for EPS.

Elevated plus maze (EPM): EPM represents a simple behavioural task for the assessment of anxiety responses of rodents as described originally by File et al. (1938) [494] and modified by Montgomery [495] and Handley and Mithani [496]. They introduced the elevated maze with four arms (two open and two enclosed) that are arranged to form a plus shape and provides for the evaluation of anxiety behaviour of rodents by using the ratio of time spent on the open (unsafe) arms to the time spent on the closed (safe) arms. The elevated plus maze utilizes rodents' inclination toward dark, enclosed spaces (approach) and an unconditioned fear of heights/open spaces (avoidance). Each animal is placed in the centre of the maze and the amount of time spent in each arm was recorded automatically by video tracking software. EPM is adapted and used for a range of applications including the anxiolytic and anxiogenic impact of therapeutics and behavioural assay for mechanisms underlying the action of neuromodulators [496,497]. Mittal et al. (2011) used EPM as a behavioural assessment of the anxiety in ovarectomized and D-gal treated animals which exhibited a higher degree of anxiety. Treatment with estradiol loaded PLGA NPs was found to be effective in attenuating the impairment, indicating its neuroprotective action on brain [34]. There are several other studies that have used EPM as an assessment for the therapeutic efficacy of BNDS in AD [167,171,498]. The general considerations while using EPM as a tool of behavioural analysis includes its susceptibility to test timing [499], prior handling [500], strain [501], age [502], sex and estrous cycle [503] of the animals used.

Novel object recognition (NOR) test: Described originally by Ennaceur and Delacour (2003) [504], the object recognition test is the evaluation of recognition memory which harnesses the natural propensity of rodents to investigate a novel object and the innate instinct to explore when they are presented with a novel environment. The choice to explore the novel object, as well as the reactivation of exploration after displacement of the object, reflects the use of learning and recognition memory processes. The available object-recognition tasks to test

cognition in rodents use different numbers of available objects and environments in which the animals are tested, as well as types of configuration aimed to test spatial recognition and novelty, among other things. The adapted version of valuation of age-related deficit detection using the object recognition test is widely used for AD models, wherein a rodent is placed in an open field filled with different objects for a finite time. After a series of training trials to habituate the animals to the properties and configurations of the objects, some objects are either switched from one location to another to test the spatial recognition or are replaced with new ones to evaluate novel object recognition. The discrimination (D^2) index is described as magnitude of discrimination between novel and familiar objects which corrects for total exploratory activity of each animal [504] and is calculated using the difference in time spent exploring the novel and familiar objects divided by the total exploration time for both objects:

$$D^2 = (\text{novel} - \text{familiar})/(\text{novel} + \text{familiar})$$

Interspecies comparison of exploratory behaviour using the NOR test is not viable because different species may use different investigatory strategies. The mechanisms underlying the failure of the animal to recognize a familiar object along with other novel object recognition are not well elucidated [505]. Vedagiri et al. (2016) have demonstrated the use of NOR test to evaluate the recovery of visual recognition memory by treatment of the rats with chrysin loaded SLNs. They showed a significant loss of exploratory behaviour in $A\beta_{25-35}$ injected group compared to the control group. This was duly restored by the treatment with chrysin loaded SLNs which were very effective *in vivo* at significantly lower doses than free chrysin [173]. Major advantages of this test include no requirement for external motivation, minimal training and habituation and short duration of analysis [506].

Y-maze test: Y-Maze Spontaneous Alternation is a behavioural test for investigating the predisposition of rodents to explore a new environment, where they typically delve into the new arm of the maze rather than return to a previously visited one. General testing setting involves a Y-shaped maze with three opaque plastic arms angled at 120°. The animal is left at the centre of maze and over the course of multiple arm entries, there should be a reduction in the tendency to visit the more explored arm. The number of arm entries and the number of triads are recorded to calculate the percentage of alternation and evaluate cognitive deficits in AD and to evaluate therapeutics for the amelioration of these deficits. The more frequently used version of the Y-maze for AD is the spontaneous alternation version of the Y-maze. In this instance, the alteration rate is determined for test animals as the degree of arm entries without repetitions when these are placed in a Y-shaped maze for a finite time. Sustained cognition is deciphered by a high alternation rate as the animals must remember which arm was entered last so as not to enter it [507]. Y-maze test was used by Mittal et al. (2016) to study the effect of chrysin-loaded SLNs and free chrysin on spatial working in $A\beta_{25-35}$ injected rats. They demonstrated a significant reduction in the % alternation in the Y-maze in the $A\beta_{25-35}$ treated rats compared to the control group. This was effectively attenuated by SLNs at a low dose when compared to that of free CN at a higher dose *in vivo* [173].

A limitation of the Y-Maze is the inherent bias introduced by the fact that the animal is faced with a single point choice that enhances the probability of success to 50%. The other concern is that the animal may use a strategy other than spatial learning to solve the maze. A major strength of the Y-Maze is the simple approach unlike that of other spatial tasks which require minimal time and training and produce reproducible results. The Y-Maze also places minimal stress on the animals.

Forced swim test (FST): Originally described by Porsolt et al. (1977, 1978) [508,509] in rats and modified for mice [510], FST is one of the most widely used tests to test depression. The test is based on the tendency of animals to give up when forced to swim in a no-escape scenario, after an initial high-activity phase. This behavioural immobility mimics the state of depression. The conventional set-up consists of a plexi-glass cylinder containing water maintained at 25°C into which the animals are plunged for a finite period and show immobility for 75% of this period. Yusuf et al. (2013) demonstrated a decrease in the immobility time following the treatment of the AD induced rats with piperine loaded SLNs. This attenuation of immobilization was found to be better than donepezil [169]. A major drawback of the test is the inability to determine the cause of immobility of the animals. The protocol is not very well adapted for mice, which show a sufficiently stable level of immobility during the last four min of a six min swim test [511]. The immobility may be influenced by a plethora of factors including the water temperature [512], emotional state [513], strain of mice [514], among the others. Benefits of FST include the ease of use, standardisation and efficacy in screening of several anti-depressants [510].

3.4.3. Psychotic disorders

Catalepsy test: Catalepsy is defined as an inability to correct an externally imposed incorrect posture and is measured by the latency of the animals to get back to the normal posture. It is a paradigm of interest because of its close resemblance to symptoms of neural disorders such as Parkinsonism, schizophrenia and basal ganglia damage as well as to study the behavioural mechanisms of neurochemical therapeutics. Most commonly used analysis for catalepsy is the 'bar test' originally described by Kuschinsky and Hornykiewicz (1972) [515]. Another variant of this behavioural test, was adapted from Rocha et al. (1991) [516], is the grid test. The set-up for this variant uses a grid inclined at 45° relative to the bench top. Each animal is placed with its forepaws near the edge of the grid and the amount of time spent in this atypical position is recorded.Muthu et al. (2014) used the bar test for catalepsy to investigate the therapeutic efficacy of paliperidone micelles in terms of their antipsychotic behaviour in swiss albino mice. The paliperidone palmitate control formulation failed to show any antipsychosis which could be attributed to the poor absorption/release of formulation from the intramuscular administration. The nano-micelles, however, showed a significant reduction in catalepsy owing to modified release patterns [110]. This assessment has also been used in rat models by Katare et al. (2015). They found that the IN administration of dendrimer bound haloperidol exhibited a cataleptic response which was similar to that achieved by IP administration at a much higher dose [89]. Major limitations in using catalepsy as a behavioural assessment paradigm are the influence of repeated testing or learning on catalepsy and standardization of catalepsy scores [517,518]. However, it is cheap, simple, reproducible and easy to perform.

Locomotor activity test (actophotometer): This test is used to determine the alertness of mental activity and its modulation using various therapeutics. An actophotometer operates on photoelectric cells which are connected in circuit with a counter and as the circuit is disrupted by motion of the animal, a count is recorded. Yadav et al. (2017) used an actophotometer to investigate the amelioration of psychosis using doxycycline hydrochloride encapsulated chitosan NPs in a ketamine-induced mice model. Encapsulated doxycycline showed a significant reduction in hyperlocomotor activity induced by ketamine compared to the free formulation at a very high dose and was comparable to the effect of olanzapine treated controls [61]. An actophotometer could have either a circular or square chamber and can be used for both mice and rats. It represents a cheaper system with minimal calibration time but it lacks the versatility of other motor assessment protocols.

Basal locomotor activity (BLA): General hypo-or hyperactivity of animals maybe instrumental in modulating the behavioural response to pharmacotherapies or genetic alterations. Basal locomotor activity of control and experimental animals is determined using the open field task in which the animal is allowed to freely run and explore an open area. The number of line crossing and the number of rearings is recorded. The crossing and rearing numbers are indicators of locomotor and exploratory activity, respectively. Dimer et al. (2015) showed the

significant decrease in stereotypic movements using the nanoencapsulated olanzapine for longer time periods as compared to the free formulation of the drug [519].

Amphetamine-induced locomotor activity (AILA): Antagonism of DA receptors by various anti-psychotics gave way to the hypothesis that psychosis is mediated by DA deregulation. This could be the result of over-release or limited re-uptake of DA or over-expression of specific DA receptors which causes the positive symptoms of psychosis, particularly those associated with schizophrenia. Featherstone et al. (2007) [520] demonstrated the effectiveness of amphetamine-induced models of schizophrenia through various sensorimotor outcomes and amphetamine is also known to induce a psychotic state in healthy individuals and augments psychosis in patients [521,522]. Dopaminergic neurotransmission plays a crucial role in the filtering (or gating) of repetitive auditory stimuli and amphetamine-induced alterations of the deficits in the filtering of auditory stimulus common to psychotic conditions is well characterized in rodents [523,524]. AILA is usually recorded after the measurement of basal locomotor activity. Dordevic et al. (2017) reported sa significant reduction in amphetamine induced hyperlocomotion after treatment with risperidone nanoemulsions as compared to free risperidone [525].

Apomorphine- induced climbing and sniffing test: Apomorphine is known to induce psychosis as a side effect, reinforcing the link between increased DA activity and psychosis [526]. Several pharmacological investigations use apomorphine to evaluate the performance of antipsychotics [527,528]. Apomorphine-induced stereotypy arises from the stimulation of post-synaptic striatal and mesolimbic DA receptors [529] and has been applied as an appropriate method for *in vivo* screening of anti-psychotic drugs by the evaluation of climbing and sniffing response of the animals. The set up involves animals being placed into cylindrical cage and scoring the climbing behaviour. Animals were also rated for repetitive sniffing as a measure of stereotypy. Scores for both behaviours are added and used as a measure of the capability of the drug to inhibit apomorphine-induced psychosis. Muthu et al. (2008) studied the efficacy of PCL NP encapsulated risperidone in inhibiting apomorphine-induced climbing and sniffing in a mice model of psychosis. They reported prolonged inhibition of climbing and sniffing in risperidone-PCL NP treatment group as compared to free risperidone treatment. They also found that increase in PCL content promoted a sustained inhibition [59].

Prepulse Inhibition of Startle Reflex (PPI): PPI is used to evaluate the sensorimotor responses and attention-indulging processes in schizophrenia models and is also useful for measurements in animal models of psychosis. This test involves exposing the subjects to an unexpected weak acoustic or tactile pre-stimulus (pre-pulse) followed by a stronger startling stimulus (pulse) [530]. The weak stimulus exposure should avoid the occurrence of startling response which does not occur in the subjects with schizophrenia or psychotic disorders [531,532]. Physical response to the startle stimulus is measured with and without pre-stimulus. This difference quantitatively relates to the motor inhibition which is associated to neuronal inhibitory mechanisms. This link is further consolidated by the treatment with direct or indirect DA agonists impairs PPI which is effectively reversed by the use of several anti-psychotics [533,534]. This test measures pre-attentive processes in animal models of diseases marked by an inability to sieve irrelevant sensorimotor and cognitive information. Dimer et al. (2015) studied the impact of free and lipid-core nanocapsule encapsulated formulations of olanzapine in prepulse inhibition disruption induced by apomorphine model of schizophrenia. They reported significant inhibition of deficit induced by apomorphine in the prepulses at doses lower than the free formulation [519]. Limitations of this procedure include the requirement of a habituation phase and susceptibility to non-specific parameters of the 'gating' response. PPI levels vary based on sex and estrous cycles, both in humans and in rodents [535]. A great advantage of this test is comparability and objectivity of the analysis in mice, rats, and humans, as it applies across all vertebrate species [532]

Stereotypy: Stereotypy is an identifying feature of schizophrenia and other psychotic disorders characterized by repetitive and functionless behaviour [536]. It is categorised as repetitive motor actions distinct from cognition and has been identified in patients as well as in pharmacological human and animal models of psychosis [537,538]. Assessment of this repetitive behaviour involves a battery of tests inclusive of but not limited to repetitive licking, chewing, grooming, head movements, sniffing, circling, or climbing. Behavioural stereotypy can be determined by manual observation or the use of a digital system coupled with a software program based on predetermined criteria. Stereotypy is both a qualitative and quantitative indicator in models of psychosis and efficacy of anti-psychotics can be screened by measuring their ability to counter this behaviour. A deficiency in usng stereotypy as a measure of psychotic disorders is that it manifests itself in the later stages of schizophrenia and could be potentiated by cognitive inhibition. Benvegnu et al. (2011) reported that haloperidol loaded polymeric nanocapsules showed significant inhibition of amphetamine induced stereotypic behaviour in rat model. The encapsulated formulation of haloperidol also showed a prolonged anti-psychotic effect as compared to free haloperidol at the equivalent dose [539].

Paw test: Catatonia, i.e. the inability of animals to regain a normal posture after being forced into an incorrect one can be estimated using the paw test. Here, the animal is placed on a Perspex platform containing two holes for the forelimbs (40 mm), two for the hindlimbs (50 mm), and a slit for the tail [540]. The rat is held by the forelimbs by the experimenter and the hindlimbs are inserted into the holes followed by placement of forelimbs in the holes. The forelimb retraction time (FRT) and the hindlimb retraction time (HRT) were specified as the time required by the animal to withdraw a forelimb and a hindlimb from the hole, respectively [384]. FRT is associated with the ability to induce extra pyramidal side effects and HRT gives an estimate of antipsychotic activity. Patel et al. (2010) observed a significant rise in HRT for mice treated with risperidone loaded SLNs (RSLNs) when compared with free risperidone. Intravenously administered RSLNs showed higher HRT values than those of free risperidone implying that significantly higher targeting to brain by the SLNs [425]. Another study by Singh et al. (2016) showed the use of the paw test in a rat model of psychosis to show the behavioural recovery following the treatment with asenapine loaded nanostructured lipid carriers [177].

Other behavioural analysis paradigms used for the investigation of psychosis and screening the impact of therapeutics include FST, passive avoidance test, rota rod test, tail suspension test and open field test, all of which have been described previously.

3.4.4. Ischemic/haemorrhagic stroke

Grip strength: Amongst the non-invasive methods for evaluation of muscular strength in neuromuscular disorders, grip strength tests have been widely used to evaluate the effects of various chemicals on motor performance as a screen for neurobehavioural toxicity. Described by Meyer et al. (1979) [541], the grip strength test mimics the hand grip test for humans in the assessment of muscular strength and ability to grip an object. The most commonly used variant of the grip test is the forelimb grip strength test in which an experimenter horizontally pulls the tail of a rodent that grips a bar connected to a monitoring device, and the maximal value is recorded as the forelimb grip strength [542]. Ahmed et al. (2013) observed a significant decrease in grip strength in the MCAO treated rats compared to the sham group. Pretreatment with PNIPAM nanoformulation of curcumin, demethoxycurcumin, and bisdemethoxycurcumin showed improvement in grip strength when compared with MCAO group [63]. The rodent grip test is however susceptible to a multitude of factors like operational parameters, disruption of peripheral sensory function and changes in body weight [543]. Other factors that can introduce imprecision in measurement include the motivation of the rodent to keep gripping the bar, inconsistent procedures by inspectors and erratic handling by experimenters. Advantages of using this method are its non-invasiveness,

less stress to the animals, ease of performance, reproducibility and the test has been previously shown to be an indicator of frailty in ageing mice [544]

Tail suspension test (TST): Originally described by Steru et al. (1985) [545] as a screening test for antidepressants, it is used as a behavioural index in cerebral ischaemia. Each animal was tested only once and out of view from the other animals. The mice were suspended from a flat metal bar for a predetermined time. Escape behaviour includes strong shake of the body and run-like movements of the limbs. Pendulum-like movements and subtle movements of forelimbs without hindlimbs are excluded from the analysis. After the test, the time of mice which did not show typical escape-related behaviours during the last 4 min was measured. The test is followed by cage cleaning to remove any signs of distress. Harris et al. (2016) used the tail suspension test in the focal ischemic mice model where they observed that nano-BDNF treated mice showed significant reduction in their immobility. This was indicative of reduction in depressive behaviour as compared to saline controls [546]. The chief limitation of the protocol is that it is exclusively for mice [547] and cannot be used on rats or heavier mice due to the pain induced by suspending them through their tails. Also, tail climbing behaviour of certain mice could lead to the aberrations in the test [548]. Weight of the animal is a major concern and calls for alternative testing options. Any genetic or pharmacological alteration that might affect mobility will have an impact on TST and hence the conclusions should always be backed up by another behavioural assay. Because of this, it is important to verify the results of TST with separate behavioural tests that measure overall activity levels in mice such as the open-field test [549]. The main advantages of this procedure are the use of a simple test paradigm and the agreement of the results with the validated "behavioural despair" test [545]

Neurological Scoring Scales: Bederson et al. [550] defined a neurological assessment scale for quantitative assessment of neurological deficits following stroke. The Bederson scale is a global scale which is based on three parametric assays of: forelimb flexion, resistance to lateral push and circling behaviour. Behavioural deficits are scored on a scale of 0–3, with ischaemic animals having higher score than controls [551]. Forelimb flexion was tested by suspending the rat one meter above the floor using its tail as a response to which both rats reach out to the floor using both forelimbs. Animals with any consistent contralateral forelimb flexion and no other abnormality were graded 1. Animals' resistance to lateral movement induced by holding the tail by hand was equal in both directions in normal or mildly dysfunctional animals but reproducibly reduced to lateral push toward the injured side and these animals were graded 2. Rats circling towards the paretic side consistently were graded 3. Limitations of this method include the subjectivity of neurological ratings on this scale and quick recovery of the deficits scored in common stroke models, rendering it inefficient for long-term assessment. This scoring scale is, however, a simple way to reveal basic neurological deficits and is very quick. This scale has been used by several studies to investigate the impact of nano-delivery systems on the neurological deficits in ischemic models [138,546,552].

Modified Neurological Severity Scores (mNSS): A more updated scale of neurological deficits in animal models of stroke is represented by the modified neurological severity scores (mNSS). The mNSS involves a conglomerate of motor (muscle status and abnormal movement), sensory (visual, tactile and proprioceptive), reflex and balance tests to cover the sensorimotor evaluation post-ischaemia and therapeutic efficacy of treatment paradigms [553]. The mNSS scores the deficits in neurological functioning on a scale of 14 or 18 in mice or rats respectively. Individual deficits in certain functional modality could be masked by the overall score and the reflexes accounted for in mNSS are the pinna and startle reflexes. Li et al. (2013) used mNSS to grade neurological functions including motor (flexion of limb and walk on the floor), sensory (limb placing test and proprioceptive test) and reflex (pinna reflex, corneal reflex and startle reflex) in the mice MCAO model. They observed a tremendous improvement in neurobehavioral deficiency in magnetic field induced-SiO4 coated iron oxide NP -EPCs treated mice compared to that of controls [554].A major benefit of mNSS is that this ambidextrous assay includes a battery of simply-administered tests which can be used for long-term assessment and this makes it unlike the neurological scoring scales. Other facets of behavioural analysis in models of cerebral ischemia or stroke include Novel object recognition task (NORT), Contextual Fear test, Morris water maze (MWM) test, elevated plus maze (EPM) test and Neurological severity score which have been described earlier.

Behavioural paradigm for assessment of functional recovery following the treatment with BNDS in haemorrhagic stroke comprises chiefly of tests similar to ischemic stroke including neurological severity score, open field tests, footfault asymmetry test and placing task. In addition to this battery of tests, studies investigating the impact of BNDS in haemorrhagic stroke have also used corner tests and the beam walking test.

Corner test: Originally described for mice models by Zhang et al. (2002), this test aims to detect a range of mild to moderate ischemia induced sensory and postural asymmetries [555]. Here, the mouse is placed between the two angled boards and both sides of the vibrissae are stimulated together when entering deep into the corner. The non-ischemic mouse turns either side, but the ischemic mouse preferentially turns toward the non-impaired side. The number of turns in either side are recorded in multiple trials while ignoring the turns which were not a part of rearing. This test was used by Cha et al. (2018) to assess the improvement in neurological outcomes in the ICH model as a result of the treatment with lipid-coated magnetic mesoporous silica NPs [196]. The chief advantages of this test are that it is easy to perform, sensitive and correlates well to striatal infarct volumes after stroke in the mice models. It is also very useful in evaluating long term functional deficits after stroke giving it an edge over neurological scoring system and foot fault tests.

Beam walking test: Originally described by Schallert et al. (2005), the beam-walking test detects placement dysfunction of the hindlimbs after unilateral brain damage [556]. Here, the animals are made to walk across an elevated beam and hind limb foot faults are recorded as deficits in hind limb function. Following stroke, there is an increase in the animal's footfaults on the contralateral side. This task requires pre-training of the animals and breaks between trials to prevent habituation. This task is instrumental in determining the extent of brain repair achieved by experimental therapies and the extent of motor learning [557] This task is more sensitivein the detection of hindlimb placing deficits while the grid walking test is more sensitive to forelimb impairments [558]. This test was used by Galho et al. (2016) in the rat ICH model to test the locomotor activity, balance and motor function recovery following quercetin-loaded nanoemulsion treatment. There was a significant decrease in the score for ICH positive animals treated with quercetin nanoemulsions. This was indicative of reversion in the motor deficit and balance caused by ICH [559]. This test has also been used previously in mice models of stroke for behavioural assessment [560].

3.4.5. Pain models

Hot plate test: The hot plate test first described by Eddy and Leimbach (1953) [561], represents a simple behavioural screening in pain models. It is considered to be a supraspinally organized response involving higher brain function. The setup involves a plate heated to a constant temperature by a thermode or a boiling liquid. Heat as a noxious stimulus produces two behavioural responses estimated in terms of reaction times: paw licking and jumping. To screen the analgesic properties of a therapeutic, latency in the responses of treated and control animals is compared, and an increase in the latency to respond is conceived as an analgesic response. The conventional assay involves placing the animal on the hot plate and measuring latency in its response by either jumping or paw licking. Further variations in the protocol involve introduction of paw thermal stimulator and focusses the heat source to a particular area and recording the paw withdrawal

time [562]. The latency in response is inversely proportional to the intensity of the stimulus. Hot plate test was used by Chen et al. (2011) to o assess the impact of the surfactant coatings on the stability of NPs and consequently on their analgesic effect. They observed that the poloxamer 188 coating was better than PS 80 to deliver the loperamide loaded NPs across BBB to the central nervous system. They also found an enhancement in the anti-noceceptive effect after surface modification with poloxamer 188 of the NPs [80]. The weakness in this method for assessing nociception is the reduction in hot plate latency resulting from repeated testing [563,564]. Hot plate assay produces a more complicated response in rats than it does in mice [565]. Other factors that affect the outcomes of this test involve oestrus cycle [566], circadian rhythm of animals [567], strain, experimenter, season, humidity, and cage density [568]. The advantages of this test are that it is short in duration, easy to standardize, objective, quantifiable and does not require long training sessions.

Tail flick test: Initially described by D'Amour and Smith (1941) [569], this is one of the most common tests in pain models to evaluate the anti-nociceptive or analgesic impact of therapeutics and is based on an intermittent high intensity stimulus. Two variants of this test have been reported in literature. The first of these uses water heated at 55°C and the second uses the quartz projection bulb to apply radiant heat to a small area of the tail. This elicits a flick of the tail away from the heat source. Alyautdin et al. (1997) used the quartz projection bulb to test anti-nociceptive effect of surface coated loperamide loaded PBCA NPs in the mice pain model. They observed a significant and prolonged analgesic effect in the mice treated with PS-80 coated NPs as compared to the PS-80 loperamide solution. However, the uncoated particles failed to produce any analgesic effect at all [79]. Lu et al. (2006) investigated the analgesic impact of PS-80 coated endomorphine-1 loaded NPs using the hot water variant of tail flick test [570]. Using the reflex response is an advantage as it allows the test to be performed in lightly anesthetized animals and is almost independent of animals' motor coordination. A disadvantage is that tail temperature can be a confounder in this test as shown by the Berge et al. (1988) [571], who observed an increase in tail flicking with a decrease in tail temperatures. Tjølsen et al. (1989) [572] described a better method for monitoring the analgesic effects by coupling the tail flick with simultaneous recording of tail skin temperature. Additionally, restraint and handling in the course of testing could impact the latency in response.

Formalin test: The formalin test for nociception involves the use of a chemical as a noxious stimulus to generate a moderate, persistent response, closely mimicking the clinical pain rather than the transient response facilitated by a brief stimuli of threshold intensity. It also requires minimal restraining of experimental animals during the testing protocol [573]. Formalin induces a two-phase pharmacologically distinct nociceptive response. Phase 1, predicted to be caused by a burst of activity from pain fibres, begins immediately after the formalin injection and lasts ~10 min. Phase 2, typically mediated by peripheral inflammation begins 15 to 20 min after the formalin injection and continues for ≥60 min. Dubuisson and Dennis [573] devised a nociception scale of 0 to 3 to score the animal's response, where: 0 = the formalin-injected paw remains pressed to the floor and bears the animal's weight; 1 = the animal puts less weight on the injected paw, resting it lightly on the floor; 2 = the animal elevates the injected paw (no surface contact maintained); 3 = the animal licks, bites, or shakes the formalin-injected paw. Another way to quantify nociceptive behaviour involves counting the number of flinches in rats and licking in the formalin-injected paw for mice [574,575]. Chen et al. (2011) used this test to assess the systemic and nociceptive effects of loperamide encapsulated NPs on the modulation of acute pain. They observed that licking duration for loperamide encapsulated NPs with poloxamer 188 coating is significantly shorter than that of PS80 coated NPs [80]. The formalin test is found to be less sensitive than other pain behavioural analysis strategies and requires a higher number of animals to arrive at a conclusion about nociceptive behaviour. However, it is also the model that very closely re-creates the clinical pain scenario in humans [576].

3.4.6. TBI

Neurological severity score (NSS): NSS established by Chen et al. [577], portrays the Glasgow Outcome Scale, which is the clinical standard used to evaluate the functional neurological and cognitive impairments in TBI patients [578]. It provides a quantitative standardized evaluation of neurological motor function deficit in rodents after TBI. NSS has been shown to correlate well with histological examinations and MRI abnormalities in TBI and thus reflects injury of brain tissue [579]. The original protocol set out to have 25 tests to assess the motor and cognitive deficits has now been modified to have 10 tests [580] which are outlined below. The scoring system awards one point for the lack of a tested reflex or for the inability to perform the tasks and no point for succeeding. Higher scores are reflective of the severity of neurological dysfunction, with failure in the majority of the tasks.

Task 1: Exit circle: A healthy animal that is placed in the centre a the circle shows an intrinsic tendency to leave the circle within 3 min. The time needed for the animal to exit the apparatus is recorded.

Task 2: Seeking behaviour: The animal is placed in the circle with a closed exit and its innate tendency to explore the surroundings and sniffing is scored.

Task 3: Monoparesis/hemiparesis: This represents a quantification of gait. Monoparesis or hemiparesis is represented by the inability to use either one or two paws while walking. Paw grip and grip strength is assessed using anatomic forceps. Inability of the animal to grip the forceps on being touched by them is scored.

Task 4: Straight walk: This investigates the motor ability and alertness of the animal wherein, when it is placed onto empty surface, the animal investigates its surroundings and displays a straight walking pattern. If the mouse demonstrates impaired gait pattern and fails to actively explore environs, the behaviour is scored.

Task 5: Startle reflex: Inability to respond to a loud clap by startling reflex was scored.

Task 6: Beam balance: Inability of the animal to perch on a beam (0.5 × 0.5 mm^2) for a designated time is scored.

Tasks 7, 8, 9: Beam walk: The animal is placed at the end of 3-, 2-, 1-cm-wide beam of predetermined length. Inability of the mouse to reach the other side of the beam is reflective of impairment in seeking behaviour and is scored. If it fails to cross 3-cm- (or 2-cm) wide beam, further tasks with 2-cm (or 1-cm) wide beam would not be carried out and 3 or 2 points are given, respectively.

Task 10: Round stick balance: Inability of the animal to balance itself on a round stick for a designated time is scored.

Khalin et al. (2016) used the NSS to evaluate the efficacy of BDNF-loaded PLGA NPs in the closed head injury mice model. This test was used to assess motor, reflex and balance ability of the mouse post-injury. The authors reported a significant improvement in the neurological deficit in the group treated with BDNF-loaded PLGA NPs as compared to the other treatment groups [66].

Passive avoidance task: Passive avoidance includes a battery of fear-actuated tests to assess the cognitive deficits in TBI. It utilizes the subject's learning capability to display a paradoxical response to their innate tendencies to prefer of dark areas and avoid bright ones. The setup for this task consists of dark poorly illuminated compartment chamber and a bright illuminated chamber separated by a door. The test comprises two phases of learning [581]. In the acquisition/conditioning phase, the animal is placed in the bright compartment and allowed to investigate it before being given access to the dark one. On

being exposed to the dark chamber, the animal, driven by its innate tendencies, almost immediately crosses to the investigate it. As it does so, it receives a mild foot shock. The shock conditions the animal by acquainting it with the negative consequences of moving to a 'safer' place. The test phase, then recreates this scenario and the passive avoidance response is evaluated as the latency of the animal to reach out to the dark chamber with a certain cut-off time. Cognitive performance is directly proportional to latency in movement towards the preferred regions. Some avoidance tests require the animals to acquire motion to escape the adverse stimuli whereas this task requires them to remain in the illuminated chamber to do so. Passive avoidance was used by Khalin et al (2016) to assess the cognitive deficits in the mice model of TBI where they observed that cognitive deficits could be detected seven days post injury. They reported the effective reversal of cognitive deficits through treatment with BDNF-loaded PLGA particles coated with poloxamer 188 in the mice model [66].

Prior learning in pain could be a confounder in this analysis. Other drawbacks of passive avoidance task, including large inter-subject and different sensitivity to the shock exposures, make it necessary to use a large sample size. The memory retention is influenced by many factors including the mental state, emotional reactivity and responses to stress hormones [582]. Passive avoidance learning could be prevented by attenuated pain perception by pharmacological or genetic induction of analgesia [583]. The benefits of this procedure is that it is a single-trial task which provides consistency in results for both mice and rats. It has a simple setup and an easy protocol for testing. Since the task can be performed at variable time intervals after initial training, short-term (STM) and long-term memory (LTM) can be assessed separately.

3.4.7. Epilepsy

Behavioural seizure severity (BSS) or Racine's scale: Seizure severity is estimated by specific scoring systems catering to different types of seizures. For the focal seizures which are the most widely used model systems for evaluation of therapeutic nano-systems, Racine's scale is used. This provides a close simulation of seizure behaviour as it progresses from the focal point to other structures. It is, however, not a suitable scale for PTZ- induced seizures [584]. Racine et al. (1972) specifically targeted the hippocampus and the amygdala of the test animals and the reaction was categorized into five stages, which are of increasing severity [585]. The five stages include mouth and facial movement, head nodding, forelimb clonus rearing with forelimb clonus, rearing and falling with forelimb clonus (generalized motor convulsions). A limitation of the use of this scale is the impact of repetitive testing on the score. Repeated exposure to stimulus is known to reduce the threshold of seizure [586]. Levya Gomez et al. (2016) used the Racine's scale to demonstrate that the latency to the onset of paroxystic activity was significantly delayed in rats Clonazepam- loaded SLNs. The authors observed a reduction in the severity of behavioral scores in rats treated with Clonazepam alone, but the most significant inhibition of convulsive behavior was observed when the rats were treated with Clonazepam- loaded SLNs [587].Other paradigms use MWM test and test the latency in onset of convulsion phases as well as latency to myoclonus, tonic clonic and tonic seizures for behavioural estimation in epileptic models.

3.4.8. Glioma/glioblastoma

A substantial portion of the nano-delivery systems targeting the brain is aimed at the treatment of glioma/gliobastoma. The efficacy of these systems is predominantly assessed by their tumor-targeting properties and reduction in tumor size. There are no behavioural analysis *per se* available thus far for glioma models. Survival is a related paradigm of investigation which measures the life of treated animals' vs the control glioma implanted animals [386,588–590]. Increase in the mean survival of the animals is a measure of the *in vivo* efficacy of the therapeutic delivery system. It is critical to keep in mind that the review focusses only on the strategies used to date in the studies using brain-targeting nano-delivery systems. The application of these behavioural assays for testing the efficacy of BNDS in different pre-clinical disease targets has been summarised in Table 6. A summary of different evaluation strategies used for behavioural analysis of BNDS efficacy for various brain disorders is presented in Fig. 5.

4. Critique

BNDS are still in their infancy and most proof-of-concept studies were performed using unloaded, oversimplified nano-systems to study their bio-distribution and safety in healthy animal models. However, the key challenge is to couple them with a cargo of interest and assess their therapeutic effect in pre-clinical models of brain disorders. From all the modalities addressed, it is obvious clear that a synergistic investigation is required, blending the multiple techniques so as to validate the nano-systems used.

Histological assessment is necessity to evaluate the therapeutic efficacy of nano-systems. It is implemented not only to confirm the establishment of the disease model but also to evaluate the effect of the therapies employed. Even though it allows a specific marker study, tailored to the individual cases, it is nevertheless semi-quantitative analysis requiring animal sacrifice to harvest tissue, and it therefore raises ethical and financial concerns. The greater part of this analysis is done only at the end of the study, instead of conducting a possibly more accurate timeline-based assessment through the course of the disease and treatment.

On the other hand, real-time analysis can be done through bio-imaging, allowing a follow up of the pathological condition, trajectory and distribution of the BDNS on a timeline. However, even though these are already a paradigm in the clinic and allow the functional assessment of the effect of the nano systems with the exception of brain tumors, they are very expensive for use in pre-clinical models.

The behavioural paradigm represents the archetype of an assessment category for different brain disorders. There are a disease-specific battery of behavioural tests that tend to cover the sensorimotor and cognitive responses of the subjects. However, most of these tasks fail to model the clinical pathophysiology of the diseases. A greater part of behavioural analysis is prone to errors resulting from experimenter handling and scaling of the behavioural scoring systems to a standardized set-up that could be used across different species yet to be actualized. Despite these downsides, it still represents the functional recovery in disease targets and hence is instrumental in determining the success of the BNDS in the pre-clinical disease models.

Molecular evaluation modality is a quantitative course of analyzing the BNDS efficacy *in vivo*. The greater part of this analysis caters to the investigation of bio-distribution of nanoparticles and their efficacy in targeting the brain adjudged by their accumulation in the brain. Pharmacokinetic analysis determining the bio-availability of the nanoparticles is also recurrently investigated. Another facet of this modality deals with the investigation of inflammatory responses elicited in the brain owing to the administration of the nanoparticles as neuro-inflammation remains the root cause or aftermath of several brain diseases. Target-specific molecular alterations are investigated using gene and proteomic analysis. However, thus far there are very few studies that investigate the regio-specific alterations in tissue molecular signature in response to the nanoparticles which would help to elucidate the mechanistic aspects of their interaction and therapeutic activity. Besides, there is a dearth of studies redressing the modulation of tissue glycome and the role of these glycans in mediating the nanoparticle interaction with tissues/organ target.

Despite the plethora of literature on the nano-delivery systems for several brain disorders, there are still some unfathomed disease targets which are in urgent need of the potential of nano-systems for therapeutic delivery like Huntington's disease, Multiple Sclerosis, ALS, amongst others. An ideal evaluation assortment would test the applicability of nano-delivery systems in the clinical settings. It should, therefore, be a meticulously designed combination of the aforementioned modalities

which can be standardized for cross-species investigation and should be closely related to the temporal changes in disease pathophysiology.

Acknowledgments

This publication has emanated from research supported in part by a research grant from Science Foundation Ireland (SFI), co-funded under the European Regional Development Fund under Grant number 13/RC/2073, Hardiman Fellowship (NUI Galway) and supported by the BrainMatTrain project, which is funded by the European Union Horizon 2020 Programme (H2020-MSCA-ITN-2015) under the Marie Skłodowska-Curie Initial Training Network and Grant Agreement No. 676408. The authors would like to express sincere gratitude towards Mr. Keith Feerick and Mr. Anthony Sloan for their contribution in editorial assessment and proof-reading of the manuscript. The authors would also like to acknowledge Mr. Maciek Doczyk for the illustrations in the manuscript.

References

[1] L. Sakka, G. Coll, J. Chazal, Anatomy and physiology of cerebrospinal fluid, Eur. Ann. Otorhinolaryngol. Head Neck Dis. 128 (2011) 309–316, https://doi.org/10.1016/j.anorl.2011.03.002.
[2] R. Weller. Anatomy of the Meninges: Structural and functional aspects. In: M. Christodoulides, editor. Meningitis: cellular and molecular basis. (2013) 17–31. 3.
[3] J.-F. Ghersi-Egea, Y. Sugiyama, Drug Transfer in the Choroid Plexus. Multiplicity and Substrate Specificities of Transporters, Adv Drug Deliver Rev 56 (2004) 1693–1890.
[4] K.-T. Callixte, T.B. Clet, D. Jacques, Y. Faustin, D.J. François, T.-T. Maturin, The pattern of neurological diseases in elderly people in outpatient consultations in Sub-Saharan Africa, BMC Res. Notes. 8 (2015) 159, https://doi.org/10.1186/s13104-015-1116-x.
[5] C. Glorioso, S. Oh, G.G. Douillard, E. Sibille, Brain molecular aging, promotion of neurological disease and modulation by Sirtuin5 longevity gene polymorphism, Neurobiol. Dis. 41 (2011) 279–290, https://doi.org/10.1016/j.nbd.2010.09.016.
[6] T.M. Barchet, M.M. Amiji, Challenges and opportunities in CNS delivery of therapeutics for neurodegenerative diseases, Expert Opin. Drug Deliv. 6 (2009) 211–225, https://doi.org/10.1517/17425240902758188.
[7] P. Ballabh, A. Braun, M. Nedergaard, The blood–brain barrier: an overview, Neurobiol. Dis. 16 (2004) 1–13, https://doi.org/10.1016/j.nbd.2003.12.016.
[8] S. Pasha, K. Gupta, Various drug delivery approaches to the central nervous system, Expert Opin. Drug Deliv. 7 (2010) 113–135, https://doi.org/10.1517/17425240903405581.
[9] J. Kreuter, Nanoparticles—a historical perspective, Int. J. Pharm. 331 (2007) 1–10, https://doi.org/10.1016/J.IJPHARM.2006.10.021.
[10] H.B. Newton, Advances in strategies to improve drug delivery to brain tumors, Expert Rev. Neurother. 6 (2006) 1495–1509, https://doi.org/10.1586/14737175.6.10.1495.
[11] S.P. Vyas, A. Singh, V. Sihorkar, Ligand-receptor-mediated drug delivery: an emerging paradigm in cellular drug targeting, Crit. Rev. Ther. Drug Carrier Syst. 18 (2001) 1–76 http://www.ncbi.nlm.nih.gov/pubmed/11326743 (accessed January 16, 2018).
[12] M. Masserini, Nanoparticles for brain drug delivery, ISRN Biochem. 2013 (2013) 1–18, https://doi.org/10.1155/2013/238428.
[13] S.R. Mudshinge, A.B. Deore, S. Patil, C.M. Bhalgat, Nanoparticles: Emerging carriers for drug delivery, Saudi Pharm. J. 19 (2011) 129–141, https://doi.org/10.1016/j.jsps.2011.04.001.
[14] Y.H. Tsou, X.Q. Zhang, H. Zhu, S. Syed, X. Xu, Drug delivery to the brain across the blood–brain barrier using nanomaterials, Small. 13 (2017) 1–17, https://doi.org/10.1002/smll.201701921.
[15] L. Han, Y. Ren, L. Long, Y. Zhong, C. Shen, P. Pu, X. Yuan, C. Kang, Inhibition of C6 glioma in vivo by combination chemotherapy of implantation of polymer wafer and intracarotid perfusion of transferrin-decorated nanoparticles, Oncol. Rep. 27 (2012) 121–128, https://doi.org/10.3892/or.2011.1459.
[16] Y. Çirpanli, E. Allard, C. Passirani, E. Bilensoy, L. Lemaire, S. Çaliş, J.P. Benoit, Antitumoral activity of camptothecin-loaded nanoparticles in 9L rat glioma model, Int. J. Pharm. 403 (2011) 201–206, https://doi.org/10.1016/j.ijpharm.2010.10.015.
[17] T. Hekmatara*, C. Bernreuther*, A.S. Khalansky, A. Theisen, J. Weissenberger, J. Matschke, S. Gelperina, J. Kreuter, M. Glatzel, Efficient systemic therapy of rat glioblastoma by nanoparticle-bound doxorubicin is due to antiangiogenic effects, Clin. Neuropathol. 28 (2009) 153–164, https://doi.org/10.5414/NPP28153.
[18] B. Petri, A. Bootz, A. Khalansky, T. Hekmatara, R. Müller, R. Uhl, J. Kreuter, S. Gelperina, Chemotherapy of brain tumour using doxorubicin bound to surfactant-coated poly(butyl cyanoacrylate) nanoparticles: Revisiting the role of surfactants, J. Control. Release. 117 (2007) 51–58, https://doi.org/10.1016/j.jconrel.2006.10.015.
[19] A.E. Gulyaev, S.E. Gelperina, I.N. Skidan, A.S. Antropov, G.Y. Kivman, J. Kreuter, Significant transport of doxorubicin into the brain with polysorbate 80-coated nanoparticles, Pharm Res 16 (1999) 1564–1569.
[20] S. Gelperina, O. Maksimenko, A. Khalansky, L. Vanchugova, E. Shipulo, K. Abbasova, R. Berdiev, S. Wohlfart, N. Chepurnova, J. Kreuter, Drug delivery to the brain using surfactant-coated poly(lactide-co-glycolide) nanoparticles: Influence of the formulation parameters, Eur. J. Pharm. Biopharm. 74 (2010) 157–163, https://doi.org/10.1016/j.ejpb.2009.09.003.
[21] C.X. Wang, L.S. Huang, L.B. Hou, L. Jiang, Z.T. Yan, Y.L. Wang, Z.L. Chen, Antitumor effects of polysorbate-80 coated gemcitabine polybutylcyanoacrylate nanoparticles in vitro and its pharmacodynamics in vivo on C6 glioma cells of a brain tumor model, Brain Res. 1261 (2009) 91–99, https://doi.org/10.1016/j.brainres.2009.01.011.
[22] H. Xin, X. Sha, X. Jiang, W. Zhang, L. Chen, X. Fang, Anti-glioblastoma efficacy and safety of paclitaxel-loading Angiopep-conjugated dual targeting PEG-PCL nanoparticles, Biomaterials. 33 (2012) 8167–8176, https://doi.org/10.1016/j.biomaterials.2012.07.046.
[23] S. Wohlfart, A.S. Khalansky, S. Gelperina, D. Begley, J. Kreuter, Kinetics of transport of doxorubicin bound to nanoparticles across the blood-brain barrier, J. Control. Release. 154 (2011) 103–107, https://doi.org/10.1016/j.jconrel.2011.05.010.
[24] J. Guo, X. Gao, L. Su, H. Xia, G. Gu, Z. Pang, X. Jiang, L. Yao, J. Chen, H. Chen, Aptamer-functionalized PEG-PLGA nanoparticles for enhanced anti-glioma drug delivery, Biomaterials. 32 (2011) 8010–8020, https://doi.org/10.1016/j.biomaterials.2011.07.004.
[25] H. Xin, L. Chen, J. Gu, X. Ren, Z. wei, J. Luo, Y. Chen, X. Jiang, X. Sha, X. Fang, Enhanced anti-glioblastoma efficacy by PTX-loaded PEGylated poly(ε-caprolactone) nanoparticles: In vitro and in vivo evaluation, Int. J. Pharm. 402 (2010) 238–247, https://doi.org/10.1016/j.ijpharm.2010.10.005.
[26] X.H. Tian, X.N. Lin, F. Wei, W. Feng, Z.C. Huang, P. Wang, L. Ren, Y. Diao, Enhanced brain targeting of temozolomide in polysorbate-80 coated polybutylcyanoacrylate nanoparticles, Int. J. Nanomedicine. 6 (2011) 445–452, https://doi.org/10.2147/IJN.S16570.
[27] T. Schneider, A. Becker, K. Ringe, A. Reinhold, R. Firsching, B.A. Sabel, Brain tumor therapy by combined vaccination and antisense oligonucleotide delivery with nanoparticles, J. Neuroimmunol. 195 (2008) 21–27, https://doi.org/10.1016/j.jneuroim.2007.12.005.
[28] F. Lu, Z. Pang, J. Zhao, K. Jin, H. Li, Q. Pang, L. Zhang, Z. Pang, Angiopep-2-conjugated poly(ethylene glycol)-co-poly(ε-caprolactone) polymersomes for dual-targeting drug delivery to glioma in rats, Int. J. Nanomedicine. 12 (2017) 2117–2127, https://doi.org/10.2147/IJN.S123422.
[29] X. Zhang, X. Li, H. Hua, A. Wang, W. Liu, Y. Li, F. Fu, Y. Shi, K. Sun, Cyclic hexapeptide-conjugated nanoparticles enhance curcumin delivery to glioma tumor cells and tissue, Int. J. Nanomedicine. 12 (2017) 5717–5732, https://doi.org/10.2147/IJN.S138501.
[30] A. Arshad, B. Yang, A.S. Bienemann, N.U. Barua, M.J. Wyatt, M. Woolley, D.E. Johnson, K.J. Edler, S.S. Gill, Convection-enhanced delivery of carboplatin PLGA nanoparticles for the treatment of glioblastoma, PLoS One. 10 (2015) 1–16, https://doi.org/10.1371/journal.pone.0132266.
[31] E. Nance, C. Zhang, T.Y. Shih, Q. Xu, B.S. Schuster, J. Hanes, Brain-penetrating nanoparticles improve paclitaxel efficacy in malignant glioma following local administration, ACS Nano. 8 (2014) 10655–10664, https://doi.org/10.1021/nn504210g.
[32] C. Zhang, X. Zheng, X. Wan, X. Shao, Q. Liu, Z. Zhang, Q. Zhang, The potential use of H102 peptide-loaded dual-functional nanoparticles in the treatment of Alzheimer's disease, J. Control. Release. 192 (2014) 317–324, https://doi.org/10.1016/J.JCONREL.2014.07.050.
[33] C. Zhang, J. Chen, C. Feng, X. Shao, Q. Liu, Q. Zhang, Z. Pang, X. Jiang, Intranasal nanoparticles of basic fibroblast growth factor for brain delivery to treat Alzheimer's disease, Int. J. Pharm. 461 (2014) 192–202, https://doi.org/10.1016/J.IJPHARM.2013.11.049.
[34] G. Mittal, H. Carswell, R. Brett, S. Currie, M.N.V.R. Kumar, Development and evaluation of polymer nanoparticles for oral delivery of estradiol to rat brain in a model of Alzheimer's pathology, J. Control. Release. 150 (2011) 220–228, https://doi.org/10.1016/J.JCONREL.2010.11.013.
[35] K.K. Cheng, C.F. Yeung, S.W. Ho, S.F. Chow, A.H.L. Chow, L. Baum, Highly stabilized curcumin nanoparticles tested in an in vitro blood–brain barrier model and in Alzheimer's Disease Tg2576 Mice, AAPS J. 15 (2013) 324–336, https://doi.org/10.1208/s12248-012-9444-4.
[36] S.K. Tiwari, S. Agarwal, B. Seth, A. Yadav, S. Nair, P. Bhatnagar, M. Karmakar, M. Kumari, L.K.S. Chauhan, D.K. Patel, V. Srivastava, D. Singh, S.K. Gupta, A. Tripathi, R.K. Chaturvedi, K.C. Gupta, Curcumin-loaded nanoparticles potently induce adult neurogenesis and reverse cognitive deficits in Alzheimer's disease model via canonical Wnt/β-Catenin pathway, ACS Nano. 8 (2014) 76–103, https://doi.org/10.1021/nn405077y.
[37] B. Wilson, M.K. Samanta, K. Santhi, K.P.S. Kumar, N. Paramakrishnan, B. Suresh, Poly(n-butylcyanoacrylate) nanoparticles coated with polysorbate 80 for the targeted delivery of rivastigmine into the brain to treat Alzheimer's disease, Brain Res. 1200 (2008) 159–168, https://doi.org/10.1016/j.brainres.2008.01.039.
[38] B. Wilson, M.K. Samanta, K. Santhi, K.P.S. Kumar, N. Paramakrishnan, B. Suresh, Targeted delivery of tacrine into the brain with polysorbate 80-coated poly(n-butylcyanoacrylate) nanoparticles, Eur. J. Pharm. Biopharm. 70 (2008) 75–84, https://doi.org/10.1016/j.ejpb.2008.03.009.
[39] B. Wilson, M.K. Samanta, K. Santhi, K.P.S. Kumar, M. Ramasamy, B. Suresh, Chitosan nanoparticles as a new delivery system for the anti-Alzheimer drug tacrine, Nanomedicine Nanotechnology, Biol. Med. 6 (2010) 144–152, https://doi.org/10.1016/j.nano.2009.04.001.
[40] K.R. Gajbhiye, V. Gajbhiye, I.A. Siddiqui, S. Pilla, V. Soni, Ascorbic acid tethered polymeric nanoparticles enable efficient brain delivery of galantamine: An in vitro-in vivo study, Sci. Rep. 7 (2017) 1–12, https://doi.org/10.1038/s41598-017-11611-4.

[41] E. Muntimadugu, R. Dhommati, A. Jain, V.G.S. Challa, M. Shaheen, W. Khan, Intranasal delivery of nanoparticle encapsulated tarenflurbil: A potential brain targeting strategy for Alzheimer's disease, Eur. J. Pharm. Sci. 92 (2016) 224–234, https://doi.org/10.1016/j.ejps.2016.05.012.
[42] Y. Chen, C. Pan, A. Xuan, L. Xu, G. Bao, F. Liu, J. Fang, D. Long, Treatment efficacy of NGF nanoparticles combining neural stem cell transplantation on Alzheimer's disease model rats, Med. Sci. Monit. 21 (2015) 3608–3615, https://doi.org/10.12659/msm.894567.
[43] Y.S.R. Elnaggar, S.M. Etman, D.A. Abdelmonsif, O.Y. Abdallah, Intranasal piperine-loaded chitosan nanoparticles as brain-targeted therapy in Alzheimer's disease: optimization, biological efficacy, and potential toxicity, J. Pharm. Sci. 104 (2015) 3544–3556, https://doi.org/10.1002/jps.24557.
[44] S. Md, R.A. Khan, G. Mustafa, K. Chuttani, S. Baboota, J.K. Sahni, J. Ali, Bromocriptine loaded chitosan nanoparticles intended for direct nose to brain delivery: pharmacodynamic, pharmacokinetic and scintigraphy study in mice model, Eur. J. Pharm. Sci. 48 (2013) 393–405, https://doi.org/10.1016/j.ejps.2012.12.007.
[45] R. Pahuja, K. Seth, A. Shukla, R.K. Shukla, P. Bhatnagar, L.K.S. Chauhan, P.N. Saxena, J. Arun, B.P. Chaudhari, D.K. Patel, S.P. Singh, R. Shukla, V.K. Khanna, P. Kumar, R.K. Chaturvedi, K.C. Gupta, Trans-blood brain barrier delivery of dopamine-loaded nanoparticles reverses functional deficits in Parkinsonian rats, ACS Nano. 9 (2015) 4850–4871, https://doi.org/10.1021/nn506408v.
[46] Y.H. Siddique, W. Khan, B.R. Singh, A.H. Naqvi, Synthesis of alginate-curcumin nanocomposite and its protective role in transgenic Drosophila model of Parkinson's disease, ISRN Pharmacol. 2013 (2013) 794582, https://doi.org/10.1155/2013/794582.
[47] P.Y. Gambaryan, I.G. Kondrasheva, E.S. Severin, A.A. Guseva, A.A. Kamensky, Increasing the efficiency of Parkinson's disease treatment using a poly(lactic-co-glycolic acid) (PLGA) based L-DOPA delivery system, Exp. Neurobiol. 23 (2014) 246, https://doi.org/10.5607/en.2014.23.3.246.
[48] C. Saraiva, J. Paiva, T. Santos, L. Ferreira, L. Bernardino, MicroRNA-124 loaded nanoparticles enhance brain repair in Parkinson's disease, J. Control. Release. 235 (2016) 291–305, https://doi.org/10.1016/J.JCONREL.2016.06.005.
[49] G. da Rocha Lindner, D. Bonfanti Santos, D. Colle, E.L. Gasnhar Moreira, R. Daniel Prediger, M. Farina, N.M. Khalil, R. Mara Mainardes, Improved neuroprotective effects of resveratrol-loaded polysorbate 80-coated poly(lactide) nanoparticles in MPTP-induced Parkinsonism, Nanomedicine. 10 (2015) 1127–1138, https://doi.org/10.2217/nnm.14.165.
[50] K. Hu, Y. Shi, W. Jiang, J. Han, S. Huang, X. Jiang, Lactoferrin conjugated PEG-PLGA nanoparticles for brain delivery: Preparation, characterization and efficacy in Parkinson's disease, Int. J. Pharm. 415 (2011) 273–283, https://doi.org/10.1016/J.IJPHARM.2011.05.062.
[51] Z. Wen, Z. Yan, K. Hu, Z. Pang, X. Cheng, L. Guo, Q. Zhang, X. Jiang, L. Fang, R. Lai, Odorranalectin-conjugated nanoparticles: Preparation, brain delivery and pharmacodynamic study on Parkinson's disease following intranasal administration, J. Control. Release. 151 (2011) 131–138, https://doi.org/10.1016/J.JCONREL.2011.02.022.
[52] A. Trapani, E. De Giglio, D. Cafagna, N. Denora, G. Agrimi, T. Cassano, S. Gaetani, V. Cuomo, G. Trapani, Characterization and evaluation of chitosan nanoparticles for dopamine brain delivery, Int. J. Pharm. 419 (2011) 296–307, https://doi.org/10.1016/j.ijpharm.2011.07.036.
[53] K.B. Kurakhmaeva, I.A. Djindjikhashvili, V.E. Petrov, V.U. Balabanyan, T.A. Voronina, S.S. Trofimov, J. Kreuter, S. Gelperina, D. Begley, R.N. Alyautdin, Brain targeting of nerve growth factor using poly(butyl cyanoacrylate) nanoparticles, J. Drug Target. 17 (2009) 564–574, https://doi.org/10.1080/10611860903112842.
[54] C.C. Bi, A.P. Wang, Y.C. Chu, S. Liu, H.J. Mu, W.H. Liu, Z.M. Wu, K.X. Sun, Y.X. Li, Intranasal delivery of rotigotine to the brain with lactoferrin-modified PEG-PLGA nanoparticles for Parkinson's disease treatment, Int. J. Nanomedicine. 11 (2016) 6547–6559, https://doi.org/10.2147/IJN.S120939.
[55] S. Di Gioia, A. Trapani, D. Mandracchia, E. De Giglio, S. Cometa, V. Mangini, F. Arnesano, G. Belgiovine, S. Castellani, L. Pace, M. Angelo Lavecchia, G. Trapani, M. Conese, G. Puglisi, T. Cassano, Intranasal delivery of dopamine to the striatum using glycol chitosan/sulfobutylether-β-cyclodextrin based nanoparticles, Eur. J. Pharm. Biopharm. 94 (2015) 180–193, https://doi.org/10.1016/j.ejpb.2015.05.019.
[56] K.S. Rao, M.K. Reddy, J.L. Horning, V. Labhasetwar, TAT-conjugated nanoparticles for the CNS delivery of anti-HIV drugs, Biomaterials. 29 (2008) 4429–4438, https://doi.org/10.1016/j.biomaterials.2008.08.004.
[57] G. Yurtdaş Kırımlıoğlu, Y. Menceloğlu, K. Erol, Y. Yazan, In vitro/in vivo evaluation of gamma-aminobutyric acid-loaded N, N -dimethylacrylamide-based pegylated polymeric nanoparticles for brain delivery to treat epilepsy, J. Microencapsul. 33 (2016) 625–635, https://doi.org/10.1080/02652048.2016.1234515.
[58] D. Sharma, D. Maheshwari, G. Philip, R. Rana, S. Bhatia, M. Singh, R. Gabrani, S.K. Sharma, J. Ali, R.K. Sharma, S. Dang, Formulation and optimization of polymeric nanoparticles for intranasal delivery of lorazepam using Box-Behnken design: In vitro and in vivo evaluation, Biomed Res. Int. 2014 (2014)https://doi.org/10.1155/2014/156010.
[59] M.S. Muthu, S. Singh, Studies on biodegradable polymeric nanoparticles of risperidone: *in vitro* and *in vivo* evaluation, Nanomedicine. 3 (2008) 305–319, https://doi.org/10.2217/17435889.3.3.305.
[60] D.M. Benvegnú, R.C.S. Barcelos, N. Boufleur, C.S. Pase, P. Reckziegel, F.C. Flores, A.F. Ourique, M.D. Nora, C. de B. da Silva, R.C.R. Beck, M.E. Bürger, Haloperidol-loaded polysorbate-coated polymeric nanocapsules decrease its adverse motor side effects and oxidative stress markers in rats, Neurochem. Int. 61 (2012) 623–631, https://doi.org/10.1016/J.NEUINT.2012.06.015.
[61] M. Yadav, M. Parle, N. Sharma, S. Dhingra, N. Raina, D.K. Jindal, Brain targeted oral delivery of doxycycline hydrochloride encapsulated Tween 80 coated chitosan nanoparticles against ketamine induced psychosis: behavioral, biochemical, neurochemical and histological alterations in mice, Drug Deliv. 24 (2017) 1429–1440, https://doi.org/10.1080/10717544.2017.1377315.
[62] D.M. Benvegnú, K. Roversi, R.C.S. Barcelos, F. Trevizol, C.S. Pase, H.J. Segat, V.T. Dias, A.L. Savian, B.L. Piccoli, J. Piccolo, C.S. Dutra-Filho, T. Emanuelli, C. de Bona da Silva, R.C.R. Beck, M.E. Burger, Effects of fish and grape seed oils as core of haloperidol-loaded nanocapsules on oral dyskinesia in rats, Neurochem. Res. 43 (2018) 477–487, https://doi.org/10.1007/s11064-017-2444-0.
[63] N. Ahmad, S. Umar, M. Ashafaq, M. Akhtar, Z. Iqbal, M. Samim, F.J. Ahmad, A comparative study of PNIPAM nanoparticles of curcumin, demethoxycurcumin, and bisdemethoxycurcumin and their effects on oxidative stress markers in experimental stroke, Protoplasma. 250 (2013) 1327–1338, https://doi.org/10.1007/s00709-013-0516-9.
[64] N. Nagai, C. Yoshioka, Y. Ito, Y. Funakami, H. Nishikawa, A. Kawabata, Intravenous administration of cilostazol nanoparticles ameliorates acute ischemic stroke in a cerebral ischemia/reperfusion-induced injury model, Int. J. Mol. Sci. 16 (2015) 29329–29344, https://doi.org/10.3390/ijms161226166.
[65] Y. Lin, Y. Pan, Y. Shi, X. Huang, N. Jia, J.Y. Jiang, Delivery of large molecules via poly (butyl cyanoacrylate) nanoparticles into the injured rat brain, Nanotechnology. 23 (2012)https://doi.org/10.1088/0957-4484/23/16/165101.
[66] I. Khalin, R. Alyautdin, T.W. Wong, J. Gnanou, G. Kocherga, J. Kreuter, Brain-derived neurotrophic factor delivered to the brain using poly (lactide-co-glycolide) nanoparticles improves neurological and cognitive outcome in mice with traumatic brain injury, Drug Deliv. 23 (2016) 3520–3528, https://doi.org/10.1080/10717544.2016.1199609.
[67] N. Ahmad, R. Ahmad, A.A. Naqvi, M.A. Alam, M. Ashafaq, M. Samim, Z. Iqbal, F.J. Ahmad, Rutin-encapsulated chitosan nanoparticles targeted to the brain in the treatment of Cerebral Ischemia, Int. J. Biol. Macromol. 91 (2016) 640–655, https://doi.org/10.1016/j.ijbiomac.2016.06.001.
[68] H. Karatas, Y. Aktas, Y. Gursoy-Ozdemir, E. Bodur, M. Yemisci, S. Caban, A. Vural, O. Pinarbasli, Y. Capan, E. Fernandez-Megia, R. Novoa-Carballal, R. Riguera, K. Andrieux, P. Couvreur, T. Dalkara, A Nanomedicine Transports a Peptide Caspase-3 Inhibitor across the Blood-Brain Barrier and Provides Neuroprotection, J. Neurosci. 29 (2009) 13761–13769, https://doi.org/10.1523/JNEUROSCI.4246-09.2009.
[69] D. Sun, A. Xue, B. Zhang, H. Lou, H. Shi, X. Zhang, Polysorbate 80-coated PLGA nanoparticles improve the permeability of acetylpuerarin and enhance its brain-protective effects in rats, J. Pharm. Pharmacol. 67 (2015) 1650–1662, https://doi.org/10.1111/jphp.12481.
[70] M.K. Reddy, V. Labhasetwar, Nanoparticle-mediated delivery of superoxide dismutase to the brain: an effective strategy to reduce ischemia-reperfusion injury, FASEB J. 23 (2009) 1384–1395, https://doi.org/10.1096/fj.08-116947.
[71] D. Hänggi, J. Perrin, S. Eicker, K. Beseoglu, N. Etminan, M.A. Kamp, H.-J. Heiroth, N. Bege, S. Macht, K. Frauenknecht, C. Sommer, T. Kissel, H.-J. Steiger, Local delivery of nimodipine by prolonged-release microparticles—feasibility, effectiveness and dose-finding in experimental subarachnoid hemorrhage, PLoS One. 7 (2012), e42597.
[72] C. Chung, J. Yang, Y. Kuo, Biomaterials Polybutylcyanoacrylate nanoparticles for delivering hormone response element-conjugated neurotrophin-3 to the brain of intracerebral hemorrhagic rats, Biomaterials. 34 (2013) 9717–9727, https://doi.org/10.1016/j.biomaterials.2013.08.083.
[73] Z. Zhang, M. Jiang, J. Fang, M. Yang, S. Zhang, Y. Yin, D. Li, L. Mao, X. Fu, Y. Hou, X. Fu, Enhanced therapeutic potential of nano-curcumin against subarachnoid hemorrhage-induced blood – brain barrier disruption through inhibition of inflammatory response and oxidative stress, Mol. Neurobiol. (2017) 1–14, https://doi.org/10.1007/s12035-015-9635-y.
[74] N. Zhang, Y. Luo, L. He, L. Zhou, W. Wu, A self-assembly peptide nanofibrous scaffold reduces inflammatory response and promotes functional recovery in a mouse model of intracerebral hemorrhage, Nanomedicine Nanotechnology, Biol. Med. 12 (2016) 1205–1217, https://doi.org/10.1016/j.nano.2015.12.387.
[75] J. Li, L. Feng, L. Fan, Y. Zha, L. Guo, Q. Zhang, J. Chen, Z. Pang, Y. Wang, X. Jiang, V.C. Yang, L. Wen, Targeting the brain with PEG-PLGA nanoparticles modified with phage-displayed peptides, Biomaterials. 32 (2011) 4943–4950, https://doi.org/10.1016/j.biomaterials.2011.03.031.
[76] J. Kreuter, R.N. Alyautdin, D.A. Kharkevich, A.A. Ivanov, Passage of peptides through the blood-brain barrier with colloidal polymer particles (nanoparticles), Brain Res. 674 (1995) 171–174, https://doi.org/10.1016/0006-8993(95)00023-J.
[77] D.H. Kim, D.C. Martin, Sustained release of dexamethasone from hydrophilic matrices using PLGA nanoparticles for neural drug delivery, Biomaterials. 27 (2006) 3031–3037, https://doi.org/10.1016/j.biomaterials.2005.12.021.
[78] H. Liu, J. Ni, R. Wang, In vitro release performance and analgesic activity of endomorphin-1 loaded nanoparticles, Pharmazie. 61 (2006) 450–452.
[79] R.N. Alyautdin, V.E. Petrov, K. Langer, A. Berthold, D.A. Kharkevich, J. Kreuter, Delivery of loperamide across the blood-brain barrier with polysorbate 80-Coated polybutylcyanoacrylate nanoparticles, Pharm. Res. 14 (1997) 325–328, https://doi.org/10.1023/A:1012098005098.
[80] Y.C. Chen, W.Y. Hsieh, W.F. Lee, D.T. Zeng, Effects of surface modification of PLGA-PEG-PLGA nanoparticles on loperamide delivery efficiency across the blood-brain barrier, J. Biomater. Appl. 27 (2013) 909–922, https://doi.org/10.1177/0885328211429495.
[81] K. Gao, X. Jiang, Influence of particle size on transport of methotrexate across blood brain barrier by polysorbate 80-coated polybutylcyanoacrylate nanoparticles, Int. J. Pharm. 310 (2006) 213–219, https://doi.org/10.1016/j.ijpharm.2005.11.040.
[82] T. Parikh, M.M. Bommana, E. Squillante, Efficacy of surface charge in targeting pegylated nanoparticles of sulpiride to the brain, Eur. J. Pharm. Biopharm. 74 (2010) 442–450, https://doi.org/10.1016/j.ejpb.2009.11.001.

[83] R.N. Alyautdin, E.B. Tezikov, P. Ramge, D.A. Kharkevich, D.J. Begley, J. Kreuter, Significant entry of tubocurarine into the brain of rats by adsorption to polysorbate 80-coated polybutylcyanoacrylate nanoparticles: An in situ brain perfusion study, J. Microencapsul. 15 (1998) 67–74, https://doi.org/10.3109/02652049809006836.
[84] T. Miyazawa, K. Nakagawa, T. Harigae, R. Onuma, F. Kimura, T. Fujii, T. Miyazawa, Distribution of β-carotene-encapsulated polysorbate 80-coated poly(D, L-lactide-co-glycolide) nanoparticles in rodent tissues following intravenous administration, Int. J. Nanomedicine. 10 (2015) 7223–7230, https://doi.org/10.2147/IJN.S94336.
[85] A. Bagad, K.Z.A. Received, Y. Review, W.M. Bagad, Z. Ahmed, K. Medical, B. Division, V.T. Nadu, Poly (n Butylcyanoacrylate) Nanoparticles for Oral Delivery of Quercetin : preparation, characterization, and pharmacokinetics and biodistribution studies in Wistar rats, 2015 1–12.
[86] R. Huang, H. Ma, Y. Guo, S. Liu, Y. Kuang, K. Shao, J. Li, Y. Liu, L. Han, S. Huang, S. An, L. Ye, J. Lou, C. Jiang, Angiopep-conjugated nanoparticles for targeted long-term gene therapy of parkinson's disease, Pharm. Res. 30 (2013) 2549–2559, https://doi.org/10.1007/s11095-013-1005-8.
[87] R. Huang, L. Han, J. Li, F. Ren, W. Ke, C. Jiang, Y. Pei, Neuroprotection in a 6-hydroxydopamine-lesioned Parkinson model using lactoferrin-modified nanoparticles, J. Gene Med. 11 (2009) 754–763, https://doi.org/10.1002/jgm.1361.
[88] S. Kannan, H. Dai, R.S. Navath, B. Balakrishnan, NIH Public Access, 4, 2012 https://doi.org/10.1126/scitranslmed.3003162.Dendrimer-Based.
[89] Y.K.K. Katare, R.P.P. Daya, C. Sookram Gray, R.E.E. Luckham, J. Bhandari, A.S.S. Chauhan, R.K.K. Mishra, Brain targeting of a water insoluble antipsychotic drug haloperidol via the intranasal route using PAMAM dendrimer, Mol. Pharm. 12 (2015) 3380–3388, https://doi.org/10.1021/acs.molpharmaceut.5b00402.
[90] P. Jeon, M. Choi, J. Oh, M. Lee, Dexamethasone-conjugated polyamidoamine dendrimer for delivery of the meme oxygenase-1 gene into the ischemic brain, Macromol. Biosci. 15 (2015) 1021–1028, https://doi.org/10.1002/mabi.201500058.
[91] Y. Liu, J. Li, K. Shao, R. Huang, L. Ye, J. Lou, C. Jiang, A leptin derived 30-amino-acid peptide modified pegylated poly-l-lysine dendrigraft for brain targeted gene delivery, Biomaterials. 31 (2010) 5246–5257, https://doi.org/10.1016/j.biomaterials.2010.03.011.
[92] W. Ke, K. Shao, R. Huang, L. Han, Y. Liu, J. Li, Y. Kuang, L. Ye, J. Lou, C. Jiang, Gene delivery targeted to the brain using an Angiopep-conjugated polyethyleneglycol-modified polyamidoamine dendrimer, Biomaterials. 30 (2009) 6976–6985, https://doi.org/10.1016/j.biomaterials.2009.08.049.
[93] L. Albertazzi, L. Gherardini, M. Brondi, S. Sulis Sato, A. Bifone, T. Pizzorusso, G.M. Ratto, G. Bardi, In vivo distribution and toxicity of PAMAM dendrimers in the central nervous system depend on their surface chemistry, Mol. Pharm. 10 (2013) 249–260, https://doi.org/10.1021/mp300391v.
[94] S. Somani, D.R. Blatchford, O. Millington, M.L. Stevenson, C. Dufès, Transferrin-bearing polypropylenimine dendrimer for targeted gene delivery to the brain, J. Control. Release. 188 (2014) 78–86, https://doi.org/10.1016/j.jconrel.2014.06.006.
[95] R. Huang, W. Ke, Y. Liu, C. Jiang, Y. Pei, The use of lactoferrin as a ligand for targeting the polyamidoamine-based gene delivery system to the brain, Biomaterials. 29 (2008) 238–246, https://doi.org/10.1016/j.biomaterials.2007.09.024.
[96] B. Srinageshwar, S. Peruzzaro, M. Andrews, K. Johnson, A. Hietpas, B. Clark, C. McGuire, E. Petersen, J. Kippe, A. Stewart, O. Lossia, A. Al-Gharaibeh, A. Antcliff, R. Culver, D. Swanson, G. Dunbar, A. Sharma, J. Rossignol, PAMAM dendrimers cross the blood–brain barrier when administered through the carotid artery in C57BL/6J mice, Int. J. Mol. Sci. 18 (2017)https://doi.org/10.3390/ijms18030628.
[97] A. Zarebkohan, F. Najafi, H.R. Moghimi, M. Hemmati, M.R. Deevband, B. Kazemi, Synthesis and characterization of a PAMAM dendrimer nanocarrier functionalized by SRL peptide for targeted gene delivery to the brain, Eur. J. Pharm. Sci. 78 (2015) 19–30, https://doi.org/10.1016/j.ejps.2015.06.024.
[98] T. Kanazawa, H. Taki, K. Tanaka, Y. Takashima, H. Okada, Cell-penetrating peptide-modified block copolymer micelles promote direct brain delivery via intranasal administration, Pharm. Res. 28 (2011) 2130–2139, https://doi.org/10.1007/s11095-011-0440-7.
[99] D. Press, c (RGDyK) -decorated Pluronic micelles for enhanced doxorubicin and paclitaxel delivery to brain glioma, (2016) 1629–1641.
[100] A. Saxena, S. Khosraviani, S. Noel, D. Mohan, T. Donner, A.R.A. Hamad, HHS Public Access 74 (2016) 27–34, https://doi.org/10.1016/j.cyto.2014.10.031.Interleukin-10.
[101] P. Agrawal Sonali, R.P. Singh, C.V. Rajesh, S. Singh, M.R. Vijayakumar, B.L. Pandey, M.S. Muthu, Transferrin receptor-targeted vitamin E TPGS micelles for brain cancer therapy: preparation, characterization and brain distribution in rats, Drug Deliv. 23 (2016) 1788–1798, https://doi.org/10.3109/10717544.2015.1094681.
[102] R. Zhang, R. Saito, Y. Mano, A. Sumiyoshi, M. Kanamori, Y. Sonoda, R. Kawashima, T. Tominaga, Convection-enhanced delivery of SN-38-loaded polymeric micelles (NK012) enables consistent distribution of SN-38 and is effective against rodent intracranial brain tumor models, Drug Deliv. 23 (2016) 2780–2786, https://doi.org/10.3109/10717544.2015.1081994.
[103] A.J. Li, Y.H. Zheng, G.D. Liu, W.S. Liu, P.C. Cao, Z.F. Bu, Efficient delivery of docetaxel for the treatment of brain tumors by cyclic RGD-tagged polymeric micelles, Mol. Med. Rep. 11 (2015) 3078–3086, https://doi.org/10.3892/mmr.2014.3017.
[104] X. Tan, G. Kim, D. Lee, J. Oh, M. Kim, C. Piao, J. Lee, M. Sang Lee, J. Hoon Jeong, M. Lee, A curcumin-loaded polymeric micelle as a carrier of a microRNA-21 antisense-oligonucleotide for enhanced anti-tumor effects in a glioblastoma animal model, Biomater. Sci. 6 (2018) https://doi.org/10.1039/c7bm01088e.
[105] Y. Li, L. Baiyang, B. Leran, W. Zhen, X. Yandong, D. Baixiang, Z. Dandan, Z. Yufu, L. Jun, Y. Rutong, L. Hongmei, Reduction-responsive PEtOz-SS-PCL micelle with tailored size to overcome blood–brain barrier and enhance doxorubicin antiglioma effect, Drug Deliv. 24 (2017) 1782–1790, https://doi.org/10.1080/10717544.2017.1402218.
[106] D. Ran, J. Mao, Q. Shen, C. Xie, C. Zhan, R. Wang, W. Lu, GRP78 enabled micelle-based glioma targeted drug delivery, J. Control. Release. 255 (2017) 120–131, https://doi.org/10.1016/j.jconrel.2017.03.037.
[107] W.G. Singleton, A.M. Collins, A.S. Bienemann, C.L. Killick-Cole, H.R. Haynes, D.J. Asby, C.P. Butts, M.J. Wyatt, N.U. Barua, S.S. Gill, Convection enhanced delivery of panobinostat (LBH589)-loaded pluronic nano-micelles prolongs survival in the F98 rat glioma model, Int. J. Nanomedicine. 12 (2017) 1385–1399, https://doi.org/10.2147/IJN.S125300.
[108] Y. Bi, L. Liu, Y. Lu, T. Sun, C. Shen, X. Chen, Q. Chen, S. An, X. He, C. Ruan, Y. Wu, Y. Zhang, Q. Guo, Z. Zheng, Y. Liu, M. Lou, S. Zhao, C. Jiang, T7 peptide-functionalized PEG-PLGA micelles loaded with carmustine for targeting therapy of glioma, ACS Appl. Mater. Interfaces. 8 (2016) 27465–27473, https://doi.org/10.1021/acsami.6b05572.
[109] T. Chen, Y. Li, C. Li, X. Yi, R. Wang, S.M.Y. Lee, Y. Zheng, Pluronic P85/F68 micelles of baicalein could interfere with mitochondria to overcome MRP2-Mediated efflux and offer improved anti-Parkinsonian activity, Mol. Pharm. 14 (2017) 3331–3342, https://doi.org/10.1021/acs.molpharmaceut.7b00374.
[110] M.S. Muthu, A.K. Sahu, A. Abdulla Sonali, D. Kaklotar, C.V. Rajesh, S. Singh, B.L. Pandey, Solubilized delivery of paliperidone palmitate by d- alpha-tocopheryl polyethylene glycol 1000 succinate micelles for improved short-term psychotic management, Drug Deliv. 23 (2016) 230–237, https://doi.org/10.3109/10717544.2014.909907.
[111] M. Das, C. Wang, R. Bedi, S.S. Mohapatra, S. Mohapatra, Magnetic micelles for DNA delivery to rat brains after mild traumatic brain injury, Nanomedicine Nanotechnology, Biol. Med. 10 (2014) 1539–1548, https://doi.org/10.1016/j.nano.2014.01.003.
[112] K. Shao, R. Huang, J. Li, L. Han, L. Ye, J. Lou, C. Jiang, Angiopep-2 modified PE-PEG based polymeric micelles for amphotericin B delivery targeted to the brain, J. Control. Release. 147 (2010) 118–126, https://doi.org/10.1016/j.jconrel.2010.06.018.
[113] S.A. Nour, N.S. Abdelmalak, M.J. Naguib, H.M. Rashed, A.B. Ibrahim, Intranasal brain-targeted clonazepam polymeric micelles for immediate control of status epilepticus: in vitro optimization, ex vivo determination of cytotoxicity, in vivo biodistribution and pharmacodynamics studies, Drug Deliv. 23 (2016) 3681–3695, https://doi.org/10.1080/10717544.2016.1223216.
[114] A. Yu, J. Lv, F. Yuan, Z. Xia, K. Fan, G. Chen, J. Ren, C. Lin, S. Wei, F. Yang, mPEG -PLA/TPGS mixed micelles via intranasal administration improved the bioavailability of lamotrigine in the hippocampus, Int. J. Nanomedicine. 12 (2017) 8353–8362, https://doi.org/10.2147/IJN.S145488.
[115] S. Hagl, A. Kocher, C. Schiborr, N. Kolesova, J. Frank, G.P. Eckert, Curcumin micelles improve mitochondrial function in neuronal PC12 cells and brains of NMRI mice - impact on bioavailability, Neurochem. Int. 89 (2015) 234–242, https://doi.org/10.1016/j.neuint.2015.07.026.
[116] Y. Li, P. Zhang, L. Hu, Y. Wang, J. Wang, L. Feng, Poly(ε-caprolactone)-Block-poly (Ethyl Ethylene Phosphate) micelles for brain-targeting drug delivery: In vitro and in vivo valuation, Pharm. Res. 27 (2010) 2657–2669, https://doi.org/10.1007/s11095-010-0265-9.
[117] J. Shen, C. Zhan, C. Xie, Q. Meng, B. Gu, C. Li, Y. Zhang, W. Lu, Poly(ethylene glycol)-block-poly(d,l-lactide acid) micelles anchored with angiopep-2 for brain-targeting delivery, J. Drug Target. 19 (2011) 197–203, https://doi.org/10.3109/1061186X.2010.483517.
[118] X. Meng, J. Liu, X. Yu, J. Li, X. Lu, T. Shen, Pluronic F127 and D-α-Tocopheryl Polyethylene Glycol Succinate (TPGS) mixed micelles for targeting drug delivery across the blood brain barrier, Sci. Rep. 7 (2017) 1–12, https://doi.org/10.1038/s41598-017-03123-y.
[119] E.B. Basalious, R.N. Shamma, Novel self-assembled nano-tubular mixed micelles of Pluronics P123, Pluronic F127 and phosphatidylcholine for oral delivery of nimodipine: In vitro characterization, ex vivo transport and in vivo pharmacokinetic studies, Int. J. Pharm. 493 (2015) 347–356, https://doi.org/10.1016/J.IJPHARM.2015.07.075.
[120] X. Ying, H. Wen, W.L. Lu, J. Du, J. Guo, W. Tian, Y. Men, Y. Zhang, R.J. Li, T.Y. Yang, D. W. Shang, J.N. Lou, L.R. Zhang, Q. Zhang, Dual-targeting daunorubicin liposomes improve the therapeutic efficacy of brain glioma in animals, J. Control. Release. 141 (2010) 183–192, https://doi.org/10.1016/j.jconrel.2009.09.020.
[121] L.H. Treat, N. McDannold, Y. Zhang, N. Vykhodtseva, K. Hynynen, Improved anti-tumor effect of liposomal doxorubicin after targeted blood-brain barrier disruption by MRI-guided focused ultrasound in rat glioma, Ultrasound Med. Biol. 38 (2012) 1716–1725, https://doi.org/10.1016/J.ULTRASMEDBIO.2012.04.015.
[122] H. Chen, Y. Qin, Q. Zhang, W. Jiang, L. Tang, J. Liu, Q. He, Lactoferrin modified doxorubicin-loaded procationic liposomes for the treatment of gliomas, Eur. J. Pharm. Sci. 44 (2011) 164–173, https://doi.org/10.1016/j.ejps.2011.07.007.
[123] Y. Qin, H. Chen, W. Yuan, R. Kuai, Q. Zhang, F. Xie, L. Zhang, Z. Zhang, J. Liu, Q. He, Liposome formulated with TAT-modified cholesterol for enhancing the brain delivery, Int. J. Pharm. 419 (2011) 85–95, https://doi.org/10.1016/j.ijpharm.2011.07.021.
[124] V. Soni, D.V. Kohli, S.K. Jain, Transferrin-conjugated liposomal system for improved delivery of 5-fluorouracil to brain, J. Drug Target. 16 (2008) 73–78, https://doi.org/10.1080/10611860701725381.
[125] Q. Lin, K.L. Mao, F.R. Tian, J.J. Yang, P.P. Chen, J. Xu, Z.L. Fan, Y.P. Zhao, W.F. Li, L. Zheng, Y.Z. Zhao, C.T. Lu, Brain tumor-targeted delivery and therapy by focused ultrasound introduced doxorubicin-loaded cationic liposomes, Cancer Chemother. Pharmacol. 77 (2016) 269–280, https://doi.org/10.1007/s00280-015-2926-1.
[126] J. Gao, Z. Wang, H. Liu, L. Wang, G. Huang, Liposome encapsulated of temozolomide for the treatment of glioma tumor: preparation, characterization and evaluation, Drug Discov. Ther. 9 (2015) 205–212, https://doi.org/10.5582/ddt.2015.01016.

[127] S.A. Shein, N.V. Nukolova, A.A. Korchagina, T.O. Abakumova, I.I. Kiuznetsov, M.A. Abakumov, V.P. Baklaushev, O.I. Gurina, V.P. Chekhonin, Site-directed delivery of VEGF-targeted liposomes into intracranial C6 glioma, Bull. Exp. Biol. Med. 158 (2015) 371–376, https://doi.org/10.1007/s10517-015-2765-4.
[128] Y. Wang, X. Ying, H. Xu, H. Yan, X. Li, H. Tang, The functional curcumin liposomes induce apoptosis in C6 glioblastoma cells and C6 glioblastoma stem cells in vitro and in animals, Int. J. Nanomedicine. 12 (2017) 1369–1384, https://doi.org/10.2147/IJN.S124276.
[129] Y. Shen, Z. Pi, F. Yan, C.K. Yeh, X. Zeng, X. Diao, Y. Hu, S. Chen, X. Chen, H. Zheng, Enhanced delivery of paclitaxel liposomes using focused ultrasound with microbubbles for treating nude mice bearing intracranial glioblastoma xenografts, Int. J. Nanomedicine. 12 (2017) 5613–5629, https://doi.org/10.2147/IJN.S136401.
[130] A.K. Al Asmari, Z. Ullah, M. Tariq, A. Fatani, Preparation, characterization, and in vivo evaluation of intranasally administered liposomal formulation of donepezil, Drug Des. Devel. Ther. 10 (2016) 205–215, https://doi.org/10.2147/DDDT.S93937.
[131] M.F. Ismail, A.N. Elmeshad, N.A.-H. Salem, Potential therapeutic effect of nanobased formulation of rivastigmine on rat model of Alzheimer's disease, Int. J. Nanomedicine. 8 (2013) 393–406, https://doi.org/10.2147/IJN.S39232.
[132] A.C. Granholm, C. Backman, F. Bloom, T. Ebendal, G.A. Gerhardt, B. Hoffer, L. Mackerlova, L. Olson, S. Soderstrom, L.R. Walus, NGF and anti-transferrin receptor antibody conjugate: short and long-term effects on survival of cholinergic neurons in intraocular septal transplants, J. Pharmacol. Exp. Ther. 268 (1994) 448–459.
[133] S. Nageeb El-Helaly, A. Abd Elbary, M.A. Kassem, M.A. El-Nabarawi, Electrosteric stealth Rivastigmine loaded liposomes for brain targeting: preparation, characterization, *ex vivo*, bio-distribution and *in vivo* pharmacokinetic studies, Drug Deliv. 24 (2017) 692–700, https://doi.org/10.1080/10717544.2017.1309476.
[134] Y.C. Kuo, C.Y. Lin, J.S. Li, Y.I. Lou, Wheat germ agglutinin-conjugated liposomes incorporated with cardiolipin to improve neuronal survival in Alzheimer's disease treatment, Int. J. Nanomedicine. 12 (2017) 1757–1774, https://doi.org/10.2147/IJN.S128396.
[135] Y. Zhang, F. Calon, C. Zhu, R.J. Boado, W.M. Pardridge, Intravenous nonviral gene therapy causes normalization of striatal tyrosine hydroxylase and reversal of motor impairment in experimental Parkinsonism, Hum. Gene Ther. 14 (2003) 1–12, https://doi.org/10.1089/10430340360464660.
[136] Y.S. Kang, H.J. Jung, J.S. Oh, D.Y. Song, Use of PEGylated immunoliposomes to deliver dopamine across the blood–brain barrier in a rat model of Parkinson's disease, CNS Neurosci. Ther. 22 (2016) 817–823, https://doi.org/10.1111/cns.12580.
[137] R. Narayan, M. Singh, O.P. Ranjan, Y. Nayak, S. Garg, G.V. Shavi, U.Y. Nayak, Development of risperidone liposomes for brain targeting through intranasal route, Life Sci. 163 (2016) 38–45, https://doi.org/10.1016/j.lfs.2016.08.033.
[138] Y.-Z. Zhao, M. Lin, Q. Lin, W. Yang, X.-C. Yu, F.-R. Tian, K.-L. Mao, J.-J. Yang, C.-T. Lu, H.L. Wong, Intranasal delivery of bFGF with nanoliposomes enhances in vivo neuroprotection and neural injury recovery in a rodent stroke model, J. Control. Release. 224 (2016) 165–175, https://doi.org/10.1016/J.JCONREL.2016.01.017.
[139] P.M. Friden, L.R. Walus, G.F. Musso, R.M. Starzyk, Anti-transferrin receptor antibody and antibody-drug conjugates cross the blood-brain barrier, Med. Sci. Nat. 88 (1991) 4771–4775, https://doi.org/10.1073/pnas.88.11.4771.
[140] S. Wu, G. Li, X. Li, C. Lin, D. Yu, S. Luan, C. Ma, Transport of glial cell line-derived neurotrophic factor into liposomes across the blood-brain barrier: In vitro and in vivo studies, Int. J. Mol. Sci. 15 (2014) 3612–3623, https://doi.org/10.3390/ijms15033612.
[141] Y. Qin, Q. Zhang, H. Chen, W. Yuan, R. Kuai, F. Xie, L. Zhang, X. Wang, Z. Zhang, J. Liu, Q. He, Comparison of four different peptides to enhance accumulation of liposomes into the brain, J. Drug Target. 20 (2012) 235–245, https://doi.org/10.3109/1061186X.2011.639022.
[142] H. Chen, L. Tang, Y. Qin, Y. Yin, J. Tang, W. Tang, X. Sun, Z. Zhang, J. Liu, Q. He, Lactoferrin-modified procationic liposomes as a novel drug carrier for brain delivery, Eur. J. Pharm. Sci. 40 (2010) 94–102, https://doi.org/10.1016/j.ejps.2010.03.007.
[143] Y. Qin, H. Chen, Q. Zhang, X. Wang, W. Yuan, R. Kuai, J. Tang, L. Zhang, Z. Zhang, Q. Zhang, J. Liu, Q. He, Liposome formulated with TAT-modified cholesterol for improving brain delivery and therapeutic efficacy on brain glioma in animals, Int. J. Pharm. 420 (2011) 304–312, https://doi.org/10.1016/j.ijpharm.2011.09.008.
[144] N. Shi, W.M. Pardridge, Noninvasive gene targeting to the brain, Proc. Natl. Acad. Sci. U. S. A. 97 (2000) 7567–7572, https://doi.org/10.1073/pnas.130187497.
[145] N. Shi, R.J. Boado, W.M. Pardridge, Receptor-mediated gene targeting to tissues in vivo following intravenous administration of pegylated immunoliposomes, Pharm. Res. 18 (2001) 1091–1095, https://doi.org/10.1023/A:1010910523202.
[146] A. Estella-Hermoso De Mendoza, V. Préat, F. Mollinedo, M.J. Blanco-Prieto, In vitro and in vivo efficacy of edelfosine-loaded lipid nanoparticles against glioma, J. Control. Release. 156 (2011) 421–426, https://doi.org/10.1016/j.jconrel.2011.07.030.
[147] J. Jin, K.H. Bae, H. Yang, S.J. Lee, H. Kim, Y. Kim, K.M. Joo, S.W. Seo, T.G. Park, D.H. Nam, In vivo specific delivery of c-Met siRNA to glioblastoma using cationic solid lipid nanoparticles, Bioconjug. Chem. 22 (2011) 2568–2572, https://doi.org/10.1021/bc200406n.
[148] S.M. Martins, B. Sarmento, C. Nunes, M. Lúcio, S. Reis, D.C. Ferreira, Brain targeting effect of camptothecin-loaded solid lipid nanoparticles in rat after intravenous administration, Eur. J. Pharm. Biopharm. 85 (2013) 488–502, https://doi.org/10.1016/j.ejpb.2013.08.011.
[149] S. Martins, I. Tho, I. Reimold, G. Fricker, E. Souto, D. Ferreira, M. Brandl, Brain delivery of camptothecin by means of solid lipid nanoparticles: Formulation design, in vitro and in vivo studies, Int. J. Pharm. 439 (2012) 49–62, https://doi.org/10.1016/j.ijpharm.2012.09.054.
[150] A. Zanotto-Filho, K. Coradini, E. Braganhol, R. Schröder, C.M. De Oliveira, A. Simões-Pires, A.M.O. Battastini, A.R. Pohlmann, S.S. Guterres, C.M. Forcelini, R.C.R. Beck, J.C.F. Moreira, Curcumin-loaded lipid-core nanocapsules as a strategy to improve pharmacological efficacy of curcumin in glioma treatment, Eur. J. Pharm. Biopharm. 83 (2013) 156–167, https://doi.org/10.1016/j.ejpb.2012.10.019.
[151] S. Jose, S.S. Anju, T.A. Cinu, N.A. Aleykutty, S. Thomas, E.B. Souto, In vivo pharmacokinetics and biodistribution of resveratrol-loaded solid lipid nanoparticles for brain delivery, Int. J. Pharm. 474 (2014) 6–13, https://doi.org/10.1016/j.ijpharm.2014.08.003.
[152] R.G. Madane, H.S. Mahajan, Curcumin-loaded nanostructured lipid carriers (NLCs) for nasal administration: design, characterization, and *in vivo* study, Drug Deliv. 7544 (2014) 1–9, https://doi.org/10.3109/10717544.2014.975382.
[153] Z.R. Cohen, S. Ramishetti, N. Peshes-Yaloz, M. Goldsmith, A. Wohl, Z. Zibly, D. Peer, Localized RNAi therapeutics of chemoresistant grade IV glioma using hyaluronan-grafted lipid-based nanoparticles, ACS Nano. 9 (2015) 1581–1591, https://doi.org/10.1021/nn506248s.
[154] Z. Chen, X. Lai, S. Song, X. Zhu, J. Zhu, Nanostructured lipid carriers based temozolomide and gene co-encapsulated nanomedicine for gliomatosis cerebri combination therapy, Drug Deliv. 7544 (2015) 1–5, https://doi.org/10.3109/10717544.2015.1038857.
[155] S. Song, G. Mao, J. Du, X. Zhu, Novel RGD containing, temozolomide-loading nanostructured lipid carriers for glioblastoma multiforme chemotherapy, Drug Deliv. 23 (2016) 1404–1408, https://doi.org/10.3109/10717544.2015.1064186.
[156] M. Wu, Y. Fan, S. Lv, B. Xiao, M. Ye, X. Zhu, Vincristine and temozolomide combined chemotherapy for the treatment of glioma: a comparison of solid lipid nanoparticles and nanostructured lipid carriers for dual drugs delivery, Drug Deliv. 23 (2016) 2720–2725, https://doi.org/10.3109/10717544.2015.1058434.
[157] Y. Chen, L. Pan, M. Jiang, D. Li, L. Jin, Nanostructured lipid carriers enhance the bioavailability and brain cancer inhibitory efficacy of curcumin both in vitro and in vivo, Drug Deliv. 23 (2016) 1383–1392, https://doi.org/10.3109/10717544.2015.1049719.
[158] D. Yu, O.F. Khan, M.L. Suvà, B. Dong, W.K. Panek, T. Xiao, M. Wu, Y. Han, A.U. Ahmed, I.V. Balyasnikova, H.F. Zhang, C. Sun, R. Langer, D.G. Anderson, M.S. Lesniak, Multiplexed RNAi therapy against brain tumor-initiating cells via lipopolymeric nanoparticle infusion delays glioblastoma progression, Proc. Natl. Acad. Sci. 114 (2017) E6147–E6156.
[159] J.E. Dahlman, C. Barnes, O.F. Khan, A. Thiriot, S. Jhunjunwala, T.E. Shaw, Y. Xing, H.B. Sager, G. Sahay, L. Speciner, A. Bader, R.L. Bogorad, H. Yin, T. Racie, Y. Dong, S. Jiang, D. Seedorf, A. Dave, K. Singh Sandhu, M.J. Webber, T. Novobrantseva, V.M. Ruda, A. K.R. Lytton-Jean, C.G. Levins, B. Kalish, D.K. Mudge, M. Perez, L. Abezgauz, P. Dutta, L. Smith, K. Charisse, M.W. Kieran, K. Fitzgerald, M. Nahrendorf, D. Danino, R.M. Tuder, U.H. Von Andrian, A. Akinc, D. Panigrahy, A. Schroeder, V. Koteliansky, R. Langer, D.G. Anderson, In vivo endothelial siRNA delivery using polymeric nanoparticles with low molecular weight, Nat. Nanotechnol. 9 (2014) 648–655, https://doi.org/10.1038/nnano.2014.84.
[160] V. Kakkar, S.K. Muppu, K. Chopra, I.P. Kaur, Curcumin loaded solid lipid nanoparticles: An efficient formulation approach for cerebral ischemic reperfusion injury in rats, Eur. J. Pharm. Biopharm. 85 (2013) 339–345, https://doi.org/10.1016/j.ejpb.2013.02.005.
[161] Z. Liu, L. Zhang, Q. He, X. Liu, O. Chukwunweike Ikechukwu, L. Tong, L. Guo, H. Yang, Q. Zhang, H. Zhao, X. Gu, Effect of Baicalin-loaded PEGylated cationic solid lipid nanoparticles modified by OX26 antibody on regulating the levels of baicalin and amino acids during cerebral ischemia-reperfusion in rats, Int. J. Pharm. 489 (2015) 131–138, https://doi.org/10.1016/j.ijpharm.2015.04.049.
[162] S.H. Hsu, C.J. Wen, S.A. Al-Suwayeh, H.W. Chang, T.C. Yen, J.Y. Fang, Physicochemical characterization and in vivo bioluminescence imaging of nanostructured lipid carriers for targeting the brain: Apomorphine as a model drug, Nanotechnology. 21 (2010) https://doi.org/10.1088/0957-4484/21/40/405101.
[163] C.V. Pardeshi, V.S. Belgamwar, A.R. Tekade, S.J. Surana, Novel surface modified polymer-lipid hybrid nanoparticles as intranasal carriers for ropinirole hydrochloride: In vitro, ex vivo and in vivo pharmacodynamic evaluation, J. Mater. Sci. Mater. Med. 24 (2013) 2101–2115, https://doi.org/10.1007/s10856-013-4965-7.
[164] Y.M. Gabal, A.O. Kamel, O.A. Sammour, A.H. Elshafeey, Effect of surface charge on the brain delivery of nanostructured lipid carriers in situ gels via the nasal route, Int. J. Pharm. 473 (2014) 442–457, https://doi.org/10.1016/j.ijpharm.2014.07.025.
[165] Y.Z. Zhao, X. Li, C.T. Lu, M. Lin, L.J. Chen, Q. Xiang, M. Zhang, R.R. Jin, X. Jiang, X.T. Shen, X.K. Li, J. Cai, Gelatin nanostructured lipid carriers-mediated intranasal delivery of basic fibroblast growth factor enhances functional recovery in hemiparkinsonian rats, Nanomedicine Nanotechnology, Biol. Med. 10 (2014) 755–764, https://doi.org/10.1016/j.nano.2013.10.009.
[166] E. Esposito, M. Fantin, M. Marti, M. Drechsler, L. Paccamiccio, P. Mariani, E. Sivieri, F. Lain, E. Menegatti, M. Morari, R. Cortesi, Solid lipid nanoparticles as delivery systems for bromocriptine, Pharm. Res. 25 (2008) 1521–1530, https://doi.org/10.1007/s11095-007-9514-y.
[167] P.A. Patel, S.C. Patil, D.R. Kalaria, Y.N. Kalia, V.B. Patravale, Comparative in vitro and in vivo evaluation of lipid based nanocarriers of Huperzine A, Int. J. Pharm. 446 (2013) 16–23, https://doi.org/10.1016/j.ijpharm.2013.02.014.
[168] S. Dhawan, R. Kapil, B. Singh, Formulation development and systematic optimization of solid lipid nanoparticles of quercetin for improved brain delivery, J. Pharm. Pharmacol. 63 (2011) 342–351, https://doi.org/10.1111/j.2042-7158.2010.01225.x.
[169] M. Yusuf, M. Khan, R.A. Khan, B. Ahmed, Preparation, characterization, *in vivo* and biochemical evaluation of brain targeted Piperine solid lipid nanoparticles in an experimentally induced Alzheimer's disease model, J. Drug Target. 21 (2013) 300–311, https://doi.org/10.3109/1061186X.2012.747529.
[170] F. Meng, S. Asghar, S. Gao, Z. Su, J. Song, M. Huo, W. Meng, Q. Ping, Y. Xiao, A novel LDL-mimic nanocarrier for the targeted delivery of curcumin into the brain to treat Alzheimer's disease, Colloids Surfaces B Biointerfaces. 134 (2015) 88–97, https://doi.org/10.1016/j.colsurfb.2015.06.025.

[171] A.K. Sachdeva, S. Misra, I. Pal Kaur, K. Chopra, Neuroprotective potential of sesamol and its loaded solid lipid nanoparticles in ICV-STZ-induced cognitive deficits: Behavioral and biochemical evidence, Eur. J. Pharmacol. 747 (2015) 132–140, https://doi.org/10.1016/j.ejphar.2014.11.014.
[172] S. Misra, K. Chopra, U.N. Saikia, V.R. Sinha, R. Sehgal, M. Modi, B. Medhi, Effect of mesenchymal stem cells and galantamine nanoparticles in rat model of Alzheimer's disease, Regen. Med. 11 (2016) 629–646, https://doi.org/10.2217/rme-2016-0032.
[173] A. Vedagiri, S. Thangarajan, Mitigating effect of chrysin loaded solid lipid nanoparticles against Amyloid β25–35 induced oxidative stress in rat hippocampal region: An efficient formulation approach for Alzheimer's disease, Neuropeptides. 58 (2016) 111–125, https://doi.org/10.1016/j.npep.2016.03.002.
[174] N. Gandomi, R. Varshochian, F. Atyabi, M.H. Ghahremani, M. Sharifzadeh, M. Amini, R. Dinarvand, Solid lipid nanoparticles surface modified with anti-Contactin-2 or anti-Neurofascin for brain-targeted delivery of medicines, Pharm. Dev. Technol. 22 (2017) 426–435, https://doi.org/10.1080/10837450.2016.1226901.
[175] R. Tiwari, K. Pathak, Nanostructured lipid carrier versus solid lipid nanoparticles of simvastatin: Comparative analysis of characteristics, pharmacokinetics and tissue uptake, Int. J. Pharm. 415 (2011) 232–243, https://doi.org/10.1016/j.ijpharm.2011.05.044.
[176] S. Patel, S. Chavhan, H. Soni, A.K. Babbar, R. Mathur, A.K. Mishra, K. Sawant, Brain targeting of risperidone-loaded solid lipid nanoparticles by intranasal route, J. Drug Target. 19 (2011) 468–474, https://doi.org/10.3109/1061186X.2010.523787.
[177] S.K. Singh, P. Dadhania, P.R. Vuddanda, A. Jain, S. Velaga, S. Singh, Intranasal delivery of asenapine loaded nanostructured lipid carriers: formulation, characterization, pharmacokinetic and behavioural assessment, RSC Adv. 6 (2016) 2032–2045, https://doi.org/10.1039/C5RA19793G.
[178] S.M. M., G.A. Elmenoufy, G.A. Elmenoufy, Evaluation of quetiapine fumarate and its solid lipid nanoparticles as antipsychotic drug in rat model of schizophrenia, Biomed. Res. Ther. 4 (2017) 1480, https://doi.org/10.15419/bmrat.v4i08.203.
[179] M.I. Alam, S. Baboota, A. Ahuja, M. Ali, J. Ali, J.K. Sahni, Intranasal administration of nanostructured lipid carriers containing CNS acting drug: Pharmacodynamic studies and estimation in blood and brain, J. Psychiatr. Res. 46 (2012) 1133–1138, https://doi.org/10.1016/j.jpsychires.2012.05.014.
[180] C.Y. Zhuang, N. Li, M. Wang, X.N. Zhang, W.S. Pan, J.J. Peng, Y.S. Pan, X. Tang, Preparation and characterization of vinpocetine loaded nanostructured lipid carriers (NLC) for improved oral bioavailability, Int. J. Pharm. 394 (2010) 179–185, https://doi.org/10.1016/j.ijpharm.2010.05.005.
[181] C. Lin, F. Chen, T. Ye, L. Zhang, W. Zhang, D. Liu, W. Xiong, X. Yang, W. Pan, A novel oral delivery system consisting in "drug-in cyclodextrin-in nanostructured lipid carriers" for poorly water-soluble drug: Vinpocetine, Int. J. Pharm. 465 (2014) 90–96, https://doi.org/10.1016/j.ijpharm.2014.02.013.
[182] M.J. Tsai, P.C. Wu, Y. Bin Huang, J.S. Chang, C.L. Lin, Y.H. Tsai, J.Y. Fang, Baicalein loaded in tocol nanostructured lipid carriers (tocol NLCs) for enhanced stability and brain targeting, Int. J. Pharm. 423 (2012) 461–470, https://doi.org/10.1016/j.ijpharm.2011.12.009.
[183] P. Vergara-Aragón, L.E. Domínguez-Marrufo, P. Ibarra-Guerrero, H. Hernandez-Ramírez, B. Hernández-Téllez, I.E. López-Martínez, I. Sánchez-Cervantes, P. Santiago-Jacinto, J.A. García-Macedo, G. Valverde-Aguilar, J. Santiago, Tio2-dopamine complex implanted unilaterally in the caudate nucleus improves motor activity and behavior function of rats with induced hemiparkinsonism, Proc. West. Pharmacol. Soc. 54 (2011) 15–20. https://www.researchgate.net/profile/Patricia_Vergara2/publication/221712025_Tio2-dopamine_complex_implanted_unilaterally_in_the_caudate_nucleus_improves_motor_activity_and_behavior_function_of_rats_with_induced_hemiparkinsonism/links/595c4eeba6fdcc36b4dc (accessed February 20, 2018).
[184] M.A. Hegazy, H.M. Maklad, D.M. Samy, D.A. Abdelmonsif, B.M. El Sabaa, F.Y. Elnozahy, Cerium oxide nanoparticles could ameliorate behavioral and neurochemical impairments in 6-hydroxydopamine induced Parkinson's disease in rats, Neurochem. Int. 108 (2017) 361–371, https://doi.org/10.1016/J.NEUINT.2017.05.011.
[185] J. Yoo, E. Lee, H.Y. Kim, D. Youn, J. Jung, H. Kim, Y. Chang, W. Lee, J. Shin, S. Baek, W. Jang, W. Jun, S. Kim, J. Hong, H.-J. Park, C.J. Lengner, S.H. Moh, Y. Kwon, J. Kim, Electromagnetized gold nanoparticles mediate direct lineage reprogramming into induced dopamine neurons in vivo for Parkinson's disease therapy, Nat. Nanotechnol. 12 (2017) 1006–1014, https://doi.org/10.1038/nnano.2017.133.
[186] S. Niu, L.-K. Zhang, L. Zhang, S. Zhuang, X. Zhan, W.-Y. Chen, S. Du, L. Yin, R. You, C.-H. Li, Y.-Q. Guan, Inhibition by multifunctional magnetic nanoparticles loaded with alpha-Synuclein RNAi plasmid in a Parkinson's Disease model, Theranostics. 7 (2017) 344–356, https://doi.org/10.7150/thno.16562.
[187] R. Prades, S. Guerrero, E. Araya, C. Molina, E. Salas, E. Zurita, J. Selva, G. Egea, C. López-Iglesias, M. Teixidó, M.J. Kogan, E. Giralt, Delivery of gold nanoparticles to the brain by conjugation with a peptide that recognizes the transferrin receptor, Biomaterials. 33 (2012) 7194–7205, https://doi.org/10.1016/j.biomaterials.2012.06.063.
[188] J. Tang, N. Huang, X. Zhang, T. Zhou, Y. Tan, J. Pi, L. Pi, S. Cheng, H. Zheng, Y. Cheng, Aptamer-conjugated PEGylated quantum dots targeting epidermal growth factor receptor variant III for fluorescence imaging of glioma, Int. J. Nanomedicine. 12 (2017) 3899–3911, https://doi.org/10.2147/IJN.S133166.
[189] S. Ruan, M. Yuan, L. Zhang, G. Hu, J. Chen, X. Cun, Q. Zhang, Y. Yang, Q. He, H. Gao, Tumor microenvironment sensitive doxorubicin delivery and release to glioma using angiopep-2 decorated gold nanoparticles, Biomaterials. 37 (2015) 425–435, https://doi.org/10.1016/j.biomaterials.2014.10.007.
[190] L. Su, B. Zhang, Y. Huang, H. Zhang, Q. Xu, J. Tan, Superparamagnetic iron oxide nanoparticles modified with dimyristoylphosphatidylcholine and their distribution in the brain after injection in the rat substantia nigra, Mater. Sci. Eng. C. 81 (2017) 400–406, https://doi.org/10.1016/j.msec.2017.08.049.
[191] B. Pham, E. Colvin, N. Pham, B. Kim, E. Fuller, E. Moon, R. Barbey, S. Yuen, B. Rickman, N. Bryce, S. Bickley, M. Tanudji, S. Jones, V. Howell, B. Hawkett, Biodistribution and clearance of stable superparamagnetic maghemite iron oxide nanoparticles in mice following intraperitoneal administration, Int. J. Mol. Sci. 19 (2018) 205, https://doi.org/10.3390/ijms19010205.
[192] F. Sousa, S. Mandal, C. Garrovo, A. Astolfo, A. Bonifacio, D. Latawiec, R.H. Menk, F. Arfelli, S. Huewel, G. Legname, H.-J. Galla, S. Krol, Functionalized gold nanoparticles: a detailed in vivo multimodal microscopic brain distribution study, Nanoscale. 2 (2010) 2826, https://doi.org/10.1039/c0nr00345j.
[193] R.G. Thorne, C. Nicholson, In vivo diffusion analysis with quantum dots and dextrans predicts the width of brain extracellular space, Proc. Natl. Acad. Sci. 103 (2006) 5567–5572, https://doi.org/10.1073/pnas.0509425103.
[194] Y. Huang, B. Zhang, S. Xie, B. Yang, Q. Xu, J. Tan, Superparamagnetic Iron Oxide Nanoparticles Modified with Tween 80 Pass through the Intact Blood-Brain Barrier in Rats under Magnetic Field, ACS Appl. Mater. Interfaces. 8 (2016) 11336–11341, https://doi.org/10.1021/acsami.6b02838.
[195] S. Paris-Robidas, D. Brouard, V. Emond, M. Parent, F. Calon, Internalization of targeted quantum dots by brain capillary endothelial cells in vivo, J. Cereb. Blood Flow Metab. 36 (2016) 731–742, https://doi.org/10.1177/0271678X15608201.
[196] B.G. Cha, H. Jeong, D. Kang, M. Nam, C.K. Kim, D.Y. Kim, Customized lipid-coated magnetic mesoporous silica nanoparticle doped with ceria nanoparticles for theragnosis of intracerebral hemorrhage, 11, 2018.
[197] D. Kang, C.K. Kim, H. Jeong, M. Soh, T. Kim, I. Choi, S. Ki, D.Y. Kim, W. Yang, T. Hyeon, S. Lee, Biocompatible custom ceria nanoparticles against reactive oxygen species resolve acute inflammatory reaction after intracerebral hemorrhage, 10, 2017 2743–2760, https://doi.org/10.1007/s12274-017-1478-6.
[198] N.A. Singh, V. Bhardwaj, C. Ravi, N. Ramesh, EGCG nanoparticles attenuate aluminum chloride induced neurobehavioral deficits, beta Amyloid and Tau pathology in a rat model of Alzheimer ' s Disease, 10, 2018 1–13, https://doi.org/10.3389/fnagi.2018.00244.
[199] Q. Chen, Y. Du, K. Zhang, Z. Liang, J. Li, H. Yu, R. Ren, J. Feng, Z. Jin, F. Li, J. Sun, M. Zhou, Q. He, X. Sun, H. Zhang, M. Tian, D. Ling, Tau-targeted multifunctional nanocomposite for combinational therapy of Alzheimer's Disease, 12, 2018 1321–1338.
[200] P.T. Schoenemann, M.J. Sheehan, L.D. Glotzer, Prefrontal white matter volume is disproportionately larger in humans than in other primates, Nat. Neurosci. 8 (2005) 242–252, https://doi.org/10.1038/nn1394.
[201] S.W. Bihaqi, N.H. Zawia, Enhanced taupathy and AD-like pathology in aged primate brains decades after infantile exposure to lead (Pb), Neurotoxicology. 39 (2013) 95–101, https://doi.org/10.1016/j.neuro.2013.07.010.
[202] C.A. Lemere, J. Oh, H.A. Stanish, Y. Peng, I. Pepivani, A.M. Fagan, H. Yamaguchi, S.V. Westmoreland, K.G. Mansfield, Cerebral Amyloid-Beta protein accumulation with aging in cotton-top tamarins: A model of early Alzheimer's Disease? Rejuvenation Res. 11 (2008) 321–332, https://doi.org/10.1089/rej.2008.0677.
[203] A. Uchida, H. Sasaguri, N. Kimura, M. Tajiri, T. Ohkubo, F. Ono, F. Sakaue, K. Kanai, T. Hirai, T. Sano, K. Shibuya, M. Kobayashi, M. Yamamoto, S. Yokota, T. Kubodera, M. Tomori, K. Sakaki, M. Enomoto, Y. Hirai, J. Kumagai, Y. Yasutomi, H. Mochizuki, S. Kuwabara, T. Uchihara, H. Mizusawa, T. Yokota, Non-human primate model of amyotrophic lateral sclerosis with cytoplasmic mislocalization of TDP-43, Brain. 135 (2012) 833–846, https://doi.org/10.1093/brain/awr348.
[204] I.H. Philippens, B.A. 't Hart, G. Torres, The MPTP marmoset model of Parkinsonism: a multi-purpose non-human primate model for neurodegenerative diseases, Drug Discov. Today. 15 (2010) 985–990, https://doi.org/10.1016/j.drudis.2010.08.009.
[205] R. Saito, M.T. Krauze, J.R. Bringas, C. Noble, T.R. McKnight, P. Jackson, M.F. Wendland, C. Mamot, D.C. Drummond, D.B. Kirpotin, K. Hong, M.S. Berger, J.W. Park, K.S. Bankiewicz, Gadolinium-loaded liposomes allow for real-time magnetic resonance imaging of convection-enhanced delivery in the primate brain, Exp. Neurol. 196 (2005) 381–389, https://doi.org/10.1016/j.expneurol.2005.08.016.
[206] M.T. Krauze, S.R. Vandenberg, Y. Yamashita, R. Saito, J. Forsayeth, C. Noble, J. Park, K. S. Bankiewicz, Safety of real-time convection-enhanced delivery of liposomes to primate brain: a long-term retrospective, Exp. Neurol. 210 (2008) 638–644, https://doi.org/10.1016/j.expneurol.2007.12.015.
[207] J. Hirota, S. Shimizu, The Laboratory Mouse, Chapter 5, 2, 2012 https://doi.org/10.1016/B978-0-12-382008-2.00001-5.
[208] S.K. Bardal, J.E. Waechter, D.S. Martin, Chapter 2 - Pharmacokinetics, in: S.K. Bardal, J.E. Waechter, D.S.B.T.-A.P. Martin (Eds.),Content Repository Only!, Philadelphia 2011, pp. 17–34, https://doi.org/10.1016/B978-1-4377-0310-8.00002-6.
[209] P.V. Turner, T. Brabb, C. Pekow, M.A. Vasbinder, Administration of substances to laboratory animals: routes of administration and factors to consider, J. Am. Assoc. Lab. Anim. Sci. 50 (2011) 600–613.
[210] L. Yildirimer, N.T.K. Thanh, M. Loizidou, A.M. Seifalian, Toxicology and clinical potential of nanoparticles, Nano Today. 6 (2011) 585–607, https://doi.org/10.1016/j.nantod.2011.10.001.
[211] T. Patel, J. Zhou, J.M. Piepmeier, W.M. Saltzman, Polymeric nanoparticles for drug delivery to the central nervous system, Adv. Drug Deliv. Rev. 64 (2012) 701–705, https://doi.org/10.1016/j.addr.2011.12.006.
[212] S.T. Jahan, S.M.A. Sadat, M. Walliser, A. Haddadi, Targeted therapeutic nanoparticles: An immense promise to fight against cancer, J. Drug Deliv. 2017 (2017) 1–24, https://doi.org/10.1155/2017/9090325.
[213] M.M. Nguyen, N.C. Gianneschi, K.L. Christman, Developing injectable nanomaterials to repair the heart, Curr. Opin. Biotechnol. 34 (2015) 225–231, https://doi.org/10.1016/j.copbio.2015.03.016.
[214] E.M. Pridgen, F. Alexis, O.C. Farokhzad, Polymeric nanoparticle drug delivery technologies for oral delivery applications, Expert Opin. Drug Deliv. 12 (2015) 1459–1473, https://doi.org/10.1517/17425247.2015.1018175.

[215] P. Batista, P.M. Castro, A.R. Madureira, B. Sarmento, M. Pintado, Recent insights in the use of nanocarriers for the oral delivery of bioactive proteins and peptides, Peptides. 101 (2018) 112–123, https://doi.org/10.1016/j.peptides.2018.01.002.
[216] M. Sun, K. Wang, D. Oupický, Advances in stimulus-responsive polymeric materials for systemic delivery of nucleic acids, Adv. Healthc. Mater. 7 (2018) 1701070, https://doi.org/10.1002/adhm.201701070.
[217] J. Kreuter, Drug delivery to the central nervous system by polymeric nanoparticles: What do we know? Adv. Drug Deliv. Rev. 71 (2014) 2–14, https://doi.org/10.1016/j.addr.2013.08.008.
[218] I. Craciun, G. Gunkel-Grabole, A. Belluati, C.G. Palivan, W. Meier, Expanding the potential of MRI contrast agents through multifunctional polymeric nanocarriers, Nanomedicine. 12 (2017) 811–817, https://doi.org/10.2217/nnm-2016-0413.
[219] C. Saraiva, C. Praça, R. Ferreira, T. Santos, L. Ferreira, L. Bernardino, Nanoparticle-mediated brain drug delivery: Overcoming blood-brain barrier to treat neurodegenerative diseases, J. Control. Release. 235 (2016) 34–47, https://doi.org/10.1016/j.jconrel.2016.05.044.
[220] J. Kreuter, R.N. Alyautdin, D.A. Kharkevich, A.A. Ivanov, Passage of peptides through the blood-brain barrier with colloidal polymer particles (nanoparticles), Brain Res. 674 (1995) 171–174, https://doi.org/10.1016/0006-8993(95)00023-J.
[221] J. Kreuter, Influence of the surface properties on nanoparticle-mediated transport of drugs to the brain, J. Nanosci. Nanotechnol. 4 (2004) 484–488.
[222] J. Kreuter, P. Ramge, V. Petrov, S. Hamm, S.E. Gelperina, B. Engelhardt, R. Alyautdin, H. von Briesen, D.J. Begley, Direct evidence that polysorbate-80-coated poly (butylcyanoacrylate) nanoparticles deliver drugs to the CNS via specific mechanisms requiring prior binding of drug to the nanoparticles, Pharm. Res. 20 (2003) 409–416.
[223] U. Schroeder, H. Schroeder, B.A. Sabel, Body Distribution of 3H-labelled dalargin bound to poly(butyl cyanoacrylate) nanoparticles after I.V. injections to mice, Life Sci. 66 (2000) 495–502.
[224] L.S. Nair, C.T. Laurencin, Biodegradable polymers as biomaterials, Prog. Polym. Sci. 32 (2007) 762–798, https://doi.org/10.1016/j.progpolymsci.2007.05.017.
[225] K.E. Washington, R.N. Kularatne, V. Karmegam, M.C. Biewer, M.C. Stefan, Recent advances in aliphatic polyesters for drug delivery applications, Wiley Interdiscip. Rev. Nanomedicine Nanobiotechnology. 9 (2017) https://doi.org/10.1002/wnan.1446.
[226] K.S.S. Rao, M.K.K. Reddy, J.L.L. Horning, V. Labhasetwar, TAT-conjugated nanoparticles for the CNS delivery of anti-HIV drugs, Biomaterials. 29 (2008) 4429–4438, https://doi.org/10.1016/j.biomaterials.2008.08.004.
[227] U.D. Bret, N.S. Lakshmi, C.T. Laurencin, Biomedical Applications of Biodegradable Polymers, J. Polym. Sci. Part B Polym. Phys. 3 (2011) 832–864, https://doi.org/10.3390/polym3031377.Poly.
[228] Y.C.C. Chen, W.Y.Y. Hsieh, W.F.F. Lee, D.T.T. Zeng, Effects of surface modification of PLGA-PEG-PLGA nanoparticles on loperamide delivery efficiency across the blood-brain barrier, J. Biomater. Appl. 27 (2013) 909–922, https://doi.org/10.1177/0885328211429495.
[229] D.H.H. Kim, D.C.C. Martin, Sustained release of dexamethasone from hydrophilic matrices using PLGA nanoparticles for neural drug delivery, Biomaterials. 27 (2006) 3031–3037, https://doi.org/10.1016/j.biomaterials.2005.12.021.
[230] N.D. Sonawane, F.C. Szoka, A.S. Verkman, Chloride accumulation and swelling in endosomes enhances DNA transfer by polyamine-DNA polyplexes, J. Biol. Chem. 278 (2003) 44826–44831, https://doi.org/10.1074/jbc.M308643200.
[231] D.W. Hwang, S. Son, J. Jang, H. Youn, S. Lee, D. Lee, Y.S. Lee, J.M. Jeong, W.J. Kim, D.S. Lee, A brain-targeted rabies virus glycoprotein-disulfide linked PEI nanocarrier for delivery of neurogenic microRNA, Biomaterials. 32 (2011) 4968–4975, https://doi.org/10.1016/j.biomaterials.2011.03.047.
[232] C. Zhan, Q. Meng, Q. Li, L. Feng, J. Zhu, W. Lu, Cyclic RGD-polyethylene glycol-polyethylenimine for intracranial glioblastoma-targeted gene delivery, Chem. - An Asian J. 7 (2012) 91–96, https://doi.org/10.1002/asia.201100570.
[233] M. Rodriguez, J. Lapierre, C.R. Ojha, A. Kaushik, E. Batrakova, F. Kashanchi, S.M. Dever, M. Nair, N. El-Hage, Intranasal drug delivery of small interfering RNA targeting Beclin1 encapsulated with polyethylenimine (PEI) in mouse brain to achieve HIV attenuation, Sci. Rep. 7 (2017) 1–10, https://doi.org/10.1038/s41598-017-01819-9.
[234] R. Gabathuler, Approaches to transport therapeutic drugs across the blood-brain barrier to treat brain diseases, Neurobiol. Dis. 37 (2010) 48–57, https://doi.org/10.1016/j.nbd.2009.07.028.
[235] H. Karatas, Y. Aktas, Y. Gursoy-Ozdemir, E. Bodur, M. Yemisci, S. Caban, A. Vural, O. Pinarbasli, Y. Capan, E. Fernandez-Megia, R. Novoa-Carballal, R. Riguera, K. Andrieux, P. Couvreur, T. Dalkara, A nanomedicine transports a peptide Caspase-3 inhibitor across the blood-brain barrier and provides neuroprotection, J. Neurosci. 29 (2009) 13761–13769, https://doi.org/10.1523/JNEUROSCI.4246-09.2009.
[236] J. Li, L. Feng, L. Fan, Y. Zha, L. Guo, Q. Zhang, J. Chen, Z. Pang, Y. Wang, X. Jiang, V.C.C. Yang, L. Wen, Targeting the brain with PEG-PLGA nanoparticles modified with phage-displayed peptides, Biomaterials. 32 (2011) 4943–4950, https://doi.org/10.1016/j.biomaterials.2011.03.031.
[237] E. Nance, C. Zhang, T.Y.Y. Shih, Q. Xu, B.S.S. Schuster, J. Hanes, Brain-penetrating nanoparticles improve paclitaxel efficacy in malignant glioma following local administration, ACS Nano. 8 (2014) 10655–10664, https://doi.org/10.1021/nn504210g.
[238] S. Wohlfart, A.S.S. Khalansky, S. Gelperina, D. Begley, J. Kreuter, Kinetics of transport of doxorubicin bound to nanoparticles across the blood-brain barrier, J. Control. Release. 154 (2011) 103–107, https://doi.org/10.1016/j.jconrel.2011.05.010.
[239] A. Abuchowski, J.R. Mccoy, N.C. Palczuk, T. Van Es, F.F. Davis, Effect of Covalent Attachment of Polyethylene Glycol on Immunogenicity and Circulating Life of Bovine Liver Catalase, J. Biol. Chem. 252 (1976) 3582–3586.
[240] C. Chang, C. Chen, B. Chen, Y. Su, Y. Chen, M.S. Hersh, M.M. Lee, T. Cheng, Y. Chen, S. R. Rof, J. Wu, A genome-wide association study identifies a novel susceptibility locus for the immunogenicity of polyethylene glycol, Nat. Commun. (2017) 1–7, https://doi.org/10.1038/s41467-017-00622-4.
[241] T. Ishida, M. Ichihara, X. Wang, K. Yamamoto, J. Kimura, Injection of PEGylated liposomes in rats elicits PEG-specific IgM, which is responsible for rapid elimination of a second dose of PEGylated liposomes, 112, 2006 15–25, https://doi.org/10.1016/j.jconrel.2006.01.005.
[242] A. Judge, K. McClintock, J.R. Phelps, I. MacLachlan, Hypersensitivity and loss of disease site targeting caused by antibody responses to PEGylated liposomes, Mol. Ther. 13 (2006) 328–337, https://doi.org/10.1016/j.ymthe.2005.09.014.
[243] Y. Yao, Accelerated blood clearance phenomenon upon cross-administration of PEGylated nanocarriers in beagle dogs, 2015 3533–3545.
[244] Y. Hsieh, H. Wang, W. Lin, S.R. Roffler, T. Cheng, Y. Su, T h e r a n o s t i c s Pre-existing anti-polyethylene glycol antibody reduces the therapeutic efficacy and pharmacokinetics of PEGylated liposomes, 8, 2018 https://doi.org/10.7150/thno.22164.
[245] P. Zhang, F. Sun, S. Liu, S. Jiang, HHS Public Access 244 (2017) 184–193, https://doi.org/10.1016/j.jconrel.2016.06.040.Anti-PEG.
[246] A. Chanan-Khan, J. Szebeni, S. Savay, L. Liebes, N.M. Rafique, C.R. Alving, F.M. Muggia, Complement activation following first exposure to pegylated liposomal doxorubicin (Doxil®): possible role in hypersensitivity reactions, Ann. Oncol. 14 (2003) 1430–1437, https://doi.org/10.1093/annonc/mdg374.
[247] K. Nagpal, S.K. Singh, D.N. Mishra, Chitosan nanoparticles: A promising system in novel drug delivery, Chem. Pharm. Bull. (Tokyo). 58 (2010) 1423–1430, https://doi.org/10.1248/cpb.58.1423.
[248] M.C. Bergonzi, C. Guccione, C. Grossi, V. Piazzini, A. Torracchi, I. Luccarini, F. Casamenti, A.R. Bilia, Albumin nanoparticles for brain delivery: A comparison of chemical versus thermal methods and in vivo behavior, ChemMedChem. (2016) 1840–1849, https://doi.org/10.1002/cmdc.201600080.
[249] Y.S.R. Elnaggar, S.M. Etman, D.A. Abdelmonsif, O.Y. Abdallah, Novel piperine-loaded Tween-integrated monoolein cubosomes as brain-targeted oral nanomedicine in Alzheimer's disease: pharmaceutical, biological, and toxicological studies, Int. J. Nanomedicine. 10 (2015) 5459–5473, https://doi.org/10.2147/IJN.S87336.
[250] T. Lin, P. Zhao, Y. Jiang, Y. Tang, H. Jin, Z. Pan, H. He, V.C. Yang, Y. Huang, Blood-brain-barrier-penetrating albumin nanoparticles for biomimetic drug delivery via albumin-binding protein pathways for antiglioma therapy, ACS Nano. 10 (2016) 9999–10012, https://doi.org/10.1021/acsnano.6b04268.
[251] H.J. Byeon, L.Q. Thao, S. Lee, S.Y. Min, E.S. Lee, B.S. Shin, H.G. Choi, Y.S. Youn, Doxorubicin-loaded nanoparticles consisted of cationic- and mannose-modified-albumins for dual-targeting in brain tumors, J. Control. Release. 225 (2016) 301–313, https://doi.org/10.1016/j.jconrel.2016.01.046.
[252] S. Lahkar, M.K. Das, Surface modified polymeric nanoparticles for brain, Curr. Trends Biotechnol. Pharm. 7 (2013) 914–931.
[253] H. Brem, M.S. Mahaley, N.A. Vick, K.L. Black, S.C. Schold, P.C. Burger, A.H. Friedman, I.S. Ciric, T.W. Eller, J.W. Cozzens, J.N. Kenealy, Interstitial chemotherapy with drug polymer implants for the treatment of recurrent gliomas, J. Neurosurg. 74 (1991) 441–446, https://doi.org/10.3171/jns.1991.74.3.0441.
[254] L.K. Fung, M. Shin, B. Tyler, H. Brem, W.M. Saltzman, Chemotherapeutic drugs released from polymers: distribution of 1,3-bis(2-chloroethyl)-l-nitrosourea in the rat brain, Pharm. Res. 13 (1996) 671–682, https://doi.org/10.1023/A:1016083113123.
[255] R.H. Bobo, D.W. Laske, A. Akbasak, P.F. Morrison, R.L. Dedrick, E.H. Oldfield, Convection-enhanced delivery of macromolecules in the brain, Proc. Natl. Acad. Sci. 91 (1994) 2076–2080, https://doi.org/10.1073/pnas.91.6.2076.
[256] G.M. Bernal, M.J. LaRiviere, N. Mansour, P. Pytel, K.E. Cahill, D.J. Voce, S. Kang, R. Spretz, U. Welp, S.E. Noriega, L. Nunez, G.F. Larsen, R.R. Weichselbaum, B. Yamini, Convection enhanced delivery and in vivo imaging of polymeric nanoparticles for the treatment of malignant glioma, Nanomedicine. 31 (2013) 1713–1723, https://doi.org/10.1016/j.nano.2013.07.003.
[257] A.J. Sawyer, J.K. Saucier-Sawyer, C.J. Booth, J. Liu, T. Patel, J.M. Piepmeier, W.M. Saltzman, Convection-enhanced delivery of camptothecin-loaded polymer nanoparticles for treatment of intracranial tumors, Drug Deliv. Transl. Res. 1 (2011) 34–42, https://doi.org/10.1007/s13346-010-0001-3.
[258] S. Kunwar, S. Chang, M. Westphal, M. Vogelbaum, J. Sampson, G. Barnett, M. Shaffrey, Z. Ram, J. Piepmeier, M. Prados, D. Croteau, C. Pedain, P. Leland, S.R. Husain, B.H. Joshi, R.K. Puri, Phase III randomized trial of CED of IL13-PE38QQR vs Gliadel wafers for recurrent glioblastoma, Neuro. Oncol. 12 (2010) 871–881, https://doi.org/10.1093/neuonc/nop054.
[259] M.A. Vogelbaum, M.K. Aghi, Convection-enhanced delivery for the treatment of glioblastoma, Neuro. Oncol. 17 (Suppl. 2) (2015) ii3–ii8, https://doi.org/10.1093/neuonc/nou354.
[260] Clinical trials, https://clinicaltrials.gov/show/NCT01655693 2012 (accessed March 11, 2018).
[261] S. Somani, C. Dufès, Applications of dendrimers for brain delivery and cancer therapy, Nanomedicine. 9 (2014) 2403–2414, https://doi.org/10.2217/nnm.14.130.
[262] K. Madaan, S. Kumar, N. Poonia, V. Lather, D. Pandita, Dendrimers in drug delivery and targeting: Drug-dendrimer interactions and toxicity issues, J. Pharm. Bioallied Sci. 6 (2014) 139–150, https://doi.org/10.4103/0975-7406.130965.
[263] L. Han, A. Zhang, H. Wang, P. Pu, X. Jiang, C. Kang, J. Chang, Tat-BMPs-PAMAM Conjugates Enhance Therapeutic Effect of Small Interference RNA on U251 Glioma Cells In Vitro and In Vivo, Hum, Gene Ther. 21 (2009) 417–426, https://doi.org/10.1089/hum.2009.087.
[264] M. Yokosawa, Y. Sonoda, S.-I. Sugiyama, R. Saito, Y. Yamashita, M. Nishihara, T. Satoh, T. Kumabe, M. Yokoyama, T. Tominaga, Convection-enhanced delivery of a synthetic retinoid Am80, loaded into polymeric micelles, prolongs the survival of

rats bearing intracranial glioblastoma xenografts, Tohoku J. Exp. Med. 221 (2010) 257–264, https://doi.org/10.1620/tjem.221.257.
[265] Y.K. Huang, W.C. Liu, F. Gao, X.L. Fang, Y.Z. Chen, C(RGDyK)-decorated pluronic micelles for enhanced doxorubicin and paclitaxel delivery to brain glioma, Int. J. Nanomedicine. 11 (2016) 1629–1641, https://doi.org/10.2147/IJN.S104162.
[266] G. Wang, J.J. Wang, X.J. Tang, L. Du, F. Li, In vitro and in vivo evaluation of functionalized chitosan-Pluronic micelles loaded with myricetin on glioblastoma cancer, Nanomedicine Nanotechnology, Biol. Med. 12 (2016) 1263–1278, https://doi.org/10.1016/j.nano.2016.02.004.
[267] J.W. Seo, J. Ang, L.M. Mahakian, S. Tam, B. Fite, E.S. Ingham, J. Beyer, J. Forsayeth, K.S. Bankiewicz, T. Xu, K.W. Ferrara, Self-assembled 20-nm 64 Cu-micelles enhance accumulation in rat glioblastoma, J. Control. Release. 220 (2015) 51–60, https://doi.org/10.1016/j.jconrel.2015.09.057.
[268] R.P. Singh Sonali, N. Singh, G. Sharma, M.R. Vijayakumar, B. Koch, S. Singh, U. Singh, D. Dash, B.L. Pandey, M.S. Muthu, Transferrin liposomes of docetaxel for brain-targeted cancer applications: formulation and brain theranostics, Drug Deliv. 23 (2016) 1261–1271, https://doi.org/10.3109/10717544.2016.1162878.
[269] M. Das, C. Wang, R. Bedi, S.S. Mohapatra, S. Mohapatra, Magnetic micelles for DNA delivery to rat brains after mild traumatic brain injury, Nanomedicine Nanotechnology, Biol. Med. 10 (2014) 1539–1548, https://doi.org/10.1016/j.nano.2014.01.003.
[270] S.A. Nour, N.S. Abdelmalak, M.J. Naguib, H.M. Rashed, A.B. Ibrahim, Intranasal brain-targeted clonazepam polymeric micelles for immediate control of status epilepticus: *in vitro* optimization, *ex vivo* determination of cytotoxicity, *in vivo* biodistribution and pharmacodynamics studies, Drug Deliv. 23 (2016) 3681–3695, https://doi.org/10.1080/10717544.2016.1223216.
[271] S. Hagl, A. Kocher, C. Schiborr, N. Kolesova, J. Frank, G.P.P. Eckert, Curcumin micelles improve mitochondrial function in neuronal PC12 cells and brains of NMRI mice - Impact on bioavailability, Neurochem. Int. 89 (2015) 234–242, https://doi.org/10.1016/j.neuint.2015.07.026.
[272] C. Tapeinos, M. Battaglini, G. Ciofani, Advances in the design of solid lipid nanoparticles and nanostructured lipid carriers for targeting brain diseases, J. Control. Release. 264 (2017) 306–332, https://doi.org/10.1016/j.jconrel.2017.08.033.
[273] M. Imran, S.B.T.-L.-B.N. for D.D, D. Ullah (Eds.), Index A2 - Shah, Muhammad Raza 2017, pp. 343–353, https://doi.org/10.1016/B978-0-323-52729-3.00026-3 , Micro Nano Technol.
[274] M. Budai, M. Szogyi, Liposomes as drug carrier systems. Preparation, classification and therapeutic advantages of liposomes, Acta Pharm. Hung. 71 (2001) 114–118.
[275] P.M.M. Friden, L.R.R. Walus, G.F.F. Musso, R.M.M. Starzyk, Anti-transferrin receptor antibody and antibody-drug conjugates cross the blood-brain barrier, Med. Sci. Nat. 88 (1991) 4771–4775, https://doi.org/10.1073/pnas.88.11.4771.
[276] P.M. Friden, L.R. Walus, P. Watson, S.R. Doctrow, J.W. Kozarich, C. Backman, H. Bergman, B. Hoffer, F. Bloom, A.C. Granholm, Blood-brain barrier penetration and in vivo activity of an NGF conjugate, Science. 259 (1993) 373–377.
[277] A.C.C. Granholm, C. Backman, F. Bloom, T. Ebendal, G.A.A. Gerhardt, B. Hoffer, L. Mackerlova, L. Olson, S. Soderstrom, L.R.R. Walus, NGF and anti-transferrin receptor antibody conjugate: short and long-term effects on survival of cholinergic neurons in intraocular septal transplants, J. Pharmacol. Exp. Ther. 268 (1994) 448–459.
[278] E. Paszko, M.O. Senge, Immunoliposomes, Curr. Med. Chem. 19 (2012) 5239–5277.
[279] F. Artzner, R. Zantl, J.O. Radler, Lipid-DNA and lipid-polyelectrolyte mesophases: structure and exchange kinetics, Cell. Mol. Biol. (Noisy-Le-Grand). 46 (2000) 967–978.
[280] A.L.C. Cardoso, S. Simões, L.P. de Almeida, N. Plesnila, M.C. Pedroso de Lima, E. Wagner, C. Culmsee, Tf-lipoplexes for neuronal siRNA delivery: A promising system to mediate gene silencing in the CNS, J. Control. Release. 132 (2008) 113–123, https://doi.org/10.1016/j.jconrel.2008.08.014.
[281] A.L.C. Cardoso, P. Costa, L.P. de Almeida, S. Simões, N. Plesnila, C. Culmsee, E. Wagner, M.C. Pedroso de Lima, Tf-lipoplex-mediated c-Jun silencing improves neuronal survival following excitotoxic damage in vivo, J. Control. Release. 142 (2010) 392–403, https://doi.org/10.1016/j.jconrel.2009.11.004.
[282] M.T. Girão da Cruz, A.L.C. Cardoso, L.P. de Almeida, S. Simões, M.C. Pedroso de Lima, Tf-lipoplex-mediated NGF gene transfer to the CNS: Neuronal protection and recovery in an excitotoxic model of brain injury, Gene Ther. 12 (2005) 1242–1252, https://doi.org/10.1038/sj.gt.3302516.
[283] Z. Hassani, G.F. Lemkine, P. Erbacher, K. Palmier, G. Alfama, C. Giovannangeli, J.-P. Behr, B.A. Demeneix, Lipid-mediated siRNA delivery down-regulates exogenous gene expression in the mouse brain at picomolar levels, J. Gene Med. 7 (2005) 198–207, https://doi.org/10.1002/jgm.659.
[284] M. Yusuf, M. Khan, R.A. Khan, B. Ahmed, Preparation, characterization, *in vivo* and biochemical evaluation of brain targeted Piperine solid lipid nanoparticles in an experimentally induced Alzheimer's disease model, J. Drug Target. 21 (2013) 300–311, https://doi.org/10.3109/1061186X.2012.747529.
[285] R. Müller, Solid lipid nanoparticles (SLN) for controlled drug delivery: a review of the state of the art, Eur. J. Pharm. Biopharm. 50 (2000) 161–177, https://doi.org/10.1016/S0939-6411(00)00087-4.
[286] V. Kakkar, S.K. Muppu, K. Chopra, I.P. Kaur, Curcumin loaded solid lipid nanoparticles: An efficient formulation approach for cerebral ischemic reperfusion injury in rats, Eur. J. Pharm. Biopharm. 85 (2013) 339–345, https://doi.org/10.1016/J.EJPB.2013.02.005.
[287] N. Naseri, H. Valizadeh, P. Zakeri-Milani, Solid lipid nanoparticles and nanostructured lipid carriers: structure, preparation and application, Adv. Pharm. Bull. 5 (2015) 305–313, https://doi.org/10.15171/apb.2015.043.
[288] Y. Chen, L. Pan, M. Jiang, D. Li, L. Jin, Nanostructured lipid carriers enhance the bioavailability and brain cancer inhibitory efficacy of curcumin both in vitro and in vivo, Drug Deliv. 23 (2016) 1383–1392, https://doi.org/10.3109/10717544.2015.1049719.
[289] J. Samal, S. Demir, A. Pandit, Chapter 6 - Exosomes: cellular capsules for drug delivery in Parkinson's disease, in: Micro Nano Technol., 2018: pp. 91–151.
[290] H. Valadi, K. Ekström, A. Bossios, M. Sjöstrand, J.J. Lee, J.O. Lötvall, Exosome-mediated transfer of mRNAs and microRNAs is a novel mechanism of genetic exchange between cells, Nat. Cell Biol. 9 (2007) 654–659, https://doi.org/10.1038/ncb1596.
[291] Y.S. Lee, S.H. Kim, J.A. Cho, C.W. Kim, Introduction of the CIITA gene into tumor cells produces exosomes with enhanced anti-tumor effects, Exp. Mol. Med. 43 (2011) 281–290, https://doi.org/10.3858/emm.2011.43.5.029.
[292] A. Mizrak, M.F. Bolukbasi, G.B. Ozdener, G.J. Brenner, S. Madlener, E.P. Erkan, T. Ströbel, X.O. Breakefield, O. Saydam, Genetically Engineered Microvesicles Carrying Suicide mRNA/Protein Inhibit Schwannoma Tumor Growth, Mol. Ther. 21 (2013) 101–108, https://doi.org/10.1038/mt.2012.161.
[293] M. Katakowski, B. Buller, X. Zheng, Y. Lu, T. Rogers, O. Osobamiro, W. Shu, F. Jiang, M. Chopp, Exosomes from marrow stromal cells expressing miR-146b inhibit glioma growth, Cancer Lett. 335 (2013) 201–204, https://doi.org/10.1016/j.canlet.2013.02.019.
[294] A. Kalani, P. Chaturvedi, P.K. Kamat, C. Maldonado, P. Bauer, I.G. Joshua, S.C. Tyagi, N. Tyagi, Curcumin-loaded embryonic stem cell exosomes restored neurovascular unit following ischemia-reperfusion injury, Int. J. Biochem. Cell Biol. 79 (2016) 360–369, https://doi.org/10.1016/j.biocel.2016.09.002.
[295] Y. Zhang, M. Chopp, Z.G. Zhang, M. Katakowski, H. Xin, C. Qu, M. Ali, A. Mahmood, Y. Xiong, Systemic administration of cell-free exosomes generated by human bone marrow derived mesenchymal stem cells cultured under 2D and 3D conditions improves functional recovery in rats after traumatic brain injury, Neurochem. Int. 111 (2017) 69–81, https://doi.org/10.1016/J.NEUINT.2016.08.003.
[296] M.J. Haney, N.L. Klyachko, Y. Zhao, R. Gupta, E.G. Plotnikova, Z. He, T. Patel, A. Piroyan, M. Sokolsky, A.V. Kabanov, E.V. Batrakova, Exosomes as drug delivery vehicles for Parkinson's disease therapy, J. Control. Release. 207 (2015) 18–30, https://doi.org/10.1016/J.JCONREL.2015.03.033.
[297] D. Ha, N. Yang, V. Nadithe, Exosomes as therapeutic drug carriers and delivery vehicles across biological membranes: current perspectives and future challenges, Acta Pharm. Sin. B. 6 (2016) 287–296, https://doi.org/10.1016/j.apsb.2016.02.001.
[298] K. Cherukula, K. Manickavasagam Lekshmi, S. Uthaman, K. Cho, C.-S. Cho, I.-K. Park, Multifunctional inorganic nanoparticles: recent progress in thermal therapy and imaging, Nanomaterials. 6 (2016) https://doi.org/10.3390/nano6040076.
[299] A. Fernandez-Fernandez, R. Manchanda, A.J. McGoron, Theranostic applications of nanomaterials in cancer: Drug delivery, image-guided therapy and multifunctional platforms, Appl. Biochem. Biotechnol. 165 (2011) 1628–1651, https://doi.org/10.1007/s12010-011-9383-z.
[300] Z.P. Xu, Q.H. Zeng, G.Q. Lu, A.B. Yu, Inorganic nanoparticles as carriers for efficient cellular delivery, Chem. Eng. Sci. 61 (2006) 1027–1040, https://doi.org/10.1016/j.ces.2005.06.019.
[301] A.C. Anselmo, S. Mitragotri, A review of clinical translation of inorganic nanoparticles, AAPS J. 17 (2015) 1041–1054, https://doi.org/10.1208/s12248-015-9780-2.
[302] R. Prades, S. Guerrero, E. Araya, C. Molina, E. Salas, E. Zurita, J. Selva, G. Egea, C. López-Iglesias, M. Teixidó, M.J.J. Kogan, E. Giralt, Delivery of gold nanoparticles to the brain by conjugation with a peptide that recognizes the transferrin receptor, Biomaterials. 33 (2012) 7194–7205, https://doi.org/10.1016/j.biomaterials.2012.06.063.
[303] N. Gao, H. Sun, K. Dong, J. Ren, X. Qu, Gold-nanoparticle-based multifunctional amyloid-β inhibitor against Alzheimer's disease, Chem. - A Eur. J. 21 (2015) 829–835, https://doi.org/10.1002/chem.201404562.
[304] D. Joh, L. Sun, M. Stangl, A. Al Zaki, S. Murty, P. Santoiemma, Selective targeting of brain tumors with gold nanoparticle-induced radiosensitization, PLoS One. 8 (2013).
[305] K. Mahmoudi, C.G. Hadjipanayis, The application of magnetic nanoparticles for the treatment of brain tumors, Front. Chem. 2 (2014) 109, https://doi.org/10.3389/fchem.2014.00109.
[306] M. Mahmoudi, S. Sant, B. Wang, S. Laurent, T. Sen, Superparamagnetic iron oxide nanoparticles (SPIONs): Development, surface modification and applications in chemotherapy, Adv. Drug Deliv. Rev. 63 (2011) 24–46, https://doi.org/10.1016/j.addr.2010.05.006.
[307] C.E. Probst, P. Zrazhevskiy, V. Bagalkot, X. Gao, Quantum dots as a platform for nanoparticle drug delivery vehicle design, Adv. Drug Deliv. Rev. 65 (2013) 703–718, https://doi.org/10.1016/j.addr.2012.09.036.
[308] R.G.G. Thorne, C. Nicholson, In vivo diffusion analysis with quantum dots and dextrans predicts the width of brain extracellular space, Proc. Natl. Acad. Sci. 103 (2006) 5567–5572, https://doi.org/10.1073/pnas.0509425103.
[309] B. Bracegirdle, The History of Histology: a brief survey of sources, Hist. Sci. XV (1997) 77–101, https://doi.org/10.1177/007327537701500201.
[310] L.D. Lavis, Histochemistry: Live and in Color, J. Histochem. Cytochem. 59 (2011) 139–145, https://doi.org/10.1369/0022155410395760.
[311] D. Ran, J. Mao, Q. Shen, C. Xie, C. Zhan, R. Wang, W. Lu, GRP78 enabled micelle-based glioma targeted drug delivery, J. Control. Release. 255 (2017) 120–131, https://doi.org/10.1016/j.jconrel.2017.03.037.
[312] Y.-Z. Zhao, R.-R. Jin, W. Yang, Q. Xiang, W.-Z. Yu, Q. Lin, F.-R. Tian, K.-L. Mao, C.-Z. Lv, Y.-X.J. Wáng, C.-T. Lu, Using gelatin nanoparticle mediated intranasal delivery of neuropeptide Substance P to enhance neuro-recovery in hemiparkinsonian rats, PLoS One. 11 (2016), e0148848. https://doi.org/10.1371/journal.pone.0148848.
[313] N. Ahmad, R. Ahmad, A.A.A. Naqvi, M.A.A. Alam, M. Ashafaq, M. Samim, Z. Iqbal, F.J. J. Ahmad, Rutin-encapsulated chitosan nanoparticles targeted to the brain in the treatment of Cerebral Ischemia, Int. J. Biol. Macromol. 91 (2016) 640–655, https://doi.org/10.1016/j.ijbiomac.2016.06.001.
[314] M.N. Ahsan, P.R.P. Verma, Development, optimization and pharmacodynamic assessment of olanzapine based lipidic SNEDDS for proficient management of

psychosis, J. Pharm. Investig. 47 (2017) 395–411, https://doi.org/10.1007/s40005-016-0274-8.
[315] A. Kádár, G. Wittmann, Z. Liposits, C. Fekete, Improved method for combination of immunocytochemistry and Nissl staining, J. Neurosci. Methods. 184 (2009) 115–118, https://doi.org/10.1016/j.jneumeth.2009.07.010.
[316] P. Frid, S.V. Anisimov, N. Popovic, Congo red and protein aggregation in neurodegenerative diseases, Brain Res. Rev. 53 (2007) 135–160, https://doi.org/10.1016/j.brainresrev.2006.08.001.
[317] F. Grandjean, L. Samain, G.J. Long, Characterization and utilization of Prussian blue and its pigments, Dalton Trans. 45 (2016) 18018–18044, https://doi.org/10.1039/c6dt03351b.
[318] R.J. Castellani, G. Mojica, G. Perry, The role of the iron stain in assessing intracranial hemorrhage, Open Neurol. J. 10 (2016) 136–142, https://doi.org/10.2174/1874205X01610010136.
[319] S. Liu, M.M. Grigoryan, V. Vasilevko, R.K. Sumbria, A. Paganini-Hill, D.H. Cribbs, M.J. Fisher, Comparative analysis of H&E and Prussian blue staining in a mouse model of cerebral microbleeds, J. Histochem. Cytochem. 62 (2014) 767–773, https://doi.org/10.1369/0022155414546692.
[320] C.N. Joshi, S.K. Jain, P.S.R. Murthy, An optimized triphenyltetrazolium chloride method for identification of cerebral infarcts, Brain Res. Protoc. 13 (2004) 11–17, https://doi.org/10.1016/j.brainresprot.2003.12.001.
[321] R.A. Kloner, J.R. Darsee, L.W. DeBoer, N. Carlson, Early pathologic detection of acute myocardial infarction, Arch. Pathol. Lab. Med. 105 (1981) 403–406.
[322] K. Kyrylkova, S. Kyryachenko, M. Leid, C. Kioussi, Detection of apoptosis by TUNEL assay, Methods Mol. Biol. 887 (2012) 41–47, https://doi.org/10.1007/978-1-61779-860-3_5.
[323] Y. Shen, Z. Pi, F. Yan, C.K.K. Yeh, X. Zeng, X. Diao, Y. Hu, S. Chen, X. Chen, H. Zheng, Enhanced delivery of paclitaxel liposomes using focused ultrasound with microbubbles for treating nude mice bearing intracranial glioblastoma xenografts, Int. J. Nanomedicine. 12 (2017) 5613–5629, https://doi.org/10.2147/IJN.S136401.
[324] B. Kalyanaraman, V. Darley-Usmar, K.J.A. Davies, P.A. Dennery, H.J. Forman, M.B. Grisham, G.E. Mann, K. Moore, L.J. Roberts, H. Ischiropoulos, Measuring reactive oxygen and nitrogen species with fluorescent probes: challenges and limitations, Free Radic. Biol. Med. 52 (2012) 1–6, https://doi.org/10.1016/j.freeradbiomed.2011.09.030.
[325] A.H. Coons, H.J. Creech, R.N. Jones, Immunological properties of an antibody containing a fluorescent group, Proc. Soc. Exp. Biol. Med. 47 (1941) https://doi.org/10.3181/00379727-47-13084P 200–202.
[326] D.J. Moore, A.B. West, V.L. Dawson, T.M. Dawson, Molecular pathophysiology of Parkinson's disease, Annu. Rev. Neurosci. 28 (2005) 57–87, https://doi.org/10.1146/annurev.neuro.28.061604.135718.
[327] S. Crotty, P. Fitzgerald, E. Tuohy, D.M. Harris, A. Fisher, A. Mandel, A.E. Bolton, A.M. Sullivan, Y. Nolan, Neuroprotective effects of novel phosphatidylglycerol-based phospholipids in the 6-hydroxydopamine model of Parkinson's disease, Eur. J. Neurosci. 27 (2008) 294–300, https://doi.org/10.1111/j.1460-9568.2007.06018.x.
[328] P. Kundu, M. Das, K. Tripathy, S.K. Sahoo, Delivery of dual drug loaded lipid based nanoparticles across the blood–brain barrier impart enhanced neuroprotection in a rotenone induced mouse model of Parkinson's Disease, ACS Chem. Neurosci. 7 (2016) 1658–1670, https://doi.org/10.1021/acschemneuro.6b00207.
[329] T. Schneider, A. Becker, K. Ringe, A. Reinhold, R. Firsching, B.A.A. Sabel, Brain tumor therapy by combined vaccination and antisense oligonucleotide delivery with nanoparticles, J. Neuroimmunol. 195 (2008) 21–27, https://doi.org/10.1016/j.jneuroim.2007.12.005.
[330] Y. Chen, C. Pan, A. Xuan, L. Xu, G. Bao, F. Liu, J. Fang, D. Long, Treatment Efficacy of NGF Nanoparticles Combining Neural Stem Cell Transplantation on Alzheimer's Disease Model Rats, Med. Sci. Monit. 21 (2015) 3608–3615, https://doi.org/10.12659/msm.894567.
[331] M. Yusuf, M. Khan, R.A. Khan, B. Ahmed, Preparation, characterization, *in vivo* and biochemical evaluation of brain targeted Piperine solid lipid nanoparticles in an experimentally induced Alzheimer's disease model, J. Drug Target. 21 (2013) 300–311, https://doi.org/10.3109/1061186X.2012.747529.
[332] N. Ahmad, R. Ahmad, A.A. Naqvi, M.A. Alam, M. Ashafaq, M. Samim, Z. Iqbal, F.J. Ahmad, Rutin-encapsulated chitosan nanoparticles targeted to the brain in the treatment of Cerebral Ischemia, Int. J. Biol. Macromol. 91 (2016) 640–655, https://doi.org/10.1016/J.IJBIOMAC.2016.06.001.
[333] L.Y. Sang, Y. Liang, Y. Li, A self-assembling nanomaterial reduces acute brain injury and enhances functional recovery in a rat model of intracerebral hemorrhage, Nanomedicine Nanotechnology, Biol. Med. 11 (2015) 611–620, https://doi.org/10.1016/j.nano.2014.05.012.
[334] L. Yang, F. Wang, H. Han, L. Yang, G. Zhang, Z. Fan, Functionalized graphene oxide as a drug carrier for loading pirfenidone in treatment of subarachnoid hemorrhage, Colloids Surfaces B Biointerfaces. 129 (2015) 21–29, https://doi.org/10.1016/j.colsurfb.2015.03.022.
[335] L.H. Portnow, D.E. Vaillancourt, M.S. Okun, The history of cerebral PET scanning: From physiology to cutting-edge technology, Neurology. 80 (2013) 952–956, https://doi.org/10.1212/WNL.0b013e318285c135.
[336] T. Ai, J.N. Morelli, X. Hu, D. Hao, F.L. Goerner, B. Ager, V.M. Runge, A historical overview of magnetic resonance imaging, focusing on technological innovations, Invest. Radiol. 47 (2012) 725–741, https://doi.org/10.1097/RLI.0b013e318272d29f.
[337] N. Kosaka, M. Ogawa, P.L. Choyke, H. Kobayashi, Clinical implications of near-infrared fluorescence imaging in cancer, Future Oncol. 5 (2009) 1501–1511, https://doi.org/10.2217/fon.09.109.
[338] R. Weissleder, M.J. Pittet, Imaging in the era of molecular oncology, Nature. 452 (2008) 580–589, https://doi.org/10.1038/nature06917.
[339] M.T. Madsen, Recent advances in SPECT imaging, J. Nucl. Med. 48 (2007) 661–673.
[340] H. Xin, X. Jiang, J. Gu, X. Sha, L. Chen, K. Law, Y. Chen, X. Wang, Y. Jiang, X. Fang, Angiopep-conjugated poly(ethylene glycol)-co-poly(ε-caprolactone) nanoparticles as dual-targeting drug delivery system for brain glioma, Biomaterials. 32 (2011) 4293–4305, https://doi.org/10.1016/j.biomaterials.2011.02.044.
[341] A. Sato, B. Klaunberg, R. Tolwani, In vivo bioluminescence imaging, Comp. Med. 54 (2004) 631–634.
[342] L.A. McDonnell, R.M.A. Heeren, Imaging mass spectrometry, Mass Spectrom. Rev. 26 (2007) 606–643, https://doi.org/10.1002/mas.20124.
[343] E. Patel, L.M. Cole, R. Bradshaw, A. Batubara, C.A. Mitchell, S. Francese, M.R. Clench, MALDI-MS imaging for the study of tissue pharmacodynamics and toxicodynamics, Bioanalysis. 7 (2015) 91–101, https://doi.org/10.4155/bio.14.280.
[344] M. Guan, Z. Zhang, S. Li, J. Liu, L. Liu, H. Yang, Y. Zhang, T. Wang, Z. Zhao, Silver nanoparticles as matrix for MALDI FTICR MS profiling and imaging of diverse lipids in brain, Talanta. 179 (2018) 624–631, https://doi.org/10.1016/j.talanta.2017.11.067.
[345] D.C. Barbacci, A. Roux, L. Muller, S.N. Jackson, J. Post, K. Baldwin, B. Hoffer, C.D. Balaban, J.A. Schultz, S. Gouty, B.M. Cox, A.S. Woods, Mass spectrometric imaging of ceramide biomarkers tracks therapeutic response in traumatic brain injury, ACS Chem. Neurosci. 8 (2017) 2266–2274, https://doi.org/10.1021/acschemneuro.7b00189.
[346] L. Muller, K. Baldwin, D.C. Barbacci, S.N. Jackson, A. Roux, C.D. Balaban, B.E. Brinson, M.I. McCully, E.K. Lewis, J.A. Schultz, A.S. Woods, Laser desorption/ionization mass spectrometric imaging of endogenous lipids from rat brain tissue implanted with silver nanoparticles, J. Am. Soc. Mass Spectrom. 28 (2017) 1716–1728, https://doi.org/10.1007/s13361-017-1665-4.
[347] S.D. Sherrod, A.J. Diaz, W.K. Russell, P.S. Cremer, D.H. Russell, Silver nanoparticles as selective ionization probes for analysis of olefins by mass spectrometry, Anal. Chem. 80 (2008) 6796–6799, https://doi.org/10.1021/ac800904g.
[348] H.-W. Tang, M.Y.-M. Wong, W. Lam, Y.-C. Cheng, C.-M. Che, K.-M. Ng, Molecular histology analysis by matrix-assisted laser desorption/ionization imaging mass spectrometry using gold nanoparticles as matrix, Rapid Commun. Mass Spectrom. 25 (2011) 3690–3696.
[349] F.P.Y. Barre, R.M.A. Heeren, N.O. Potocnik, Mass spectrometry imaging in nanomedicine: unraveling the potential of MSI for the detection of nanoparticles in neuroscience, Curr. Pharm. Des. 23 (2017) 1974–1984, https://doi.org/10.2174/1381612823666170111112550.
[350] A. Limbeck, P. Galler, M. Bonta, G. Bauer, W. Nischkauer, F. Vanhaecke, Recent advances in quantitative LA-ICP-MS analysis: challenges and solutions in the life sciences and environmental chemistry, Anal. Bioanal. Chem. 407 (2015) 6593–6617, https://doi.org/10.1007/s00216-015-8858-0.
[351] D.J. Hare, J.K. Lee, A.D. Beavis, A. van Gramberg, J. George, P.A. Adlard, D.I. Finkelstein, P.A. Doble, Three-dimensional atlas of iron, copper, and zinc in the mouse cerebrum and brainstem, Anal. Chem. 84 (2012) 3990–3997, https://doi.org/10.1021/ac300374x.
[352] J.S. Becker, A. Matusch, C. Palm, D. Salber, K.A. Morton, J.S. Becker, Bioimaging of metals in brain tissue by laser ablation inductively coupled plasma mass spectrometry (LA-ICP-MS) and metallomics, Metallomics. 2 (2010) 104–111, https://doi.org/10.1039/b916722f.
[353] L.-M. Wang, J.S. Becker, Q. Wu, M.F. Oliveira, F.A. Bozza, A.L. Schwager, J.M. Hoffman, K.A. Morton, Bioimaging of copper alterations in the aging mouse brain by autoradiography, laser ablation inductively coupled plasma mass spectrometry and immunohistochemistry, Metallomics. 2 (2010) 348–353, https://doi.org/10.1039/c003875j.
[354] D. Clases, S. Fingerhut, A. Jeibmann, M. Sperling, P. Doble, U. Karst, LA-ICP-MS/MS improves limits of detection in elemental bioimaging of gadolinium deposition originating from MRI contrast agents in skin and brain tissues, J. Trace Elem. Med. Biol. 51 (2019) 212–218, https://doi.org/10.1016/j.jtemb.2018.10.021.
[355] J. Bell, Elemental Imaging of MRI Contrast Agents: Benchmarking of LA-ICP-MS to MRI, 2012 1641–1649, https://doi.org/10.1007/s00216-012-5973-z.
[356] O. Reifschneider, I. Castanheira, M. Sperling, U. Karst, G. Ciarimboli, Spectrometry to Investigate Toxic Side Effects of Cisplatin, 2015 1595–1603, https://doi.org/10.1039/c5mt00226e.
[357] G.D. Kenny, A.S. Bienemann, A.D. Tagalakis, J.A. Pugh, K. Welser, F. Campbell, A.B. Tabor, H.C. Hailes, S.S. Gill, M.F. Lythgoe, C.W. Mcleod, E.A. White, S.L. Hart, Biomaterials Multifunctional receptor-targeted nanocomplexes for the delivery of therapeutic nucleic acids to the Brain, Biomaterials 34 (2013) 9190–9200, https://doi.org/10.1016/j.biomaterials.2013.07.081.
[358] F. Lu, Z.Z. Pang, J. Zhao, K. Jin, H. Li, Q. Pang, L. Zhang, Z.Z. Pang, Angiopep-2-conjugated poly(ethylene glycol)-co-poly(ε-caprolactone) polymersomes for dual-targeting drug delivery to glioma in rats, Int. J. Nanomed. 12 (2017) 2117–2127, https://doi.org/10.2147/IJN.S123422.
[359] S. Misra, K. Chopra, U.N. Saikia, V.R. Sinha, R. Sehgal, M. Modi, B. Medhi, Effect of mesenchymal stem cells and galantamine nanoparticles in rat model of Alzheimer's disease, Regen. Med. 11 (2016) 629–646, https://doi.org/10.2217/rme-2016-0032.
[360] Y.S. Kang, H.J. Jung, J.S. Oh, D.Y. Song, Use of PEGylated immunoliposomes to deliver dopamine across the blood–brain barrier in a rat model of Parkinson's disease, CNS Neurosci. Ther. 22 (2016) 817–823, https://doi.org/10.1111/cns.12580.
[361] K. Jellinger, L. Linert, E. Kienzl, E. Herlinger, M.B. Youdim, Chemical evidence for 6-hydroxydopamine to be an endogenous toxic factor in the pathogenesis of Parkinson's disease, J. Neural Transm. Suppl. 46 (1995) 297–314 http://www.ncbi.nlm.nih.gov/pubmed/8821067 (accessed March 16, 2018).
[362] A.D. Andersen, M. Blaabjerg, M. Binzer, A. Kamal, H. Thagesen, T.W. Kjaer, E. Stenager, J.B.P. Gramsbergen, Cerebrospinal fluid levels of catecholamines and its metabolites in Parkinson's disease: effect of l -DOPA treatment and changes in

levodopa-induced dyskinesia, J. Neurochem. 141 (2017) 614–625, https://doi.org/10.1111/jnc.13997.
[363] S. Nageeb El-Helaly, A. Abd Elbary, M.A.A. Kassem, M.A.A. El-Nabarawi, Electrosteric stealth Rivastigmine loaded liposomes for brain targeting: preparation, characterization, *ex vivo*, bio-distribution and *in vivo* pharmacokinetic studies, Drug Deliv. 24 (2017) 692–700, https://doi.org/10.1080/10717544.2017.1309476.
[364] V. Soni, D.V.V. Kohli, S.K.K. Jain, Transferrin-conjugated liposomal system for improved delivery of 5-fluorouracil to brain, J. Drug Target. 16 (2008) 73–78, https://doi.org/10.1080/10611860701725381.
[365] R.A. Floyd, J.M. Carney, Free radical damage to protein and DNA: mechanisms involved and relevant observations on brain undergoing oxidative stress, Ann. Neurol. 32 (Suppl) (1992) S22–S27 http://www.ncbi.nlm.nih.gov/pubmed/1510377 (accessed March 15, 2018).
[366] B. Chance, H. Sies, A. Boveris, Hydroperoxide metabolism in mammalian organs, Physiol. Rev. 59 (1979) 527–605, https://doi.org/10.1152/physrev.1979.59.3.527.
[367] D.S. Warner, H. Sheng, I. Batinić-Haberle, Oxidants, antioxidants and the ischemic brain, J. Exp. Biol. 207 (2004) 3221–3231, https://doi.org/10.1242/jeb.01022.
[368] L. Zuo, T. Zhou, B.K. Pannell, A.C. Ziegler, T.M. Best, Biological and physiological role of reactive oxygen species - the good, the bad and the ugly, Acta Physiol. 214 (2015) 329–348, https://doi.org/10.1111/apha.12515.
[369] G. Merlini, V. Bellotti, Molecular mechanisms of amyloidosis, N. Engl. J. Med. 349 (2003) 583–596, https://doi.org/10.1056/NEJMra023144.
[370] R. Kones, Mitochondrial therapy for Parkinson's disease: neuroprotective pharmaconutrition may be disease-modifying, Clin. Pharmacol. 2 (2010) 185–198, https://doi.org/10.2147/CPAA.S12082.
[371] Y. Nakabeppu, D. Tsuchimoto, H. Yamaguchi, K. Sakumi, Oxidative damage in nucleic acids and Parkinson's disease, J. Neurosci. Res. 85 (2007) 919–934, https://doi.org/10.1002/jnr.21191.
[372] D.A. Bosco, D.M. Fowler, Q. Zhang, J. Nieva, E.T. Powers, P. Wentworth, R.A. Lerner, J. W. Kelly, Elevated levels of oxidized cholesterol metabolites in Lewy body disease brains accelerate α-synuclein fibrilization, Nat. Chem. Biol. 2 (2006) 249–253, https://doi.org/10.1038/nchembio782.
[373] G.D. Zeevalk, R. Razmpour, L.P. Bernard, Glutathione and Parkinson's disease: Is this the elephant in the room? Biomed. Pharmacother. 62 (2008) 236–249, https://doi.org/10.1016/j.biopha.2008.01.017.
[374] W. Zhang, T. Wang, Z. Pei, D.S. Miller, X. Wu, M.L. Block, B. Wilson, W. Zhang, Y. Zhou, J.-S. Hong, J. Zhang, Aggregated α-synuclein activates microglia: a process leading to disease progression in Parkinson's disease, FASEB J. 19 (2005) 533–542, https://doi.org/10.1096/fj.04-2751com.
[375] C. Farina, F. Aloisi, E. Meinl, Astrocytes are active players in cerebral innate immunity, Trends Immunol. 28 (2007) 138–145, https://doi.org/10.1016/j.it.2007.01.005.
[376] H.-M. Gao, P.T. Kotzbauer, K. Uryu, S. Leight, J.Q. Trojanowski, V.M.-Y. Lee, Neuroinflammation and Oxidation/Nitration of -Synuclein Linked to Dopaminergic Neurodegeneration, J. Neurosci. 28 (2008) 7687–7698, https://doi.org/10.1523/JNEUROSCI.0143-07.2008.
[377] R.M. Friedlander, Apoptosis and caspases in neurodegenerative diseases, N. Engl. J. Med. 348 (2003) 1365–1375, https://doi.org/10.1056/NEJMra022366.
[378] Y. Zhao, B. Zhao, Oxidative stress and the pathogenesis of Alzheimer's Disease, Oxid. Med. Cell. Longev. 2013 (2013) 1–10, https://doi.org/10.1155/2013/316523.
[379] R. Castellani, K. Hirai, G. Aliev, K.L. Drew, A. Nunomura, A. Takeda, A.D. Cash, M.E. Obrenovich, G. Perry, M.A. Smith, Role of mitochondrial dysfunction in Alzheimer's disease, J. Neurosci. Res. 70 (2002) 357–360, https://doi.org/10.1002/jnr.10389.
[380] P. Picone, D. Nuzzo, L. Caruana, V. Scafidi, M. Di Carlo, Mitochondrial dysfunction: different routes to Alzheimer's disease therapy, Oxid. Med. Cell. Longev. 2014 (2014) 1–11, https://doi.org/10.1155/2014/780179.
[381] X. Wang, W. Wang, L. Li, G. Perry, H. Lee, X. Zhu, Oxidative stress and mitochondrial dysfunction in Alzheimer's disease, Biochim. Biophys. Acta Mol. Basis Dis. 1842 (2014) 1240–1247, https://doi.org/10.1016/j.bbadis.2013.10.015.
[382] A. Siderowf, A. Newberg, K.L. Chou, M. Lloyd, A. Colcher, H.I. Hurtig, M.B. Stern, R.L. Doty, P.D. Mozley, N. Wintering, J.E. Duda, D. Weintraub, P.J. Moberg, [99mTc] TRODAT-1 SPECT imaging correlates with odor identification in early Parkinson disease, Neurology 64 (2005) 1716–1720, https://doi.org/10.1212/01.WNL.0000161874.52302.5D.
[383] P.H. Chan, Reactive oxygen radicals in signaling and damage in the ischemic brain, J. Cereb. Blood Flow Metab. 21 (2001) 2–14, https://doi.org/10.1097/00004647-200101000-00002.
[384] M.D. de M, Oxidative therapy against cancer, Oxidative Stress Dis, InTech, 2012 https://doi.org/10.5772/33251.
[385] W.-T. Chiu, S.-C. Shen, J.-M. Chow, C.-W. Lin, L.-T. Shia, Y.-C. Chen, Contribution of reactive oxygen species to migration/invasion of human glioblastoma cells U87 via ERK-dependent COX-2/PGE2 activation, Neurobiol. Dis. 37 (2010) 118–129, https://doi.org/10.1016/j.nbd.2009.09.015.
[386] S.-S. Kim, A. Rait, E. Kim, K.F. Pirollo, M. Nishida, N. Farkas, J.A. Dagata, E.H. Chang, A nanoparticle carrying the p53 gene targets tumors including cancer stem cells, sensitizes glioblastoma to chemotherapy and improves survival, ACS Nano 8 (2014) 5494–5514, https://doi.org/10.1021/nn5014484.
[387] E.D. Wills, Mechanisms of lipid peroxide formation in animal tissues, Biochem. J. 99 (1966) 667–676 http://www.ncbi.nlm.nih.gov/pubmed/5964963 (accessed March 16, 2018).
[388] M. Khoubnasabjafari, K. Ansarin, A. Jouyban, Reliability of malondialdehyde as a biomarker of oxidative stress in psychological disorders, Bioimpacts 5 (2015) 123–127, https://doi.org/10.15171/bi.2015.20.
[389] G. Wu, Y.-Z. Fang, S. Yang, J.R. Lupton, N.D. Turner, Glutathione metabolism and its implications for health, J. Nutr. 134 (2004) 489–492, https://doi.org/10.1093/jn/134.3.489.
[390] D.J. Jollow, J.R. Mitchell, N. Zampaglione, J.R. Gillette, Bromobenzene-induced liver necrosis. protective role of glutathione and evidence for 3,4-bromobenzene oxide as the hepatotoxic metabolite, Pharmacology 11 (1974) 151–169, https://doi.org/10.1159/000136485.
[391] J.B. de Haan, C. Bladier, P. Griffiths, M. Kelner, R.D. O'Shea, N.S. Cheung, R.T. Bronson, M.J. Silvestro, S. Wild, S.S. Zheng, P.M. Beart, P.J. Hertzog, I. Kola, Mice with a homozygous null mutation for the most abundant glutathione peroxidase, Gpx1, show increased susceptibility to the oxidative stress-inducing agents paraquat and hydrogen peroxide, J. Biol. Chem. 273 (1998) 22528–22536 http://www.ncbi.nlm.nih.gov/pubmed/9712879 (accessed March 16, 2018).
[392] J. Mohandas, J.J. Marshall, G.G. Duggin, J.S. Horvath, D.J. Tiller, Differential distribution of glutathione and glutathione-related enzymes in rabbit kidney. Possible implications in analgesic nephropathy, Biochem. Pharmacol. 33 (1984) 1801–1807 http://www.ncbi.nlm.nih.gov/pubmed/6145422 (accessed March 16, 2018).
[393] J.M. Estrela, A. Ortega, E. Obrador, Glutathione in cancer biology and therapy, Crit. Rev. Clin. Lab. Sci. 43 (2006) 143–181, https://doi.org/10.1080/10408360500523878.
[394] M. Weisbrot-Lefkowitz, K. Reuhl, B. Perry, P.H. Chan, M. Inouye, O. Mirochnitchenko, Overexpression of human glutathione peroxidase protects transgenic mice against focal cerebral ischemia/reperfusion damage, Brain Res. Mol. Brain Res. 53 (1998) 333–338 http://www.ncbi.nlm.nih.gov/pubmed/9473716 (accessed March 16, 2018).
[395] S.J. Kish, C.L. Morito, O. Hornykiewicz, Brain glutathione peroxidase in neurodegenerative disorders, Neurochem. Pathol. 4 (1986) 23–28 http://www.ncbi.nlm.nih.gov/pubmed/2940481 (accessed March 16, 2018).
[396] G.W. Kim, T. Kondo, N. Noshita, P.H. Chan, Manganese superoxide dismutase deficiency exacerbates cerebral infarction after focal cerebral ischemia/reperfusion in mice: implications for the production and role of superoxide radicals, Stroke. 33 (2002) 809–815 http://www.ncbi.nlm.nih.gov/pubmed/11872908 (accessed March 16, 2018).
[397] R.M. Lebovitz, H. Zhang, H. Vogel, J. Cartwright, L. Dionne, N. Lu, S. Huang, M.M. Matzuk, Neurodegeneration, myocardial injury, and perinatal death in mitochondrial superoxide dismutase-deficient mice, Proc. Natl. Acad. Sci. U. S. A. 93 (1996).
[398] Y. Kono, Generation of superoxide radical during autoxidation of hydroxylamine and an assay for superoxide dismutase, Arch. Biochem. Biophys. 186 (1978) 189–195 http://www.ncbi.nlm.nih.gov/pubmed/24422 (accessed March 16, 2018).
[399] R. Dringen, P.G. Pawlowski, J. Hirrlinger, Peroxide detoxification by brain cells, J. Neurosci. Res. 79 (2005) 157–165, https://doi.org/10.1002/jnr.20280.
[400] J.M. Auerbach, M. Segal, Peroxide modulation of slow onset potentiation in rat hippocampus, J. Neurosci. 17 (1997) 8695–8701 http://www.ncbi.nlm.nih.gov/pubmed/9348338 (accessed March 16, 2018).
[401] C. A, in: R.A. Greenwald (Ed.), CRC Handbook of Methods for Oxygen Radical Research, CRC Press 1985, p. 447 https://catalog.hathitrust.org/Record/000626593 , (accessed September 19, 2018).
[402] N.R. Sims, M.F. Anderson, L.M. Hobbs, J.Y. Kong, S. Phillips, J.A. Powell, E. Zaidan, Impairment of brain mitochondrial function by hydrogen peroxide, Brain Res. Mol. Brain Res. 77 (2000) 176–184 http://www.ncbi.nlm.nih.gov/pubmed/10837913 (accessed March 16, 2018).
[403] W.-S. Choi, R.D. Palmiter, Z. Xia, Loss of mitochondrial complex I activity potentiates dopamine neuron death induced by microtubule dysfunction in a Parkinson's disease model, J. Cell Biol. 192 (2011) 873–882, https://doi.org/10.1083/jcb.201009132.
[404] T.E. King, R.L. Howard, [52] Preparations and properties of soluble NADH dehydrogenases from cardiac muscle, Methods Enzymol. 10 (1967) 275–294, https://doi.org/10.1016/0076-6879(67)10055-4.
[405] M.F. Beal, E. Brouillet, B.G. Jenkins, R.J. Ferrante, N.W. Kowall, J.M. Miller, E. Storey, R. Srivastava, B.R. Rosen, B.T. Hyman, Neurochemical and histologic characterization of striatal excitotoxic lesions produced by the mitochondrial toxin 3-nitropropionic acid, J. Neurosci. 13 (1993) 4181–4192 http://www.ncbi.nlm.nih.gov/pubmed/7692009 (accessed March 16, 2018).
[406] T.E. King, [58] Preparation of succinate dehydrogenase and reconstitution of succinate oxidase, Methods Enzymol. 10 (1967) 322–331, https://doi.org/10.1016/0076-6879(67)10061-X.
[407] T. Wei, C. Chen, J. Hou, B. Zhao, W. Xin, A. Mori, The antioxidant EPC-K1 attenuates NO-induced mitochondrial dysfunction, lipid peroxidation and apoptosis in cerebellar granule cells, Toxicology. 134 (1999) 117–126 http://www.ncbi.nlm.nih.gov/pubmed/10403631 (accessed March 16, 2018).
[408] L.C. Green, D.A. Wagner, J. Glogowski, P.L. Skipper, J.S. Wishnok, S.R. Tannenbaum, Analysis of nitrate, nitrite, and [15N]nitrate in biological fluids, Anal. Biochem. 126 (1982) 131–138, https://doi.org/10.1016/0003-2697(82)90118-X.
[409] N.C. Inestrosa, A. Alvarez, C.A. Pérez, R.D. Moreno, M. Vicente, C. Linker, O.I. Casanueva, C. Soto, J. Garrido, Acetylcholinesterase accelerates assembly of amyloid-beta-peptides into Alzheimer's fibrils: possible role of the peripheral site of the enzyme, Neuron 16 (1996) 881–891 http://www.ncbi.nlm.nih.gov/pubmed/8608006 (accessed March 16, 2018).
[410] W. Poewe, E. Wolters, M. Emre, M. Onofrj, C. Hsu, S. Tekin, R. Lane, EXPRESS Investigators, Long-term benefits of rivastigmine in dementia associated with Parkinson's disease: An active treatment extension study, Mov. Disord. 21 (2006) 456–461, https://doi.org/10.1002/mds.20700.
[411] G.L. Ellman, K.D. Courtney, V. Andres, R.M. Featherstone, A new and rapid colorimetric determination of acetylcholinesterase activity, Biochem. Pharmacol. 7 (1961) 88–95, https://doi.org/10.1016/0006-2952(61)90145-9.
[412] D. Sharma, D. Maheshwari, G. Philip, R. Rana, S. Bhatia, M. Singh, R. Gabrani, S.K.K. Sharma, J. Ali, R.K.K. Sharma, S. Dang, Formulation and optimization of polymeric nanoparticles for intranasal delivery of lorazepam using Box-Behnken design: In

vitro and in vivo evaluation, Biomed Res. Int. 2014 (2014) https://doi.org/10.1155/2014/156010.
[413] D. Psimadas, P. Bouziotis, P. Georgoulias, V. Valotassiou, T. Tsotakos, G. Loudos, Radiolabeling approaches of nanoparticles with ^{99m}Tc, Contrast Media Mol. Imaging 8 (2013) 333–339, https://doi.org/10.1002/cmmi.1530.
[414] L.H. Reddy, R.K. Sharma, K. Chuttani, A.K. Mishra, R.R. Murthy, Etoposide-incorporated tripalmitin nanoparticles with different surface charge: Formulation, characterization, radiolabeling, and biodistribution studies, AAPS J. 6 (2004) 55–64, https://doi.org/10.1208/aapsj060323.
[415] L.H. Reddy, R.K. Sharma, R.S.R. Murthy, Enhanced tumour uptake of doxorubicin loaded poly(butyl cyanoacrylate) nanoparticles in mice bearing Dalton's lymphoma tumour, J. Drug Target. 12 (2004) 443–451, https://doi.org/10.1080/10611860400011406.
[416] F. Pitossi, A. del Rey, A. Kabiersch, H. Besedovsky, Induction of cytokine transcripts in the central nervous system and pituitary following peripheral administration of endotoxin to mice, J. Neurosci. Res. 48 (1997) 287–298, https://doi.org/10.1002/(SICI)1097-4547(19970515)48:4<287::AID-JNR1>3.0.CO;2-7.
[417] M.A. Muñoz-Fernández, M. Fresno, The role of tumour necrosis factor, interleukin 6, interferon-gamma and inducible nitric oxide synthase in the development and pathology of the nervous system, Prog. Neurobiol. 56 (1998) 307–340 http://www.ncbi.nlm.nih.gov/pubmed/9770242 (accessed March 16, 2018).
[418] B. Engelhardt, F.K. Conley, P.J. Kilshaw, E.C. Butcher, Lymphocytes infiltrating the CNS during inflammation display a distinctive phenotype and bind to VCAM-1 but not to MAdCAM-1, Int. Immunol. 7 (1995) 481–491, https://doi.org/10.1093/intimm/7.3.481.
[419] I. Khalin, R. Alyautdin, T.W.W. Wong, J. Gnanou, G. Kocherga, J. Kreuter, Brain-derived neurotrophic factor delivered to the brain using poly (lactide-co-glycolide) nanoparticles improves neurological and cognitive outcome in mice with traumatic brain injury, Drug Deliv. 23 (2016) 3520–3528, https://doi.org/10.1080/10717544.2016.1199609.
[420] S. Wohlfart, A.S. Khalansky, S. Gelperina, D. Begley, J. Kreuter, Kinetics of transport of doxorubicin bound to nanoparticles across the blood-brain barrier, J. Control. Release 154 (2011) 103–107, https://doi.org/10.1016/j.jconrel.2011.05.010.
[421] A. Arshad, B. Yang, A.S.S. Bienemann, N.U.U. Barua, M.J.J. Wyatt, M. Woolley, D.E.E. Johnson, K.J.J. Edler, S.S.S. Gill, Convection-enhanced delivery of carboplatin PLGA nanoparticles for the treatment of glioblastoma, PLoS One 10 (2015) 1–16, https://doi.org/10.1371/journal.pone.0132266.
[422] W.G.G. Singleton, A.M.M. Collins, A.S.S. Bienemann, C.L.L. Killick-Cole, H.R.R. Haynes, D.J.J. Asby, C.P.P. Butts, M.J.J. Wyatt, N.U.U. Barua, S.S.S. Gill, Convection enhanced delivery of panobinostat (LBH589)-loaded pluronic nano-micelles prolongs survival in the F98 rat glioma model, Int. J. Nanomed. 12 (2017) 1385–1399, https://doi.org/10.2147/IJN.S125300.
[423] G. Yurtdaş Kırımlıoğlu, Y. Menceloğlu, K. Erol, Y. Yazan, *In vitro/in vivo* evaluation of gamma-aminobutyric acid-loaded *N, N* -dimethylacrylamide-based pegylated polymeric nanoparticles for brain delivery to treat epilepsy, J. Microencapsul. 33 (2016) 625–635, https://doi.org/10.1080/02652048.2016.1234515.
[424] R. Narayan, M. Singh, O.P.P. Ranjan, Y. Nayak, S. Garg, G.V.V. Shavi, U.Y.Y. Nayak, Development of risperidone liposomes for brain targeting through intranasal route, Life Sci. 163 (2016) 38–45, https://doi.org/10.1016/j.lfs.2016.08.033.
[425] S. Patel, S. Chavhan, H. Soni, A.K. Babbar, R. Mathur, A.K. Mishra, K. Sawant, Brain targeting of risperidone-loaded solid lipid nanoparticles by intranasal route, J. Drug Target. 19 (2011) 468–474, https://doi.org/10.3109/1061186X.2010.523787.
[426] V. Kakkar, S.K. Muppu, K. Chopra, I.P. Kaur, Curcumin loaded solid lipid nanoparticles: An efficient formulation approach for cerebral ischemic reperfusion injury in rats, Eur. J. Pharm. Biopharm. 85 (2013) 339–345, https://doi.org/10.1016/j.ejpb.2013.02.005.
[427] E.B. Basalious, R.N. Shamma, Novel self-assembled nano-tubular mixed micelles of Pluronics P123, Pluronic F127 and phosphatidylcholine for oral delivery of nimodipine: In vitro characterization, ex vivo transport and in vivo pharmacokinetic studies, Int. J. Pharm. 493 (2015) 347–356, https://doi.org/10.1016/J.IJPHARM.2015.07.075.
[428] A.R. Galho, M.F. Cordeiro, S.A. Ribeiro, M.S. Marques, M.F.D. Antunes, D.C. Luz, G. Hädrich, A.L. Muccillo-Baisch, D.M. Barros, J.V. Lima, C.L. Dora, A.P. Horn, Protective role of free and quercetin-loaded nanoemulsion against damage induced by intracerebral haemorrhage in rats, Nanotechnology 27 (2016) 175101, https://doi.org/10.1088/0957-4484/27/17/175101.
[429] P. Chonpathompikunlert, C.-H. Fan, Y. Ozaki, T. Yoshitomi, C.-K. Yeh, Y. Nagasaki, Redox nanoparticle treatment protects against neurological deficit in focused ultrasound-induced intracerebral hemorrhage, Nanomedicine 7 (2012) 1029–1043, https://doi.org/10.2217/nnm.12.2.
[430] Y.-C. Chen, W.-Y. Hsieh, W.-F. Lee, D.-T. Zeng, Effects of surface modification of PLGA-PEG-PLGA nanoparticles on loperamide delivery efficiency across the blood–brain barrier, J. Biomater. Appl. 27 (2013) 909–922, https://doi.org/10.1177/0885328211429495.
[431] F. Hefti, E. Melamed, B.J. Sahakian, R.J. Wurtman, Circling behavior in rats with partial, unilateral nigro-striatal lesions: Effect of amphetamine, apomorphine, and DOPA, Pharmacol. Biochem. Behav. 12 (1980) 185–188, https://doi.org/10.1016/0091-3057(80)90353-6.
[432] U. Ungerstedt, Postsynaptic supersensitivity after 6-Hydroxy-dopamine induced degeneration of the nigro-striatal dopamine system, Acta Physiol. Scand. 82 (1971) 69–93, https://doi.org/10.1111/j.1365-201X.1971.tb11000.x.
[433] U. Ungerstedt, Striatal dopamine release after amphetamine or nerve degeneration revealed by rotational behaviour, Acta Physiol. Scand. 82 (1971) 49–68, https://doi.org/10.1111/j.1365-201X.1971.tb10999.x.
[434] U. Ungerstedt, G.W. Arbuthnott, Quantitative recording of rotational behavior in rats after 6-hydroxy-dopamine lesions of the nigrostriatal dopamine system, Brain Res. 24 (1970) 485–493, https://doi.org/10.1016/0006-8993(70)90187-3.
[435] R. Iancu, P. Mohapel, P. Brundin, G. Paul, Behavioral characterization of a unilateral 6-OHDA-lesion model of Parkinson's disease in mice, Behav. Brain Res. 162 (2005) 1–10, https://doi.org/10.1016/J.BBR.2005.02.023.
[436] A. Abuirmeileh, R. Lever, A.E. Kingsbury, A.J. Lees, I.C. Locke, R.A. Knight, H.S. Chowdrey, C.S. Biggs, P.S. Whitton, The corticotrophin-releasing factor-like peptide urocortin reverses key deficits in two rodent models of Parkinson's disease, Eur. J. Neurosci. 26 (2007) 417–423, https://doi.org/10.1111/j.1460-9568.2007.05653.x.
[437] S.B. Dunnett, I.Q. Whishaw, D.C. Rogers, G.H. Jones, Dopamine-rich grafts ameliorate whole body motor asymmetry and sensory neglect but not independent limb use in rats with 6-hydroxydopamine lesions, Brain Res. 415 (1987) 63–78 http://www.ncbi.nlm.nih.gov/pubmed/3113665 (accessed March 13, 2018).
[438] J.M. Klug, A.B. Norman, Long-term sensitization of apomorphine-induced rotation behavior in rats with dopamine deafferentation or excitotoxin lesions of the striatum, Pharmacol. Biochem. Behav. 46 (1993) 397–403 http://www.ncbi.nlm.nih.gov/pubmed/7903458 (accessed March 13, 2018).
[439] G. Rozas, J.L. Labandeira García, Drug-free evaluation of rat models of parkinsonism and nigral grafts using a new automated rotarod test, Brain Res. 749 (1997) 188–199, https://doi.org/10.1016/S0006-8993(96)01162-6.
[440] M. Olsson, G. Nikkhah, C. Bentlage, A. Björklund, Forelimb akinesia in the rat Parkinson model: differential effects of dopamine agonists and nigral transplants as assessed by a new stepping test, J. Neurosci. 15 (1995) 3863–3875 http://www.ncbi.nlm.nih.gov/pubmed/7751951 (accessed March 13, 2018).
[441] E.I. Miklyaeva, I.Q. Whishaw, HemiParkinson analogue rats display active support in good limbs versus passive support in bad limbs on a skilled reaching task of variable height, Behav. Neurosci. 110 (1996) 117–125 http://www.ncbi.nlm.nih.gov/pubmed/8652060 (accessed March 13, 2018).
[442] K.E. Martin, J.G. Phillips, R. Iansek, J.L. Bradshaw, Inaccuracy and instability of sequential movements in Parkinson's disease., Exp, Brain Res. 102 (1994) 131–140 http://www.ncbi.nlm.nih.gov/pubmed/7895789 (accessed March 13, 2018).
[443] P. Umarao, S. Bose, S. Bhattacharyya, A. Kumar, S. Jain, Neuroprotective potential of superparamagnetic iron oxide nanoparticles along with exposure to electromagnetic field in 6-OHDA rat model of Parkinson's Disease, J. Nanosci. Nanotechnol. 16 (2016) 261–269, https://doi.org/10.1166/jnn.2016.11103.
[444] Zhang Nisi, Xiuxian Huang, Dai Zhifei, Hairong Zheng, Yan Fei, Localized delivery of curcumin-loaded nanoparticles to the brain for treatment of Parkinson's disease using focused ultrasound, in: 2016 IEEE Int. Ultrason. Symp., IEEE, 2016: pp. 1–3. https://doi.org/10.1109/ULTSYM.2016.7728663.
[445] C.V. Borlongan, P.R. Sanberg, Elevated body swing test: A new behavioral parameter for rats with 6-Hydroxydopamine-induced hemiparkinsonism, J. Neurosci. 15 (1995) 5372–5378 https://pdfs.semanticscholar.org/3b1c/8df0743f0bf83cceb63514381650d8f067f1.pdf (accessed March 13, 2018).
[446] R. Iancu, P. Mohapel, P. Brundin, G. Paul, Behavioral characterization of a unilateral 6-OHDA-lesion model of Parkinson's disease in mice, Behav. Brain Res. 162 (2005) 1–10, https://doi.org/10.1016/j.bbr.2005.02.023.
[447] M. Olsson, G. Nikkhah, C. Bentlage, A. Bjarklund, Forelimb akinesia in the rat Parkinson model: differential effects of dopamine aagonists and nigral transplants as assessed by a new stepping test, J. Neurosci. 15 (1995) 3863–3875 http://www.jneurosci.org/content/jneuro/15/5/3863.full.pdf (accessed March 13, 2018).
[448] M. Sedelis, R.K. Schwarting, J.P. Huston, Behavioral phenotyping of the MPTP mouse model of Parkinson's disease, Behav. Brain Res. 125 (2001) 109–125, https://doi.org/10.1016/S0166-4328(01)00309-6.
[449] R.N. Walsh, R.A. Cummins, The open-field test: A critical review, Psychol. Bull. 83 (1976) 482–504, https://doi.org/10.1037/0033-2909.83.3.482.
[450] Y. Liu, Y. Guo, S. An, Y. Kuang, X. He, H. Ma, J. Li, J. Lv, N. Zhang, C. Jiang, Targeting Caspase-3 as dual therapeutic benefits by RNAi facilitating brain-targeted nanoparticles in a rat model of Parkinson's Disease, PLoS One 8 (2013), e62905. https://doi.org/10.1371/journal.pone.0062905.
[451] R. Huang, H. Ma, Y. Guo, S. Liu, Y. Kuang, K. Shao, J. Li, Y. Liu, L. Han, S. Huang, S. An, L. Ye, J. Lou, C. Jiang, Angiopep-conjugated nanoparticles for targeted long-term gene therapy of Parkinson's Disease, Pharm. Res. 30 (2013) 2549–2559, https://doi.org/10.1007/s11095-013-1005-8.
[452] F.P. Valle, Effects of strain, sex, and illumination on open-field behavior of rats, Am. J. Psychol. 83 (1970) 103–111 http://www.ncbi.nlm.nih.gov/pubmed/5465190 (accessed March 13, 2018).
[453] M.D. Grounds, H.G. Radley, G.S. Lynch, K. Nagaraju, A. De Luca, Towards developing standard operating procedures for pre-clinical testing in the mdx mouse model of Duchenne muscular dystrophy, Neurobiol. Dis. 31 (2008) 1–19, https://doi.org/10.1016/j.nbd.2008.03.008.
[454] P.R. Sanberg, M. Giordano, M.D. Bunsey, A.B. Norman, The catalepsy test: its ups and downs, Behav. Neurosci. 102 (1988) 748–759 https://www.researchgate.net/profile/Magda_Giordano/publication/20252530_The_Catalepsy_Test_Its_Ups_and_Downs/links/54cbeb110cf24601c089c9c2/The-Catalepsy-Test-Its-Ups-and-Downs.pdf (accessed March 14, 2018).
[455] P.R. Sanberg, J. Pevsner, J.T. Coyle, Parametric influences on catalepsy, Psychopharmacology (Berl.) 82 (1984) 406–408 http://www.ncbi.nlm.nih.gov/pubmed/6427835 (accessed March 14, 2018).
[456] M.L. Starkey, A.W. Barritt, P.K. Yip, M. Davies, F.P.T. Hamers, S.B. McMahon, E.J. Bradbury, Assessing behavioural function following a pyramidotomy lesion of the corticospinal tract in adult mice, Exp. Neurol. 195 (2005) 524–539, https://doi.org/10.1016/j.expneurol.2005.06.017.

[457] R.B. Silvestrin, L.F. de Oliveira, C. Batassini, A. Oliveira, T.M. e Souza, The footfault test as a screening tool in the 6-hydroxydopamine rat model of Parkinson's disease, J. Neurosci. Methods. 177 (2009) 317–321, https://doi.org/10.1016/J.JNEUMETH.2008.10.030.
[458] C. Weller, C.J. O'Neill, A. Charlett, S.G. Bowes, A. Purkiss, P.W. Nicholson, R.J. Dobbs, S.M. Dobbs, Defining small differences in efficacy between anti-parkinsonian agents using gait analysis: a comparison of two controlled release formulations of levodopa/decarboxylase inhibitor, Br. J. Clin. Pharmacol. 35 (1993) 379–385 http://www.ncbi.nlm.nih.gov/pubmed/8485018 (accessed March 14, 2018).
[459] A. Bartolic, Z. Pirtosek, J. Rozman, S. Ribaric, Postural stability of Parkinson's disease patients is improved by decreasing rigidity, Eur. J. Neurol. 12 (2005) 156–159, https://doi.org/10.1111/j.1468-1331.2004.00942.x.
[460] J.L. Tillerson, W.M. Caudle, M.E. Reverón, G.W. Miller, Detection of behavioral impairments correlated to neurochemical deficits in mice treated with moderate doses of 1-methyl-4-phenyl-1,2,3,6-tetrahydropyridine, Exp. Neurol. 178 (2002) 80–90 http://www.ncbi.nlm.nih.gov/pubmed/12460610 (accessed March 14, 2018).
[461] S.M. Fleming, J. Salcedo, P.-O. Fernagut, E. Rockenstein, E. Masliah, M.S. Levine, M.-F. Chesselet, Early and Progressive Sensorimotor Anomalies in Mice Overexpressing Wild-Type Human -Synuclein, J. Neurosci. 24 (2004) 9434–9440, https://doi.org/10.1523/JNEUROSCI.3080-04.2004.
[462] H. Leblond, M. L'Esperance, D. Orsal, S. Rossignol, Treadmill locomotion in the intact and spinal mouse, J. Neurosci. 23 (2003) 11411–11419 http://www.ncbi.nlm.nih.gov/pubmed/14673005 (accessed March 14, 2018).
[463] M.A. Smith, J. Brandt, R. Shadmehr, Motor disorder in Huntington's disease begins as a dysfunction in error feedback control, Nature. 403 (2000) 544–549, https://doi.org/10.1038/35000576.
[464] N. Ogawa, Y. Hirose, S. Ohara, T. Ono, Y. Watanabe, A simple quantitative bradykinesia test in MPTP-treated mice, Res. Commun. Chem. Pathol. Pharmacol. 50 (1985) 435–441 http://www.ncbi.nlm.nih.gov/pubmed/3878557 (accessed March 14, 2018).
[465] K. Matsuura, H. Kabuto, H. Makino, N. Ogawa, Pole test is a useful method for evaluating the mouse movement disorder caused by striatal dopamine depletion, J. Neurosci. Methods. 73 (1997) 45–48, https://doi.org/10.1016/S0165-0270(96)02211-X.
[466] T. Schallert, S.M. Fleming, J.L. Leasure, J.L. Tillerson, S.T. Bland, CNS plasticity and assessment of forelimb sensorimotor outcome in unilateral rat models of stroke, cortical ablation, parkinsonism and spinal cord injury, Neuropharmacology. 39 (2000) 777–787 http://www.ncbi.nlm.nih.gov/pubmed/10699444 (accessed March 15, 2018).
[467] M. Woodlee, A. Asseogarcia, X. Zhao, S. Liu, T. Jones, T. Schallert, Testing forelimb placing across the midline reveals distinct, lesion-dependent patterns of recovery in rats, Exp. Neurol. 191 (2005) 310–317, https://doi.org/10.1016/j.expneurol.2004.09.005.
[468] R.D.S. Prediger, L.C. Batista, R.N. Takahashi, Caffeine reverses age-related deficits in olfactory discrimination and social recognition memory in rats, Neurobiol. Aging. 26 (2005) 957–964, https://doi.org/10.1016/j.neurobiolaging.2004.08.012.
[469] A.A. Castro, K. Ghisoni, A. Latini, J. Quevedo, C.I. Tasca, R.D.S. Prediger, Lithium and valproate prevent olfactory discrimination and short-term memory impairments in the intranasal 1-methyl-4-phenyl-1,2,3,6-tetrahydropyridine (MPTP) rat model of Parkinson's disease, Behav. Brain Res. 229 (2012) 208–215, https://doi.org/10.1016/j.bbr.2012.01.016.
[470] R. Dantzer, R.-M. Bluthe, G.F. Koob, M. Le Moal, Modulation of social memory in male rats by neurohypophyseal peptides, Psychopharmacology (Berl.) 91 (1987) 363–368, https://doi.org/10.1007/BF00518192.
[471] T.F. Sawyer, A.K. Hengehold, W.A. Perez, Chemosensory and hormonal mediation of social memory in male rats, Behav. Neurosci. 98 (1984) 908–913 http://www.ncbi.nlm.nih.gov/pubmed/6487419 (accessed March 15, 2018).
[472] G. da Rocha Lindner, D. Bonfanti Santos, D. Colle, E.L. Gasnhar Moreira, R. Daniel Prediger, M. Farina, N.M. Khalil, R. Mara Mainardes, Improved neuroprotective effects of resveratrol-loaded polysorbate 80-coated poly(lactide) nanoparticles in MPTP-induced Parkinsonism, Nanomedicine 10 (2015) 1127–1138, https://doi.org/10.2217/nnm.14.165.
[473] R.D.S. Prediger, A.S. Aguiar, A.E. Rojas-Mayorquin, C.P. Figueiredo, F.C. Matheus, L. Ginestet, C. Chevarin, E. Del Bel, R. Mongeau, M. Hamon, L. Lanfumey, R. Raisman-Vozari, Single intranasal administration of 1-Methyl-4-Phenyl-1,2,3,6-tetrahydropyridine in C57BL/6 mice models early preclinical phase of Parkinson's Disease, Neurotox. Res. 17 (2010) 114–129, https://doi.org/10.1007/s12640-009-9087-0.
[474] M. Lemaire, Martine Lemaire, Social recognition task in the rat, Curr. Protoc. Pharmacol, John Wiley & Sons, Inc, Hoboken, NJ, USA 2003, p. 5 , 30.1-5.30.11 https://doi.org/10.1002/0471141755.ph0530s20.
[475] R.G.M. Morris, Spatial localization does not require the presence of local cues, Learn. Motiv. 12 (1981) 239–260, https://doi.org/10.1016/0023-9690(81)90020-5.
[476] B. Gong, O.V. Vitolo, F. Trinchese, S. Liu, M. Shelanski, O. Arancio, Persistent improvement in synaptic and cognitive functions in an Alzheimer mouse model after rolipram treatment, J. Clin. Invest. 114 (2004) 1624–1634, https://doi.org/10.1172/JCI22831.
[477] F. Trinchese, S. Liu, F. Battaglia, S. Walter, P.M. Mathews, O. Arancio, Progressive age-related development of Alzheimer-like pathology in APP/PS1 mice, Ann. Neurol. 55 (2004) 801–814, https://doi.org/10.1002/ana.20101.
[478] S. Dalm, J. Grootendorst, E.R. De Kloet, M.S. Oitzl, Quantification of swim patterns in the morris water maze, Behav. Res. Methods, Instruments, Comput. 32 (2000) 134–139, https://doi.org/10.3758/BF03200795.
[479] S.J. Clapcote, N.L. Lazar, A.R. Bechard, G.A. Wood, J.C. Roder, NIH Swiss and Black Swiss mice have retinal degeneration and performance deficits in cognitive tests, Comp. Med. 55 (2005) 310–316 http://www.ncbi.nlm.nih.gov/pubmed/16158906 (accessed March 18, 2018).
[480] Y. Liu, S. An, J. Li, Y. Kuang, X. He, Y. Guo, H. Ma, Y. Zhang, B. Ji, C. Jiang, Brain-targeted co-delivery of therapeutic gene and peptide by multifunctional nanoparticles in Alzheimer's disease mice, Biomaterials 80 (2016) 33–45, https://doi.org/10.1016/J.BIOMATERIALS.2015.11.060.
[481] Q. Song, M. Huang, L. Yao, X. Wang, X. Gu, J. Chen, J. Chen, J. Huang, Q. Hu, T. Kang, Z. Rong, H. Qi, G. Zheng, H. Chen, X. Gao, Lipoprotein-based nanoparticles rescue the memory loss of mice with Alzheimer's Disease by accelerating the clearance of Amyloid-Beta, ACS Nano 8 (2014) 2345–2359, https://doi.org/10.1021/nn4058215.
[482] R. Gerlai, N.S. Clayton, Analysing hippocampal function in transgenic mice: an ethological perspective, Trends Neurosci. 22 (1999) 47–51 http://www.ncbi.nlm.nih.gov/pubmed/10092042 (accessed March 18, 2018).
[483] I.Q. Whishaw, J.A. Tomie, Of mice and mazes: similarities between mice and rats on dry land but not water mazes, Physiol. Behav. 60 (1996) 1191–1197 http://www.ncbi.nlm.nih.gov/pubmed/8916170 (accessed March 18, 2018).
[484] P. Lavenex, F. Schenk, Integration of olfactory information in a spatial representation enabling accurate arm choice in the radial arm maze, Learn. Mem. 2 (2018) 299–319 http://www.ncbi.nlm.nih.gov/pubmed/10467581 (accessed March 18, 2018).
[485] J.A. Espinoza, K. Bohmwald, P.F. Cespedes, R.S. Gomez, S.A. Riquelme, C.M. Cortes, J. A. Valenzuela, R.A. Sandoval, F.C. Pancetti, S.M. Bueno, C.A. Riedel, A.M. Kalergis, Impaired learning resulting from respiratory syncytial virus infection, Proc. Natl. Acad. Sci. U. S. A. 110 (2013) 9112–9117, https://doi.org/10.1073/pnas.1217508110.
[486] Q. Li, H.F. Zhao, Z.F. Zhang, Z.G. Liu, X.R. Pei, J.B. Wang, M.Y. Cai, Y. Li, Long-term administration of green tea catechins prevents age-related spatial learning and memory decline in C57BL/6 J mice by regulating hippocampal cyclic amp-response element binding protein signaling cascade, Neuroscience 159 (2009) 1208–1215, https://doi.org/10.1016/j.neuroscience.2009.02.008.
[487] D. Morgan, D.M. Diamond, P.E. Gottschall, K.E. Ugen, C. Dickey, J. Hardy, K. Duff, P. Jantzen, G. DiCarlo, D. Wilcock, K. Connor, J. Hatcher, C. Hope, M. Gordon, G.W. Arendash, Aβ peptide vaccination prevents memory loss in an animal model of Alzheimer's disease, Nature. 408 (2000) 982–985, https://doi.org/10.1038/35050116.
[488] S. Ikegami, Behavioral impairment in radial-arm maze learning and acetylcholine content of the hippocampus and cerebral cortex in aged mice, Behav. Brain Res. 65 (1994) 103–111 http://www.ncbi.nlm.nih.gov/pubmed/7880448 (accessed March 19, 2018).
[489] S. Hamann, E.S. Monarch, F.C. Goldstein, Impaired fear conditioning in Alzheimer's disease, Neuropsychologia. 40 (2002) 1187–1195 http://www.ncbi.nlm.nih.gov/pubmed/11931922 (accessed March 19, 2018).
[490] S.A. Balogh, J.M. Wehner, Inbred mouse strain differences in the establishment of long-term fear memory, Behav. Brain Res. 140 (2003) 97–106 http://www.ncbi.nlm.nih.gov/pubmed/12644283 (accessed March 19, 2018).
[491] P. Curzon, N.R. Rustay, K.E. Browman, Cued and contextual fear conditioning for rodents, in: J.J. Buccafusco (Ed.), Methods of Behavior Analysis in Neuroscience, 2nd editionCRC Press/Taylor & Francis, Boca Raton (FL) 2009, pp. 19–38.
[492] P. Bekinschtein, M. Cammarota, L.M. Igaz, L.R.M. Bevilaqua, I. Izquierdo, J.H. Medina, Persistence of long-term memory storage requires a late protein synthesis- and BDNF- dependent phase in the hippocampus, Neuron. 53 (2007) 261–277, https://doi.org/10.1016/j.neuron.2006.11.025.
[493] M.-L.G. Wadenberg, Conditioned avoidance response in the development of new antipsychotics, Curr. Pharm. Des. 16 (2010) 358–370 https://www.researchgate.net/profile/Marie-Louise_Wadenberg/publication/41172465_Conditioned_Avoidance_Response_in_the_Development_of_New_Antipsychotics/links/56ae866408aeaa696f2ece15/Conditioned-Avoidance-Response-in-the-Development-of-New-Antipsychotics (accessed March 19, 2018).
[494] B.F. Skinner, The behavior of organisms: an experimental analysis, Oxford, Engl. Appleton-Century. (1938) 232–262.
[495] K.C. Montgomery, The relation between fear induced by novel stimulation and exploratory behavior, J. Comp. Physiol. Psychol. 48 (1955) 254–260 http://www.ncbi.nlm.nih.gov/pubmed/13252152 (accessed March 19, 2018).
[496] S.L. Handley, S. Mithani, Effects of alpha-adrenoceptor agonists and antagonists in a maze-exploration model of 'fear'-motivated behaviour, Naunyn. Schmiedebergs. Arch. Pharmacol. 327 (1984) 1–5 http://www.ncbi.nlm.nih.gov/pubmed/6149466 (accessed March 19, 2018).
[497] B.M. Cortese, K.L. Phan, The role of glutamate in anxiety and related disorders, CNS Spectr. 10 (2005) 820–830 http://www.ncbi.nlm.nih.gov/pubmed/16400245 (accessed March 19, 2018).
[498] S. Misra, K. Chopra, U.N. Saikia, V.R. Sinha, R. Sehgal, M. Modi, B. Medhi, Effect of mesenchymal stem cells and galantamine nanoparticles in rat model of Alzheimer's disease, Regen. Med. 11 (2016) 629–646, https://doi.org/10.2217/rme-2016-0032.
[499] M.M. Andrade, M.F. Tomé, E.S. Santiago, A. Lúcia-Santos, T.G. de Andrade, Longitudinal study of daily variation of rats' behavior in the elevated plus-maze, Physiol. Behav. 78 (2003) 125–133 http://www.ncbi.nlm.nih.gov/pubmed/12536019 (accessed March 19, 2018).
[500] R.E. Adamec, T. Shallow, Lasting effects on rodent anxiety of a single exposure to a cat, Physiol. Behav. 54 (1993) 101–109 http://www.ncbi.nlm.nih.gov/pubmed/8327588 (accessed March 19, 2018).
[501] V. Carola, F. D'Olimpio, E. Brunamonti, F. Mangia, P. Renzi, Evaluation of the elevated plus-maze and open-field tests for the assessment of anxiety-related

behaviour in inbred mice, Behav. Brain Res. 134 (2002) 49–57 http://www.ncbi.nlm.nih.gov/pubmed/12191791 (accessed March 19, 2018).
[502] A.P. Carobrez, L.J. Bertoglio, Ethological and temporal analyses of anxiety-like behavior: The elevated plus-maze model 20 years on, Neurosci. Biobehav. Rev. 29 (2005) 1193–1205, https://doi.org/10.1016/j.neubiorev.2005.04.017.
[503] C.A. Frye, S.M. Petralia, M.E. Rhodes, Estrous cycle and sex differences in performance on anxiety tasks coincide with increases in hippocampal progesterone and 3alpha,5alpha-THP, Pharmacol. Biochem. Behav. 67 (2000) 587–596 http://www.ncbi.nlm.nih.gov/pubmed/11164090 (accessed March 19, 2018).
[504] A. Sik, P. van Nieuwehuyzen, J. Prickaerts, A. Blokland, Performance of different mouse strains in an object recognition task, Behav. Brain Res. 147 (2003) 49–54 http://www.ncbi.nlm.nih.gov/pubmed/14659569 (accessed March 19, 2018).
[505] M. Leger, A. Quiedeville, V. Bouet, B. Haelewyn, M. Boulouard, P. Schumann-Bard, T. Freret, Object recognition test in mice, Nat. Protoc. 8 (2013) 2531–2537, https://doi.org/10.1038/nprot.2013.155.
[506] J.M. Silvers, S.B. Harrod, C.F. Mactutus, R.M. Booze, Automation of the novel object recognition task for use in adolescent rats, J. Neurosci. Methods. 166 (2007) 99–103, https://doi.org/10.1016/j.jneumeth.2007.06.032.
[507] L.L. Jackson, VTE on an elevated T-maze, J. Comp. Psychol. 36 (1943) 99–107, https://doi.org/10.1037/h0058536.
[508] R.D. Porsolt, G. Anton, N. Blavet, M. Jalfre, Behavioural despair in rats: a new model sensitive to antidepressant treatments, Eur. J. Pharmacol. 47 (1978) 379–391 http://www.ncbi.nlm.nih.gov/pubmed/204499 (accessed March 19, 2018).
[509] R.D. Porsolt, M. Le Pichon, M. Jalfre, Depression: a new animal model sensitive to antidepressant treatments, Nature. 266 (1977) 730–732 http://www.ncbi.nlm.nih.gov/pubmed/559941 (accessed March 19, 2018).
[510] R.D. Porsolt, A. Bertin, M. Jalfre, Behavioral despair in mice: a primary screening test for antidepressants, Arch. Int. Pharmacodyn. Ther. 229 (1977) 327–336 http://www.ncbi.nlm.nih.gov/pubmed/596982 (accessed March 19, 2018).
[511] V. Castagné, P. Moser, S. Roux, R.D. Porsolt, Rodent models of depression: forced swim and tail suspension behavioral despair tests in rats and mice, Curr. Protoc. Neurosci, John Wiley & Sons, Inc, Hoboken, NJ, USA, 2011 https://doi.org/10.1002/0471142301.ns0810as55 , Unit 8.10A.
[512] I. Arai, Y. Tsuyuki, H. Shiomoto, M. Satoh, S. Otomo, Decreased body temperature dependent appearance of behavioral despair in the forced swimming test in mice, Pharmacol. Res. 42 (2000) 171–176, https://doi.org/10.1006/phrs.2000.0672.
[513] B. Petit-Demouliere, F. Chenu, M. Bourin, Forced swimming test in mice: a review of antidepressant activity, Psychopharmacology (Berl.) 177 (2005) 245–255, https://doi.org/10.1007/s00213-004-2048-7.
[514] D.J.P. David, C.E. Renard, P. Jolliet, M. Hascoët, M. Bourin, Antidepressant-like effects in various mice strains in the forced swimming test, Psychopharmacology (Berl.) 166 (2003) 373–382, https://doi.org/10.1007/s00213-002-1335-4.
[515] K. Kuschiski, O. Hornykiewicz, Morphine catalepsy in the rat: relation to striatal dopamine metabolism, Eur. J. Pharmacol. 19 (1972) 119–122, https://doi.org/10.1016/0014-2999(72)90086-6.
[516] J.B.T. Rocha, J.E.T. Santos, L.K. Rocha, E.R. Kleinpaul, Undernutrition During Suckling Changes the Sensitivity to Haloperidol and Chlorpromazine in lko Behavioural Measures in Weaning Rats, Phartnucology Toxicol. 81 (1991) https://doi.org/10.1111/j.1600-0773.1997.tb00040.x.
[517] B. Costall, J.E. Olley, Cholinergic- and neuroleptic-induced catalepsy: Modification by lesions in the caudate-putamen, Neuropharmacology 10 (1971) 297–306, https://doi.org/10.1016/0028-3908(71)90053-0.
[518] M.E. Stanley, S.D. Glick, Interaction of drug effects with testing procedures in the measurement of catalepsy, Neuropharmacology 15 (1976) 393–394, https://doi.org/10.1016/0028-3908(76)90115-5.
[519] F.A. Dimer, M.C. Pigatto, C.A. Boque, C.S. Pase, K. Roversi, A.R. Pohlmann, M.E. Burger, M.K. Rates, T. Dalla Costa, S.S. Guterres, Nanoencapsulation improves relative bioavailability and antipsychotic effect of olanzapine in rats, J. Biomed. Nanotechnol. 11 (2015) 1482–1493 http://www.ncbi.nlm.nih.gov/pubmed/26295148 (accessed February 19, 2018).
[520] R.E. Featherstone, S. Kapur, P.J. Fletcher, The amphetamine-induced sensitized state as a model of schizophrenia, Prog. Neuro-Psychopharmacology Biol. Psychiatry 31 (2007) 1556–1571, https://doi.org/10.1016/j.pnpbp.2007.08.025.
[521] B.M. Angrist, S. Gershon, The phenomenology of experimentally induced amphetamine psychosis—preliminary observations, Biol. Psychiatry 2 (1970) 95–107 http://www.ncbi.nlm.nih.gov/pubmed/5459137 (accessed March 21, 2018).
[522] A.D. Levy, P.A. Rittenhouse, A.M. Bonadonna, M.C. Alvarez Sanz, C.L. Bethea, L.D. Van de Kar, Repeated exposure to cocaine produces long-lasting deficits in the serotonergic stimulation of prolactin and renin, but not adrenocorticotropin secretion, Eur. J. Pharmacol. 241 (1993) 275–278 http://www.ncbi.nlm.nih.gov/pubmed/8243563 (accessed March 21, 2018).
[523] K.E. Stevens, J. Luthman, E. Lindqvist, R.G. Johnson, G.M. Rose, Effects of neonatal dopamine depletion on sensory inhibition in the rat, Pharmacol. Biochem. Behav. 53 (1996) 817–823, https://doi.org/10.1016/0091-3057(95)02083-7.
[524] K.E. Stevens, L.L. Fuller, G.M. Rose, Dopaminergic and noradrenergic modulation of amphetamine-induced changes in auditory gating, Brain Res. 555 (1991) 91–98 http://www.ncbi.nlm.nih.gov/pubmed/1681997 (accessed March 21, 2018).
[525] S.M. Đorđević, A. Santrač, N.D. Cekić, B.D. Marković, B. Divović, T.M. Ilić, M.M. Savić, S.D. Savić, Parenteral nanoemulsions of risperidone for enhanced brain delivery in acute psychosis: physicochemical and in vivo performances, Int. J. Pharm. 533 (2017) 421–430, https://doi.org/10.1016/J.IJPHARM.2017.05.051.
[526] L. Dépatie, S. Lal, Apomorphine and the dopamine hypothesis of schizophrenia: a dilemma? J. Psychiatry Neurosci. 26 (2001) 203–220 http://www.ncbi.nlm.nih.gov/pubmed/11394190 (accessed March 21, 2018).
[527] R. Depoortère, C. Barret-Grévoz, L. Bardin, A. Newman-Tancredi, Apomorphine-induced emesis in dogs: differential sensitivity to established and novel dopamine D2/5-HT1A antipsychotic compounds, Eur. J. Pharmacol. 597 (2008) 34–38, https://doi.org/10.1016/j.ejphar.2008.08.011.
[528] F.R.C. Dias, L.W. de Matos, M. de F. dos S. Sampaio, R.J. Carey, M.P. Carrera, Opposite effects of low versus high dose haloperidol treatments on spontaneous and apomorphine induced motor behavior: evidence that at a very low dose haloperidol acts as an indirect dopamine agonist, Behav. Brain Res. 229 (2012) 153–159, https://doi.org/10.1016/j.bbr.2011.12.042.
[529] B. Costall, R.J. Naylor, V. Nohria, Climbing behaviour induced by apomorphine in mice: A potential model for the detection of neuroleptic activity, Eur. J. Pharmacol. 50 (1978) 39–50, https://doi.org/10.1016/0014-2999(78)90251-0.
[530] B.I. Turetsky, M.E. Calkins, G.A. Light, A. Olincy, A.D. Radant, N.R. Swerdlow, Neurophysiological endophenotypes of schizophrenia: the viability of selected candidate measures, Schizophr. Bull. 33 (2006) 69–94, https://doi.org/10.1093/schbul/sbl060.
[531] Y. Du, N. Li, X. Wu, Y. Wu, Top–down modulation of prepulse inhibition of the startle reflex in humans and rats, Neurosci. Biobehav. Rev. 33 (2009) 1157–1167, https://doi.org/10.1016/J.NEUBIOREV.2009.02.001.
[532] M.A. Geyer, K.L. McIlwain, R. Paylor, Mouse genetic models for prepulse inhibition: an early review, Mol. Psychiatry 7 (2002) 1039–1053, https://doi.org/10.1038/sj.mp.4001159.
[533] M.A. Geyer, K. Krebs-Thomson, D.L. Braff, N.R. Swerdlow, Pharmacological studies of prepulse inhibition models of sensorimotor gating deficits in schizophrenia: a decade in review, Psychopharmacology (Berl.) 156 (2001) 117–154, https://doi.org/10.1007/s002130100811.
[534] N.R. Swerdlow, M.A. Geyer, Using an animal model of deficient sensorimotor gating to study the pathophysiology and new treatments of schizophrenia, Schizophr. Bull. 24 (1998) 285–301 http://www.ncbi.nlm.nih.gov/pubmed/9613626 (accessed March 20, 2018).
[535] I. Aasen, L. Kolli, V. Kumari, Sex effects in prepulse inhibition and facilitation of the acoustic startle response: implications for pharmacological and treatment studies, J. Psychopharmacol. 19 (2005) 39–45, https://doi.org/10.1177/0269881105048890.
[536] J.P. Garner, C.L. Meehan, J.A. Mench, Stereotypies in caged parrots, schizophrenia and autism: evidence for a common mechanism, Behav. Brain Res. 145 (2003) 125–134, https://doi.org/10.1016/S0166-4328(03)00115-3.
[537] C.D. Frith, D.J. Done, Stereotyped responding by schizophrenic patients on a two-choice guessing task, Psychol. Med. 13 (1983) 779–786 http://www.ncbi.nlm.nih.gov/pubmed/6665094 (accessed March 21, 2018).
[538] G. Bush, M. Fink, G. Petrides, F. Dowling, A. Francis, I. Catatonia, Rating scale and standardized examination, Acta Psychiatr. Scand. 93 (1996) 129–136, https://doi.org/10.1111/j.1600-0447.1996.tb09814.x.
[539] D.M. Benvegnú, R.C.S. Barcelos, N. Boufleur, P. Reckziegel, C.S. Pase, A.F. Ourique, R. C.R. Beck, M.E. Bürger, Haloperidol-loaded polysorbate-coated polymeric nanocapsules increase its efficacy in the antipsychotic treatment in rats, Eur. J. Pharm. Biopharm. 77 (2011) 332–336, https://doi.org/10.1016/J.EJPB.2010.12.016.
[540] B. Ellenbroek, A.R. Cools, The Paw test: an animal model for neuroleptic drugs which fulfils the criteria for pharmacological isomorphism, Life Sci. 42 (1988) 1205–1213 http://www.ncbi.nlm.nih.gov/pubmed/2894605 (accessed March 21, 2018).
[541] O.A. Meyer, H.A. Tilson, W.C. Byrd, M.T. Riley, A method for the routine assessment of fore- and hindlimb grip strength of rats and mice, Neurobehav. Toxicol. 1 (1979) 233–236 http://www.ncbi.nlm.nih.gov/pubmed/551317 (accessed March 20, 2018).
[542] J.P. Smith, P.S. Hicks, L.R. Ortiz, M.J. Martinez, R.N. Mandler, Quantitative measurement of muscle strength in the mouse, J. Neurosci. Methods 62 (1995) 15–19 http://www.ncbi.nlm.nih.gov/pubmed/8750080 (accessed March 20, 2018).
[543] J.P.J. Maurissen, B.R. Marable, A.K. Andrus, K.E. Stebbins, Factors affecting grip strength testing, Neurotoxicol. Teratol. 25 (2018) 543–553 http://www.ncbi.nlm.nih.gov/pubmed/12972067 (accessed March 20, 2018).
[544] H. Liu, T.G. Graber, L. Ferguson-Stegall, L.V. Thompson, Clinically relevant frailty index for mice, J. Gerontol. Ser. A Biol. Sci. Med. Sci. 69 (2014) 1485–1491, https://doi.org/10.1093/gerona/glt188.
[545] L. Steru, R. Chermat, B. Thierry, P. Simon, The tail suspension test: a new method for screening antidepressants in mice, Psychopharmacology (Berl.) 85 (1985) 367–370 http://www.ncbi.nlm.nih.gov/pubmed/3923523 (accessed March 20, 2018).
[546] N.M. Harris, R. Ritzel, N.S. Mancini, Y. Jiang, X. Yi, D.S. Manickam, W.A. Banks, A.V. Kabanov, L.D. McCullough, R. Verma, Nano-particle delivery of brain derived neurotrophic factor after focal cerebral ischemia reduces tissue injury and enhances behavioral recovery, Pharmacol. Biochem. Behav. 150 (151) (2016) 48–56, https://doi.org/10.1016/J.PBB.2016.09.003.
[547] V. Castagné, P. Moser, S. Roux, R.D. Porsolt, Rodent models of depression: forced swim and tail suspension behavioral despair tests in rats and mice, Curr. Protoc. Neurosci, John Wiley & Sons, Inc, Hoboken, NJ, USA, 2011 https://doi.org/10.1002/0471142301.ns0810as55 , Unit 8.10A.
[548] A.J. Mayorga, I. Lucki, Limitations on the use of the C57BL/6 mouse in the tail suspension test, Psychopharmacology (Berl.) 155 (2001) 110–112 http://www.ncbi.nlm.nih.gov/pubmed/11374330 (accessed March 20, 2018).
[549] T.D. Gould (Ed.), Mood and Anxiety Related Phenotypes in Mice, Humana Press, Totowa, NJ, 2009 https://doi.org/10.1007/978-1-60761-303-9.
[550] J.B. Bederson, L.H. Pitts, M. Tsuji, M.C. Nishimura, R.L. Davis, H. Bartkowski, Rat middle cerebral artery occlusion: evaluation of the model and development of a neurologic examination, Stroke 17 (2018) 472–476 http://www.ncbi.nlm.nih.gov/pubmed/3715945 (accessed March 20, 2018).

[551] T. Freret, S. Valable, L. Chazalviel, R. Saulnier, E.T. Mackenzie, E. Petit, M. Bernaudin, M. Boulouard, P. Schumann-Bard, Delayed administration of deferoxamine reduces brain damage and promotes functional recovery after transient focal cerebral ischemia in the rat, Eur. J. Neurosci. 23 (2006) 1757–1765, https://doi.org/10.1111/j.1460-9568.2006.04699.x.
[552] A. Gaudin, M. Yemisci, H. Eroglu, S. Lepetre-Mouelhi, O.F. Turkoglu, B. Dönmez-Demir, S. Caban, M.F. Sargon, S. Garcia-Argote, G. Pieters, O. Loreau, B. Rousseau, O. Tagit, N. Hildebrandt, Y. Le Dantec, J. Mougin, S. Valetti, H. Chacun, V. Nicolas, D. Desmaële, K. Andrieux, Y. Capan, T. Dalkara, P. Couvreur, Squalenoyl adenosine nanoparticles provide neuroprotection after stroke and spinal cord injury, Nat. Nanotechnol. 9 (2014) 1054–1062, https://doi.org/10.1038/nnano.2014.274.
[553] J. Chen, C. Zhang, H. Jiang, Y. Li, L. Zhang, A. Robin, M. Katakowski, M. Lu, M. Chopp, Atorvastatin induction of VEGF and BDNF promotes brain plasticity after stroke in mice, J. Cereb. Blood Flow Metab. 25 (2005) 281–290, https://doi.org/10.1038/sj.jcbfm.9600034.
[554] Q. Li, G. Tang, S. Xue, X. He, P. Miao, Y. Li, J. Wang, L. Xiong, Y. Wang, C. Zhang, G.-Y. Yang, Silica-coated superparamagnetic iron oxide nanoparticles targeting of EPCs in ischemic brain injury, Biomaterials 34 (2013) 4982–4992, https://doi.org/10.1016/J.BIOMATERIALS.2013.03.030.
[555] L. Zhang, T. Schallert, Z.G. Zhang, Q. Jiang, P. Arniego, Q. Li, M. Lu, M. Chopp, A test for detecting long-term sensorimotor dysfunction in the mouse after focal cerebral ischemia, J. Neurosci. Methods 117 (2002) 207–214 http://www.ncbi.nlm.nih.gov/pubmed/12100987 (accessed March 20, 2018).
[556] T. Schallert, M.T. Woodlee, S.M. Fleming, Disentangling multiple types of recovery from brain injury, in: J. Kreigelstein, S. Klumpps (Eds.),Pharmacology of cerebral ischemia. Medpharm Scientific Publishers 2002, pp. 201–216.
[557] T. Schallert, Behavioral tests for preclinical intervention assessment, NeuroRX 3 (2006) 497–504, https://doi.org/10.1016/j.nurx.2006.08.001.
[558] T.M. Barth, T.A. Jones, T. Schallert, Functional subdivisions of the rat somatic sensorimotor cortex, Behav. Brain Res. 39 (1990) 73–95.
[559] A.R. Galho, M.F. Cordeiro, S.A. Ribeiro, M.S. Marques, M.F.D. Antunes, D.C. Luz, G. Hädrich, A.L. Muccillo-Baisch, D.M. Barros, J.V. Lima, C.L. Dora, A.P. Horn, Protective role of free and quercetin-loaded nanoemulsion against damage induced by intracerebral haemorrhage in rats, Nanotechnology 27 (2016) 175101, https://doi.org/10.1088/0957-4484/27/17/175101.
[560] T.N. Luong, H.J. Carlisle, A. Southwell, P.H. Patterson, Assessment of motor balance and coordination in mice using the balance beam, J. Vis. Exp. (2011) https://doi.org/10.3791/2376.
[561] L.D. Eddy, N. B., Synthetic analgesics. II. Dithienylbutenyl-and dithienylbutylamines, J. Pharmacol. Exp. Ther. 107 (1953) 385–393.
[562] K. Hargreaves, R. Dubner, F. Brown, C. Flores, J. Joris, A new and sensitive method for measuring thermal nociception in cutaneous hyperalgesia, Pain. 32 (1988) 77–88 http://www.ncbi.nlm.nih.gov/pubmed/3340425 (accessed March 19, 2018).
[563] M.A. Plone, D.F. Emerich, M.D. Lindner, Individual differences in the hotplate test and effects of habituation on sensitivity to morphine, Pain. 66 (1996) 265–270 http://www.ncbi.nlm.nih.gov/pubmed/8880849 (accessed March 19, 2018).
[564] Y.Y. Lai, S.H. Chan, Shortened pain response time following repeated algesiometric tests in rats, Physiol. Behav. 28 (1982) 1111–1113 http://www.ncbi.nlm.nih.gov/pubmed/7111456 (accessed March 19, 2018).
[565] B. Tamba, R. Iliescu, G. Foltea, M. Leon, Chapter 14. Experimental models for the evaluation of somatic pain in rodents, 2018 http://www.umfiasi.ro/Cercetare/CentreDeCercetare/Documents/CarteExperimental models in rodents/14.pdf (accessed March 19, 2018).
[566] E.C. Stoffel, C.M. Ulibarri, R.M. Craft, Gonadal steroid hormone modulation of nociception, morphine antinociception and reproductive indices in male and female rats, Pain 103 (2003) 285–302 http://www.ncbi.nlm.nih.gov/pubmed/12791435 (accessed March 19, 2018).
[567] A.J.M. Christina, N.J. Merlin, C. Vijaya, S. Jayaprakash, N. Murugesh, Daily rhythm of nociception in rats, J. Circadian Rhythms 2 (2004) 2, https://doi.org/10.1186/1740-3391-2-2.
[568] E.J. Chesler, S.G. Wilson, W.R. Lariviere, S.L. Rodriguez-Zas, J.S. Mogil, Identification and ranking of genetic and laboratory environment factors influencing a behavioral trait, thermal nociception, via computational analysis of a large data archive, Neurosci. Biobehav. Rev. 26 (2002) 907–923 http://www.ncbi.nlm.nih.gov/pubmed/12667496 (accessed March 19, 2018).
[569] F.E. D'Amour, D.L. Smith, A method for determining loss of pain sensation, J. Pharmacol. Exp. Ther. 72 (1941).
[570] H. Liu, J. Ni, R. Wang, In vitro release performance and analgesic activity of endomorphin-1 loaded nanoparticles, Pharmazie 61 (2006) 450–452 http://www.ingentaconnect.com/content/govi/pharmaz/2006/00000061/00000005/art00014?crawler=true (accessed March 2, 2018).
[571] O.-G. Berge, I. Garcia-Cabrera, K. Hole, Response latencies in the tail-flick test depend on tail skin temperature, Neurosci. Lett. 86 (1988) 284–288, https://doi.org/10.1016/0304-3940(88)90497-1.
[572] A. Tjølsen, A. Lund, O.-G. Berge, K. Hole, An improved method for tail-flick testing with adjustment for tail-skin temperature, J. Neurosci. Methods. 26 (1989) 259–265, https://doi.org/10.1016/0165-0270(89)90124-6.
[573] D. Dubuisson, S.G. Dennis, The formalin test: a quantitative study of the analgesic effects of morphine, meperidine, and brain stem stimulation in rats and cats, Pain. 4 (1977) 161–174 http://www.ncbi.nlm.nih.gov/pubmed/564014 (accessed March 19, 2018).
[574] H. Wheeler-Aceto, A. Cowan, Standardization of the rat paw formalin test for the evaluation of analgesics, Psychopharmacology (Berl.) 104 (1991) 35–44 http://www.ncbi.nlm.nih.gov/pubmed/1882002 (accessed March 19, 2018).
[575] S. Hunskaar, O.B. Fasmer, K. Hole, Formalin test in mice, a useful technique for evaluating mild analgesics, J. Neurosci. Methods 14 (1985) 69–76 http://www.ncbi.nlm.nih.gov/pubmed/4033190 (accessed March 19, 2018).
[576] C.J. Meunier, J. Burton, J. Cumps, R.K. Verbeeck, Evaluation of the formalin test to assess the analgesic activity of diflunisal in the rat, Eur. J. Pharm. Sci. 6 (1998) 307–312 http://www.farm.ucl.ac.be/Full-texts-FARM/Meunier-1998.pdf (accessed March 19, 2018).
[577] Y. Chen, S. Constantini, V. Trembovler, M. Weinstock, E. Shohami, An experimental model of closed head injury in mice: pathophysiology, histopathology, and cognitive deficits, J. Neurotrauma. 13 (1996) 557–568, https://doi.org/10.1089/neu.1996.13.557.
[578] J.T. King, P.M. Carlier, D.W. Marion, Early glasgow outcome scale scores predict long-term functional outcome in patients with severe traumatic brain injury, J. Neurotrauma. 22 (2005) 947–954, https://doi.org/10.1089/neu.2005.22.947.
[579] J. Tsenter, L. Beni-Adani, Y. Assaf, A.G. Alexandrovich, V. Trembovler, E. Shohami, Dynamic changes in the recovery after traumatic brain injury in mice: effect of injury severity on T2-weighted MRI abnormalities, and motor and cognitive functions, J. Neurotrauma. 25 (2008) 324–333, https://doi.org/10.1089/neu.2007.0452.
[580] M.A. Flierl, P.F. Stahel, K.M. Beauchamp, S.J. Morgan, W.R. Smith, E. Shohami, Mouse closed head injury model induced by a weight-drop device, Nat. Protoc. 4 (2009) 1328–1337, https://doi.org/10.1038/nprot.2009.148.
[581] K. Tayebi Meybodi, A. Vakili Zarch, M.R. Zarrindast, B. Djahanguiri, Effects of ultra-low doses of morphine, naloxone and ethanol on morphine state-dependent memory of passive avoidance in mice, Behav. Pharmacol. 16 (2005) 139–145 http://www.ncbi.nlm.nih.gov/pubmed/15864068 (accessed March 20, 2018).
[582] J.L. McGaugh, The amygdala modulates the consolidation of memories of emotionally arousing experiences, Annu. Rev. Neurosci. 27 (2004) 1–28, https://doi.org/10.1146/annurev.neuro.27.070203.144157.
[583] P.J.J. Baarendse, G. van Grootheest, R.F. Jansen, A.W. Pieneman, S.O. Ögren, M. Verhage, O. Stiedl, Differential involvement of the dorsal hippocampus in passive avoidance in C57bl/6J and DBA/2J mice, Hippocampus. 18 (2008) 11–19, https://doi.org/10.1002/hipo.20356.
[584] A. Lüttjohann, P.F. Fabene, G. van Luijtelaar, A revised Racine's scale for PTZ-induced seizures in rats, Physiol. Behav. 98 (2009) 579–586, https://doi.org/10.1016/j.physbeh.2009.09.005.
[585] R.J. Racine, Modification of seizure activity by electrical stimulation: II. Motor seizure, Electroencephalogr. Clin. Neurophysiol. 32 (1972) 281–294, https://doi.org/10.1016/0013-4694(72)90177-0.
[586] G.V. Goddard, D.C. McIntyre, C.K. Leech, A permanent change in brain function resulting from daily electrical stimulation, Exp. Neurol. 25 (1969) 295–330 http://www.ncbi.nlm.nih.gov/pubmed/4981856 (accessed March 21, 2018).
[587] G. Leyva-Gómez, M.E. González-Trujano, E. López-Ruiz, P.-O. Couraud, B. Wekslerg, I. Romero, F. Miller, F. Delie, E. Allémann, D. Quintanar-Guerrero, Nanoparticle formulation improves the anticonvulsant effect of clonazepam on the pentylenetetrazole-induced seizures: behavior and electroencephalogram, J. Pharm. Sci. 103 (2014) 2509–2519, https://doi.org/10.1002/jps.24044.
[588] B. Wang, L. Lv, Z. Wang, Y. Jiang, W. Lv, X. Liu, Z. Wang, Y. Zhao, H. Xin, Q. Xu, Improved anti-glioblastoma efficacy by IL-13Rα2 mediated copolymer nanoparticles loaded with paclitaxel, Sci. Rep. 5 (2015) 16589, https://doi.org/10.1038/srep16589.
[589] S.C.J. Steiniger, J. Kreuter, A.S. Khalansky, I.N. Skidan, A.I. Bobruskin, Z.S. Smirnova, S.E. Severin, R. Uhl, M. Kock, K.D. Geiger, S.E. Gelperina, Chemotherapy of glioblastoma in rats using doxorubicin-loaded nanoparticles, Int. J. Cancer 109 (2004) 759–767, https://doi.org/10.1002/ijc.20048.
[590] A.C. Silva, T.R. Oliveira, J.B. Mamani, S.M.F. Malheiros, L. Malavolta, L.F. Pavon, T.T. Sibov, E. Amaro, A. Tannús, E.L.G. Vidoto, M.J. Martins, R.S. Santos, L.F. Gamarra, L. F. Gamarra, Application of hyperthermia induced by superparamagnetic iron oxide nanoparticles in glioma treatment, Int. J. Nanomedicine. 6 (2011) 591–603, https://doi.org/10.2147/IJN.S14737.
[591] M.-J. Tsai, Y.-B. Huang, P.-C. Wu, Y.-S. Fu, Y.-R. Kao, J.-Y. Fang, Y.-H. Tsai, Oral apomorphine delivery from solid lipid nanoparticles with different monostearate emulsifiers: pharmacokinetic and behavioral evaluations, J. Pharm. Sci. 100 (2011) 547–557, https://doi.org/10.1002/jps.22285.
[592] M.S. Muthu, M.K. Rawat, A. Mishra, S. Singh, PLGA nanoparticle formulations of risperidone: preparation and neuropharmacological evaluation, Nanomed. Nanotechnol. Biol. Med. 5 (2009) 323–333, https://doi.org/10.1016/j.nano.2008.12.003.
[593] A. Bernardi, R.L. Frozza, A. Meneghetti, J.B. Hoppe, A.M.O. Battastini, A.R. Pohlmann, S.S. Guterres, C.G. Salbego, Indomethacin-loaded lipid-core nanocapsules reduce the damage triggered by Aβ1-42 in Alzheimer's disease models, Int. J. Nanomed. 7 (2012) 4927–4942, https://doi.org/10.2147/IJN.S35333.
[594] Z. Liu, Y. Shen, Y. Wu, Y. Yang, J. Wu, P. Zhou, X. Lu, Z. Guo, An intrinsic therapy of gold nanoparticles in focal cerebral ischemia-reperfusion injury in rats, J. Biomed. Nanotechnol. 9 (2013) 1017–1028, https://doi.org/10.1166/jbn.2013.1597.
[595] H. Chen, F. Spagnoli, M. Burris, W.B. Rolland, A. Fajilan, H. Dou, J. Tang, J.H. Zhang, Nanoerythropoietin is 10-times more effective than regular erythropoietin in neuroprotection in a neonatal rat model of hypoxia and ischemia, Stroke 43 (2012) 884–887, https://doi.org/10.1161/STROKEAHA.111.637090.
[596] S. Namura, J. Zhu, K. Fink, M. Endres, A. Srinivasan, K.J. Tomaselli, J. Yuan, M.A. Moskowitz, Y. Capan, E. Fernandez-Megia, R. Novoa-Carballal, R. Riguera, K. Andrieux, P. Couvreur, T. Dalkara, Activation and cleavage of caspase-3 in apoptosis induced by experimental cerebral ischemia, J. Neurosci. 18 (1998) 3659–3668, https://doi.org/10.1523/jneurosci.4246-09.2009.
[597] L. Zhao, A. Liu, S. Yu, Z. Wang, X. Lin, G. Zhai, Q. Zhang, The permeability of puerarin loaded poly(butylcyanoacrylate) nanoparticles coated with polysorbate 80 on the blood–brain barrier and its protective effect against cerebral ischemia/reperfusion

injury, Biol. Pharm. Bull. 36 (2013) 1263–1270, https://doi.org/10.1248/bpb.b12-00769.
[598] A. Rosillo-de la Torre, L. Zurita-Olvera, S. Orozco-Suárez, P.E. Garcia Casillas, H. Salgado-Ceballos, G. Luna-Bárcenas, L. Rocha, Phenytoin carried by silica core iron oxide nanoparticles reduces the expression of pharmacoresistant seizures in rats, Nanomedicine 10 (2015) 3563–3577, https://doi.org/10.2217/nnm.15.173.
[599] Y. Wang, X. Ying, L. Chen, Y. Liu, Y. Wang, J. Liang, C. Xu, Y. Guo, S. Wang, W. Hu, Y. Du, Z. Chen, Electroresponsive nanoparticles improve antiseizure effect of phenytoin in generalized tonic-clonic seizures, Neurotherapeutics 13 (2016) 603–613, https://doi.org/10.1007/s13311-016-0431-9.
[600] R. Nair, A.C. Kumar, V.K. Priya, C.M. Yadav, P.Y. Raju, Formulation and evaluation of chitosan solid lipid nanoparticles of carbamazepine, Lipids Health Dis. 11 (2012) 72, https://doi.org/10.1186/1476-511X-11-72.
[601] B. Wilson, Y. Lavanya, S.R.B. Priyadarshini, M. Ramasamy, J.L. Jenita, Albumin nanoparticles for the delivery of gabapentin: Preparation, characterization and pharmacodynamic studies, Int. J. Pharm. 473 (2014) 73–79, https://doi.org/10.1016/J.IJPHARM.2014.05.056.
[602] M. Hashemian, D. Anissian, M. Ghasemi-Kasman, A. Akbari, M. Khalili-Fomeshi, S. Ghasemi, F. Ahmadi, A.A. Moghadamnia, A. Ebrahimpour, Curcumin-loaded chitosan-alginate-STPP nanoparticles ameliorate memory deficits and reduce glial activation in pentylenetetrazol-induced kindling model of epilepsy, Prog. Neuro-Psychopharmacology Biol. Psychiatry 79 (2017) 462–471, https://doi.org/10.1016/J.PNPBP.2017.07.025.